Micro and nanostructured impedance sensors for biological and biomedical applications

by

Walter Messina

ucc

Coláiste na hOllscoile Corcaigh, Éire
University College Cork, Ireland

A thesis submitted to the National University of Ireland

for the degree of Doctor of Philosophy

October 2014

Under the supervision of Dr. Eric Moore

Department of Chemistry
Tyndall National Institute
Cork

Tyndall
National Institute
Institiúid Náisiúnta

Acknowledgements

I would like to extend my sincere thanks to all those people who helped me during the course of this thesis. I would like to express my gratitude in particular to Dr. Eric Moore for giving me the opportunity to work under his supervision and for all his guidance and support. I would like to thank especially my colleague Michelle Fitzgerald for all the help and support during this thesis; without all her work done even in extra hours and during not working days most of this thesis would have never been accomplished.

To all my friends and colleagues in LSI in Tyndall, without you guys I would never have successfully completed this study. A special thanks to Eileen Hurley who has always been a good friend first and a colleague, always willing to lend a helping hand. Thanks also to Lisa Helen, with whom I worked first supervising her as a fourth year student and then became a great addition to the group, for the work done about the Smart needle project. Lynette, Karen, Niall, Shauna, Gerard, Fengjun, Kon for always listening to my complaints and problems and helping me through the tough times.

A special thanks to Lynette Keeney for the help with the AFM measurements and Suzanne Crotty in UCC for the SEM analysis. A big thanks to all the people involved in the central fabrication facility in the Tyndall Institute, in particular Richard Murphy, Dan O'Connell, Brendan McCarthy and Krimo Kalfi.

Thanks to my Mom, Dad and my Brother who have always supported me from many miles away, always giving me encouragement throughout my thesis. Their moral support has been the driving force not only for this thesis but for all my life.

Thank you all from the bottom of my heart.

Declaration

I hereby declare that this thesis is my own work, in partial fulfilment of the requirements of the Doctor of Philosophy degree. It is based on research carried out in Tyndall National Institute and the Department of Chemistry, University College Cork, Ireland between October 2010 and October 2014.

Walter Messina

Abstract

This thesis work covered the fabrication and characterisation of impedance sensors for biological applications aiming in particular to the cytotoxicity monitoring of cultured cells exposed to different kind of chemical compounds and drugs and to the identification of different types of biological tissue (fat, muscles, nerves) using a sensor fabricated on the tip of a commercially available needle during peripheral nerve block procedures.

Gold impedance electrodes have been successfully fabricated for impedance measurement on cells cultured on the electrode surface which was modified with the fabrication of gold nanopillars. These nanostructures have a height of 60nm or 100nm and they have highly ordered layout as they are fabricated through the e-beam technique. The fabrication of the three-dimensional structures on the interdigitated electrodes was supposed to improve the sensitivity of the ECIS (electric cell-substrate impedance sensing) measurement while monitoring the cytotoxicity effects of two different drugs (Antrodia Camphorata extract and Nicotine) on three different cell lines (HeLa, A549 and BALBc 3T3) cultured on the impedance devices and change the morphology of the cells growing on the nanostructured electrodes.

The fabrication of the nanostructures was achieved combining techniques like UV lithography, metal lift-off, evaporation and e-beam lithography techniques. The electrodes were packaged using a pressure sensitive, medical grade adhesive double-sided tape.

The electrodes were then characterised with the aid of AFM and SEM imaging which confirmed the success of the fabrication processes showing the nanopillars fabricated with the right layout and dimensions figures. The introduction of nanopillars on the impedance electrodes, however, did not improve much the sensitivity of the assay with the exception of tests carried out with Nicotine. HeLa and A549 cells appeared to grow in a different way on the two surfaces, while no differences where noticed on the BALBc 3T3 cells.

Impedance measurements obtained with the dead cells on the negative control electrodes or the test electrodes with the drugs can be compared to those done on the electrodes containing just media in the tested volume (as no cells are attached and cover the electrode surface). The impedance figures recorded using these electrodes were between 1.5kΩ and 2.5 kΩ, while the figures recorded on confluent cell layers range between 4kΩ and 5.5kΩ with peaks of almost 7 kΩ if there was more than one layer of cells growing on each other. There was then a very clear separation between the values of living cell compared to the dead ones which was almost 2.5 - 3kΩ. In this way it was very easy to determine whether the drugs affected the cells normal life cycle on not.

However, little or no differences were noticed in the impedance analysis carried out on the two different kinds of electrodes using cultured cells. An increase of sensitivity was noticed only in a couple of experiments carried out on A549 cells growing on the nanostructured electrodes and exposed to different concentration of a solution containing Nicotine. More experiments to achieve a higher number of statistical evidences will be needed to prove these findings with an absolute confidence.

The smart needle project aimed to reduce the limitations of the Electrical Nerve Stimulation (ENS) and the Ultra Sound Guided peripheral nerve block techniques giving the clinicians an additional tool for performing correctly the peripheral nerve block.

Bioimpedance, as measured at the needle tip, provides additional information on needle tip location, thereby facilitating detection of intraneural needle placement. Using the needle as a precision instrument and guidance tool may provide additional information as to needle tip location and enhance safety in regional anaesthesia.

In the time analysis, with the frequency fixed at 10kHz and the samples kept at 12°C, the approximate range for muscle bioimpedance was 203 – 616 Ω, the approximate bioimpedance range for fat was 5.02 - 17.8 kΩ and the approximate range for connective tissue was 790 Ω – 1.55 kΩ. While when the samples were heated at 37°C and measured again at 10kHz, the approximate bioimpedance range for muscle was 100-175Ω. The approximate bioimpedance range of fat was 627 Ω - 3.2 kΩ and the range for connective tissue was 221-540Ω.

In the experiments done on the fresh slaughtered lamb carcass, replicating a scenario close to the real application, the impedance values recorded for fat were around 17 kΩ, for muscle and lean tissue around 1.3 kΩ while the nervous structures had an impedance value of 2.9 kΩ.

With the data collected during this research, it was possible to conclude that measurements of bioimpedance at the needle tip location can give valuable information to the clinicians performing a peripheral nerve block procedure as the separation (in terms of impedance figures) was very marked between the different type of tissues. It is then feasible to use an impedance electrode fabricated on the needle tip to differentiate several tissues from the nerve tissue.

Currently, several different methods are being studied to fabricate an impedance electrode on the surface of a commercially available needle used for the peripheral nerve block procedure.

Table of Contents

Objectives and Thesis overview

The work described in this thesis focused on the development of novel impedance sensors for biological measurement and followed the engagement on two projects carried out during the thesis work. One was the fabrication of nanopillars on the surface of an interdigitated impedance electrode to study if the cells could be potentially cultured on such nanostructured substrate and if, thanks to the nanostructures, it was possible to achieve a better sensitivity in the assay compared to that carried out with flat standard electrodes. The second project was related to the fabrication of bioimpedance electrode on the tip of a commercially available needle for peripheral nerve block procedures. This sensor would allow the clinicians to identify the tissue the needle is in by measuring the bioimpedance value of the human body while the needle progresses towards the nerve structures. In this way, once recognized the proximity to the nerve bundle, the anaesthesiologist would be able to avoid an intraneural injection of drug causing irreversible chemical damages to the nerve.

Chapter 1 is a general introduction focusing mainly on the state of the art of sensors and biosensors and their fabrication methods. A section is also dedicated to an overview of the nanostructures mainly studied recently with particular regards to the nanopillars. Impedance techniques are also examined with a thorough description of the electric cell-substrate impedance spectroscopy technique used in this thesis. Also theory about bioimpedance and impedance from an electrical point of view are described. An introduction to bioimpedance used for tissue differentiation is also given here.

Chapter 2 describes the fabrication steps adopted to achieve the fabrication of nanopillars on the impedance electrodes. A description of how the electrodes with the novel structures have been characterised through the SEM and the AFM, how the electrodes have been packaged and what setup has been prepared for the impedance measurements is also presented in this chapter.

Chapter 3 focuses on to studying whether the presence of nanopillars allow a good growth of the cells on the substrate and if in electrical impedance measurements for

cytotoxicity monitoring it is possible to achieve better sensitivity in the assay compared to the same kind of electrode but flat instead. Three different cell lines have been tested for this purpose on the nanostructured electrodes and exposed to two different chemicals to determine their cytotoxicity on A549, BALB c3T3 and HeLa cell lines. The chemicals used are an extract of Antrodia Camphorata and Nicotine. The results achieved in the studies are reported in this chapter.

Chapter 4 reports a description of an alternative use of these impedance electrodes which can be used as electrochemical sensors too. This chapter proves that the nanostructures can increase the mass transport of the electrodes in this kind of measurement.

Chapter 5 describes the preliminary studies done at the Tyndall National Institute in collaboration with Cork University Hospital (Anaesthesia Dept.) for fabricating a "Smart Needle" able to identify the kind of tissue it is in in order to kind information to the anaesthesiologists of the needle tip location. The main objective of this project is to provide doctors with a further tool increase the safety of peripheral nerve block procedure by avoiding intraneural drug injection to the patients causing irreversible chemical damages to the nerves. All the preliminary studies conducted ex-vivo, fabrication and results are described in this section.

Chapter 6 discusses the general conclusions of the work carried out in this thesis and possible future work. Chapter 7 lists the publications, oral and poster presentation given during the thesis period of time.

Chapter 1

INTRODUCTION

1.1 SENSORS

Sensors are devices able to detect and respond to certain types of inputs from the physical environment. The output is generally a signal that can be converted to a readable display. This read-out can be located directly on the sensor or transmitted, often electronically, over a network of other devices and components for reading or further processing. Physical parameters (temperature, pressure, speed, etc.) are converted into signals which can be measured and interpreted. For example the mercury in the glass of a thermometer expands and contracts depending on the temperature at which it is exposed to and that can be read by the user on the calibrated glass tube.

There are many criteria and features to consider in the choice of a sensor: accuracy, environmental condition, range of measurement, resolution (the smallest increment detected by the sensor), repeatability (consistency of the measurements in the same conditions and environment), cost, calibration and biocompatibility if the sensor will be used for biological systems or medical applications.

Sensors can be classified generally in two big categories mainly by their applications. They can be differentiated between [1]:

- Industrial (process control, measurement and automation)
- Non-industrial (Aerospace engineering, Medical products, Automobiles, Consumer electronics, etc.)

They can also be classified by other characteristics, for example:

Digital or analog (distinguishing between discrete or continuous signals). For the digital sensors the signal they produce are binary or quantized, while for the analog ones the signal produced is continuous and proportional to the measurand.

Active or passive (distinguishing between those which need and those which do not need power supply). Active sensors require an external source of power (excitation voltage) that provides the majority of the output power of the signal, while the passive sensors are provided an output power by the measured signal without an excitation voltage.

There are many specific applications for the sensors and often they are the key components of many systems, if we look carefully around we could find them everywhere: phones, cars, kitchens, chemistry laboratories, medical devices, etc (Figure 1.1). The most common types of sensors are:

- Temperature - Thermistors, thermocouples, RTDs (resistance temperature detectors and many more.
- Pressure - Fibre optic, vacuum, elastic liquid based manometers, LVDT (linear variable differential transformer), electronic.
- Flow - Electromagnetic, differential pressure, positional displacement, thermal mass, etc.
- Level Sensors - Differential pressure, ultrasonic radio frequency, radar, thermal displacement, etc.
- Proximity and displacement - LVDT, photoelectric, capacitive, magnetic, ultrasonic.
- Biosensors - Resonant mirror, electrochemical, surface Plasmon resonance, light addressable potentiometric.
- Image - Charge coupled devices, CMOS
- Gas and chemical - Semiconductor, infrared, conductance, electrochemical.

- Acceleration - Gyroscopes, accelerometers.

- Others - Moisture, humidity sensor, speed sensor, mass, tilt sensor, force, viscosity.

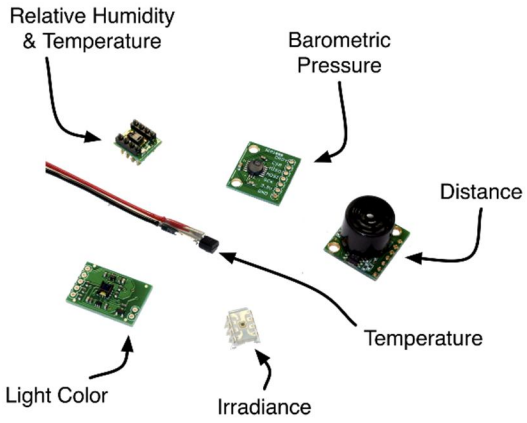

Figure 1.1: An example of various sensors available on the current market

The physical quantity, property, or condition that the system is able to measure is called measurand. The words "sensor" and "transducer" are both commonly used in the description of systems of control and measurement. The use of these devices in different fields of science contributed to create ambiguity and misinterpretation about their definitions. In literature, a sensor is "a device which is sensitive to a physical quantity and able to transform it into a measurable signal" or also it is "a device able to transform a physical quantity in an electric signal". Some books define a transducer as "a device that converts the energy from a system to another in the same or different form" or as the ensemble of a sensor and a signal conditioning circuit [2]. In summary a sensor is an element that provides an output dependent to a certain variable, while a transducer is a device that has the function of transforming the physical quantity provided by the primary sensor in an output that could be easier to read. The sensor, in respect to the transducer, is always the initial element of the measurement chain. The term transducer is used to indicate a sensor that is not the initial element of the system just explained.

The measurements done through the use of sensors are not immune to errors. In fact, in the real world, there are many factors interfering with the outputs. In theory there are three kinds of inputs in an operating sensor:

- desired inputs, which are the measurands that the sensor has been designated to identify and isolate
- interfering inputs, quantities to which the instrument is unintentionally sensitive and that inadvertently affect the instrument as a consequence of the principles used to acquire and process the desired inputs
- Modifying Input: Quantities that cause a change in the input –output relations of the instrument by altering its performance

The effects of the interfering and modifying inputs can be decreased or removed either by altering the design of the components in the instrument or by adding new parts designed to offset the undesired inputs. In reality, the elimination of the actual source of the undesired inputs occurs only very rarely. There are several ways to reduce the effects of these unwanted contributions: for example one way is to estimate or measure their magnitude and subtract them from the signal to calculate the correct output; another method is to introduce "filters" into the instrument to block or reduce the modifying or interfering inputs (filters can also be applied to the outputs; in electronic engineering for example low-pass, band-pass filters, etc. are used); or also additional interferences can be introduced to compensate or cancel the undesired effects of other interfering inputs [3].

1.2 BIOSENSORS

One of the targeted goals of this thesis will be the fabrication and the use of biosensors. A biosensor can be defined as a self-contained integrated device which is capable of providing specific quantitative or semi-quantitative analytical information using a biological recognition element which is in direct spatial contact with a transducer element (Figure 1.2). Biosensors have a range of application covering many fields; for example medicine, pharma, food and process control, environmental monitoring,

defence and security, but most of the market is driven by medical diagnostics, mainly glucose sensors for people with diabetes. The most significant trend likely to impact on biosensors is the emergence of personalised medicine. Electrochemical biosensors are currently the most widespread among this category of sensors, but are focused mostly on metabolite monitoring, while bioaffinity is examined mainly through optical techniques [4].

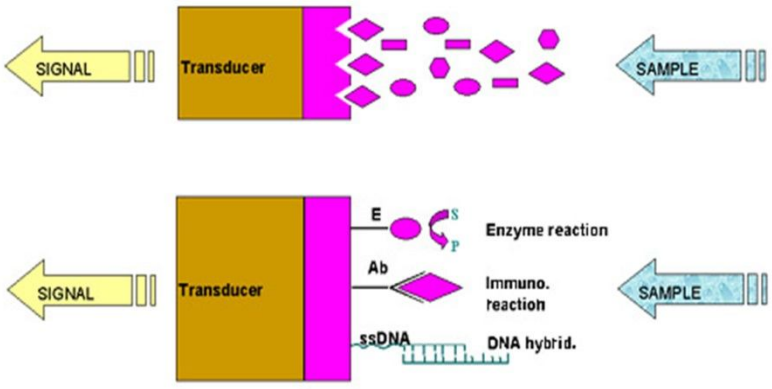

Figure 1.2: General schematic of the working principle of biosensors (http://bme240.eng.uci.edu/students/08s/vkhoshne/b.html)

1.2.1 Types of biosensors:

As mentioned before, biosensors are used in a wide variety of science and industrial sectors. For this reason these sensor are made of different material and use different kinds of transducers. A list of the main transduction modes is reported below.

1.2.1.1 Electrical Biosensors

These biosensors can measure the change of electrical properties in a system due to the proximity or contact with an analyte have become well widespread and use a raw electrical signal, such as current or impedance, that can be directly processed and read by the users. This class of sensors is well represented by devices called Field Effect Transistors (FET). FETs are able to monitor the current between two electrical terminals, source and drain, embedded in a semiconductor. A second electric field can

be applied across two terminals oriented orthogonally in respect to the source to change the concentration of charge carriers in the semiconductor. The current then reaches the drain flowing through the gate. For example, a nanowire FET biosensor is composed of a semiconductor which connects the source and drain electrodes (Figure 1.3). Charged biomolecules that are adsorbed onto the semiconductor sensor produce an electric field acting as the gate and changing the charge carrier density within the device. The drain current can be then measured and scaled for sensing applications. Besides being a sensitive label-free technology, nanowire FET biosensors can be fabricated relatively cheaply using traditional micro and nano fabrication techniques that are well-known in the semiconductor industry. These sensors are usually incorporated into microfluidic flow cells, and they require only a small amount (microliters) of sample for a measurement [5].

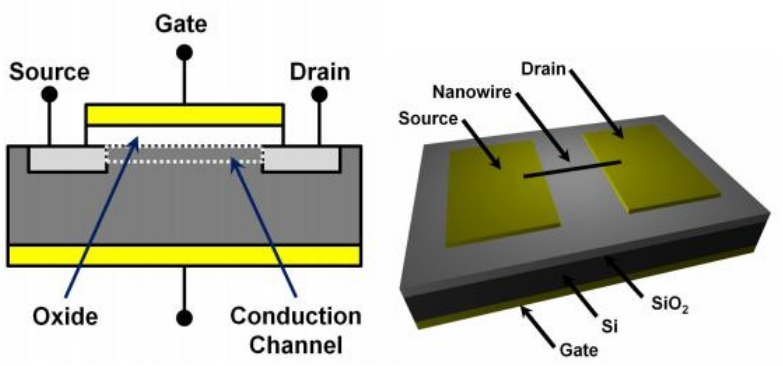

Figure 1.3: Field effect transistors (FETs). On left is represented a generic FET, including the source and drain with conduction channel between the two. A field applied using the gate can control the density of charge carriers in the conduction channel and change the current measured at the drain. On the right side is represented nanowire FET sensor, Biomolecules bound to the surface of the nanowire have a localized electric field that can distort the charge carrier in density in the nanowire. Changes in the drain current are used to track how much material has adsorbed to the device (ref 5).

Impedance based biosensors can provide information about the growth, motility, and physiology of cells growing on biocompatible electrodes. Impedance-based sensor arrays are particularly useful for performing drug screening experiments and also for studying the cells adhesion and micromotion. Cells are cultured on the electrodes and the measured AC impedance change in a way which is depending on the frequency used in the measurement, the cell coverage, and the cell-electrode gap. A basic sensor configuration includes the use of a sensing electrode and a counter electrode immersed in cell growth medium. Cells growing and spreading on the electrode adhere to it creating focal adhesion points which represent only a small (5-10%) fraction of their area. At relatively low frequencies (<100Hz), resistive behavior is predominant, while at high frequencies (>100 kHz) capacitive effects are more marked. At moderate frequencies, cells obstruct the current flow and there is an increase in the measured impedance [6].

1.2.1.2 Mechanical Biosensors

Some biosensors can exploit the use mechanical forces and motion of a certain material to identify the amount of an analyte present in a sample. An example of such devices is the microcantilever (figure 1.4), which uses mainly two modes of detection. One is the static deflection of the device that, following a specific adsorption, can be used to measure the concentration of a specific analyte. The second exploits the fact that microcantilevers oscillate at a characteristic frequency. This frequency depends strictly on the shape and material properties of the cantilever and changes upon adsorption of biomolecules. Modification of the condition of the device, i.e. deflection and change in oscillation frequency, can be observed by reflecting a laser off the device surface and tracking its position, much the same way as in an atomic force microscope. [7]

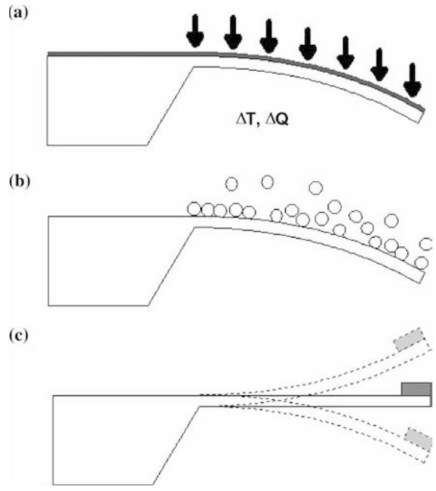

Figure 1.4: Schematic drawings of cantilever transduction principles: a bimetallic temperature and heat sensor, b surface stress sensor, c microbalance due to additional mass loading (ref. 7)

Another mechanical biosensor is the quartz crystal microbalance (QCM), which uses the piezoelectric characteristics of a crystal and the change in resonant frequency as the material, coated with a biological recognition element, adsorbs the interested analyte. The oscillation of the crystals is stimulated electronically, but the frequency change occurs when biomolecules couple mechanically on the crystal surface. Like microcantilevers, QCMs have a low limit of detection. However, these devices are relatively easy and cheap to manufacture and are easy to integrate into flow devices. They are also very well characterized and easily functionalized via surface chemistry [8].

1.2.1.3 Thermometric Biosensors

This class of biosensors measures the generation or the absorption of heat resulting from a reaction between the analyte and the biological recognition element. They are particularly useful for measuring enzymatic reactions (Figure 1.5). The selectivity is given by the nature of the target enzyme used and the reaction enthalpy cannot be confused with other reactions happening during the measurement and related to other species in the biologic mixture. If the enzyme catalyzed reaction is exothermic, two thermistors may be used to measure the difference in resistance between reactant and product and, hence, the analyte concentration. Thermistors are used more often than thermometers or thermocouples as the change of resistance of certain oxides is larger

than the change of length of a mercury column or the microvolt changes of thermocouple junctions. A new kind of thermometric sensors are fabricated using pyroelectric heat flow transducers. Heat flows from a heated region to a lower temperature region, controlled to occur in one dimension. The lower temperature side can be coated with an enzyme. When the reaction takes place the lower temperature side gets warmed. The pyroelectric material develops a spontaneous voltage difference in a thermal gradient; if the gradient is disturbed by generation or adsorption of heat, the voltage temporarily changes [9].

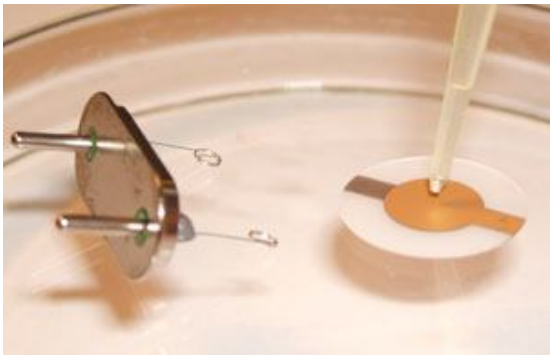

Figure 1.5: Example of a thermometric biosensor. These sensors are constructed by combining enzymes with temperature sensors. When the analyte is exposed to the enzyme, the heat of reaction of the enzyme is measured and is calibrated against the analyte concentration (ref 9).

1.2.1.4 Electrochemical biosensors

This group of biosensors is probably the most commonly used in the general category of sensors. They have great advantages in terms of high sensitivity and portability. The fundamental principle for this type of biosensors is that many chemical reactions produce or consume ions or electrons (red-ox) which cause some changes in the electrical properties of the solution which can be sensed out and used as measuring parameter. A suitable enzyme in the biological recognition layer is the most crucial part of an electrochemical biosensor and is, usually, immobilized onto the electrode allowing then the interaction with the target analyte. They can be divided in three categories: amperometric, potentiometric and conductometric. [10, 11]

Potentiometric biosensors are based on ion-selective electrodes (ISE) and ion-sensitive field effect transistors (ISFET). Their output signal is generated thanks to the accumulation of ions at the border of an ion – selective membrane (Figure 1.6). The current flow in the electrode is zero or very close to it. For example, it is possible to immobilize glucose oxidase on the surface of the pH-meter electrode. Glucose does not have a major effect on the pH of the working media but the gluconate, produced from the enzymic reaction, causes acidification. In general a normal pH-meter normally found in chemistry laboratories is a good example of potentiometric sensors. The potential difference between a working and reference electrode is proportional to the natural logarithm of the ion concentration as described by the Nernst equation (10).

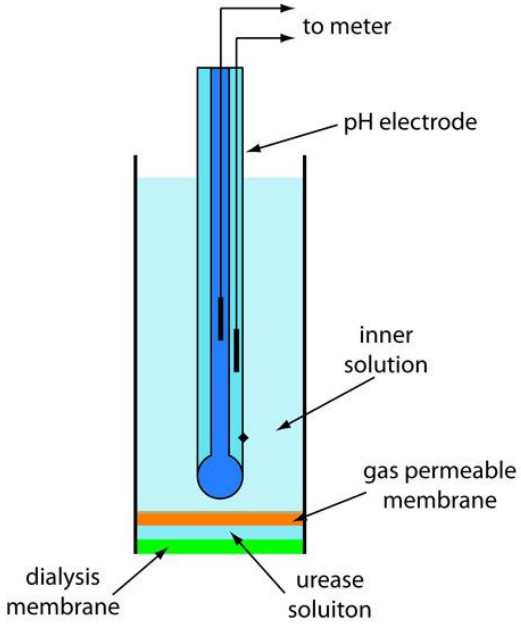

Figure 1.6: Schematic diagram showing an enzyme-based potentiometric biosensor for urea. A solution of the enzyme urease is trapped between a dialysis membrane and a gas permeable membrane. Urea diffuses across the dialysis membrane and reacts with urease, producing NH_3 that diffuses across the gas permeable membrane. The resulting change in the internal solution's pH is measured with the pH electrode (http://chemwiki.ucdavis.edu/Analytical_Chemistry/).

Amperometric biosensors, unlike the potentiometric ones, measure a current originated by the oxidation or reduction of chemical species at the working electrode interface with

a fixed potential applied between the working and the reference electrode. The current that is generated is directly proportional to the electroactive species concentration in the solution analysed (Figure 1.7). The first and most famous example of an amperometric biosensor is an enzyme-based sensor developed by Clarke in 1962 which consisted of immobilized glucose oxidation enzymes on an oxygen sensor coupled with a semi-permeable membrane which allowed the measurement of consumed oxygen by the GO enzyme.

$$glucose + O_2 \xrightarrow{glucose\ oxidase} gluconic\ acid + H_2O_2$$

Oxygen was reduced to water following the application of a negative potential on the platinum cathode.

$$O_2 + 4H^+ + 4e^- \longrightarrow 2H_2O$$

A lower concentration of oxygen corresponded to a higher concentration of GO and vice versa. The earlier generations of this kind of sensor required the application of high potentials to work but this resulted in interferences from other active species present in the investigated solution. The use of mediators in the latter generation allowed the operations at lower potential reducing the interferences as these non-physiological electron acceptors can shuttle electrons between the surface of the working electrode and the bio-recognition element. Improvements in the last generation led to the operation of glucose biosensors without mediators at low potentials as the electrons are transported to the electrode from the glucose via the enzyme active site with a very high selectivity.

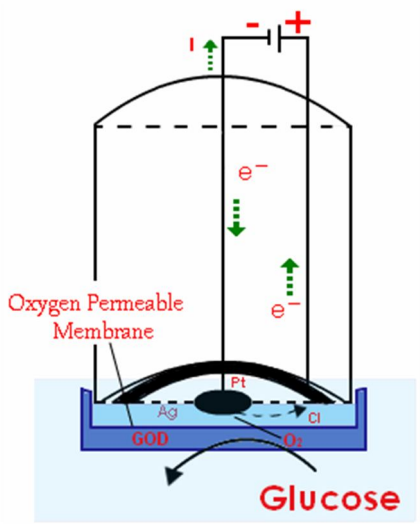

Figure 1.7: Schematic diagram of a simple amperometric biosensor. A potential is applied between the central platinum cathode and the silver anode. This generates a current(I) which is carried between the electrodes through a saturated solution of KCl. This electrode compartment is separated from the biocatalyst (here shown glucose oxidase, GOD) by a thin membrane permeable only to oxygen. The analyte solution is separated from the biocatalyst by another membrane, permeable to the substrate(s) and product(s). This biosensor is normally about 1 cm in diameter but can be scaled down to 0.25 mm diameter using a Pt wire cathode within a silver plated steel needle anode and dip-coated membranes (http://www1.lsbu.ac.uk/water/enztech/amperometric.html)

Conductometric biosensors measure the change in conductivity of solutions containing mobile electric charges. The conductivity of a liquid results from the dissociation of a dissolved electrolyte into ions and their migration induced by an electrical field. An electrical field within the electrolyte is created upon the application of a potential difference, so ions negatively charged move towards the anode, while those positively charged move towards the cathode. The current in the electrolyte is caused by the ion movement towards the electrodes where the ions are neutralized and isolated as neutral atoms (or molecules). Thus, the conductivity of the electrolyte solution depends on the ion concentration and mobility. The resistance of electrolyte solution is well-known to be in direct proportion to the distance between the immersed electrodes and reciprocal to their surface area. In general conductometric measurement commonly consists of determining the conductivity of a solution between two parallel electrodes and its value

is the sum of all the ions within the solution tested. Usually, conductometric transducers are miniaturized two-electrode devices designed to measure the conductivity of a thin electrolyte layer adjacent to the electrode surface (Figure 1.8). The most common and widely used layout for the development of conductometric biosensor is the interdigitated structure which is widely found in literature [12, 13].

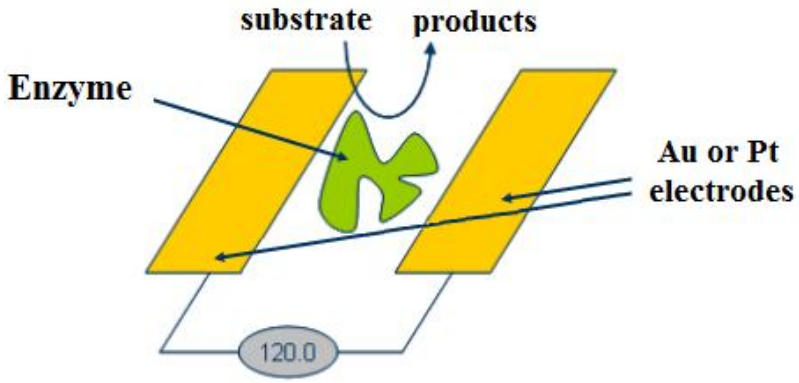

Figure 1.8: general schematic of a conductometric biosensor. The products of an enzymatic reaction change the conductibility of a solution in the proximity of the electrodes (Greppi G., "Sensors and Biosensors", University of Sassari, Italy; http://slideplayer.it/slide/598663/)

1.2.2 Biosensor Recognition Elements

Biosensing operations are strictly linked to molecular recognition. Biosensor recognition elements are usually isolated from living systems although, many biorecognition elements now available are often not naturally occurring but synthesized in a laboratory. Techniques available in modern biotechnology have enabled the use of a broad range of molecular recognition elements, including receptors, enzymes, antibodies, nucleic acids and cells to develop new biosensors.

Receptor-based biosensors: besides being physiological processes mediators, receptors are natural targets for a huge range of drugs and toxins. Receptors are transmembrane and soluble proteins that are able to bind to specific molecules (ligands). When a binding event takes place, specific cellular responses occur, causing transduction in

response to the initial receptor-ligand binding event. Although receptors as biosensor recognition elements have high ligand specificity and affinity, their low yield and relative instability, intensive and long labour associated with the isolation and purification protocols, as well as transduction difficulties have significantly limited the use and development of receptor-based devices [14].

Enzyme-based biosensors: enzymes are large molecules, mostly proteins, which carry on many metabolic processes inside the cell. These kinds of biosensors exploit the properties of high affinity and selectivity of these proteins towards the target molecules (Figure 1.9). Usually the enzymes are immobilized on the surface of the sensor or within it; the transducer converts then the effects created by the interaction of the enzyme with the analyte, usually into an electrical signal. These biosensors can work fundamentally in two different ways: one monitor an increased enzymatic activity, as it happens in the glucose sensors (glucometers); the second, on the other hand, detects an increased enzyme inhibition activity monitoring a decrease of the initial signal used often the detection of organophosphate compounds in pesticides or warfare nerve agents. The advantages of these devices are that they are very specific and that they have faster responses due to shorter diffusion paths (no cell walls). Unfortunately they are quite expensive to fabricate and take lot time and labour to isolate the enzymes which tend to be also quite unstable [15, 16].

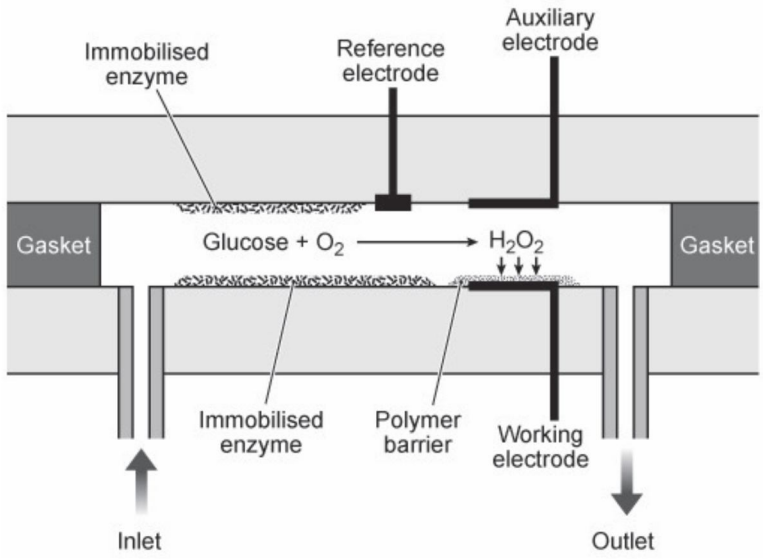

Figure 1.9: Diagram of the glucose sensor showing the electrode configuration, the polymer barrier deposited onto the working electrode and the surface where the enzyme (glucose oxidase) is immobilized (ref 15).

Antibody-based biosensors (or immunosensors): antibodies are large, Y-shaped, specialized proteins (also called Immunoglobins) produced by the body's immune system when harmful substances, called antigens, are detected. Examples of antigens include microorganisms such as bacteria, fungi, parasites, and viruses or chemicals. Antibodies have the ability to combine with the antigen that triggered their production and fight it. These types of biosensors work by using an antigen-antibody reaction to create a transduced signal (Figure 1.10): an electric current (amperometric immunosensors), a voltage difference (potentiometric immunosensors), or a resistivity change (conductimetric immunosensors). One of the biggest issues with antibody-based biosensors is that binding reactions occur only on contact with its antigen. Also, there is no biological amplification of the signal generated by the accumulation of a product which can give a measurable signal to the transducer [17, 18]http://sst-web.tees.ac.uk/external/u0003076/BIOSENSORS_WEB/antibody/AGAB1.htm.

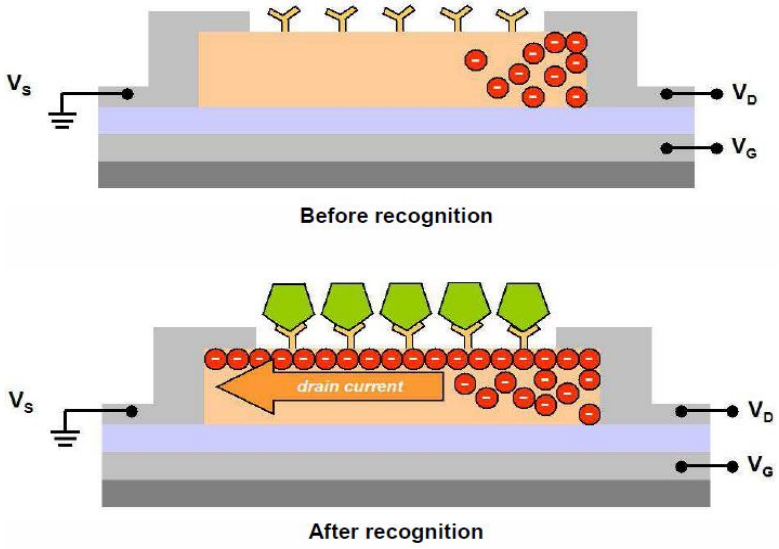

Figure 1.10: Schematic of a FET immunosensor. The formation of antigen-antibody complex at the gate terminal modulates the charge carrier flow between source and gate, generating an increase in current (ref 18).

DNA-based biosensors: Deoxyribonucleic acids (DNA) are one of the most studied and important biomolecules. The DNA has a unique structure based on the complementarity of the adenine/thymine and cytosine/guanine pairs which has been the basis and the starting point for most of the genetic analysis and experiments. The capability of a single strand of DNA (ssDNA) molecule to hybridize to its complementary strand in a sample is the foundation of DNA-based detection systems (AAA). The potential market for this simple, cheap, rapid, and quantitative detection of specific genes is huge as it includes areas like the clinical, veterinary, medico-legal, environmental and food industry. These kinds of biosensors are mostly based on optical, surface acoustic wave and electrochemical transducers. The optical ones are widely used and exploit several techniques like luminescence, fluorescence, surface plasmon resonance (SPR), etc. The acoustic ones instead have been employed to avoid the use of labels such as radiochemical or fluorescent agents and exploit piezoelectric phenomena happening at the substrate material level during the detection. Electrochemical techniques allow DNA based biosensor to be rapid, sensitive, cost effective and enable in-situ generation of reactive intermediates and detection of DNA damage (Figure 1.11). The DNA biosensor can be also used as a good model for simulating interactions that occur between the

nucleic acid with cell membranes, potential environmental carcinogenic compounds and to clarify the mechanisms of action of drugs used as chemotherapeutic agents. The electrodes in the electrochemical transduction are themselves a tuneable charged reagent as well as a detector of all surface phenomena, which greatly enhances the electrochemical DNA biosensing capabilities. However a necessary condition is that the analyte is electroactive, i.e. capable of undergoing electron transfer reaction in order to use an electrochemical transducer [19].

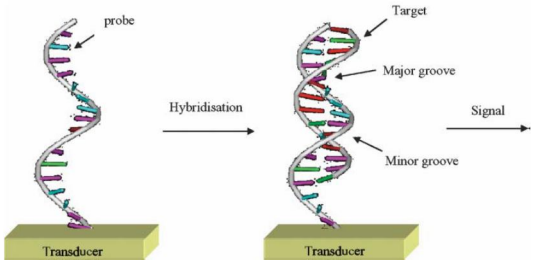

Figure 1.11: Recognition interface consisting of the immobilised DNA probe and steps in the detection of a specific DNA target strand (ref 19).

Cell-based biosensors: in this kind of sensors the cell responds to the presence of a certain analyte by generating a specific cellular signal which is converted by a secondary in a readable signal for the user. Mammalian cells and bacterial cells (prokaryote and eukaryote cells) are commonly used in this class of biosensors. Mammalian cells are the biological recognition element more widely employed in this type of sensor fabrication [20]. They are very often used for cytotoxicity monitoring, but this will be discussed more widely in the next paragraphs.

1.3 MICRO AND NANO FABRICATION

The word "lithography" means literally the transfer of an image to a surface. Current photolithographic techniques, such as ultra-violet (UV), electron-beam (e-beam), X-ray and focused ion-beam (FIB), employ light exposure to pattern a specific layout on surfaces of different materials. Non-photolithographic methods use, instead, atomic force microscopes (dip-pen), soft (soft lithography) or hard moulds (nanoimprint lithography), for example, to transfer the desired pattern. Other non-lithographic approaches (like vapour-solid and vapour-liquid-solid), do not implicate the use of prefabricated images and patterns, but could also be used to produce micro and nano structures; nanorods, nanowires and nanotubes are probably the most known examples. Moreover, different fabrication methods can be combined in order to create 3-D or hybrid micro-nano structures.

This section will outline the most important micro and nanofabrication techniques. There are several methods based on the fabrication of integrated circuit (IC), such as thin film deposition, lithography and etching, which will be discussed in detail. Nanofabrication technologies and micro electromechanical systems (MEMS) fabrication will be also discussed. Even though most of the current research is moving towards the nano domain, a general review of top-down methods for fabricating micro structured patterns and devices is essential in understanding this research.
The fabrication of nanostructures can be divided into two main general methods: top down and bottom up construction.

Top down fabrication can be compared to sculpting from a bulky block of material. This is gradually eroded until the desired design or pattern is achieved. There are several techniques in micro and nanotechnology for top down fabrication but they can be generally divided into mechanical and chemical fabrication methods. The most well-known top-down technique is the lithography.

Bottom up fabrication can be likened to the process of building a house using bricks. Instead of using bricks one by one to build a house, bottom up fabrication techniques place atoms or molecules to fabricate the desired nanostructure. These kinds of

processes are time consuming and so, usually, self-assembly techniques are employed where atoms or molecules are able to arrange themselves as required.

Micro- and nanodevices have many advantages over their macroscale counterparts. Miniaturization allows manufacturing of portable, hand-held, implantable, or even injectable devices. As a result of their smaller size, these devices need a lower sample or reagent for analysis or operation, thus saving money and time. Miniaturization also allows shortening diffusion times where processes and experiments are inhibited by the length of the same [21, 22].

1.3.1 Lithography

Introduced in the late 1950 in microelectronics manufacturing, photolithography has been extensively employed as the primary lithographic step in micro-nanofabrication. The high resolution (sub-micrometers to tens of nanometers) and reliability of the process are achieved at the expense of complicated exposure systems and toxic photo-reactive chemicals, which limits the application of this technique to the cleanroom environment [23, 24].

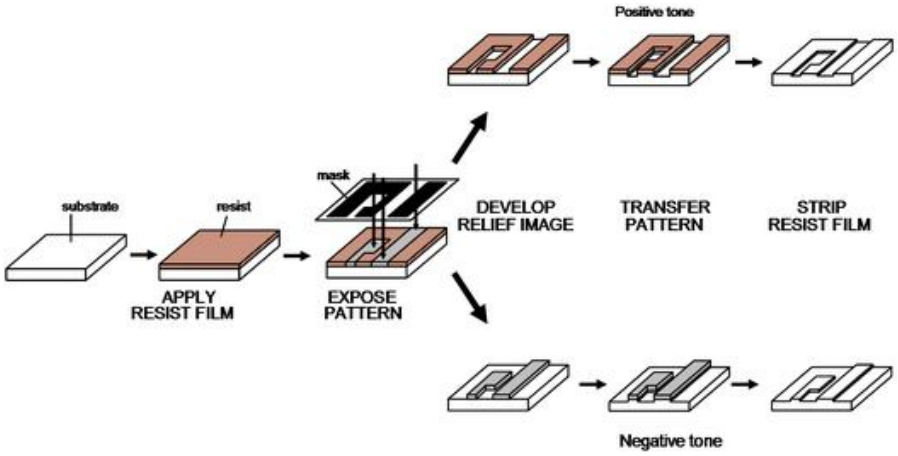

Figure 1.12: Schematic diagram showing the steps in the lithographic process to fabricate microelectronic devices (ref 23).

The photolithographic process consists of a number of steps in which a chosen design is produced on a substrate surface by exposing regions of a light-sensitive material to ultraviolet (UV) light. In the first step the substrate material, usually silicon or glass, is

spin-coated with a layer of a photoresist or light-sensitive polymer which comes in a liquid form. After spinning the photoresist onto the wafer, the substrate is soft-baked for a few minutes at 60–100 °C to remove the solvents from the resist and improve adhesion. A photo mask, with the desired shape patterned with a non-transparent material (commonly chromium) on a glass dish or other transparent material, is then aligned with the substrate covered with the photoresist. This assembly is then exposed to a source of UV light, thus irradiating the sections of the photoresist not covered by the opaque regions of the mask. Depending on the type of photoresist utilized (positive or negative), the photoresist will go through one of two possible transformations after the exposure to light. When UV light irradiates a positive photoresist, the exposed regions break down and become more soluble in a developing solution and can be removed when in contact with it. On the other hand, when UV light illuminates a negative photoresist, it becomes cross-linked becoming insoluble in the developing solution. Therefore only the parts not exposed to light will be dissolved and removed (Figure 1.12).

The patterned photoresist is then used to protect the covered parts of the substrate from etching, or from a further deposition of compounds or biomolecules on its surface. Once the process is completed, the photoresist can be removed, leaving the desired pattern design on the substrate. A hard bake step (20-30 minutes at 120-180 °C) usually precedes the developing stage to further improve adhesion. One of the most commonly used photoresist is SU-8, originally developed by IBM. It is a negative photoresist which crosslinks after the exposure of near UV radiation in the range of 350 to 400 nm, and can be developed with a number of substances including propyleneglycol monoether acetate, ethyl acetate and diacetone alcohol. One of the main advantages of SU-8 is that it permits generation of tall structures, of more than 1000 m in height [16]. Photolithography is widely used in the field of micro fabrication because of the high resolution and variety of pattern that are possible to achieve. These, however, depend on the characteristics of the photomask. A limitation of this technique is that it requires a clean-room environment [21, 22, 25].

Nanosphere lithography (NSL) is a relatively inexpensive fabrication technique for fabricating regular and homogenous arrays of nanoparticles of different sizes. This process can be divided in two main steps of which the first is the mask preparation. The flat substrate is coated with a suspension containing monodisperse spherical colloids (e.g. polystyrene) in order to enhance its hydrophilicity. After drying, a hexagonal closed packed (HCP) monolayer (or bilayer), called a colloidal crystal mask (CCM), is formed. This mask is then used to selectively pattern the substrate thanks to the deposition of the desired material of through the gaps created by the ordered spheres. The mask is then removed through sonication in an suitable solvent or by a strip-off process leaving an array of ordered nanodots on the surface of the substrate. Sometimes it could be necessary to proceed with an annealing process to crystallize the sample or induce a crystallographic phase change. The NSL is often considered as a hybrid between the bottom-up approach (due to the self-organization of the colloidal spheres in a HCP lattice) and the top-down approach (due to the achievement of dots like in a conventional lithography technique). Nanosphere Lithography is also known as colloidal lithography [26, 27] or Natural lithography [28].

1.3.2 Soft lithography

Quite similar to photolithography, soft lithography is a method used to transfer a pattern onto a surface. It uses a microstructure replica produced by moulding a polymer, in most of the cases poly-dimethylsiloxane (PDMS), to a master manufactured through other micro fabrication techniques such as photolithography, micromachining, e-beam writing, TEM grids [29], polymer beads assembled on solid supports [30], and relief structures etched in metals or Si [30, 31]. PDMS has been readily used in the biomedical and pharmaceutical fields because of its biocompatibility, and good thermal, mechanical and optical properties. Other materials that could be used are polyurethanes, polyimides, and cross-linked resins (phenol formaldehyde polymers) [29]. They have very low glass transition temperatures and therefore are fluids at room temperature. These liquid materials can be readily converted into solid elastomers by cross-linking. The formulation, fabrication, and applications of PDMS elastomers have been extensively studied and are well documented in literature [32]. Elastomers like PDMS can make conformal contact with surfaces over relatively large areas, even those that are non-

planar on the submicron scale, and because they can be released easily from rigid masters or from complex, three-dimensional structures that are being moulded. The main advantage of soft lithography is that once the reusable mould is fabricated, none of the other steps require a clean room environment. As a result, it is a less expensive technique that provides great resolution through a simpler process [21, 33].

1.3.3 Microcontact printing

Microcontact printing is used to transfer patterns from the surface of a patterned PDMS stamp to the surface of a substrate [34]. Various biomolecules, proteins, polyelectrolytes and suspensions of cells, can be patterned directly on surfaces using this technique [35 – 37]. In this technique, contact between the PDMS stamp and a substrate only transfers the biomolecules from the raised surface of the bas-relief features of the stamp to the substrate, and produces patterns with feature sizes as small as 100 nm over areas as large as a square meter. Conformal contact between the stamp and the substrate is facilitated by the elastic nature of the PDMS stamp itself, making possible the patterning onto non-planar surfaces [38]. The advantages of microcontact printing for fabricating small structures reside in the fact that the minimum feature sizes of the pattern are defined by the physical dimensions of the stamp (not optical diffraction); the flexibility of the stamp allows conformal contact between the stamp and the substrate for a range of topologies, including planar and curved substrates; a large variety of types of molecules can act as "inks" on several different materials. The major disadvantages include the blurring of the pattern because of the lateral diffusion of the ink, the deformation in the pattern that reflects deformations in the stamp, and the substantial number of defects that could be found in the film [39 – 41].

1.3.4 Replica moulding

Replica moulding is an efficient method for duplicating shapes, structure and patterns present on the surface of a mould [42]. UV- or thermally curable prepolymers are commonly used in this technique and because they usually have shrinkage of less than 3% after being cured they are able to replicate almost the same dimensions and topologies as the features in the mould. Van der Waals interactions, wetting, and kinetic factors (such as the filling of the mould) determine the fidelity of this process. These

physical interactions are short range and should potentially allow more accurate replication of small (<100 nm) features than photolithography is able to do [43]. The replica moulding has its advantages because it allows duplication of three-dimensional topologies in a single step; it enables faithful duplication of complex structures in the master in multiple copies with nanometer resolution in a simple, reliable and inexpensive way. Replica moulding against a rigid mould with thermoplastic polymer has been used for the mass-production of a wide range of structured surfaces such as compact disks [42, 44], diffraction gratings [45], holograms [46], and micro-tools [47]. The capability of this procedure can be extended to moulding against elastomeric PDMS moulds rather than against rigid moulds; the use of elastomers makes it easier to release small, fragile structures [33]. Two techniques related to RM are micromoulding in capillaries (MIMIC) and microtransfer moulding (μTM). Micromoulding in capillaries allows making isolated structures by using capillarity to fill channels in a PDMS mould with low viscosity liquid solutions, such as a photo- or thermally curable prepolymer [48]. Nanosized channels can be filled with liquids [49]; however they are slow or impossible to fill completely since resistance to flow in pressure-driven flow increases rapidly because of the channel size decreases. The capillary flow can be assisted by applying a vacuum to one end of the capillaries, heating the liquid, or applying an electric field [50]. Through microtransfer moulding it also possible to fabricate isolated structures but they are limited to a minimum feature size >100 nm [51, 52].

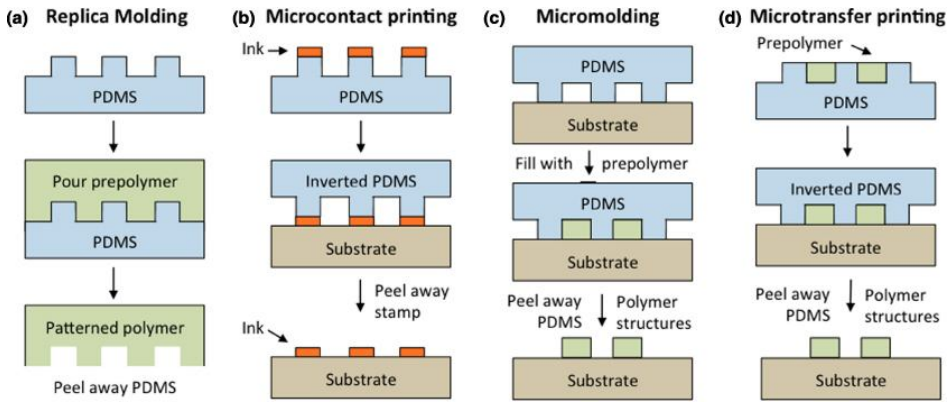

Figure 1.13: Various soft lithography techniques. (a) Replica molding, (b) microcontact printing, (c) micromolding in capillaries and (d) microtransfer printing (N.Lindquist et al 2012, Rep. Prog. Phys. 75 036501).

1.3.5 Electron beam (E-beam)

Electron Beam Lithography is a particular technique for creating extremely fine patterns of the order of few nm. Developed from the early scanning electron microscopes (SEM), this technique consists of scanning a beam of electrons on a substrate covered with a resist film sensitive to those electrons, thus depositing energy in the desired pattern onto the resist film. This kind of fabrication technique is capable of very high resolution and precision and it allows the users to work with a wide variety of materials. However, it is very slow, it is expensive and relatively complex – electron beam lithography tools can cost millions of Euros and require frequent service to stay in properly working order. The basic idea behind electron beam lithography is identical to any other lithography methods. The substrate is coated with a thin layer of resist, which changes its chemical structure upon exposure to the electron beam, so that the exposed (or non-exposed) areas can be dissolved with a specific solvent (positive or negative lithography). A thin layer of a chosen metallic material is deposited onto the substrate after the elimination of the exposed resist. On those areas exposed directly to the E-beam, the metal will adhere to the substrate while those areas not exposed will have the metal sitting on top resist surface. Once the metal deposition step is over, the parts of resist not patterned by the E-beam are dissolved with a strong solvent (lift-off). As a consequence the metal deposited on the unexposed resist is washed away, leaving only the metal in direct contact with the substrate.

The substrates used for electron beam lithography must satisfy several conditions; one of the most important is that they have to be relatively conductive otherwise the substrate might build up a certain electric charge which could cause the deflection of the electron beam, thus distorting the drawn pattern. However, in some cases, like in the fabrication of electronic circuits, the base material used should be obviously insulating otherwise the entire circuit would be short circuited. For this reason, the choice of a substrate for E-beam lithography is not an obvious thing; a compromise must be made in its selection: the substrate should be as insulating as possible. The most commonly used substrate is semiconducting silicon which has a thin insulating layer of silicon dioxide on top. Other possible substrates that can be used are glass plates coated with metals,

like ITO, Chrome (widely used for masks production), in which case the metal layer should be grounded before drawing.

Figure 1.14: Jeol 6000FS/E Electron Lithography System available in Tyndall National Institute.

Another critical part in order to perform electron beam lithography is the choice of a suitable resist. These materials are chemically modified after the exposure to the electron beam. There is quite a large number of different resists, all with different properties and requiring different chemicals for development and lift-off process. One of the first materials developed for e-beam lithography was polymethylmethacrylate (PMMA) which still today is the standard positive e-beam resist and is one of the resists which allows obtaining the highest resolutions. PMMA for this application is sold in several molecular weight forms (50 K – 950 K) and usually dissolves in chlorobenzene. PMMA is spun on the substrate and hard baked at 170 to 200 °C. E-beam exposure causes the polymer to break into fragments that can be dissolved in methyl isobutyl ketone (MIBK); both the exposed and the unexposed PMMA can be eliminated with the use of pyrrolidone or acetone. PMMA can be used as a negative resist as when it is exposed to a positive dose more than 10 times than the normal optimal dose, it will crosslink. PMMA has a low resistance to plasma etching, but it is very effective as a mask for chemically assisted ion beam etching. In order to facilitate the lift-off process it is possible to enhance an undercut on the resist by fabricating a double layer system where a high molecular weight PMMA is spun on top of a low molecular weight

PMMA. The lower weight PMMA is more sensitive than the top layer, hence creating the enhanced undercut wanted. This makes the fabrication easier, especially when lifting off thicker metal layers is required.

One of the major issues that can occur when using the e-beam is the control of the electrons scattering. When the electrons penetrate the resist, they can be subjected to many small-angle scattering events (forward scattering), which could broaden the original beam diameter. When the electrons penetrate through the resist into the substrate, the angle of these scattering events will be larger than that measured earlier (backscattering). These backscattered electrons are the cause of the 'proximity effect', which means that the dose that a pattern feature receives is affected by electrons scattered from other features nearby. During this process, the electrons are continuously slowed down, producing a series of electrons with low energy called secondary electrons. They are responsible for the bulk of the actual resist exposure process; their contribution to the proximity effect is very small but the net result can be considered to be an effective widening of the beam diameter by few nm. This resolution level can be improved by using different dose correction methods. The main effect of proximity effect is that the small features are exposed less than the larger ones, which leads to a significant distortion in very small features (that is also the reason why the exposition rate may depend on pattern geometry and size). The easiest dose correction method consists in the use of a double layer of resist, but its use is limited to quite large features (~1). The other method instead requires the calculation of the cumulative exposition rate that a certain feature receives directly from the beam and also, indirectly, from other features. The excess dose will be then compensated by adapting the beam current, the speed with which the beam scans over the substrate sample or the shape of the drawn features [53, 54].

1.3.6 Thin-film deposition

Materials deposited in the form of thin films have different properties from those of their equivalent *bulk* forms (metals for instance show higher resistivity in their thin-film form). Moreover, the techniques employed to deposit these materials greatly influence their final properties. For example, internal stress (compressive or tensile) in a film is

strongly dependent on the process used for its fabrication. Adhesion is another very important parameter that has to be taken into account when depositing thin films. In some cases to improve the adhesion of some materials, such as noble metals (e.g., gold), an intermediate layer (usually chromium or titanium) may be needed. Step coverage and conformality are two properties that can also influence the choice of different deposition technique [21].

There are many deposition techniques for thin-films formation. [55 – 57]. Thin-film deposition technologies are either purely physical (PVD), such as evaporative methods, or purely chemical, like gas- and liquid-phase chemical processes (CVD). A substantial number of processes, based on glow discharges and reactive sputtering, combine both physical and chemical reactions; these processes can be classified as physical-chemical methods.

Evaporative Technologies like thermal evaporation or vacuum evaporation are still widely used in the laboratories and in industries for depositing metal and metal alloys, although they are between the oldest techniques used for depositing thin films [58]. The process starts by generating a vapour by boiling or sublimating the source material. Then the vapour is transported from the source to the substrate onto which it condenses to a solid film on the substrate surface. The materials that can be evaporated cover a huge range of varying chemical reactivity and vapour pressures. This variety leads to a large diversity of source machineries including resistance-heated filaments, electron beams, crucibles heated by conduction, radiation, or RF-induction, arcs, exploding wires and lasers.

1.4 NANOSTRUCTURES

With the evolution of systems and machine in the field of micro and nano fabrication a large number of new nanostructures have become possible to be manufactured. The nanometre domain covers sizes bigger than several atoms but smaller than the wavelength of visible light. Nature abounds in interesting structures in this domain, ranging from microcrystals to viruses. The concept of nanostructure is not new itself

[59] but the ability to fabricate well defined patterns of complex nanostructures for specific purposes on this scale is a relatively recent achievement. Surfaces patterned with nanopillars structures are applied in different scientific fields like biology, electrochemistry, photonics, electronic engineering, information technology and many others. Several approaches have been adopted in order to achieve these nanostructures that can be conventional fabrication methods, non-conventional methods or, quite often, a combination of the two. The choice of the materials is very important first of all in terms of the application to which the manufactured device will be intended for, and then in terms of the fabrication steps that it has to undergo. The design of the structure must comply with some important parameters especially for what concerns the functionality of the device (geometry, size, costs, etc.).

Between the most relevant nanostructures it is possible to find nanofibers, nanoparticles, nanorods, nanowires, quantum dots, nanotubes and, of course, nanopillars.

1.4.1 Nanofibers

Nanofibers are a new class of material used in several fields; their properties make them suitable for a wide range of applications such as medical (especially tissue regeneration, drug delivery systems and wound healing) [60, 61], electrochemical (battery separators, energy storage, fuel cells) [62].

The general definition of a nanofiber is a fiber that has a diameter of less than one micron, although more than often, it must have a diameter measuring less than 100 nanometer (nm).

When compared to conventional fibers, nanofibers offer numerous advantages, most notably high surface area, small pore size and high pore volume [63].

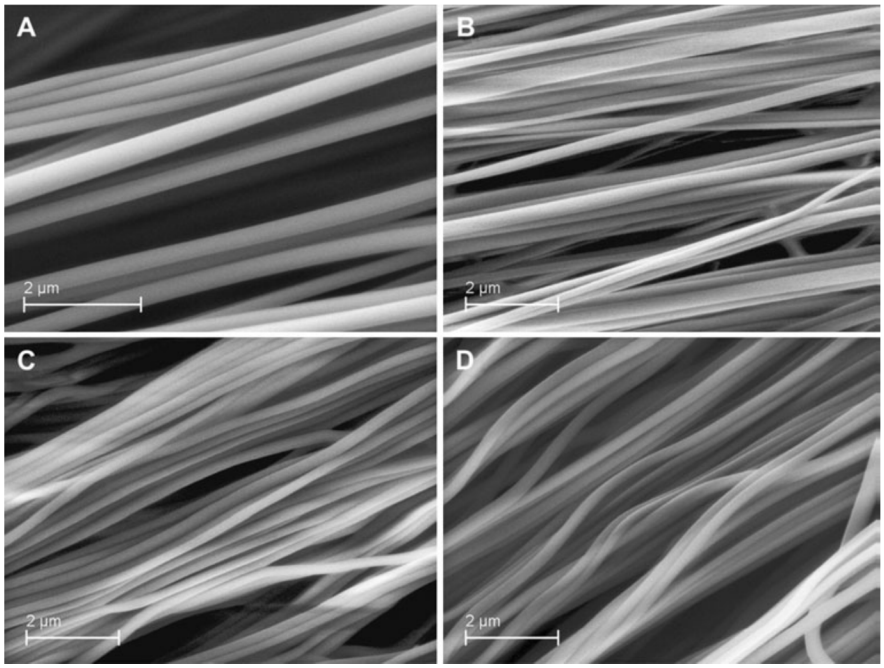

Figure 1.15: SEM images showing representative morphologies of the electrospun PAN copolymer nanofiber bundle (a), the stretched nanofiber bundles with the final lengths being 2 (b), 3 (c), and 4 (d) times of original lengths (ref. 71).

1.4.2 Nanoparticles

Nanoparticles are defined as a particulate dispersions or solid particles with a size in the range of 10-1000nm. Their unique optical-electronic properties have been researched and used in high technology applications such as organic photovoltaics, sensory probes, therapeutic agents, drug delivery in biological and medical applications, electronic conductors and catalysis. The characteristics and properties of gold nanoparticles can be modified by changing their size, shape, surface chemistry, or aggregation state.

The properties of conventional materials change when transformed from bulk to nanoparticles. This is because nanoparticles have a bigger surface area per weight than larger particles and this causes them to be more reactive to some other molecules.

Nanoparticles have made major contributions to clinical medicine in the areas of medical imaging [64, 65] and drug/gene delivery [66 – 68].

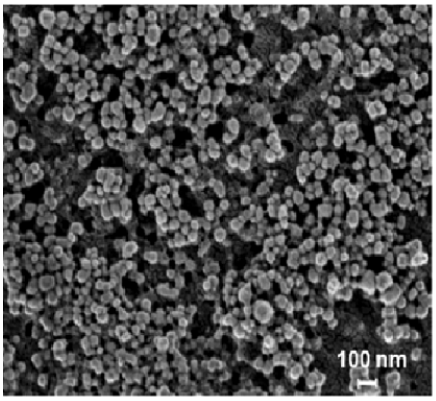

Figure 1.16: Ag nanoparticles on the surface of Ti/PEI/(Gel/Chi/$Ag_{0.1}$)$_4$/Gel substrate (ref 80).

Gold nanoparticles are probably the most generally used in many fields as preferred materials for their optical, physical and electrical properties, such as surface plasmon oscillations for labelling, imaging, and sensing. Au-NPs could be prepared and functionalized with many different molecules and material like polymers, surfactants, ligands, drugs, DNA, RNA, proteins, peptides and oligonucleotides.

1.4.3 Nanotubes

Single-walled carbon nanotubes (SWNTs) are cylinders with diameters of the orders of few nanometers and they consist of a single graphene sheet wrapped up to form a tube (figure 1.17). Several studies and experiments have backed up the theory that these tubes can be either metals or semiconductors, and their electrical properties can be considered similar, or even better than those of the best metals or semiconductors known. The remarkable electrical properties of SWNTs come from the unusual electronic structure of the two-dimensional material, graphene, from which they are constructed. Graphene is a single atomic layer of graphite and it consists of a 2D honeycomb structure of sp^2 bonded carbon atoms [69].

The properties of Carbon nanotubes find utility in an eclectic range of new and enhanced applications in printed electronics, sensors, flexible displays, e-readers, medical treatment, energy storage and more. Since their discovery in 1991 by Ijima [70], SWNTs have inspired a lot of research in both the academic community and industry,

and have attracted many investments in manufacturing methods, characterization and application development.

As mentioned before, SWNTs are an allotrope of sp2 hybridized carbon. Their structure is a cylindrical tube comprised of 6-membered carbon rings, as in graphite. The cylindrical tubes may (or may not) have one or both ends capped with a hemisphere of the so-called bucky-ball or fullerene structure. Understanding the structure of SWNT requires familiarity with the concept of nanotube chirality, since the chirality of a SWNT dictates many of its properties. The chirality gives information on both the orientation and diameter to which the sheet is rolled. Each SWNT on the chirality map is defined by two integers, (n,m).

Nanotubes have excellent mechanical properties; for example they are considerably stronger than steel as their tensile strength is approximately 100 times greater at nearly 1/16th the weight. The highest measured value is roughly half of the expected theoretical strength but this difference is possibly due to some imperfections in the structure [71]. From the electrical point of view they have current carrying capacities higher than those of copper or gold [72], and semiconducting types exhibit higher electron mobility than silicon. In Optical applications SWNTs have been found to have distinct optical absorptions and fluorescence responses because each chirality has its own characteristic absorption and fluorescence spectrum [73]. Another interesting property that characterizes nanotubes is that at room temperature the thermal conductivity of a single nanotube is similar to that of diamond or in-plane graphite, which is commonly thought to be the highest measured thermal conductivity of any known material at moderate temperatures [74].

Nanotubes can be fabricated with different methods like arc discharge [75], laser ablation [76], chemical vapour deposition [77, 78] and Hydrothermal Synthesis [79].

Multi-walled carbon nanotubes (MWNTs) are made of multiple rolled layers of graphene. MWNTs have a structure more complex and more varied compared to SWNTs and for this reason they have not been perfectly characterized yet. However, MWNTs exhibit some advantages over SWNTs, such as ease of mass production, lower

production cost per unit and enhanced thermal and chemical stability. The electrical and mechanical properties of SWNTs may change when functionalized because of the structural defects occurred by C=C bond breakages during chemical processes. Yet, the essential properties of carbon nanotubes can be maintained by modifying the surface of MWNTs, where the outer wall of MWNTs is exposed to chemical modifiers.

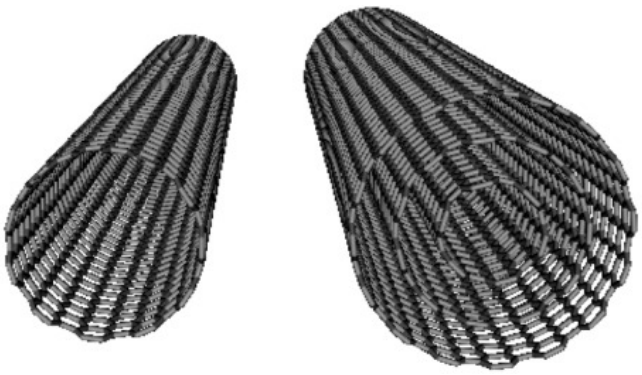

Figure 1.17: Schematic of single- and multi-walled carbon nanotubes (ref. 96).

1.4.4 Nanopillars

There are several methods, in literature, used to fabricate nanopillars and other similar nanostructures that could be conventional or non-conventional; some of them make also possible the creation of highly ordered surface and very high aspect ratio.

In [80] Wu and colleagues fabricate nanopillars and nanoholes using the nanosphere photolithography (NSP) technique. They use a self-assembled planar ordered single layer of transparent spheres to generate sub wavelength regular patterns over a large area on a common photoresist. Porous alumina templates are used to fabricate gold nanopillars by Schröper et al [81]. A silicon substrate is covered sequentially with e-beam evaporated thin films of titanium (10 nm), gold (200 nm), and thermal evaporated aluminium (400–500 nm). The anodisation of the sample in oxalic acid (0.3M) at 40V leads to the formation of a porous alumina template on the topside of the sample. A thin barrier layer at the bottom of the pores is removed via etching in phosphoric acid (5%) so that the nanochannels in the alumina matrix are connected to the underlying gold

surface. Subsequently, the nanochannels are filled with gold by electrochemical deposition.

A similar approach in the nanopillar fabrication is used in [82] where Palacios et al use the method of the template wetting through a nanoporous alumina template. Instead of using gold they infiltrate a polymer, Poly(9,9-dioctylfluorene), into the pores of the alumina with an average pore diameter of 225 nm and a pore depth of 500 nm.

Nanoporous anodic alumina oxides (AAO) membranes are used in the fabrication of gold nanopillars by Shin and his group. In their work [83] they describe a homemade system to deposit gold through the pores of the membrane.

Santos too in his research work [84] uses alumina membranes to fabricate polymeric nanopillars. Commercial Al foils are annealed in N_2 environment to homogenize their crystalline phase and grain size. They are then electropolished in a mixture of ethanol and perchloric acid to reduce their surface roughness. Finally, the Al foils are washed with deionized water, dried under a draught and stored in dry environment. Nanoporous anodic alumina templates (NAAT) are fabricated using direct anodization (figure 1.20).

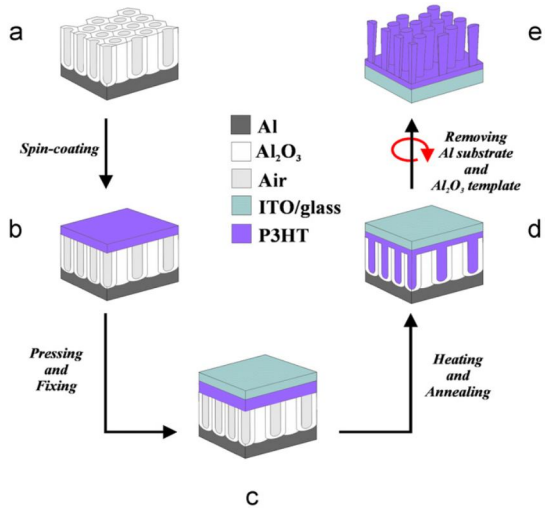

Figure 1.18: Slanted cross-section view diagram describing the fabrication process of the high-density arrays of semiconducting Poly(3-hexylthiophene) nanopillars on ITO/glass substrates. (a) NAAT template on aluminium substrate once the second step of the anodization process has finished (ordered pores). (b) P3HT spin-coated NAAT. (c) P3HT-covered NAAT pressed and fixed to an ITO/glass substrate. (d) NAAT infiltrated with P3HT after heating and annealing treatment. (e) Arrays of semiconducting P3HT nanopillars on ITO/glass substrate after removing the Al substrate and the NAAT (ref 84).

Another way to produce nanopillars is the inductively coupled plasma (ICP) cryogenic dry etching process which is used by Stranz [85] for the fabrication of nanostructures in silicon. The etching process is carried out at 75 C in SF_6/O_2 plasma. The etching rate for silicon can reach up to 4μm/min. After the etching, the pillars have an aspect ratio greater than 10 and a diameter that ranges between 1 μm and 3.5 μm. During the etching process the bottom surface of the sample is etched, while the sidewalls are passivated. The pillars show a regular shape, arrangement and a uniform height. In order to reduce the diameter of the pillars they use a thermal oxidation of the dry-etched pillars followed by oxide etching in HF acid. The oxidation-etching sequence is repeated several times, achieving a reduction in diameter from 1.6 μm to 288 nm.

Nomura et al. in [86] describe how to obtain nanopillars using the technique of nanoimprinting. Polystyrene (PS) films 1.0 m thick are spin-coated onto glass substrates (figure 1.19). Then they use nanomoulds made of silicon wafer fabricated using photolithography and press them onto the PS films heated at 423K. Then the moulds are lifted from the films at room temperature, so that nanopillar structures can be formed. The diameters of the nanopillars range between 0.16 and 1.0 m according to the patterns drawn on the nanomoulds while the height of the nanopillars is 1.0 m.

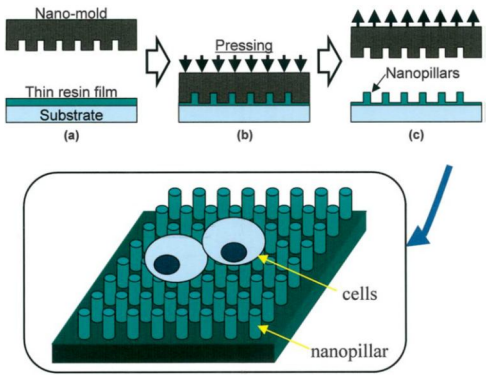

Figure 1.19: Fabrication of fine structures using nanoimprinting to create a new type of culture dish (ref. 86).

Panaitov et al [87] report on results of fabrication of micron and submicron golden spines by means of e-beam lithography and electroplating.

In [88] Chang describes the fabrication of nanopillars by using the conventional reactive ion etching process (RIE). This method allows a precise control of the height, positioning and configuration of the nanostructured array.

Wolfrum and his group in [89] show how micrometre and nanometre-sized arrays of gold nanopillars can be fabricated at predefined positions on a silicon substrate by combining an imprint method with template-assisted electrodeposition (figure 1.20).

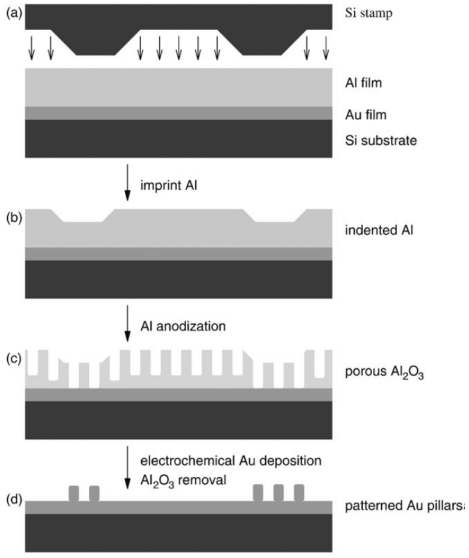

Figure 1.20: Process sketch for the fabrication of patterned arrays of Au nanopillars. a) A silicon stamp is used to indent the aluminum layer of a substrate. b, c) The imprinted Al film (b) is subsequently anodized to create nanoporous alumina (c). Only the pores originating from the imprinted patterns connect to the underlying gold film. Gold is electrochemically deposited inside these pores. Removal of the template material reveals the patterned Au-nanopillar arrays (ref. 89).

Cheung describes a fabrication method to produce hexagonally close packed semiconductor nanopillars which involve three fundamental steps [90]: spin coating of polystyrene beads on silicon, reactive ion etching (RIE) with oxygen to tailor the size of the polystyrene beads and deep RIE of silicon to etch the pillar structures.

Another way to produce nanopillars via porous alumina is published by Sanetra et al [91]. Silicon wafers serve as substrates for all samples.

Hu in his project about growing cells on a nanostructured surface [92] discusses about the method of fabrication of high aspect ratio polymer nanopillars using controlled elongation of the imprinted pillars during mould release.

Kouklin is one of the first to report in his letter [93] the use of anodized aluminum oxide membrane for the fabrication of nanopores and nanopillars.

Hsu [94] uses the principles of the Langmuir-Blodgett (LB) technique to fabricate silicon nanopillars and nanocones on a 4 inch wafer exploiting LB assembled nanoparticles as a mask for reactive ion etching (RIE) to fabricate nanopillars with uniform coverage over a silicon wafer.

Nanosphere lithography is also often used to fabricate nanostructures. The advantages of using nanosphere lithography for nanofabrication include its low cost, ease of preparation and ability to fabricate the structures on large areas. In his publication Kuo et al. [95] use nanosphere lithography as a method for fabricating nanopillars (figure 1.21).

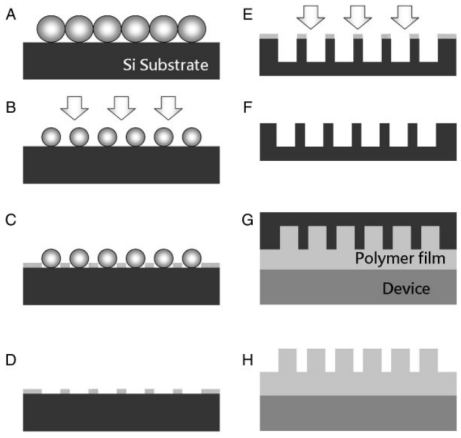

Figure 1.21: Schematic for the fabrication of nanopillar arrays. (A) Nanosphere lithography is used to prepare a monolayer of close-packed polystyrene beads with preselected diameters. (B) The diameter of polystyrene beads can be trimmed by oxygen plasma. (C) A layer of nickel is deposited on top of the polystyrene beads. (D) The polystyrene beads are removed by dichloromethane, leaving a nickel film with periodic holes. (E) ICP is used to etch a silicon template using the nickel film as an etching mask. (F) Nickel film is removed by nickel etchant. (G) Silicon template is used as the master in a nano-moulding process. (H) A well-ordered periodic nanopillar array can be obtained after curing and mould release (ref. 95).

There are a large number of applications for this type of nano-structured electrodes that range across different fields of science. From the literature found it is more than clear that most of the applications are focused towards the biological field especially those based on the studies of cells growth and tissue cultures, followed by the fairly widespread use in solar cells for improving the efficiency of the same. Other applications include the fabrication of batteries, plasmonic sensors, fuel cells, spin torque magnetic memory and others.

As mentioned before, most of the biological applications are dedicated to the study of the cells and their growth on this kind of substrates as well as in the tissue cultures. The interactions between the living samples and the nanopillars, the behaviour of and the effects of the nanostructures on the cells are the centre of these kinds of studies. Also the biosensing applications cover a large area in this field as the nanopillars can be functionalized to work as biosensors or also as useful elements in the separations of different biological samples.

Nomura et al. investigate a modified substrate for the growth of cell cultures which includes the use of nanopillars and make a comparison between commercially available culturing dishes, nanopillars and polystyrene dishes [80]. In [96] Cheung et al. show a method to improve neural recording by fabricating polysilicon nanopillars on their electrodes. In this way they want to reduce the impedance of their electrodes and increase their effective surface. Also Bruggemann and colleagues in [97] fabricate nanopillars on top of their electrodes to decrease their impedance and improve the signal to noise ratio. In their research they used biocompatible nanostructured microelectrode array for signal recording from electrogenic cells. The gold nanopillars provided a method for lowering the electrode impedance without altering the chemical properties of gold. In [98] Hanson investigates cellular interactions with vertically-aligned nanopillars of several materials, and the interface between the cells and said vertical nanopillars. He observes significantly decreased cell motility on the nanostructured surface compared to a standard flat surface. In another research [99], it is investigated the effect of nanopillars and nanopores on PC12 cells neurite extensions where the neurites are very few and quite short compared to a normal culture of this type of cells on a standard culture dish (figure 1.22).

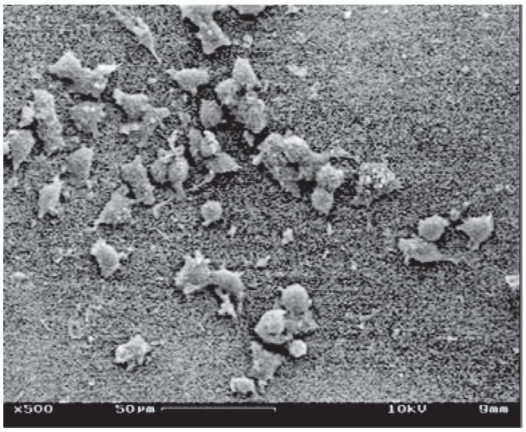

Figure 1.22: SEM images of cells: on nanopillars – cells with short and few neurites and a relatively high cell density (ref. 99)

The fact that the cells are not well spread on nanopillar substrates could be explained also by looking at the results obtained by Arnold et al [100] where they show that a spacing between nanodots higher than 70nm leads to a limited cell spreading, attachment and focal adhesion. Here they suggest that an ideal spacing would be between 58nm and 70nm, while Haq and colleagues uses spacing slightly higher than 70nm between the nanopillars. In another research [92] by Hu, human dermal fibroblasts are cultured on ultrahigh aspect ratio polymer nanopillars formed in a novel procedure which uses a controlled elongation of the imprinted pillars during mould release. The nanopillar topography shows strong effects on the cell morphology, with pillars of widely varying aspect ratios and surface energies resisting cell spreading. The fact that nanoscale topographies significantly affect cell response to a biomaterial surface is also confirmed by Sjöström [101]. He fabricates well-defined Titania nanopillars with tuneable feature sizes from 15 to 100 nm on bulk titania (Ti) substrates (figure 1.23) using a through-mask anodization technique and studies their effects on initial attachment and spreading of osteoblast-like cells (MG63).

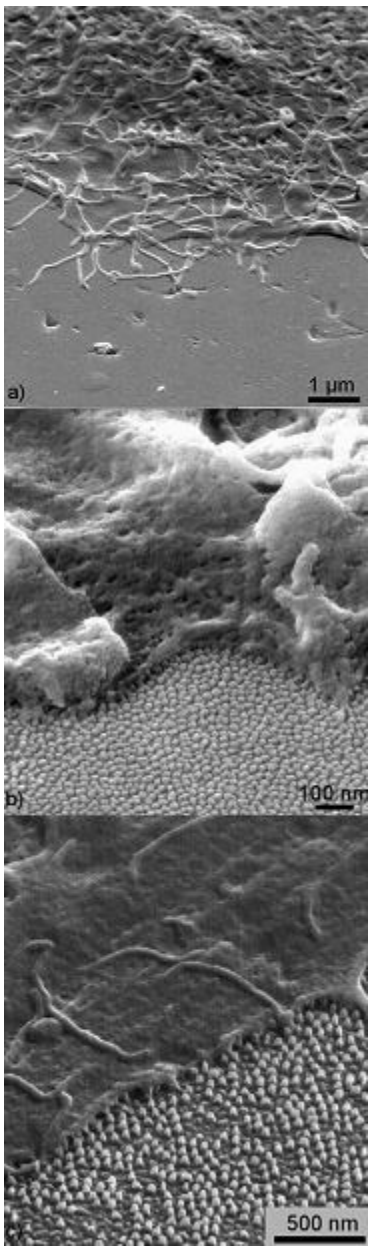

Figure 1.23: SEM images of cells on the different surfaces interacting with the nanotopography features: (a) shows a cell spreading out on the smooth as polished surface, (b) shows a cell on the 15nm surface with the cell attaching to the pillar structures and (c) shows a cell on the 100nm surface, using the pillar features as anchoring points (ref. 101).

In a study conducted to probe the mesenchymal stem cell (MSC) response and differentiation using only the topographic features of the culture substrate, Brammer et al [102] investigated nanopillars with micro and nanoscale diameters to determine if the size of the tall hydrophobic pillars used affects growth and differentiation of MSCs.

Again, in neural engineering, the effect of nanotopographies has been studied and evaluated. As we can see in [103], Fozdar and colleagues investigate the effects of arrays of lines and holes patterned on quartz, at the micro (~2 m) and nanoscale (~300 nm) dimensions, on the adhesion, axon establishment (polarization), axon length, axon alignment and cell morphology of rat embryonic hippocampal neurons, to study the response of the neurons to feature dimension and geometry (figure 1.24). Nanopillars can be also used to enhance the biosensing performance of an electrode. In fact Anandan et al in [104] find out that a nanostructured electrode shows a 7-fold increase in its sensitivity compared to a flat electrode. Such a significant increase in the sensitivity of the nanostructured electrodes is attributed to the higher surface area due to the nanopillar array structures.

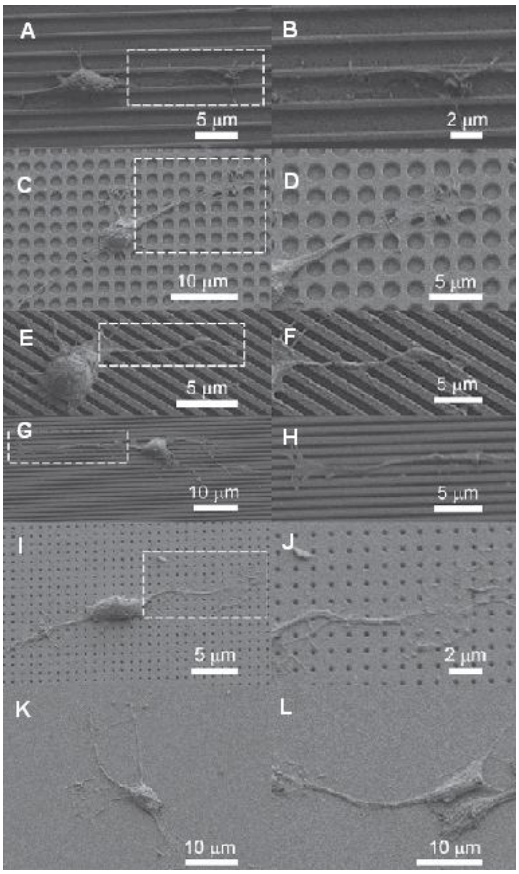

Figure 1.24: Soma and axon orientation and morphology based on topography. The images in the right column show the enlarged areas indicated in the white boxes shown in the juxtaposing images in the left column. Sample cells on (*A*), (*B*) 2 m lines, (*C*), (*D*) 2 m holes, (*E*)–(*H*) 300 nm lines, (*I*), (*J*) 300 nm holes and (*K*), (*L*) smooth surface (ref. 103).

Enzymes are often immobilized onto the electrode surface for catalytic reactions to functionalise these electrochemical biosensors and then make them sensitive. In the case of electrochemical glucose sensors, the electrodes are usually functionalized with glucose oxidase (GOx) for catalyzing the oxidation of glucose [105]. Gangadharan et al. fabricated gold nanopillars, on the electrodes by electrodepositing gold through porous anodic alumina templates in gold plating solution, which were functionalized using GOx/PPY in order to achieve enhanced current performances in glucose detection compared to flat electrodes. In the paper published in 2007 by Anandan [106], where he studies the role of reaction kinetics and mass transport in glucose sensing using an array of electrodes enhanced with gold nanopillars, we can find that, in an electrochemical based detection, the increased active surface area due to the addition of nanopillars may lead to enhanced sensing performances only when the reaction rate constant of the target species is low. At a higher reaction rate constant, only the top part of the electrodes modified with nanopillar serves the purpose of transferring electrons. Nanopillars find their applications also in DNA analysis systems like in [107] where Murthy reports a study in which the use of ordered, high-aspect ratio nanopillar arrays on the surface of silicon-based chips enhances the signal intensity in DNA microarrays. Another interesting application of the nanopillars in bionanotechnology is the use of these nanostructures for capturing circulating tumour cells (CTC) (figure 1.25) in blood samples [108].

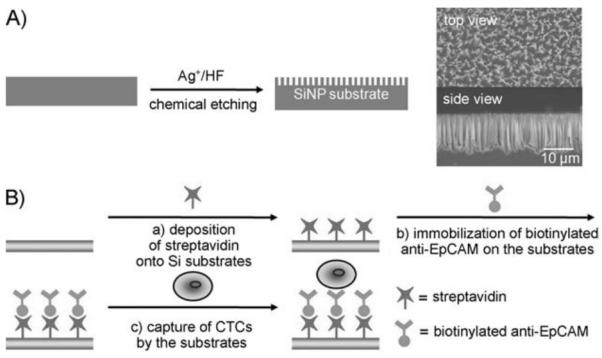

Figure 1.25: A) Chemical etching by Ag+ and HF was employed to produce a silicon nanopillar (SiNP) array on a silicon wafer. The SEM images reveal that well-defined SiNPs with diameters ranging from 100 to 200 nm and lengths around 10 mm were produced. B) Grafting of biotinylated epithelial-cell adhesion-molecule antibody (anti EpCAM) onto silicon substrates (ref. 108).

Another interesting research is described by Xie et al [109] in which they use vertically aligned SiO_2 nanopillars to achieve below-the-diffraction limit observation volume in vitro and inside live cells. Transparent SiO_2 nanopillars embedded in a non-transparent substrate restrict the light propagation and allow evanescence wave excitation along its vertical surface.

In solar cells applications, the researchers focused their work mainly to improve existing technologies by using these nanostructures. The increased area of light collection introduced with the use of nanopillars enhances the efficiency of these solar cells making these devices better and more attractive in terms of market and more economically viable.

In a review article by Fan et al [110], it is highlighted that silicon nanopillars (or nanowires) arrays used in a photovoltaic (PV) cell can increase the probability of an incident photon of being absorbed and generate carriers for the subsequent collection thus increasing the efficiency of the PV itself (figure 1.26).
A similar theory is reported also by Wong et al in his research on Si nanopillar based solar cells [111]. Ryder in his research [112] describes a method for functionalizing organic photovoltaic (OPV) cells by introducing indium tin oxide (ITO) nanopillars on one or both of the electrodes of the cell in order to reduce the charge carrier transport distance and increase the interfacial area for charge extraction.

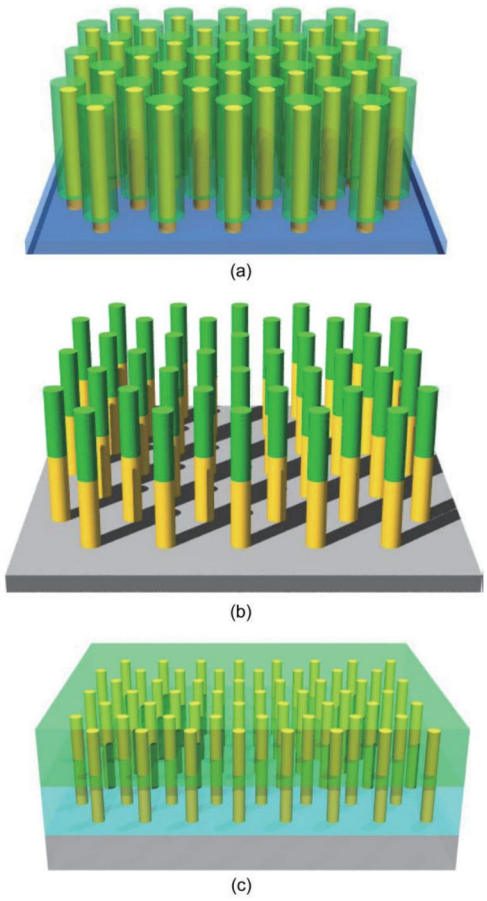

Figure 1.26: Nanopillar solar cell architectures. Three commonly explored PV device structures include: (a) NPL radial junctions; (b) NPL axial junctions; (c) NPL arrays embedded in thin film of an absorber (ref. 110).

Another solar cell that uses the concept of nanopillars to enhance its performances is the one published by Mariani et al [113] in which they describe the fabrication of a GaAs nanopillar based catalyst-free solar cell. Kapadia and his research group in [114] fabricated a new low-cost, efficient, flexible solar cell for the conversion of light energy to electricity (figure 1.27). The cell consists of arrays of optically active semiconductors arranged as nanoscale pillars on aluminum substrates. A more accurate and specific overview of flexible photovoltaic cells can be found in a paper published on Nature by Fan et al [115].

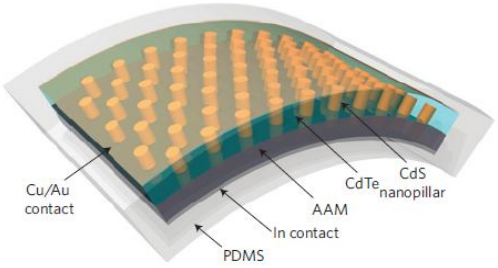

Figure 1.27: Mechanically flexible SNOP cells. (a) Schematic diagram of a bendable SNOP module embedded in PDMS (ref. 114).

The concept of nanopillars can be applied to a wide range of other applications in several different fields. As follows we can see some of these applications, such as plasmonic sensors, electroluminescent devices, fuel cells, lithium batteries and capacitors.

Kubo and Fujikawa [116] fabricated a plasmonic sensor made of a double nanopillar (DNP) array with nanogaps that would measure a few tens of nanometers. Another application found in literature is for nanoscale electroluminescent devices based on AlGaAs±GaAs. Manimaran et al. [117] fabricated these devices using the conventional optical lithographic and RIE techniques and studied the electrical and light emitting properties of the devices. Tang et al. [118] report, in their paper, improved performances of methanol fuel cells enhanced with nanopillars which increased the contact surface area between the catalyst and the fuel cell. In [119] Chang fabricated a silicon nanopillar-based nanocapacitor array. He and his group found an expected trend as a function of pillar height and array period in the capacitance measurements that they did. In [120] Ji and colleagues fabricated a Sn-nanopillar array which acts as a binder-free anode in high capacity lithium batteries devices. This nanostructured film is made of graphene and Sn-nanopillars.

A good variety of materials has been exploited for the purpose of manufacturing nanostructures. A great part of the projects interested in the fabrication of nanopillars have chosen metals like gold. Gold is definitely one of the most widespread materials used for this kind of nanostructure due to its good chemical and electrical properties and also because it is a well-known biocompatible material and, as described in the earlier

paragraphs, it is used very frequently in the biological applications [81, 83, 87, 89, 97, 99, 100, 102, 106, 116, 121]. Probably the most used material in this nanotechnology area is silicon because it is an easy material to work with; it is relatively cheap, has great electrical properties and shows also some good biocompatibility properties [85, 88, 90, 94, 107, 108, 109, 111, 119, 122]. Another material used for manufacturing these structures is indium tin oxide (ITO). This solid solution is well known for its main properties which are optical transparency, electrical conductivity and biocompatibility and it is mainly used in the fabrication of nanostructures for photovoltaic or biological applications [112, 123, 124]. Polymers also represent another class of materials used for making nanopillars and nanostructures. They are mainly used for their biocompatibility characteristics but also for their low cost and their ease of use (in most of the cases at least). Some of these polymers have also electrical conductivity properties which makes them more attractive materials for future improvements and new applications [82, 84, 92, 105, 125 – 127]. There are then many several other materials used in different projects which use AlGaAs-GaAs [117], silver [127], quartz [103, 128], titanium dioxide [101], tin [120], polysilicon [96], cadmium sulphide [115] and gallium nitride [93].

Table 1.1: Summary of applications, fabrication methods and materials used to fabricate the nanopillars

Application	Fabrication	Material
Tissue culture substrate	Nanosphere photolithography	Gold
Cell growth substrate	Reactive Ion Etching (RIE)	Silicon
Biosensors functionalization	Sputtering	Indium Tin Oxide
Plasmonic sensor	Evaporation	Polymers
Fuel Cell	Template wetting	Silver
Nanocapacitor	E-beam lithography	Quartz
Lithium batteries	Anodization of porous alumina templates	Titanium Dioxide
		Tin
		Polysilicon
		Gallium Nitride
		Cadmium Sulphide

It is quite clear, in conclusion, that the main applications for this kind of nanostructures lay mainly in the biological field and more specifically in the cell-adhesion studies. Also the photonic field looks to be well orientated to go deeper into the matter especially for what concerns the fabrication of solar cells. The most common materials used are certainly Au and Si due to their good electrical and biocompatibility properties as well as their ease to use them in the fabrication processes since they are "well-known" materials. In terms of methods of fabrication the most common way to produce nanopillars is to go through the use of anodized alumina oxide membranes and then using other steps like evaporation techniques to prepare free standing pillars. Nanosphere lithography is also very often used to fabricate this kind of nanostructure in combination with etching techniques.

Nanopillars and nanostructures in general, have the potential to improve existing technologies and renew radically the way of looking at certain kind of applications.

1.5 CELL-BASED BIOSENSORS AND ASSAYS

Cell based assay have been object of continuous and extensive studies and they have been improved so much since their first application at the beginning of the 20^{th} century that today they have become central in the role of drug discovery and development. Test performed on cell culture allow for a direct and non-invasive method to the evaluation of therapeutic compounds under study on biological systems without using live subjects. The introduction of tough new regulations for the testing and approval of chemicals and the demand of sacrifice of less animals for the experiments has led to increased interest in cell-based assays.

These refer to a number of different tests based on the use of live cells. In general they can include a range of assays that measure cell proliferation, toxicity, motility, production of a determinate product and morphology. Assays on cell cultures can give an accurate representation of the *in-vivo* model since live cells are used, and also offer the chance of a dynamic investigation through monitoring the behaviour of the living cells.

Cell-based assays are founded on four main essential components, the first of which is certainly the cellular one. It could be a single cell, a culture or a primary cell population. A target substrate or molecule able to record the cellular response is then needed as much as an instrument capable of conducing and monitoring the experiment. Informatics components and statistical analysis are then needed to manage and evaluate the data collected during the tests.

They also offer certain advantages over biochemical assays; first of all they provide information on the conformation and activity of the target molecule in a cellular context; assays do not require purification of the target molecule, it is possible to screen compounds or potential drugs that are generally cytotoxic or that cannot permeate cellular membranes to reach intracellular sites; they help saving time and costs in development of new drugs; cell-based assay can visualize all potential drug-target interactions.

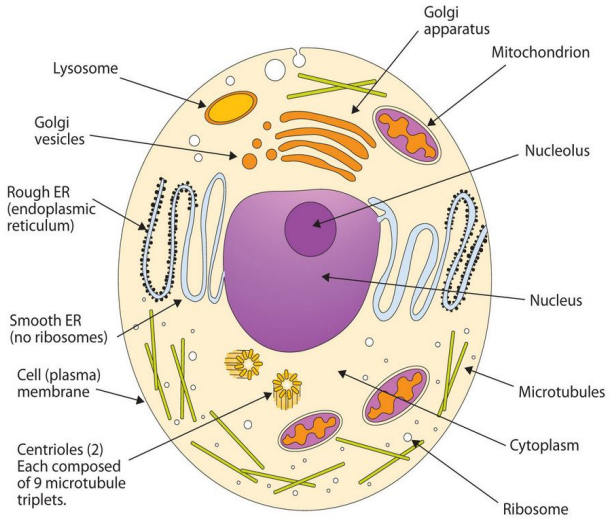

Figure 1.28: Diagram of a typical animal cell (http://pulpbits.com/5-animal-cell-drawing/animal-cell-coloring-printing/)

There is a certain protocol to follow to create and culture cell lines. In a very general way the user has to attain to strict sterility and aseptic techniques before stepping into checking the morphology of cells to evaluate mainly their health and other parameters. Then a quantification of the cell number is needed before cryopreserving them. Cells

can then be thawed and prepared for a new subcultivation. Another important role in the cell culture is played by the media in which the cells are grown in. In general they are made of Carbohydrates (glucose, fructose, galactose); Amino acids; water soluble vitamins; some elements in traces (Se, Fe^{2+}, Zn^{2+}, Mn^{2+}, Cu^{2+}, etc); inorganic ions (maintenance of membrane potentials, pumps and osmotic pressure, cofactors for enzymatic reactions); some other components (nucleosides, pyruvate, lipids, linoleic and oleic acid); pH buffers (sodium bicarbonate, HEPES) and indicators (phenol red pH 7.4); serum (horse, foetal calf, new born calf). They are rich in nutrients but are susceptible to contamination.

The morphology differs from each of the different kinds of cell cultures. In general they can be classified as monolayers, where the cells attach to the bottom of the flask, suspension culture which cells do not or loosely attach to a surface, and semi-adherent cultures such as human leukaemia, mammary glands and breast cancer [129, 130].

1.5.1 Mammalian cell cultures

Mammalian cell cultures are one class of cultures mainly used in the drug and cytotoxicity testing. They are growths of immortalized cell cultures in liquid media that come in tissue culture flasks or dishes. The cells grow onto the surface of their containers and they are subcultured by transferring them into a different vessel in order to allow further proliferation of the cells. The amount of times the cells are subcultured or split is defined as the passage number [131]. The subculture starts when the cells are detached from the surface of the tissue culture flask using a trypsin/EDTA solution. Trypsin is a digestive enzyme able to catalyze the hydrolysis of peptide bonds. Polymeric materials as well as glass and porous filter membranes are commonly used as a substrate for mammalian cells to adhere to and grow. One of the most typical plastic used for this application is polystyrene, which is a hydrophobic material that can be treated to make it more hydrophilic hence improving the cell attachment. Techniques like gas-plasma discharge are often used to oxidize the growth surface of commercially available polystyrene tissue culture containers. This treatment causes the growth surface to be negatively charged, however, cells can adhere to both positively and negatively charged surfaces. It goes without saying that the culture environment must meet the cells

biological requirements in order for the cells to survive and grow especially by using specific culture media and growing the cells in suitable conditions [131].

When doing a cell culture, it is possible to observe four distinct phases. The first is a Lag Phase, which usually lasts no more than 1-2 days, and during which there is little or no increase in cell quantity. In this phase, the cells condition the media, by undergoing internal cytoskeletal and enzyme changes and adjusting to the new media. When cells are seeded at a low density, it could take them longer to adapt to the media increasing then the time of the lag phase.

In the following stage, Log Phase, the number of cells increases exponentially. The proliferation will continue as long as there are enough nutrients to support the increasing cell number until, eventually, some critical nutrient will be missing. Other factors influencing this phase are the seeding and saturation density and the cell growth rate.

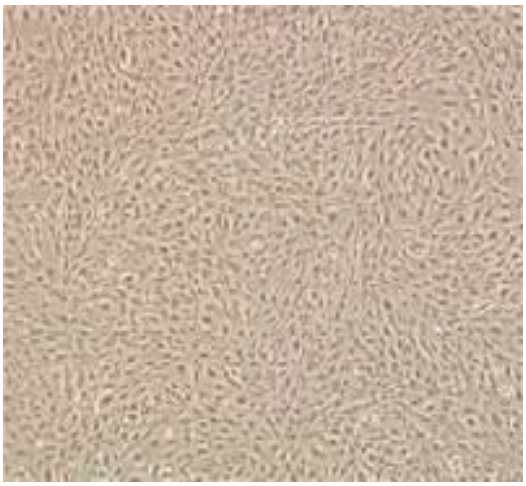

Figure 1.29: Human umbilical vein endothelial cells (HUVECs) grown for seven days on BD BioCoat Gelatin 6-well Multiwell Plates seeded at a density of $2x10^4$ in the presence of E-STIM™ Endothelial Cell Culture Medium (440x) (https://www.bd.com/resource.aspx?IDX=17646)

At some point the culture would reach a level of complete confluency (that means that the cells have covered 100% of the available growth surface) which inhibits then further growth. This phase is called plateau or stationary Phase. During this phase the rate of cell growth slows down and the number of cells remains quite constant because of the accumulation of cell waste and nutrient depletion. Eventually, of course, the cells will

die unless subcultured or fresh media is added. Some cell lines however, are not limited by contact inhibition and may continue to divide and form layers on top of the parent cells.

If subcultured the cells may continue to grow on the surface of the vessel and give rise to a monolayer culture. The cells will cease to divide when they reach over-confluency. Here starts the fourth, and final, phase called decline phase in which the rate of dead cells is higher than the rate of cells growing [132].

1.5.2 Cell based biosensors: examples

1.5.2.1 Field effect transistors sensors

Field effect transistors (FET) can be used for monitoring the cell microenvironment. Cell metabolism parameters like the changes of the extracellular pH value, ion concentrations, oxygen consumption, carbon dioxide production, and other metabolic products can be monitored using these kinds of devices. The ISFET (ion sensitive field effect transistor) can be used to measure more cell physiology information, mainly focusing on the extracellular acidification rate since protons are the main regulator in the living cells microenvironment and involved in various biochemical reactions. More important ions in cellular metabolism, like potassium, sodium, and calcium, can also be monitored at the same time using ion-sensitive membrane-modified ISFETs (figure 1.30) [133].

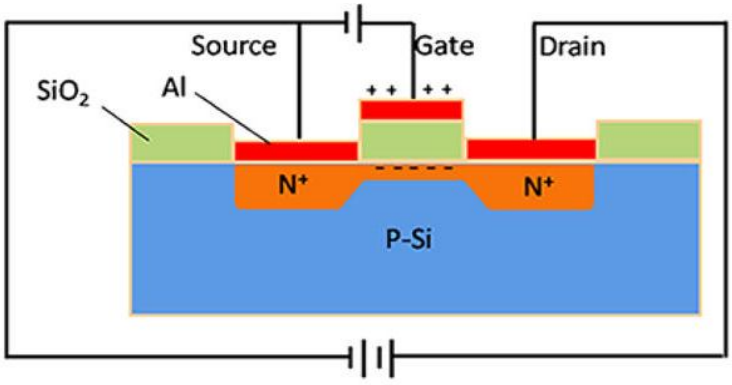

Figure 1.32: Basic structure of an n-channel enhancement-mode MOSFET with a positive gate voltage (ref. 133).

1.5.2.2 Light addressable potentiometric sensors LAPS

In biological applications, LAPS commonly monitor the cellular metabolism, especially what is concerned to energy metabolism (figure 1.31). The heterotrophic cells use several different nutrients, transform them into energy, and release the wastes produced during the growth process. The carbon source (e.g., sugars, amino acids, and fatty acid) mainly produces metabolic energy [134]. In a normal aerobic situation, cells convert glucose into carbon dioxide. In an anaerobic condition, cells glucose is converted into lactic acid. The generation of acidic products (e.g., H^+, CO2, and lactic acid) leads to a pH drop in the extracellular environment, which can be measured by a microphysiometer [135]. The extracellular acidification rate (ECAR) is the most significant factor to give information about the state of cellular metabolism.

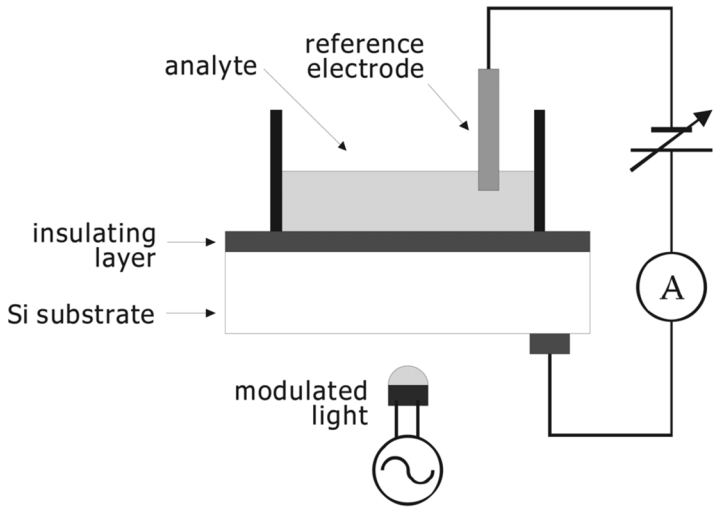

Figure 1.31: Schematic of the light-addressable potentiometric sensor (LAPS). LAPS measurement is spatially resolved. The measured area on the sensing surface is defined by illumination, which generates the ac photocurrent to be measured (ref. 134).

The ECAR of the cells is influenced by many other biochemical factors, such as receptor−ligand reactions, that, however, could be measured by a microphysiometer. This device can also help in the investigation and evaluation of pharmaceutical effects on ECAR, like for example antitumor drugs for chemotherapy [136]. For monitoring the

extracellular environment, LAPS more ideal than the ISFET approach because they are easier to fabricate, to encapsulate, and to be incorporated into the micro-volume compartments for bioassays [137].

1.5.2.3 Patch clamp technique

The patch clamp is a laboratory technique that allows the study of single or multiple ion channels in cells. It can be used with many different cells, but is particularly suitable for the study of excitable cells like neurons, cardiomyocytes, and muscle fibers. A fire-polished glass pipet with an open tip diameter of approximately 1 m is used to isolate a small membrane patch for recording. The tip has a smooth surface that creates a Gigaohm resistance seal with the cell membrane, which is the most important aspect of this technique. In fact, the currents of the ion channels can be measured by the cell membrane patch on the basis of the high resistance seal with the cell membrane and electronic isolation.

The patch clamp allows the study of single-channel behaviours on a small membrane patch or the macroscopic current from the whole cellular membrane which play crucial roles in cellular signal transduction, impulse conduction, and cellular microenvironment balance. Ion channels are, although, essential drug targets since many drugs are agonists or antagonists of ion channels. Still, this technique suffers from some fundamental limitations, including being of low throughput and requiring high precision operation, vibration damping, and great experience and skills on behalf of the user [138]. The challenge for chip fabrication is achieving a smooth aperture on the chip with a diameter smaller than 1 m. With the progresses accomplished in the years in micro and nano fabrication technology, several patch clamp devices have been fabricated using different materials. At present, patch clamp chips have been fabricated with silicon [139], glass [140], PDMS [141] and Teflon [142].

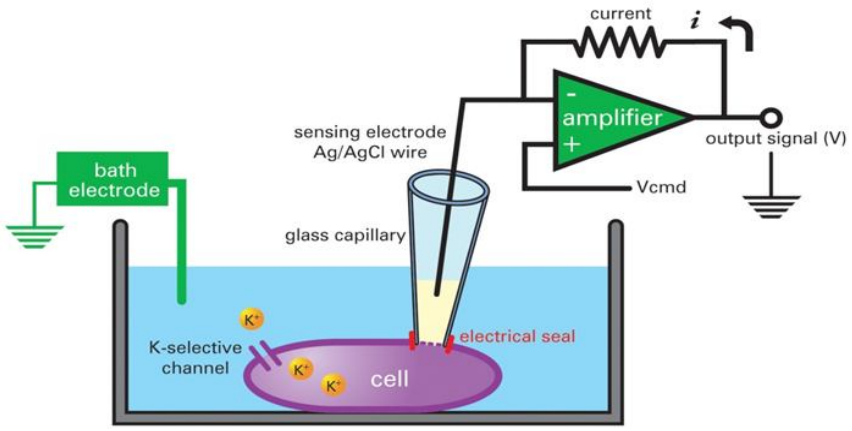

Figure 1.32: Diagram of a "whole-cell patch clamp": a micromanipulator is used to position the tip of a glass micropipette containing an electrode onto the surface membrane of an individual cell. Suction is then applied to form a high resistance electrical seal and to pull away the piece of plasma-membrane enclosed by the pipette tip. This gives electrical continuity between the pipette electrode and the inside of the cell and also allows the membrane potential to be precisely controlled or "clamped." Currents passing across the entire cell membrane, representing the overall activity of all channels expressed in the plasma-membrane, can then be recorded with reference to a second electrode positioned in the external medium (J. Clare, http://www.discoverymedicine.com/).

1.5.2.4 Quartz Crystal Microbalance (QCM)

QCM is a mass sensitive device which measures changes of its characteristic oscillation frequency when a certain mass binds to the crystal surface. A tiny mass variation causes a pressure modification on the crystal surface subsequently leading an oscillation frequency shift of the crystal. When cells attach to the device, the mass bound to the quartz crystal surface increase causing a decrease of the oscillation frequency (figure 1.33). To apply QCM as cell-based biosensors, it is necessary that a cell culture incubator is integrated with the QCM device to guarantee a suitable environment for the cell growth. The cell-culture medium or liquid samples can be delivered directly to the QCM electrode surface via syringe, micropipette, or flow injection analysis systems [143].

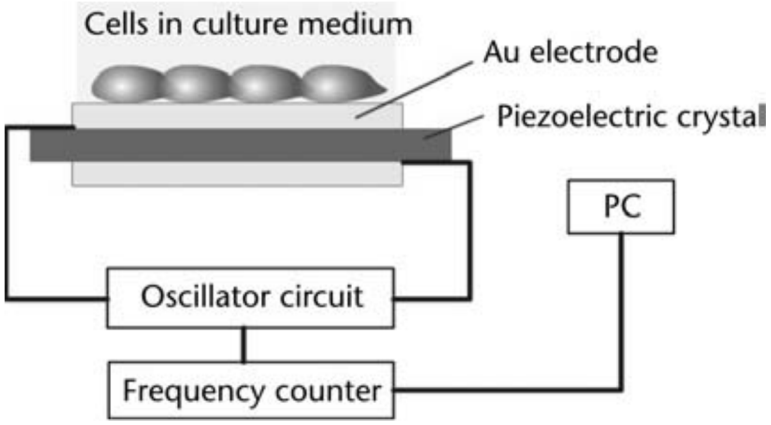

Figure 1.33: The process of cells attachment and spreading onto a quartz crystal surface. The oscillation frequency shift and energy dissipation, which are due to mass changes and medium viscoelastic properties, give quantitative information about the cell attachment process (ref. 143).

1.5.2.5 Surface Plasmon Resonance biosensors (SPR)

SPR exploits an optical detection technique which occurs when a polarized light hits a prism covered by a thin metallic layer which is normally made of gold. Several parameters like wavelength, polarization, and incidence angle have to be set in order to allow for the free electrons at the surface of the gold layer to absorb incident photons and convert them into surface plasmon waves (figure 1.34). Modification of resonance conditions of the gold surface of the biochip show a possible interaction between probe molecules immobilized on the chip and captured target molecules, which is measured as a change in reflectivity. For cell-based biosensors, cells are often directly cultured on the sensor surface as sensitive elements for probing target molecules [143].

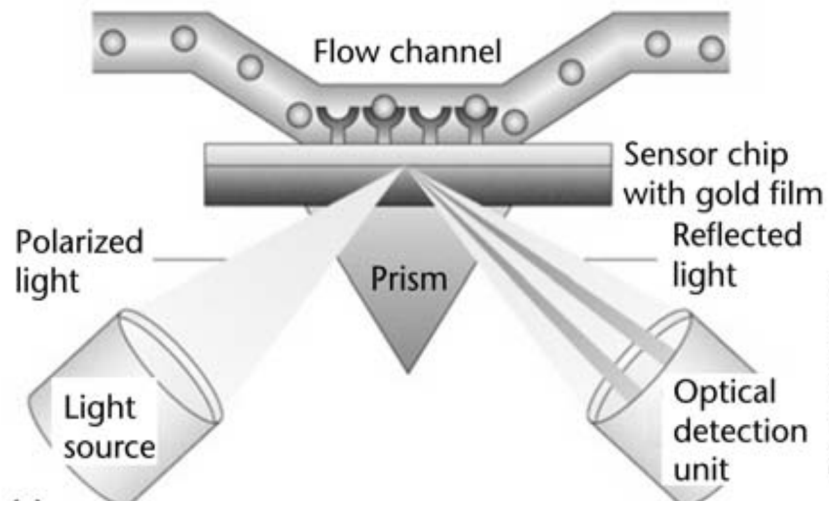

Figure 1.34: SPR detects changes in the refractive index in the immediate vicinity of the surface layer of a sensor chip. (a) SPR is observed as a sharp shadow in the reflected light from the surface at an angle that is dependent on the mass of material at the surface (ref. 143).

1.5.2.6 Immune cell-based biosensors

Immune cells play a central role in immune mechanisms of the human body. Different classes of this kind of cells carry out very specific tasks; they synthesize and secrete particular molecules that act as messengers, regulators, or helpers in the process of defending against external infections. Immune cells recognize and respond to antigens with very high sensitivity and specificity and this characteristic make them ideal candidates as sensitive elements in cell-based biosensors for antigens or pathogens detection. Several immune cells have been considered to explore the feasibility of being used as sensitive elements in cell-based biosensors; a good example would be mast cells (which release chemical mediators after a degranulation activated by the binding of the antigen-antibody) and B cells (or B lymphocytes) [143, 144].

1.5.3 Impedance based biosensors

When we talk about electrical biosensor it is possible to distinguish between two main ways to measure a signal which could be through voltammetric, amperometric/coulometric or impedimetric techniques.

Voltammetry and amperometry measure the current at the level electrode as a function of an applied electrode-solution voltage; these methods are DC or pseudo-DC and change the electrode conditions.

Impedance biosensors, instead, measure the electrical impedance in AC steady state with constant DC bias conditions; this is normally achieved by setting a small sinusoidal voltage at a certain frequency and measuring the resulting current; the process can be replicated in a range of different frequencies. The current-voltage ratio gives the impedance figures. This technique, also known as Electrochemical Impedance Spectroscopy (EIS), allows the examination of a broad variety of electrochemical phenomena in a wide frequency range. The impedance or capacitance of the electrode-solution interface can also be measured at a selected particular single frequency. Impedance measurements do not require the use of special reagents and is a label-free technique.

Impedance based microelectrode sensor arrays have emerged as a promising means for cell activity monitoring since 1986 when Giaever and Keese developed an electrical cell-substrate impedance sensor to control cell proliferation, morphology, and motility [145]. They reported of a sensor consisting of one large common reference electrode and one smaller working electrode while the cells were cultured on the electrodes surface. The AC impedance, at a certain frequency, between the two electrodes was measured, recorded and correlated with cell activity. After this, Ehret and his group observed the impedance change during cell growth and tested the toxic effect of cadmium ions with an interdigitated electrode structure [146]. Due to the size of the electrodes, the measured impedance changes in all these studies represent the average effect of a large number of cells [147].

Impedance techniques have been used not only to study anchorage dependent cell cultures or cultured cell suspensions, but also for organs in the body, explanted neural

tissues, whole blood and erythrocytes, and bacterial growth. There is a large amount of relevant information on the characteristics of the biological material that can be potentially defined through this technique. Most significant are the frequency dependent dielectric properties of biological materials that yield insight into the behaviour within different frequency ranges (figure 1.35). In many cases, the capacitance of the cell membrane, cell-substrate gap, and cell-cell gap can all be monitored and determined [143].

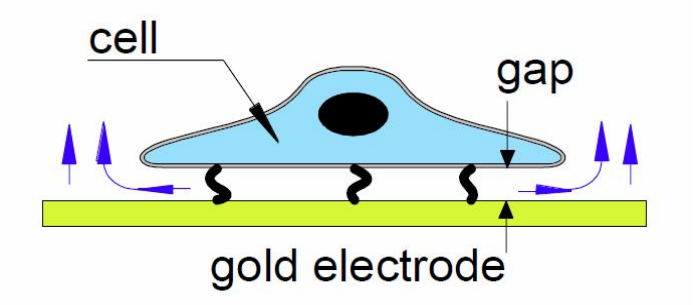

Figure 1.35: Cell-electrode junction showing cell focal adhesion contacts and current flowing (blue arrows) laterally through the cell-electrode gap (ref. 147).

1.5.3.1 Applications

In the last 20-30 years, significant changes in technology have led to improved and numerous applications regarding cell impedance. Many publications can be found in literature describing the applications of monitoring cellular events, such as cell adhesion and spreading on different substrate [148, 149], barrier function of endothelial cells [150], cell micromotion [151], cell migration [152], cell morphology [153] and cell shape change [154] due to various factors, and cell responses to cytotoxic compounds [155 –157]. The ECIS techniques covers many areas of applications, but the most common one is the investigation of the effect of chemicals on cells in pharmacology, cytotoxicity, and cell biology [143].

As mentioned above, ECIS is very useful in experiments that aim to monitoring cell adhesion, spreading, morphology and proliferation. Adhesion and motility are strongly influenced by the way that cells interact with the extra-cellular matrix (ECM) substrates. When a suspended cell encounters an adhesion surface, the cell starts flattening and deforming. This stage is characterized by passive adhesion and spreading [158]. Then, the cell keeps spreading further, reorganizing its cytoskeleton and forming points of

focal adhesions. This mechanism changes from cell to cell and the time and strength of adhesion are different depending on the specific amount of receptors and ligands on both the cell and substrate and the type of surface (material, energy, hydrophobicity). ECIS is mainly based on the cell adhesion and spreading on the surface process as the viability and proliferation of the cell culture depend on the cell-substrate interactions. Different ECM can be used to help and promote cell adhesion such as fibronectin, collagen, laminin, poly-l-lysine and vitronectin through integrins. These recognize and bind to specific sites mediating the adhesion and the information going to the cell for starting further processes.

Cell migration can also be investigated through ECIS techniques. The migration has a central role in different complex processes like embryonic development, homeostasis, immune response, wound healing and so on. There are many assays to monitor and measure the migration like Boyden chamber assay, time-lapse microscopy and wound healing. Of these, the last one has attracted a lot of attention in the impedance-based research. One of the first to report such application was Noiri and colleagues [159] followed by many others in the following years. Keese et al. in [160] introduced a method which provided highly reproducible results comparable to those obtained with the traditional assays.

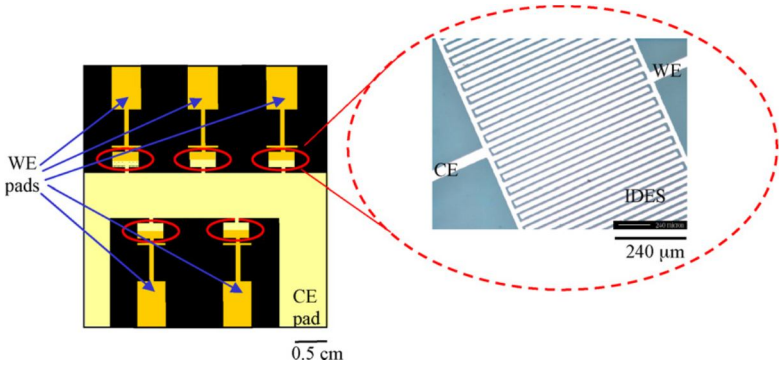

Figure 1.36: Diagram of the chip with five interdigitated electrode structures (IDES) integrated on a glass slide for impedance measurements. Working electrode pads (WE pads), IDES and the common counter electrode (CE) are realized by lithography, PVD and lift off techniques on the slide. On the right is the gold IDES with 23µm wide fingers and interspace is presented (ref. 161).

Cytotoxicity assays aim to analyze the reaction of the cells exposed to cytotoxins. The usual response is a loss of adhesion of the cells which tend to get a round shape, membrane protrusions and formation of apoptotic bodies. These cellular dynamics though depend mainly on the cell type under investigation, cytotoxins properties and concentration and time of exposure to them. These changes in adhesion and morphology lead to a modification of the cell-substrate impedance signal. Many articles have demonstrated the applicability of the ECIS for cytotoxicity testing on different cell types [154, 161].

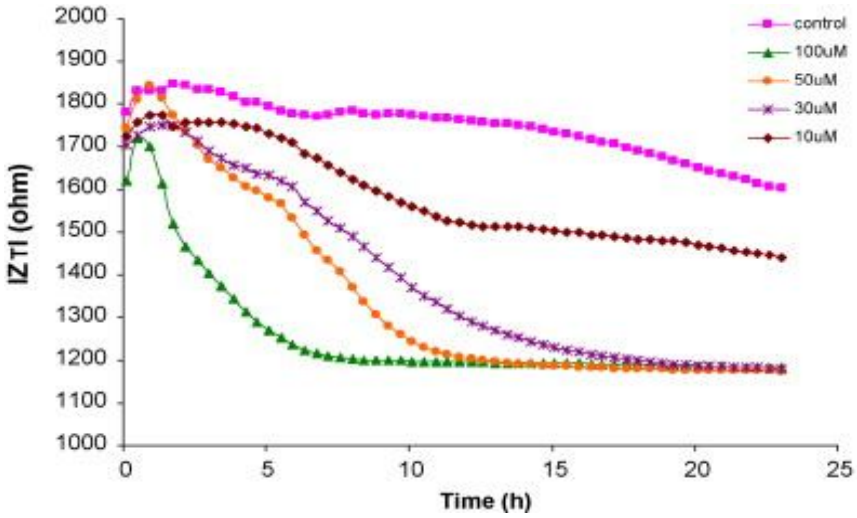

Figure 1.37: On-line monitoring of impedance modulus (|ZT|) at 10 kHz of BALB/3T3 cell adhesion for five wells of the chip after addition (time = 0) of fresh medium alone (control) or medium containing 10, 30, 50 and 100 M sodium arsenite (ref. 161).

In-vitro toxicity assay have the potential to become a solid alternative to in-vivo testing thus alleviating the demand of animals that would be sacrificed in laboratories (figure 1.37).

1.6 DETECTION TECHNIQUES

1.6.1 Impedance: Concept of Complex Impedance

While Ohm's Law applies directly to resistors in DC or in AC circuits, the form of the current-voltage relationship in AC circuits in general is modified to a different form. The concept of electrical resistance is fairly simple and it can be defined as the ability of a circuit element to resist the flow of electrical current. Ohm's law (Eq. 1) defines resistance in terms of the ratio between voltage, E, and current, I.

$$R \equiv \frac{E}{I} \quad (1)$$

This well-known relationship is limited to only one circuit element which is an ideal resistor. This element has several basic properties: it follows Ohm's Law at all current and voltage levels, its resistance value is independent of frequency, AC current and voltage signals passing through it are in phase with each other.

However, the real world circuit elements behave differently and exhibit a much more complex behaviour. These elements force us to abandon the simpler concept of resistance which has to be replaced with impedance, a more general circuit parameter. Similar to resistance, impedance is a measure of the ability of a circuit to resist the flow of electrical current, but it is not limited by the simplifying properties cited earlier.

Electrochemical impedance is measured by applying an AC potential (with a certain sinusoidal potential excitation) to an electrochemical cell and then measuring the current flowing through it. The response to this potential is an AC current signal that can be analysed as a sum of sinusoidal functions (Fourier series).

Normally, electrochemical impedance is measured using a small excitation signal so that the response of the cell is pseudo-linear. In a linear (or pseudo-linear) system, the current response to a sinusoidal potential is a sinusoid at the same frequency but shifted in phase (see Figure 1.38).

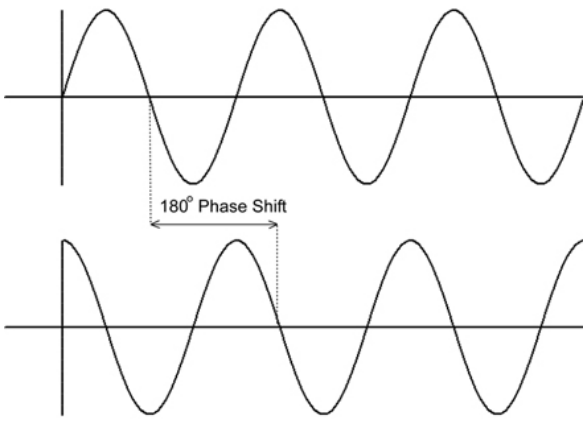

Figure 1.38: Sinusoidal Current Response in a Linear System
(http://www.jiscdigitalmedia.ac.uk/guide/the-physical-principles-of-sound)

The excitation signal, expressed as a function of time, has the form

$$E_t = E_0 \sin(\omega t) \quad (2)$$

where E_t is the potential at time t, E_0 is the amplitude of the signal, and ω is the radial frequency. The relationship between radial frequency ω (rad/s) and frequency f (Hertz [Hz]) is:

$$\omega = 2\pi f \quad (3)$$

In linear systems, the response signal, I_t is shifted in phase (φ) and has a different amplitude than I_0.

$$I_t = I_0 \sin(\omega t + \varphi) \quad (4)$$

An expression analogous to Ohm's Law allows us to calculate the impedance of the system as:

$$Z = \frac{E_t}{I_t} = \frac{E_0 \sin(\omega t)}{I_0 \sin(\omega t+\varphi)} = Z_0 \frac{E_0 \sin(\omega t)}{I_0 \sin(\omega t+\varphi)} \quad (5)$$

The impedance is then expressed in terms of a magnitude Z_0 and a phase shift φ.

If we plot the applied sinusoidal signal Et on the X-axis of a graph and the sinusoidal response signal I(t) on the Y-axis, the result is an oval also known as a "Lissajous plot". Analysis of Lissajous graphs on oscilloscope screens was a method of impedance measurement prior to the availability of modern EIS instrumentation.

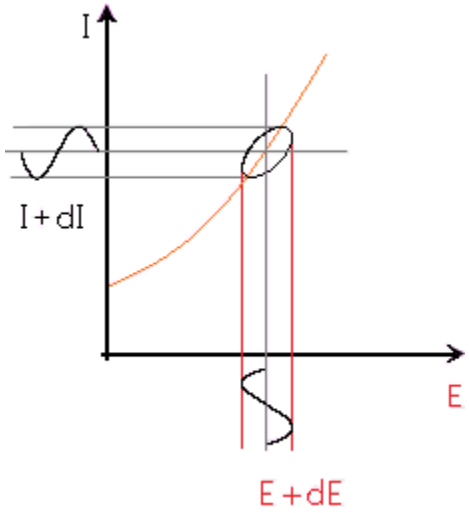

Figure 1.39: Origin of Lissajous Figure

With Eulers relationship, it is possible to express the impedance as a complex function.

$$\exp(j\varphi) = \cos\varphi + j\sin\varphi \quad (6)$$

The potential is described as

$$E_t = E_0 \exp(j\omega t) \quad (7)$$

While the current response as

$$I_t = I_0 \exp(j\omega t - \varphi) \quad (8)$$

The impedance can be then represented as a complex number,

$$Z(\omega) = \frac{E}{I} = Z_0 \exp(j\varphi) = Z_0 (\cos\varphi + j\sin\varphi) \quad (9)$$

In the last equation 9, Z(ω) is composed of a real and an imaginary part. In order to get a "Nyquist Plot" (see Figure 1.40) the real part must be plotted on the X-axis and the imaginary part on the Y-axis of a chart. In this plot the Y-axis is actually negative and each point on the Nyquist Plot is the impedance figure at one frequency. Low frequency data are represented on the right side of the plot while higher frequencies are on the left.

On the Nyquist Plot the impedance can be represented as a vector of length |Z|. The angle between this vector and the X-axis is φ, the "phase angle"

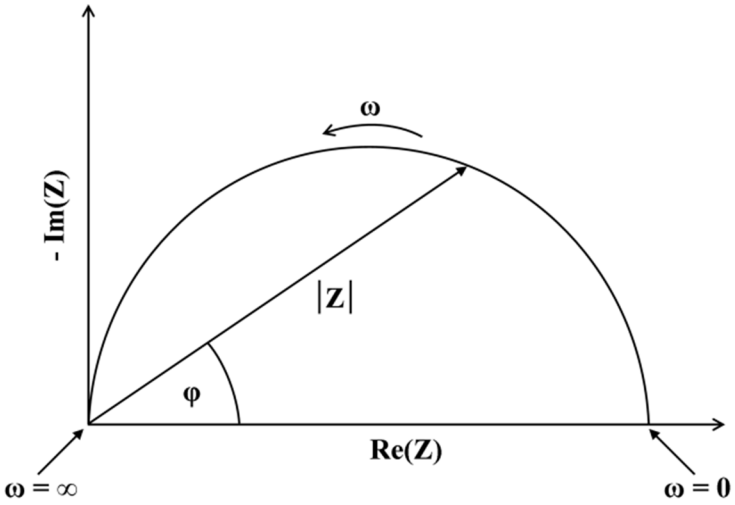

Figure 1.40: Nyquist Plot with Impedance Vector

The major limitation of Nyquist Plots is that they cannot tell what frequency was used to record a specific data point on the plot.

This Nyquist Plot represents the results from an electrical circuit like the one shown in Figure 1.41. The semicircle is characteristic of a single "time constant". Often electrochemical impedance Nyquist plots contain more than one semicircles but usually only a portion of a semicircle is seen.

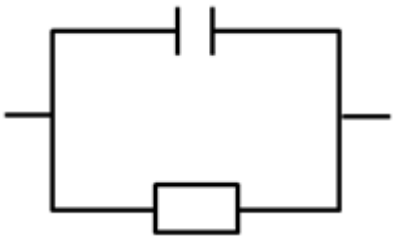

Figure 1.41: Simple Equivalent Circuit with One Time Constant

Another standard and quite common presentation method is the Bode Plot. The impedance is plotted with log frequency on the X-axis and both the absolute values of the impedance ($|Z|=Z_0$) and the phase-shift on the Y-axis.

The Bode Plot for the electric circuit of Figure 1.41 is shown in Figure 1.42. Unlike the Nyquist Plot, the Bode Plot shows frequency information.

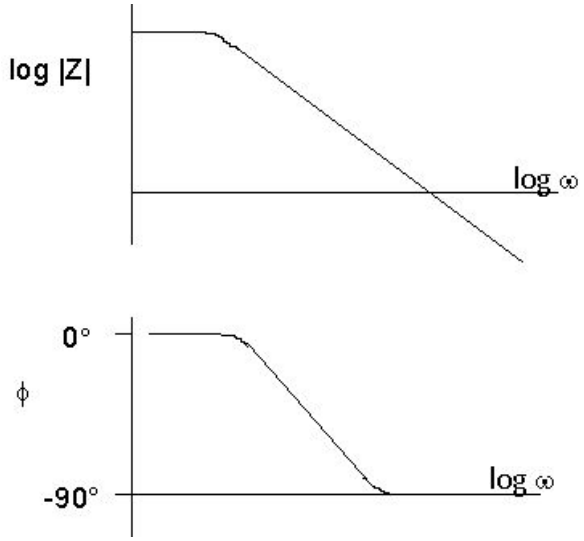

Figure 1.42: Bode Plot with One Time Constant
(http://www.labelettro.altervista.org/biografie/Bode_biografia.htm)

There are 3 fundamental conditions for EIS to be working correctly: Linearity, Stability and Causality. [162, 163]

1.6.1.1 Linearity/Non linearity of Electrochemistry Systems

Electrical circuits can be, theoretically, distinguished between linear and non-linear systems. Impedance analysis of linear circuits is less complicated than that of non-linear ones.

In a potentiostated electrochemical cell, the potential is considered to be the input while the output is the current. Electrochemical cells are not necessarily linear; in fact doubling the voltage won't automatically double the current.

Looking at a small enough portion of a cell's current versus voltage curve might give the impression to be dealing with a linear system while it is in fact pseudo-linear. (Figure 1.43)

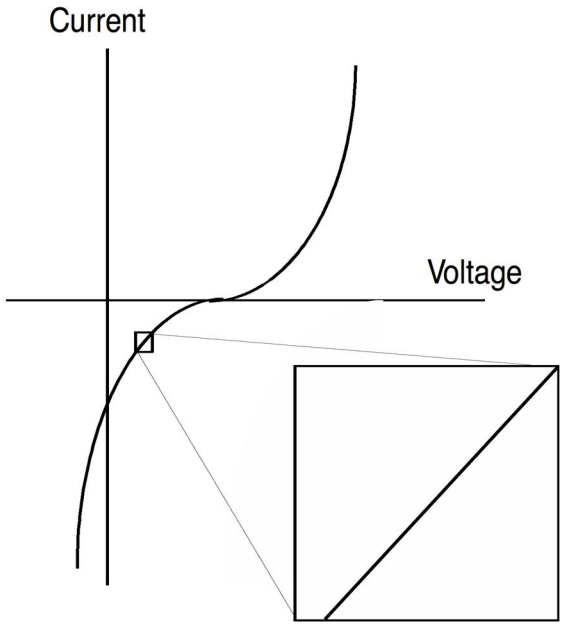

Figure 1.43: Current versus Voltage Curve Showing Pseudo-Linearity
(http://www.gamry.com/application-notes/basics-of-electrochemical-impedance-spectroscopy/)

A small AC signal (1 to 10 mV) is normally applied to the cell during an EIS analysis. With this potential signal, the system can be assumed to be pseudo-linear. It won't be possible in fact to see the larger non-linear response of the cell to the DC potential because the cell current is measured only at a certain excitation frequency.

1.6.1.2 Steady State Systems

The analysis of EIS spectra could occasionally take a lot of time, sometimes up to several hours. This happens, especially when the experiments are done including a range of very low frequencies. The system under investigation must be at a steady state during the course of the time required to measure the EIS spectrum. A common cause of problems in EIS measurements and analysis is the drift in the conditions of the measured system.

In practice a perfect steady state can be difficult, or rather impossible to achieve. The cell can change through adsorption of solution impurities, growth of an oxide layer, building-up of reaction products in solution, coating degradation, or temperature changes, to list just a few factors.

1.6.1.3 Causality

The measured AC response of the system must be directly correlated to the applied AC stimulus. The shielding of the cell from outside perturbations is important in this case.

1.6.1.4 Kramers-Kronig Analysis

The Kramers-Kronig (K-K) relations can be used to evaluate data quality. This analysis requires that causal, complex plane spectral data shows dependence between magnitude and phase. The real part of a spectrum can be obtained by integration of the imaginary part and vice versa.

The K-K relations will always be true for EIS data that is linear, causal, and stable. If measured real and imaginary data do not comply with the K-K relations, the data is violating at least one of these conditions.

Unfortunately, the K-K transform is quite complicated and requires integration over a range of frequency from zero to infinity. Evaluating the K-K relations via integration always involves assumptions about the behaviour of a spectrum beyond the frequencies over which it was measured.

1.6.1.5 Electrical Circuit Elements

Circuit elements used in the model of the analysed system are commonly simple electrical elements such as resistors, capacitors, and inductors and distributed elements such as constant phase element and Warburg impedance. These elements can be

combined in series and/or in parallel to give complex equivalent circuits. All of them have a certain physical meaning assigned in the equivalent circuit.

Table 1.2: Common Electrical Elements

Component	Current Vs. Voltage	Impedance
Resistor (R)	E = IR	Z = R
Inductor (L)	E = L dI/dt	Z = jωL
Capacitor (C)	I = C dE/dt	Z = jωC

The impedance of a resistor is independent of frequency and has no imaginary component. With only a real impedance component, the current through a resistor is always in phase with the voltage across the resistor. Some examples of the use of Resistance, R, to describe electrochemical phenomena are:

1.6.1.6 Electrolyte Resistance

The resistance of an ionic solution is strictly dependent on the ions concentration, type of ions, temperature and geometry of the area in which the current flows. Electrolyte resistance is a very important parameter to factor in the impedance analysis of an electrochemical cell. In a confined area A, of length l, in which flows a uniform current, the resistance is defined as,

$$R = \rho \frac{l}{A} \quad (10)$$

ρ is the solution resistivity, however this is usually expressed in the form of κ, which is the conductivity of the solution. So the equation can be re-written as:

$$R = \frac{1}{\kappa} \cdot \frac{l}{A} = \kappa = \frac{l}{RA} \quad (11)$$

The unit of κ is Siemens per meter (S/m). The Siemen is the reciprocal of the ohm, so 1 S = 1/ohm.

1.6.1.7 Ohmic resistance R_Ω

The potential drop between the reference electrode and the working electrode, is the ohmic resistance, or the uncompensated resistance and can be modelled using R. The ohmic resistance depends on the conductivity of the electrolyte and the geometry of the electrode. For a rotating disc electrode, the ohmic resistance is given by:

$$R_\Omega = \frac{1}{4\kappa R} \quad (12)$$

where κ is the specific conductivity of the bulk electrolyte, r is the radius of the disc. For more complex geometries the ohmic resistance is determined experimentally and can be estimated by impedance spectroscopy. In a Nyquist plot, the intersection of the impedance data with the real part of the axis at the high frequency end gives the ohmic resistance.

1.6.1.8 Polarization resistance, Rp

An electrode is polarized when its potential is forced away from its value at open circuit. Polarization of an electrode causes current to flow due to electrochemical reactions it induces at the electrode surface. The magnitude of the current is controlled by reaction kinetics and diffusion of reactants both towards and away from the electrode. When an electrode undergoes uniform corrosion at open circuit, the open circuit potential is controlled by the equilibrium between anodic and cathodic reactions resulting in anodic and cathodic currents. The open circuit potential is the potential where the two currents are equal. The value of the current for either of the reactions is known as the corrosion current. When the two reactions are under kinetic control, the potential of the cell can be related to the current by the Butler-Volmer equation:

$$i = i_0 \left(e^{\beta\alpha} - e^{\beta c}\right) \quad (13)$$

where, i is the measured cell current, i_0 is the exchange current, e is the over potential, β_α and β_c are the anodic and cathodic Tafel coefficients, respectively. For small e the above equation can be transformed to:

$$i_0 = \frac{\beta_\alpha \beta_c}{\beta_\alpha + \beta_c}\left(\frac{1}{R_p}\right) \quad (14)$$

The parameter R_p (polarization resistance) behaves like a resistor. If the Tafel constants are known, one can calculate the i_0 from R_p. The exchange current, i_0 can be used to calculate the corrosion rate, for example.

The impedance of an inductor increases as frequency increases. Inductors have only an imaginary impedance component. As a result, the current through an inductor is phase-shifted -90 degrees with respect to the voltage.

The impedance vs. frequency behaviour of a capacitor is the opposite of that of an inductor. A capacitor's impedance decreases as the frequency is raised. Capacitors also have only an imaginary component. The current through a capacitor is phase shifted -90 degrees with respect to the voltage.

1.6.1.9 Double Layer Capacitance

At the interface between the electrode and the electrolyte there is an electrical double layer. This is formed as ions from the solution adsorb onto the surface of the electrode. The charged electrode is separated from the charged ions by an insulating space, usually very small (few angstroms). In theory, charges separated by an insulating material form a capacitor, so a metal immersed in an electrolyte will behaves like a capacitor. You can estimate that there will be 20 to 60 F of capacitance for every 1 cm^2 of electrode area, though the value of the double layer capacitance depends on many variables. Electrode potential, temperature, ionic concentrations, types of ions, oxide layers, electrode roughness, impurity adsorption, etc. are all factors.

1.6.1.10 Coating Capacitance

A capacitor is formed when two conducting plates are separated by a non-conducting media, called the dielectric. The value of the capacitance depends on the size of the plates, the distance between the plates and the properties of the dielectric. The relationship is,

$$C = \frac{\varepsilon_0 \varepsilon_r}{d} A \quad (15)$$

With, ε_o = permittivity of free space; ε_r = dielectric constant (relative electrical permittivity); A = surface of one plate; d = distances between two plates

Whereas the permittivity of free space is a physical constant, the dielectric constant depends on the material. Table 3 gives you some useful e_r values.

Table 1.3: Typical Dielectric Constants

Material	ε_r
Vacuum	1
Water	80.1 (20 °C)
Organic coating	4 - 8

Notice the large difference between the dielectric constant of water and that of an organic coating. The capacitance of a coated substrate changes as it absorbs water. EIS can be used to measure that change.

1.6.1.11 Constant Phase Element

When modelling an electrochemical phenomenon with an ideal capacitor it is assumed that the surface under investigation is homogeneous although is normally not the case. This lack of homogeneity is modelled with a Q element, used to represent the CPE:

$$Z_Q = \frac{1}{Y_0 (j\omega)^n} \quad (16)$$

Where Y_0 is the admittance of an ideal capacitance and n is an empirical constant, ranging from 0 to 1. It is noteworthy that when n = 1, the CPE behaves as a pure capacitor, while when n = 0, the CPE behaves as a pure resistor. Furthermore, when n = 0.5, the CPE is the equivalent of the so-called Warburg element, described below

1.6.1.12 Warburg Impedance, W

In electrochemical systems, diffusion of ionic species at the interface is common. The Warburg impedance was developed to model this phenomenon. Several expressions, based on different assumptions, are used to describe diffusion impedance. Under the assumption of semi-infinite diffusion layer, the impedance is:

$$Z_W = \frac{1}{Y_0 \sqrt{j\omega}} \quad (17)$$

Y_0 is the diffusion admittance. Warburg impedance is characterized by having identical real and imaginary contributions, resulting in a phase angle of 45°. Under the assumption of a finite diffusion layer thickness (Nernst hypothesis), the diffusion impedance is modelled by:

$$Z_0 = \frac{1}{Y_0}\tanh(B\sqrt{j\omega}) \quad (18)$$

B is given by:

$$B = \frac{\delta}{\sqrt{D}} \quad (19)$$

Where δ is the diffusion layer thickness and D is the diffusion coefficient. When B is large enough, Z_0 is basically Z_W.

1.6.1.13 Serial and Parallel Combinations of Circuit Elements

Electrochemical cells can be rarely modeled using a single circuit element. Usually are made of several elements in a network which can be both serial (Figure 1.44) and parallel (Figure 1.45) combinations.

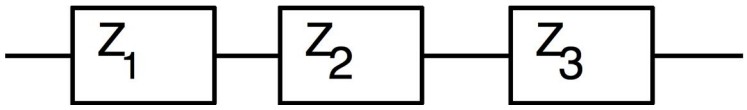

Figure 1.44: Impedances in Series

For linear impedance elements in series, impedance can be calculated as:

$$Z_{eq} = Z_1 + Z_2 + Z_3 \quad (20)$$

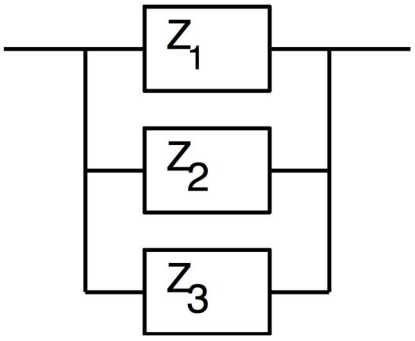

Figure 1.45: Impedances in Parallel

While the equivalent impedance for elements in parallel can be calculated as:

$$\frac{1}{Z_{eq}} = \frac{1}{Z_1} + \frac{1}{Z_2} + \frac{1}{Z_3} \quad (21)$$

When purely resistive elements are combined in series, both resistance and impedance go up.

When capacitive elements are connected in series, instead, impedance goes up but capacitance figures go down as a consequence of the inverse relationship between capacitance and impedance.

1.6.1.14 Common Equivalent Circuit Models

To recap, in the following table 4 there are the impedance and admittance relationship for the most common elements used for modelling circuits

Table 1.4: Impedance and admittance for the most common elements used for modelling circuits

Equivalent Element	Admittance	Impedance
R	1/R	R
C	jωC	1/ jωC
L	1/ jωL	jωL
W (Warburg)	$Y_0\sqrt{j\omega}$	$1/Y_0\sqrt{j\omega}$
Q (CPE)	$Y_0(j\omega)^{\alpha}$	$1/Y_0(j\omega)^{\alpha}$

1.6.1.15 Purely Capacitive Coating

A metallic sample covered with a uniform and undamaged coating generally has very high impedance. The equivalent circuit for this situation is represented in Figure 1.46.

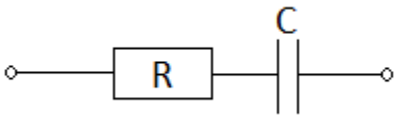

Figure 1.46: Purely Capacitive Coating

The resistor represents the electrolyte resistance while the capacitor models the coating.

In a Nyquist plot this model would like approximately like this:

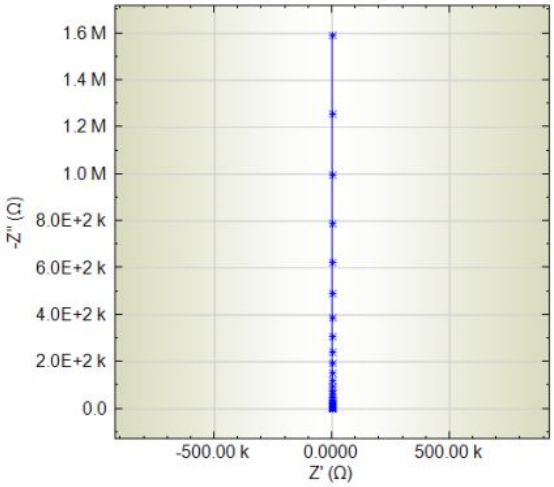

Figure 1.47: Typical Nyquist Plot for an Excellent Coating (Autolab Application Note EIS06)

1.6.1.16 Randles Cell

The Randles cell (figure 1.48) is a very common element used in the circuit modelling and it is usually the starting point for more complex models. It consists of a solution resistance, a double layer capacitor and a polarization resistance. The double-layer capacitance is in parallel with the polarization resistance

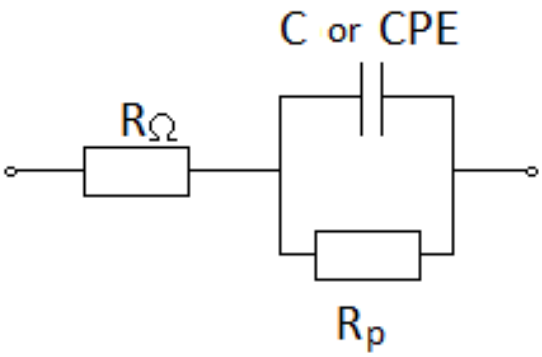

Figure 1.48: Randles Cell Schematic Diagram

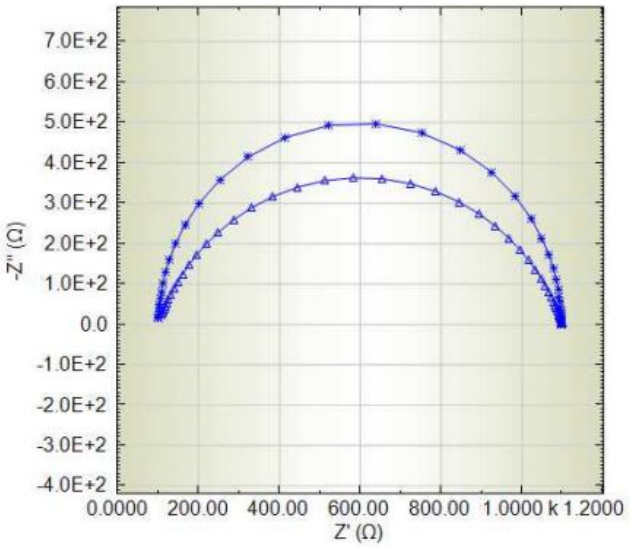

Figure 1.49: Nyquist Plot for Randles cells (Autolab Application Note EIS06)

The Nyquist Plot for a Randles cell (figure 1.49) has always the shape of a semicircle. The electrolyte resistance figure can be read on the real axis at the high frequency intercept. The intercept of the real axis value at low frequency is the sum of R_p and R_Ω. The diameter of the semicircle represents then the polarization resistance.

1.6.1.17 Mixed Kinetic and Diffusion Control

If a cell has semi-infinite diffusion with a series solution resistance as the only other cell impedance. The Warburg impedance in a Nyquist plot looks as a line with a slope of 45°.

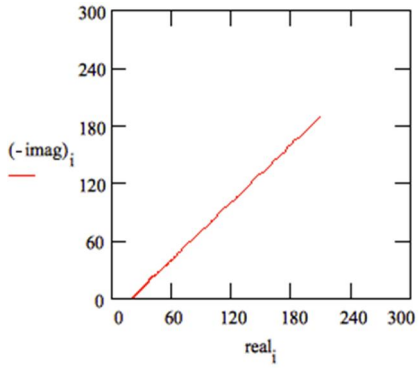

Figure 1.50: Nyquist Plot for Warburg Impedance (Gamry.com, Basics of Electrochemical Impedance Spectroscopy)

The same data is plotted in the Bode format in Figure 1.51. The phase angle of Warburg impedance is 45˚.

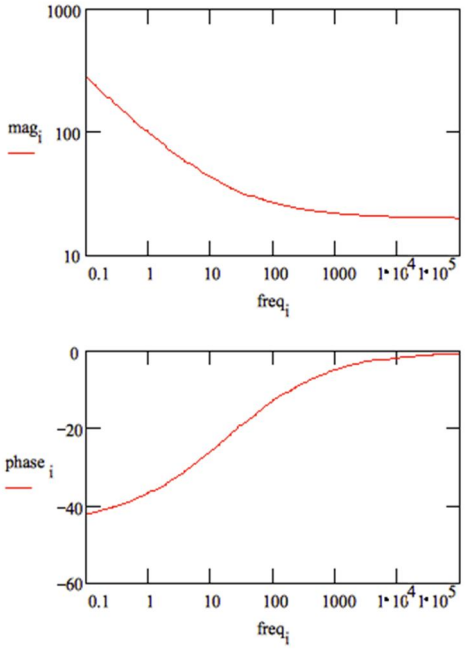

Figure 1.51: Bode Plot for Warburg Impedance (Gamry.com, Basics of Electrochemical Impedance Spectroscopy)

If double layer capacitance and charge transfer impedance are added to this condition, the equivalent circuit looks as below in Figure 1.52. As no simple element can model the Warburg impedance, it is not possible to create a cell that models the Randles Cell.

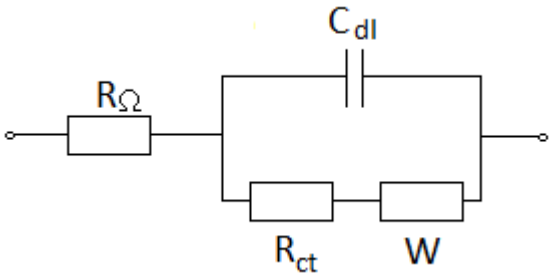

Figure 1.52: Randles Cell: Equivalent Circuit with Mixed Kinetic and Charge-Transfer Control

This circuit models a cell where polarization is due to a combination of kinetic and diffusion processes.

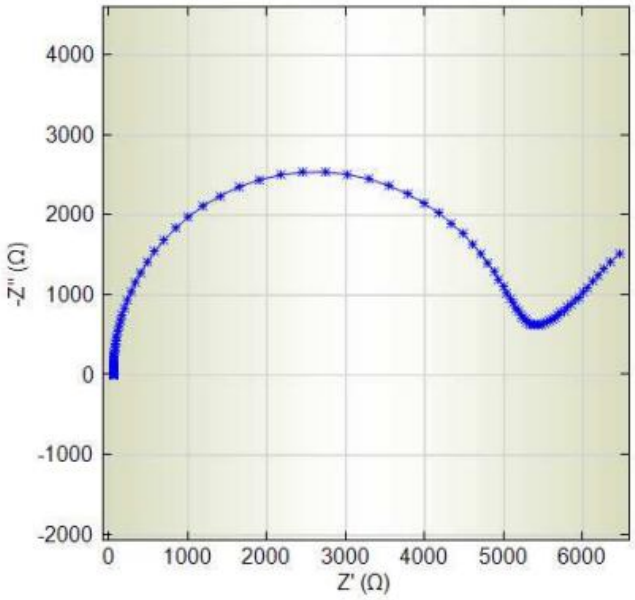

Figure 1.53: Nyquist Diagram for Mixed Control Circuit (Autolab Application Note EIS06)

An example of what a Bode plot would look like for an equivalent circuit like the one shown in figure 1.52 is as follows in Figure 1.54.

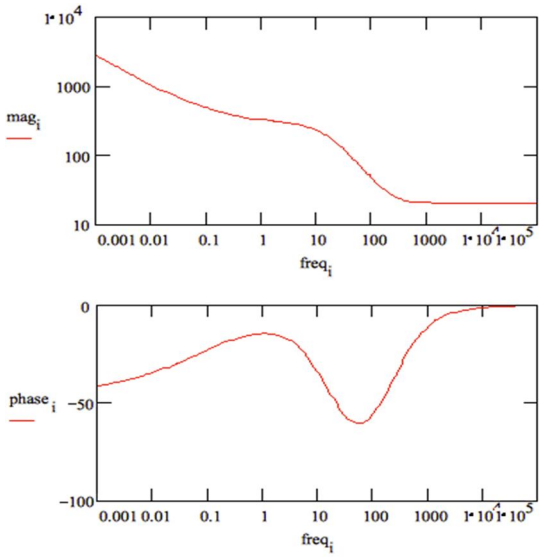

Figure 1.54: Bode Plot for the Mixed Control Circuit (Gamry.com, Basics of Electrochemical Impedance Spectroscopy)

1.6.1.18 Complex Circuits

In more complicated situation, such as the impedance analysis of an organic coating on a metal substrate in contact with an electrolyte, it is very difficult to model the experimental conditions. Some complex circuit like those shown below (figure 1.55) will lead to multiple semi-circles on the Nyquist plot (figure 1.56).

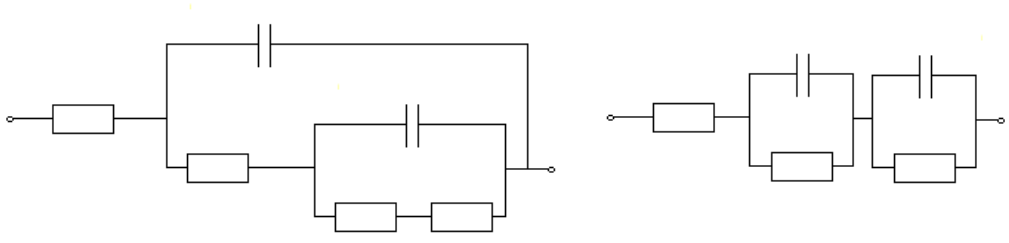

Figure 1.55 Examples of more complex circuits that lead to multiple semi-circles in the Nyquist plot

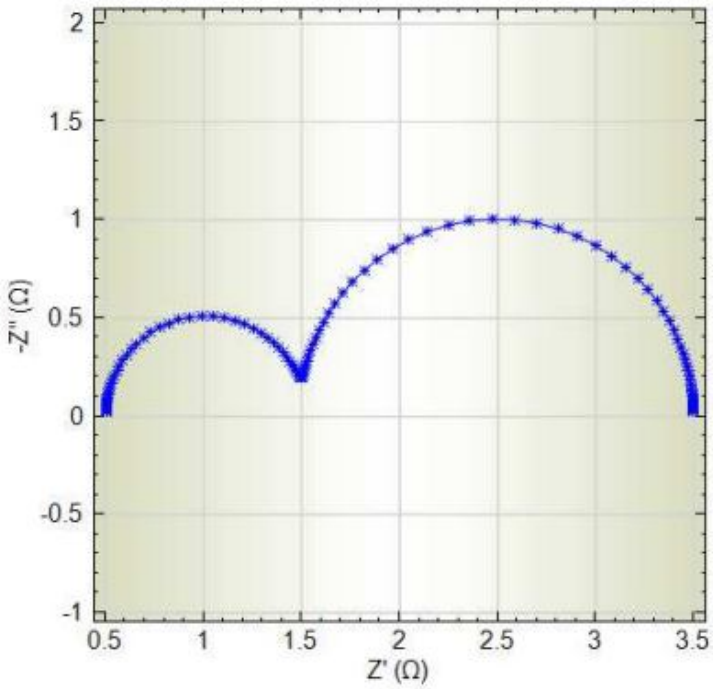

Figure 1.56: Nyquist plost of complex circles showing two semi-circles (Autolab Application Note EIS06)

1.6.1.19 Non-uniqueness of models

Modelling an equivalent circuit is a technique that tries to match an ideal model of an electrochemical setup with an experimental set of data. Circuit elements can only be assigned properly when enough information about the chemical and electrochemical phenomena taking place at the interface is known. Furthermore, it is important to observe that several models are possible for a certain set of data and that some equivalent circuits are mathematically identical [164 – 168].

1.6.2 ECIS

1.6.2.1 Intro

The basic idea of monitoring cell electrically came about in the 80s when Giaver and Keese started studying this approach at General Electric laboratories and described their work in [169] which is the first time that ECIS is reported in literature. They basically placed gold film electrodes on the bottom of a tissue culture dish, inoculated these

electrodes with cells and then applied a very weak AC signal. If the electrodes were small such that they could eliminate the solution resistance, they were able to see clearly the cells activity. ECIS stands for electric cell-substrate impedance sensing but the acronym could be also intended as electric cell impedance spectroscopy because the AC frequency that is used in making these measurements is very important in terms of what specific activity of the cells can be detected.

The cells grow in tissue culture medium which serves as the electrolyte for the measurement. To make this kind of analysis it is necessary to apply a very weak AC signal anywhere in the range of frequencies from 100Hz up to 100 kHz and the current density has to be kept sufficiently low so that the measurement is not invasive. This broad range of frequencies is chosen to have a comprehensive understanding of the cell behaviour in a wide spectrum. Measurements conducted at lower frequencies would show a predominance of resistive effects, while those at higher frequencies would show a predominance of capacitive effects [170, 171]. The cells are unaware they are being monitored and the voltage drop across their membranes is not sufficiently large to be detected by the cells. The voltage across the electrodes is monitored through the electronic system and computers and after a data analysis is possible to report the impedance values which is the equivalent of resistance in DC circuits (although this is an AC circuit). Impedance is represented with Z and is measured in Ohms (Ω). Most instruments in addition to monitoring the voltage across the electrodes are able to follow and determine the phase difference between the current and the voltage as it oscillates back and forth. Using this information is possible to describe the complex impedance which can be represented roughly as a resistance in series to a capacitor. So the output of an ECIS system would be either Z measured in Ohms or the resistive portion of the impedance again measured in Ohms, or the capacitance of the gold plates in the solution which would be of the order of nanofarads.

The reason why we see this change in impedance with these electrodes is quite simple. The gold film electrode is carrying the current, which is actually carried by the ions in the electrolytic solution. The electronic system ensures that the current is constant at all time so even when the cell layer grows evenly over the insulating film and the electrode, the current flows through the cell layer. When the cells are in place, the current must

flow out from beneath the cell around the adhesion plaques and go through this narrow space between the electrode and the basal membrane. Then the current passes through the cell-cell junctions into the electrolyte to find the counter electrode or another small electrode.

The dotted line indicates that some current will capacitively couple through the insulating membrane of the cells because this is after all an AC measurement. The degree to which it couples through the cell membrane is dependent upon the AC frequency and by studying the behaviour of cells at different AC frequencies we can discern different activities of the cells. In conclusion anything that impinges on the site of the cell and changes the morphology of the cells will change this current path and this will lead to a measurable impedance change that is detected by ECIS. These changes can come about from a variety of conditions from signal transduction, viral infection, DNA transfection, changes in the chemical and physical conditions of the cells and cultures. It is indeed and extremely versatile measurement (figure 1.57).

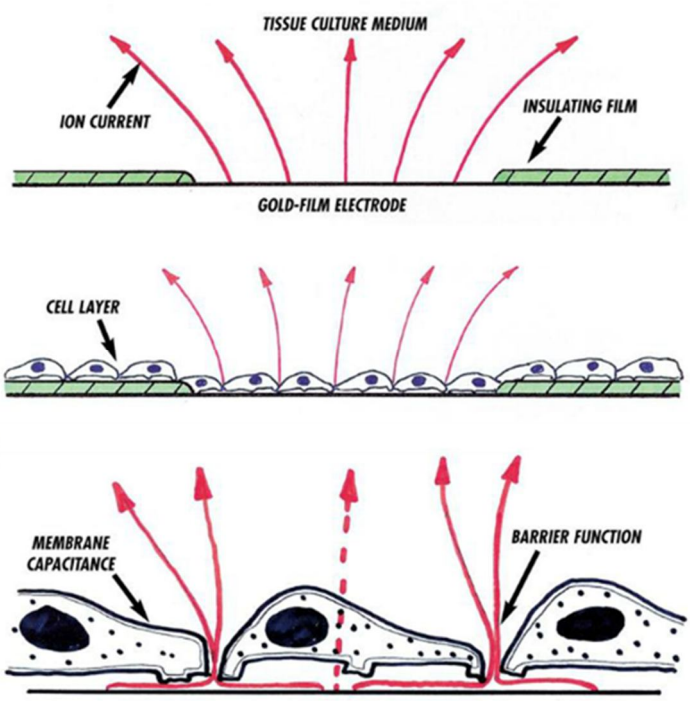

Figure 1.57: Current flow in an ECIS experiment when the electrode is free from cell growth (top) and when the cells are growing on the substrate (middle and bottom) (http://www.biophysics.com/)

1.6.2.2 ECIS theory

Let's consider first an electrode without any cells on it. There are two main sources of impedance: one is the exchange of electrons that takes place at the electrode's surface, the faradaic resistance (R_f); the other is the passage of current through the solution due to the mobility of the ions, the solution resistance (R_s). We are interested of course to see what happens at the surface, where the cells are located, and we are really not interested in the R_s but unfortunately if the electrodes are too large, the R_s will predominate in the measurement. The reason for this is shown in the right hand side (figure 1.58) where we are considering a small circular electrode of radius r. As we make this electrode smaller, the R_s does increase as the current has to funnel into the electrode, the so-called spreading or contact resistance. But this change in R_s goes as 1/r whereas the faradaic resistance, which is related to the area of the electrode, is $1/r^2$. Because of this mathematical relationship as we make the electrode smaller and smaller, eventually the faradaic resistance will predominate and it is in this size that we see the activity of the cells. This usually happens when the radius is around 100µm.

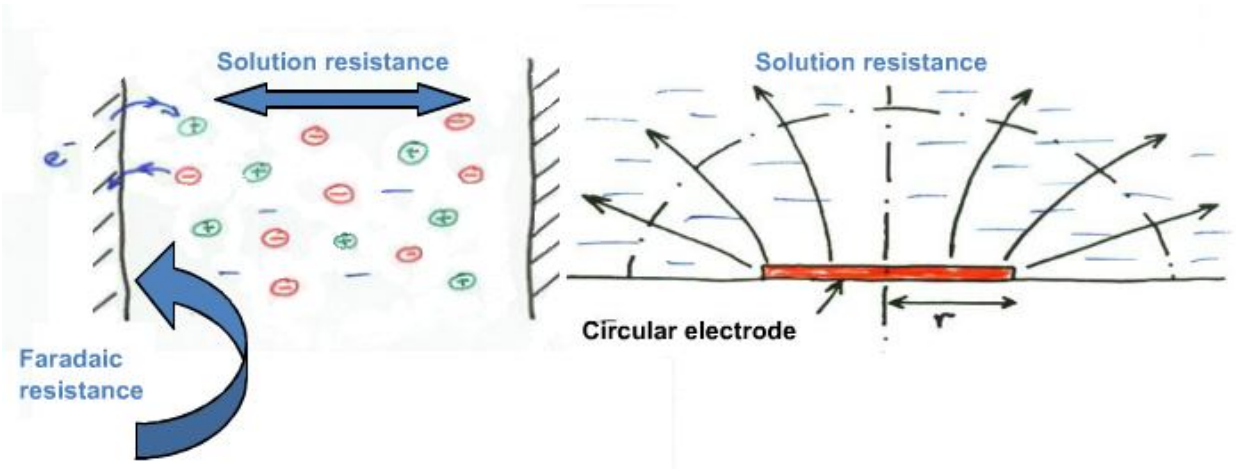

Figure 1.58: Effects of Solution Resistance (R_s) and Faradaic Resistance (R_f) in ECIS measurements (http://www.biophysics.com/)

There is another way to minimize the solution resistance and that is to use interdigitated electrodes. In this case the R_s is maintained small by minimizing the solution to very thin skin near the electrode surface rather than the entire bulk of the solution. This approach

is very useful in the proliferation experiments. The drawback of this method is that we cannot mathematically model what is going on and also the micromotion, which is an interesting part of the ECIS measurement, is almost entirely lost using this large surface area. Nevertheless these kinds of arrays are excellent for monitoring cell proliferation.

The reason why we see these changes in impedance when the cells attach and spread on the can be easily explained. As the cells attach and spread they tend to flatten out (figure 1.59), cover the electrode and block the area available for current flow. The current flows under the cells, in the space between the electrode and the basal membrane as the cell stand on small adhesion plaques (focal contacts). The dotted line points out the fact that because this is an AC measurement some current will be capacitively coupling with through the cell membrane and passing directly through without passing beneath the cells or between the cells. The AC frequency used in the measurement will determine how much current capacitively couples through the membrane. The low frequency is indicated by the red line, the current flows between spaces beneath cells and through the cell-cell junctions whereas at very high frequencies (30-40 kHz) more of the current is going to couple with the membrane. This allows taking apart different activities of the cells using EIS.

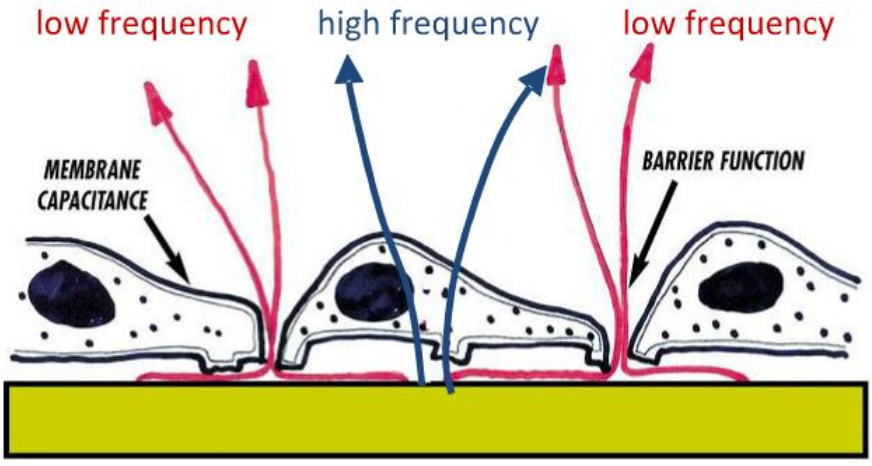

Figure 1.59: Differences in the current path caused by different frequencies in ECIS measurements (http://www.biophysics.com/)

By using different frequencies we are able to sort out differences in cell behavior. At high frequencies, we can monitor cell attachment and spreading and at lower frequencies we can start to see the current going between the cells or the barrier function of the cell layer.

More sophisticated instruments monitor the complex impedance, where in addition to monitoring the voltage between the electrodes they can control the phase difference between the voltage and the current. This allows the users to break the Impedance down to its components, resistance and capacitance. These data can be used to define all the parameters and their changes in real time. In cell attachment and spreading using complex Z, where instead of looking at Z or R, we look at the capacitance of the Au. As the cells attach and spread, the capacitance drops as cells block the Au electrode. It is interesting to notice that C monitored at high frequencies varies in a linear manner with the percentage of the cell coverage.

1.6.2.3 Toxicology with ECIS

For both economic and ethical reasons there has been growing attention for alternative methods to replace the use of animals in toxicity testing of chemical agents. Tissue cultures have been proved to have the potential to replace tests on animal; but for this kind of in-vitro approach to be successful, new and more sensitive techniques to detect cellular activities are required.

In 1992, Giaever and Keese published an article "*Toxic? Cells Can Tell*" [172], suggesting the application of cell impedance measurement for this purpose. Since then, many researchers developed ECIS-based assays for toxicity testing and have obtained a considerable amount of data to validate the efficacy of this method. The ECIS approach supplies quantitative data, and since instruments are normally computer controlled, very little technician labor is required to acquire large amounts of data. Precision and cost efficiency are important attributes of ECIS.

In 1998 an article aiming at monitoring dose response curves using ECIS was published by Keese et al. [173]. In this study cells were exposed to different potential toxicants and their response was monitored through ECIS. Confluent monolayers of WI-38/VA13 fibroblastic and MDCK epithelial cells were exposed to different concentrations of four detergents (Tween 20, benzalkonium chloride, Triton X100 and sodium lauryl sulfate). Changes of the overall impedance of the cell monolayer and of cell micromotions detected as impedance fluctuations were observed. Analysis of these measurements correctly ranked the detergents according to their established in vivo toxicity. A dramatic increase of impedance fluctuations was recorded from cells upon exposure to the toxicants.

At high concentrations of detergent, a rapid drop in the resistive portion of the impedance is observed that begins near the time of detergent addition. At intermediate concentrations there is a delay in response followed by a slower decline in the resistance.

1.6.2.4 Microelectrode arrays

The most common ECIS system is the microelectrode array setup [174]. With this design, measurements are taken between multiple sensing electrodes and a common reference electrode on a planar substrate. Cells attach to the sensing electrodes while the reference electrode is typically cell-free. The surface area of the reference electrode is often made much larger than that of the sensing electrodes so that the impedance measurement is dominated by the cell layer [175]. Another method reported to reduce electrical interference is to add grounded electrodes on either side of the sensing electrodes in a coplanar arrangement [42 176]. Ideally, cells should cover the whole sensing electrode to avoid a direct electrical shunt to the media via the exposed regions. For example, microelectrode array have been used for cardiomyocyte extracellular matrix adhesion measurements [177], in finding the capacitance of ovarian cancer epithelial cells [178], and to observe the effect of forskolin on MCF-7 cells [179].

1.6.2.5 Interdigitated electrodes

Interdigitated electrodes are arranged on a flat substrate, where the electrodes are all connected to either one of two contact pads. These electrodes are usually patterned on insulating and biocompatible substrates by using standard lithography techniques. An electric field, which is used to measure impedance, develops in the region between the adjacent fingers of the interdigitated electrodes. As a result, the bulk impedance of cell suspensions and monolayers can be measured. Such setups have been used to measure, for example, bacterial suspensions [180], changes in cell adhesion [181] and the cell cycle [182]. Other applications for interdigitated electrodes have been reported to be used as biosensors for Escherichia coli [183] and in cell differentiation studies [184]. Setups have integrated interdigitated electrodes with silicon or glass micro chambers [180], Poly- dimethylsiloxane (PDMS) culture wells [181] and plastic culture dishes [182].

1.6.2.6 Cytotoxicity and cell death

Dying cells exhibit changes in their impedance spectrum. Therefore, impedance measurements can be used to measure the effects of certain chemicals on cell mortality. Typical cytotoxicity experiments involve the exposure of cells to varying concentrations of toxicants and then recording the changes in the cell impedance value. ECIS is definitely one of the most popular methods for detecting cytotoxicity. Dying cells exhibit detachment, spreading, micro-motion, changes in substrate adhesion, and a reduced affinity for other cells. Impedance experiments on cytotoxicity include observing the effects of cytochalasin B on human umbilical vein epithelial cells [185], monomers and co-monomers of dental resin composites on human gingival fibroblasts [186], gemcitabine and mercury chloride on human hepatocarcinoma cells (BEL7404) [187], quantum dots on fibroblastic V79 cells [188] and sodium arsenite on immortalized mouse fibroblasts BALB3T3 [181]. The data from these studies show significant differences in time based cell impedance values with changing toxicant concentrations. Flow cytometry, combined with impedance measurements, has also been used discriminate between live and dead cells, for example Bacillus megaterium cells [189]. The literature shows that impedance has the potential to screen for the cytotoxicity of various agents, such as chemicals, drugs, cell labels, and implants, along

with allowing the observation of the effect of various stresses induced on cells. In these setups, the cell is used as a biosensor for rapid and real-time measurements and can replace slower, invasive and destructive traditional cytotoxicity assays.

1.6.2.7 Drug screening platform

Drug screening provides a reliable assay with which to evaluate the ability of a specific drug to induce apoptosis and cell death [190]. These kinds of events are usually marked by significant modifications in the impedance spectra, so the effect of the drug can be observed at varying concentrations. In cancer research, impedance has been used to test the effect of cisplatin on human esophageal cancer cell lines KYSE 30 [191], the ion channel inhibitor chlorotoxin on U87MG human glioblastoma cells [174], retinoic acid on human esophageal squamous epithelial cancer cells [192], and doxorubicin on MCF-7 cells [193]. Data in these studies show a higher drop in cell impedance with higher drug concentrations and longer incubation time with the drug. If the drug quantity is beneath an effective concentration then there is little difference in impedance between cells under test and drug free controls. These kinds of studies can be extended to observe the potential effects of cancer treatments on healthy tissues. For example, impedance measurements were used to investigate the effects of drugs on kidney cell nephrotoxicity [194]. Impedance measurements have also been used to assess ampicillin resistance in bacteria [195]. Studies on Drugs effects extend beyond cytotoxicity or killing unwanted organisms. The pharmaceutical research has a particular interest in cell barrier biology in relation to drugs to determine, for example, how permeable the gastrointestinal barrier is to orally administered drugs. Since the impedance of cellular monolayers is correlated to their permeability, impedance spectroscopy is an ideal tool for cell barrier studies. Microfluidic devices that use impedance spectroscopy have been produced to evaluate the barrier strength (or permeability) of cell monolayers and in the future these studies can be extended to monitor the effects caused by the drugs under test [196].

Cell-based assays have been used as an alternative method for animal experiments in pre-clinical research and development of drugs and toxicological testing [197, 198]. It has been concluded that *in vitro* cytotoxicity assay can be used as an addition to animal testing to improve dose level selection and thus further reduce the number of animals sacrificed for the purpose [199]. ECIS has been proven valuable and reliable in real-time

monitoring of dynamic changes induced by cell–toxicant interactions [200]. Keese *et al.* [201] demonstrated the applicability of the ECIS system for toxicological testing of fibroblasts and epithelial cells. Subsequently, many chemicals have been tested for cytotoxicity evaluation with various types of cells [202, 200, 203]. The effect of cytotoxins on cells is usually presented with time-response and dose-response curves using ECIS technology in a label-free way.

1.7 BIOIMPEDANCE MEASUREMENT AS ADDITIONAL POSSIBILITY

1.7.1 Bioimpedance

Bioimpedance is the response of a living organism to an externally applied electric current. It is, just like impedance, a measure of the opposition to the flow of an electric current through a certain material, which in this case is biological. The carriers of the electric charge in living tissues are, with some exceptions, ions. Tissues could be regarded as a volume conductor, or more commonly, as a dielectric. In frequencies lower than 100 kHz they are mostly electrolytic conductors.

Bioimpedance is about biomaterials which are not exclusively from living organisms. They can be living, dead tissues or building blocks for living tissues. Tissues of interest can include plants, fruits, eggs, fishes or animals and human body. Also dead biological material can be examined through bioimpedance observation like hairs or nails for example or ex-vivo material such as a piece of stratum corneum to cite one. Cells are of course the essential building block of living organisms and the basic requisite for its life is that they have to be surrounded by an electrolytic solution. When testing a biological material it is essential to keep in account its conditions as the situation can change completely from an in-vivo to an ex-vivo sample.

Tissue is a very heterogeneous material as the cells of which it is made of could be all of different sizes with different functions. This naturally influences its conductivity properties and it is impossible, from an electrical point of view, to assume any tissue as a homogeneous material. It can be regarded as an anisotropic material because of it complex structure and the orientation of the cells, membranes and micro-organelles.

Tissue is classified in epithelium, muscle, connective tissue and nervous tissue in medicine. If it is investigated at a cellular level, its parameter may change a lot even if moving of few micrometers from each point of analysis. Bioimpedance values of tissues are dependent on frequency, temperature, water content, blood perfusion, etc. An interesting thing is that the differences between mammalian and human tissue figures are usually very small.

Muscle tissue has been observed to have a large alpha-dispersion (areas where outer cell membranes are able to charge and discharge fully) and strongly anisotropic with a low frequency conductance ratio of 1:8 between the transversal and longitudinal directions. In the last one, the high conductance is not frequency dependent as there are free liquid channels that dominate the current path (figure 1.60). The transversal properties are more influenced by a beta-dispersion. In beta-dispersions the membranes are able to be charged only partially and the current is able to charge the small intracellular space structures which behave as capacitances. At frequencies between 10 kHz and 10 MHz the current can flow through the lipidic membranes introducing a capacitive component. This makes higher frequencies sensitive to intracellular changes due to structural relaxation [204 – 206].

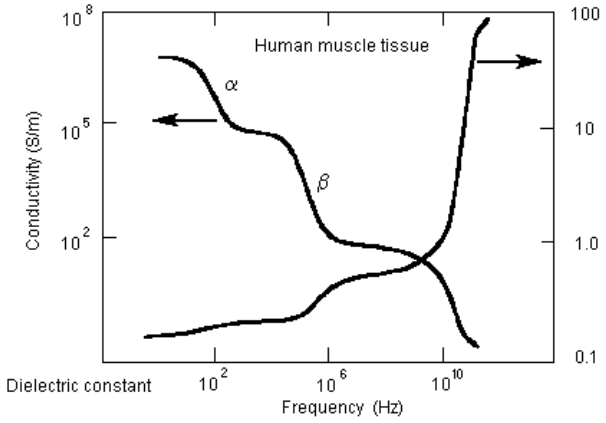

Figure 1.60: Dielectric constant and conductivity of typical biological tissue as functions of frequency (ref. 200)

Nerve tissue is, as expected, largely found in the brain. The other nervous tissue found elsewhere in the body has an electrical behaviour similar to that of an electrical cable to which can be applied the general rules of electricity and conduction. The myelin sheath

that can be found in myelinated nerves increases the impedance of these structures. Adipose tissue, bone and bone marrow have a variable permittivity and conductivity. They can be roughly seen as insulators but their properties depend mostly on the degree of blood and liquid perfusion.

Bioimpedance follows the same theory of the normal electrical impedance, only in this case it is applied to biological materials. The biomaterial could be living or dead tissue or any other organic material related to a living organism. The measurement of its impedance could give valuable information about its composition or a physiological event of interest. For bioimpedance measurements, a different number of electrodes can be used depending on the applications: on one (or more) a small current is applied while other electrodes measure the resulting voltage [207].

As the conductivity in biological materials is electrolytic and based on Na^+ and Cl^- ions, in body fluids, changes in the content of liquid or the ion-concentration lead to changes in the impedance. Furthermore, cell membranes have a low conductivity, hence the concentration of cells influences the impedance as well [207, 208]. However, they are separating two electrolytic systems which make the cells operate as capacitors [207, 209]. That is why in biological tissue there are resistive and capacitive components which are both well described by the concept of complex impedance [210].

1.7.2 Why bioimpedance? - Impedance in relation to medical purpose

In the past, bioimpedance measurements were mentioned to offer the possibility to be used as potential tool for medical diagnostics in many different ways. One reason for this is that impedance values are characteristic features of one material. Besides, it offers easy-to-apply techniques related with reasonably low costs [211]. These techniques currently in use all exploit the fact that electrical bioimpedance is dependent on the content of liquid and the concentration of ions in the sample. That is why different kinds of tissue show different values of impedance.

1.7.3 Electrical Impedance Tomography

There are two different approaches for Electrical Impedance Tomography (EIT): The adjacent drive and current pattern design. For the adjacent drive setup, an array of adjacent electrodes is placed on the part of body under examination. A current is applied

to one electrode of this array and the potential is measured on the other electrode(s). These measurements are repeated for all electrodes of the array. The second setup forms a current pattern within the body of interest applying a current to several electrodes at the same time. This pattern rotates around the body while the resulting voltage is measured. The data collected in this way is transformed into a 2D-image with an image reconstruction software [212].

This imaging technique allows a very fast and non-invasive collection of data so that changes in structure or function are measureable. On the other hand, it is possible to monitor physiological functions over a long period of time. Besides this, this technique is relatively cheap, portable and till today, there are no known hazards to the patient [212, 213].

Concerning these possibilities, EIT is considered for many medical purposes. It could be used to detect breast cancer, since the impedance of a malignant breast tumour tissue is lower than impedance of normal breast tissue [214 - 216].

Furthermore, EIT is used to monitor the regional lung function bed-side and non-invasively which is a helpful application especially for intensive care medicine [217 - 219]. It helps to control lung water, lung composition and ventilation as well as to detect pulmonary embolus and to observe patients under artificial ventilation [212]. This is not only used for intensive care patients, but also for the observation of neonates, because it is the only non-invasive technique for this purpose known till today [212, 217].

EIT could be used to analyse slow metabolic related changes in the brain. This could be increasing blood flow or cell swelling related to epilepsy diagnostic, changes occurring to evoked activity of the brain or to make a diagnose of acute stroke, a ischemia caused loss of brain function [213, 220]. Furthermore, it offers the possibility to follow fast neuronal depolarization occurring during electrical activity of brain which, in the future, could be a tool to help neuroscientist to understand the function of the brain [213].

Another application of EIT is the possibility to measure gastric emptying during continuous infusion of liquid feed [221 - 224].

1.7.4 Bioelectrical Impedance Analysis

Bioelectrical Impedance Analysis (BIA) is a technique for non-invasive measurement of human body composition. Since content of electrolytic solution is influencing the value

of impedance, it could be used to deduce the total body water [225, 226]. This knowledge allows conclusions on the fat free mass of the patient's body [225].

1.7.5 Skin Impedance

Measurement of skin impedance can be used to detect and to classify skin cancer [227 - 232]. There are existing generally two different kinds of probes for determining differences in skin impedance, a non-invasive screening tool and a micro invasive probe, which penetrates the stratum corneum into the epidermis without touching deeper layers of skin with blood vessels and nerves. According to the position of the cancer – superficially into the stratum corneum or in between epidermal and dermal layers – the one or the other lead to better results [86 230].

Further applications for non-invasive impedance measurement of skin are diagnostic or analysis of allergic reactions [233, 234], of diabetes mellitus [235], of skin irritations [236, 237] and of skin moisture [238].

1.7.6 Impedance Cardiography

Impedance Cardiography offers non-invasive and operator-independent method to monitor cardiac output and stroke volume continuously. For this changes of bioimpedance of the thorax are measured during heartbeats with a set of four electrodes placed on neck and thorax. In this way, Bioimpedance offers a potentially great tool for diagnostic, treatment and observation of patients with cardiovascular diseases [239, 240].

1.7.7 Electrical impedance can help to determine different kinds of tissue

It is well known, that different kinds of biological material show different values of impedance. In the past, several studies and measurement were taken on this field. They are well reviewed by Durney et al [241] and Gabriel et al [242]. In table 5.2 some of the results related to human tissue are presented. They clearly show that impedance is a characteristic property of the tissue and demonstrate as well that it is strictly dependent on the signal frequency of the measurement. Furthermore, they show that blood is a very good electrical conductor, lung, skin, fat and bone conduct very poor, while liver and

muscle show an intermediate level of conductance [208, 243 -246]. This offers the possibility to determine different kind of tissues at certain frequencies.

Table 1.5: Conductivity [S/m] of Various Body Tissues

Freq. [kHz]	Ref.	Conductivity [S/m]								
		Muscle	Fat tissue	Blood	Liver	Lung	Kidney	Heart muscle	Bone	Skin
100	Rajevski/ 1938 [243]	0.85 – 1.04	0.083		0.63 – 0.87	0.77 – 1.15	0.85 – 1.0	0.78 – 0.92		0.21 – 0.625
200	Schwan and Li/ 1953 [245]	0.833 – 0.909	0.02 – 0.067	1.042	0.588 – 0.8	0.526	0.962	0.769 – 0.909		
300		0.909 – 0.952		1.11	0.645 – 0.833	0.588	0.980 – 1	0.833 – 0.952		
400		0.952 – 1	0.075 – 0.77	1.099	0.667 – 0.833	0.613	1.02	0.87 – 1		
600		1 – 1.064		1.087	0.714 – 0.909	0.641	1.064 – 1.11	0.87 – 1.053		
700		1.075 – 1.49		1.176	0.769 – 1	0.658	1.11 – 1.12	0.909 – 1.082		
900		1.19 – 1.235	0.029 – 0.091	1.25	0.73	0.73	1.22 – 1.235	1 – 1.205		
1780	Cook/ 1951 [246]	2.245	0.270						0.149	1.926
2980		2.984	0.341						0.219	2.244
3590		3.186	0.309						0.258	2.557
4630		4.808	0.381						0.335	3.606
3000	England/ 1950 [244]		0.267	2.503						2.754
9430			0.498	12.066					0.761	8.394
23620			1.445	26.28					1.445	17.082

1.8 NEEDLE AS A PROBE FOR ELECTRICAL IMPEDANCE MEASUREMENT

In the past there had been several investigations about the use of a needle as a probe for impedance measurement for medical purposes. The results collected during these studies encouraged further analysis for using a general injection needle for detection of needle-to-nerve contact in regional anaesthesia by measuring impedance. The most remarkable are reviewed below:

1.8.1 Electrical Impedance of stainless steel needle electrodes

Important work was done by Kalvøy et al in 2010 [247]. They analyzed *in vitro* stability and variability of stainless steel needle electrodes used for medical purposes. Different types of needles were treated with anodic or cathodic DC current of 1 A and then stored in a saline tank in 0.9% NaCl. Monopolar impedance spectra were measured before and after treatment as well as after 5 to 48 h of saline exposure, the saline tank was used to model the tissue. They found out that the characteristic impedance figures of the analysed needles were varying. On one hand, new needles showed different values of impedance due to electrode size, material and roughness; on the other hand impedance was decreasing after electrical treatment and increasing again after the storage in saline solution [248].

1.8.2 Stereotactic biopsy for brain tumors

In stereotactic biopsy, deep brain tumours are characterized by CT and trans-tumoral impedance monitoring. The tumour is first localized by CT imaging and then a stainless steel electrode is inserted through a small hole in the skull through a cannula. Impedance is measured during the insertion. The electrode is then removed and samples are taken with biopsy forceps at the positions identified with the impedance profile [249, 250]. Broggi and Franzini presented a study with 35 patients with deep brain tumours, treated with stereotactic biopsy. In 10 cases the results of the histological diagnosis were different from the expected one so they were able to correct and optimize the therapy planned in the earlier stages [249].

1.8.3 Impedance based tissue discrimination for needle guidance

Kalvøy et al made several investigations to use bioimpedance measurement to determine the position of a needle within different kinds of tissue. For this, they used a three-electrode setup configuration consisting of an insulated needle with conductive tip (active electrode) and two Ag/AgCl electrodes (counter and reference electrode). Reference and counter electrodes were placed on the skin of a pig; the active electrode was inserted into different kinds of tissues and organs like muscle, liver, spleen, fat etc. Current flowed between working and counter electrodes and impedance was measured at each position while the potential value was controlled between working and reference electrodes. As a result, they found out that it is possible to determine different kinds of tissues in vivo using impedance measurement and (with further research on the sensitivity of the system) could be used for needle guidance in medical purposes [247].

1.8.4 Bioimpedance used as a minimally invasive technique for cancer localisation in intact prostate

In 1997 a minimally invasive probe to localise cancer in intact prostate was developed. It consists of two insulated stainless steel needles (diameter 1 mm, length 30 mm) with the distal part of 1.0 mm in length uncoated. They are fixed in parallel configuration at a distance of 1 mm. In several studies this probe was *ex vivo* inserted into prostate tissue and impedance was measured. It was shown, that the impedance values of cancerous regions were higher compared to those of normal prostate tissue [251, 252]. Furthermore, it is possible to distinguish different gradations of tumours based on measured impedance values [252].

1.8.5 Bioimpedance for lung cancer analysis

Kimura et al designed an impedance analysis system to distinguish pulmonary mass in vivo through impedance measurement. This system was made up of a coaxial bipolar needle electrode which was connected to a counter electrode plate. The needle was inserted into skeletal muscle, pulmonary tissue and pulmonary mass while the plate electrode was placed on the lower portion of the leg. A pulsed current was applied between the outer conductive part of the needle electrode and the counter electrode and a response voltage was measured between the counter electrode and the inner conductor at each position in the tissue. The results showed that impedance of pulmonary mass and

lung cancer was lower than impedance of normal lung tissue. This offers a possibility to generate data that allows diagnosis of the pulmonary mass and (in combination with needle biopsy) to guide the tip of the biopsy needle at the right place of the lung [253].

1.8.6 Smart needle to confirm percutaneous kidney access

Hernandez et al developed a smart needle to verify a successful performance of a percutaneous kidney access. They used a modified percutaneous access needle to measure electrical impedance during the needle placement. It consisted of a metal trocar and a metal inner stylet with a sharp needle, insulated from each other by insulating coating. The distal part of the needle was uncoated for 3 mm; that enables to measure impedance at the tip. During access performance, impedance was measured and, afterwards, resistance was plotted against depth of needle. As a result, Hernandez et al found out that the graphs of resistivity versus depth of successful and unsuccessful access attempts were divergent. During a successful needle placement they observed a characteristic drop of resistivity when the needle enters the collecting system of the kidney while resistivity did not decrease below 1.5 Ωm when the procedure was unsuccessful. This confirmed that the needle could be a sensitive electrical probe that could help surgeons to confirm percutaneous access more accurately, safely and quicker. [254]

1.8.7 Impedance measurement for detection of penetration of spinal cord

In 1969, Gildenberg et al discussed the possibility to detect the entering of needle into spinal cord in anterior percutaneous cervical cordotomy using bioimpedance measurement. The principle was the fact that the impedance figures of the spinal cord were higher than of the cerebrospinal fluid but less than of the surrounding space filled with air. That was the reason why there can be observed a significant change in impedance when the needle enters the spinal cord. The probe designed for this purpose consisted of a needle electrode with a conductive tip and a Teflon coated stylet. The distal 2 mm were left uncoated. With this needle probe, impedance was measured at a frequency of 500 kHz. The observation of a change of the impedance value confirmed that the electrode reached the right position [255].

1.8.8 Electrical Impedance to distinguish intraneural from extraneural needle placement

Tsui et al have shown in 2008 [256] that there is a significant difference in bioimpedance between extraneural and intraneural tissue. For this, they connected an externally insulated needle to a nerve stimulator. It was placed directly next to the nerve and then inserted into the nerve of a pig under direct vision and under ultrasonic guidance. At both positions, impedance was measured. Impedance of extra neural tissue was significantly lower compared to neural area. As a conclusion to their investigation, Tsui et al suggested that impedance measurement could be a useful warning signal to avoid intraneural injection in the future [257].

1.9 Electrochemical measurements

Electrochemistry is the branch of chemistry that deals with the relations between electrical and chemical phenomena (Oxford dictionary). It has important applications in everyday life ranging from the battery fabrication that we use in every electronic device to the electrorefining to manufacture the copper pipes carrying drinking water in the houses. Electrochemical techniques use oxidation and reduction reactions. Oxidation happens when a chemical species loses one or more electrons while reduction implies the gain of electrons by a chemical species. When the two are combined together in a red-ox reaction, electrons can flow from the oxidized species (the reductant) to the reduced species (the oxidant). Electrons can flow spontaneously in a reaction and converted into electricity and in this is the case of a galvanic cell. When the flow is imposed using an external source it is the case of an electrolytic cell [258].

One of the techniques used for the electrodes characterization in this thesis is the cyclic voltammetry. Below there is a short description of voltammetric methods.

1.9.1 Linear Sweep Voltammetry (LSV)

Linear sweep voltammetry (LSV) uses a fixed potential range while the voltage is scanned from a lower limit to an upper limit as shown below in Figure 1.61 [259].

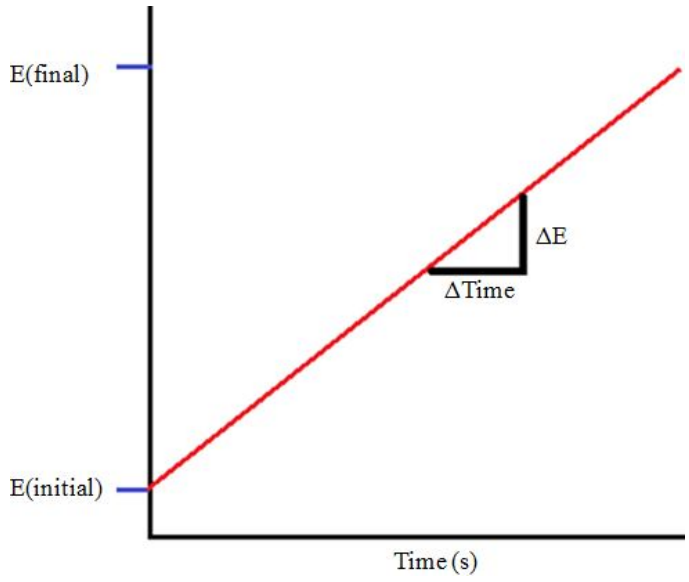

Figure 1.61: Representation of a typical LSV graph where the potential applied across the electrode-solution interface is scanned linearly from an initial value E_i to a final value E_f at a constant rate v.

In LSV the potential applied across the electrode-solution interface is scanned linearly from an initial value E_i to a final value E_f at a constant rate v.

The slope of the line depends on the voltage scan that is used in the analysis. By changing the sweep time the scan rate changes accordingly. When the potential goes towards the positive direction, (increasingly positive), it is termed as a positive scan.

The voltammograms acquired during LSV would change their aspect depending on a certain number of factors such as [259]: the rate of the electron transfer reaction(s), the chemical reactivity of the electroactive species and the voltage scan rate.

The initial potential scan E_i would not cause any reaction scanning then through the standard electrode potential(s) of the species in solution, so the reaction layer is not altered at the start by the application potential. The peak potential is the potential where the peak current is observed and is represented with Ep. All the redox species are consumed at the surface of the electrode when the peak potential is reached and diffusion is the limiting factor for the current. The amount of electron transfer between the species and the electrode is indicated by the intensity of the Faradaic current, Ipa (anodic peak current) or Ipc (cathodic peak current). The electron transmission in LSV

experiments can be regarded as a: reversible process, irreversible process or quasi-reversible process.

In reversible processes the half-wave potential ($E^{1/2}$) is equivalent to the formal potential (Eo′) and their relationship with the standard potential (Eo) is described below in equation 22:

$$E^{1/2} = E_{o\prime} = E_o + \frac{RT}{2F}\ln\frac{[O]}{[R]} \qquad (22)$$

Equation 22: The half-wave potential ($E^{1/2}$) for a reversible process is equal to the formal potential (Eo′) and their relation with the standard potential (Eo).

Where; R is the gas constant, T is the temperature (in Kelvin), F is the Faraday's constant (96485 C mol^{-1}), [O] is the concentration of oxidized species (mol L^{-1}) and [R] indicates concentration of reduced species (mol L^{-1}).

The formal redox potential can be expressed as

$$E_{o\prime} = E_{pa} + \frac{E_{pc}}{2} \quad (23)$$

Equation 23: To compute the formal redox potential

Epa is the anodic peak potential and Epc is the cathodic peak potential.

The number of electrons transmitted during a reversible process can be calculated using this equation:

$$\Delta E = E_{pc} - E_{pa} = \frac{RT}{nF} \quad (24)$$

Equation 24: To calculate the number of electrons transmitted during a reversible process

At 25° C, ΔE = 0.059V/n. *n* represents number of electrons transferred.

The peak current i_p value in a reversible process at 25°C, can be calculated using the Randles-Sevcik Equation (25):

$$i_p = 2.69 \cdot 10^5 n^{3/2} A D^{1/2} C v^{1/2} \qquad (25)$$

Equation 25: The Randles-Sevcik Equation

Where n = number of electrons transferred, A is the electrode area (cm^2), D is the diffusion coefficient (cm^2/s), C is the concentration of the species in the bulk solution (mol/cm^3) and v is the scan rate (V/s).

Through the Randles-Sevcik Equation it is possible to achieve a linear plot of Ip vs. $v^{1/2}$ for a planar diffusion [260, 261] at the surface of the electrode. If the plot loses its linearity, it indicates that oxidized, reduced or both species have participated in the chemical reaction. Irreversible processed may include only forward oxidation or reduction peak, sometimes with a weak reverse peak.

In an irreversible process the electron transfer can be very slow or show mostly sluggish chemical reactions at the electrode's end [262]. This kind of process does not follow the Nernst equation because the electron transfer is not fast enough to reach the equilibrium. I_p in this case can be calculated using the following equation:

$$i_p = (2.69 \cdot 10^5) n(\alpha n_a)^{1/2} A C D^{1/2} v^{1/2} \quad (26)$$

Equation 26: To calculate peak current, i_p, for an irreversible process.

α is the transfer coefficient, n_a is the number of electrons transferred. The peak current is still related to the bulk concentration, but it will have a lower height depending on the value of α.

ΔEp can be calculated as follows if the system is completely irreversible

$$E_p = E^0 - \left(\frac{RT}{\alpha n_a F}\right)\left[0.78 - ln\left(\frac{k^0}{D^{\frac{1}{2}}}\right) + ln\left(\frac{\alpha n_a F v}{RT}\right)^{\frac{1}{2}}\right] \quad (27)$$

Equation 27: To calculate ΔE_p for an irreversible process

Where; k^o symbolizes heterogeneous electron transfer constant (cms^{-1}).

In quasi-reversible processes, both charge transfer kinetics and mass transport play their parts in handling the current [263, 264] as these kinds of processes lie in between the reversible and irreversible ones. A quasi-reversible process takes place when the relative rate of electron transfer with reference to that of mass transport is incapable of achieving Nernst equilibrium at the surface of the electrode. During quasi-reversible process, $\upsilon^{1/2}$

increases with the Ip but not in a linear way, and an increase in $\Delta E > 59/n$ mV is observed when υ increases.

1.9.2 Cyclic Voltammetry

Cyclic voltammetry (CV) is possibly the most common electrochemical technique used for the description of red-ox systems. This method observes electron transfer throughout reactions, providing data concerning kinetics and formal reduction, reversibility, stability and oxidation potentials of a system [265]. CV is an extension of the LSV concept, so the same theory and equations formulated are valid for both techniques.

CV is a quick and convenient method for the evaluation of redox potentials, redox species and for determining the effects of media on the redox process. In CVs, the current that flows between the electrode of interest (the potential is monitored with respect to a reference electrode) and the counter electrode, is measured with the aid of a potentiostat. On the voltammetry plot it is possible to determine the potentials at which the different electrochemical processes occur. The working electrode is subjected to a triangular potential sweep: the potential rises from a start value Ei to a set final value Ef then returns back to the starting potential at a constant potential sweep rate. To complete a CV analysis, single or multiple cycles can be executed depending on the information required and the sweep rate applied can range from a few millivolts per second to a hundred volts per second. The current measured during a CV is normalised to the electrode surface area and referred to as the current density. This is then plotted against the applied potential, and the resulting graph is referred to as a cyclic voltammogram [266]. Every electrode has a characteristic potential at which the reaction takes place and there a peak in the measured current can be observed. The width and height of the peak for a particular process are strictly dependent on the sweep rate, electrolyte concentration and the electrode material [267].

Cyclic voltammetry provides information about the kinetics of electrochemical reactions taking place at electrode surfaces [268]. In a voltammogram, there could be several different peaks. By analysing the sweep-rate dependence of the peak amplitudes, widths and potentials of the peaks observed in the plot, it is possible to investigate the role of diffusion, adsorption, and coupled homogeneous chemical reaction mechanisms [269]. The most important parameters of a cyclic voltammetry are the peak currents i_{pa} (anodic

peak current) and i_{pc} (cathodic peak current) magnitude and the potentials at which the E_{pa} and E_{pc} peaks occur.

A reversible system will contain all of these parameters thus CV can be also used as a method for determining whether a system is reversible or not. A red-ox couple in which both the oxidative and reductive species exchange electrons with the working electrode is defined as an electrochemically reversible couple, and in a cyclic voltammogram it is possible to recognise the presence of two peaks, one for the oxidation and one for the reduction; the potential difference between the potentials of these two peaks can be expressed as:

$$\Delta E = E_{pa} - E_{pc} \approx \frac{0.058}{n} \quad (28)$$

Equation 28: Electrochemically reversible couple

n is the number of electrons transferred. The value in the formula (0.058/n V) is independent of scan rate for a reversible couple but is, to some extent, dependent on the cycle number and switching potential. If the scan rate is increased, the anodic and cathodic peak potentials both increase proportionally with the scan rate. For an irreversible couple, instead, the anodic and cathodic peak potentials plotted versus the scan rate are linear with the intercepts at the origin. The values of i_{pa} and i_{pc} should be similar in magnitude for a reversible couple with no kinetic complications, i.e., $i_{pa}/i_{pc} \approx 1$.

The irreversibility is caused by the slow electron exchange of the redox species with the working electrode; the separation peak potential is bigger than 0.058/n V and is dependent on the scan rate value. The presence of a single peak in the voltammogram (i_{pa} or i_{pc}) is usually a strong clue of irreversibility. In quasi-reversible Voltammograms of a system are more stretched and show a larger separation in peak potentials compared to those of a reversible system [263]. In these systems, the current is controlled by both the mass transport and the charge transfer. Figure 1.62 shows a typical potential-time excitation signal for voltammetry and a cyclic voltammogram for a reversible process while Figure 1.63 shows cyclic voltammograms for irreversible and quasi-reversible redox processes.

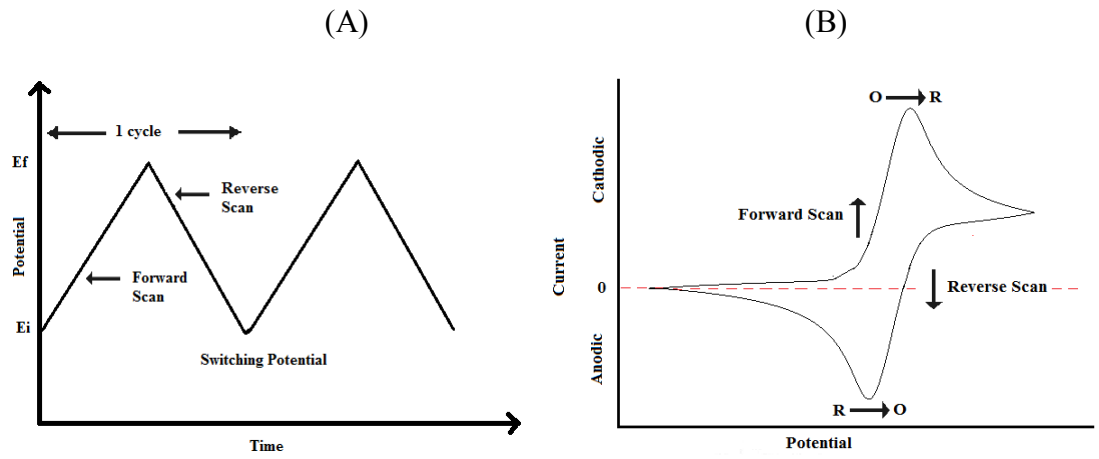

Figure 1.62: (A) Typical potential-time excitation signal for voltammetry, where E_i is the initial potential and E_f is the final potential, and (B) is a typical voltammogram for a reversible process.

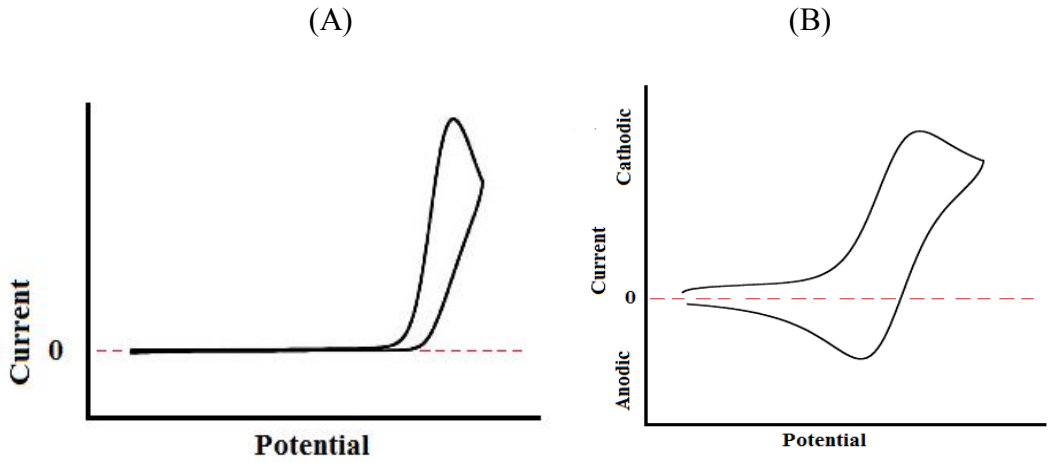

Figure 1.63: (A) Typical voltammogram for an irreversible process and (B) is a typical voltammogram for a quasi-reversible process.

1.10 REFERENCES

[1] J. Fraden, "Handbook of Modern Sensors: Physics, Designs, and Applications", 4th ed. 2010, p 1-11, Springer Ed.

[2] Kumari S. et al, "Types of Sensors and Their Applications", International Journal of Engineering Research and Development, Vol. 10, Issue 4 2014, PP.72-85

[3] "Sensors: Types and Characteristics", Academic Resource Center, Illinois Institute of Technology, http://iit.edu/arc/workshops/pdfs/SENSORS.pdf

[4] Anthony P. F. Turner, "Biosensors: sense and sensibility", Chem. Soc. Rev., 2013, 42, 3184

[5] Gamba J., "The role of transport phenomena in whispering gallery mode optical biosensor performance", California Institute of Technology, Thesis, Ch. 2

[6] X. Huang, D.W. Greve, I Nausieda, D. Nguyen and M.M. Domach, "Impedance-based Biosensors", Carnegie Mellon University, Pittsburgh, PA, USA

[7] Christiane Ziegler, "Cantilever-based biosensors", Anal Bioanal Chem (2004) 379: 946–959, Springer-Verlag

[8] K.A. Marx, "Quartz Crystal Microbalance: A Useful Tool for Studying Thin Polymer Films and Complex Biomolecular Systems at the Solution-Surface Interface", Biomacromolecules, American Chemical Society Vol. 4, N. 5

[9] R.P. Buck, "Bioanalytic sensors, The Biomedical Engineering Handbook", 2nd edition Volume 1, J. Bronzino, Springer-Verlag 2000

[10] J. Tokas, "Biosensors: general principles and applications", PITT, University Of Pittsburgh Supercourse Lecture presentation 2009

[11] Nada F. Atta, Ahmed Galal and Shimaa Ali, "Nanobiosensors for health care, Biosensors for Health,Environment and Biosecurity", P. A. Serra (Ed.), ISBN: 978-953-307-443-6, InTech(2011).

[12] M. A. Iqbal, S.G. Gupta, Hussaini S.S., "A Review on Electrochemical Biosensors: Principles and Applications", Advances in Bioresearch Volume 3, December 2012: 158 - 163© 2012 Society of Education, India

[13] N. Jaffrezic-Renault, S. V. Dzyadevych, "Conductometric Microbiosensors for Environmental Monitoring", Sensors 2008, 8, 2569-2588

[14] J. P. Chambers, B. P. Arulanandam, L. L. Matta, A. Weis, J. J. Valdes, "Biosensor Recognition Elements", Curr. Issues Mol. Biol., 2008, 10: 1–12.

[15] J.R. Rao, C. Fleming, J. Moore, "Molecular Diagnostics: Current Technology and Applications, Horizon Scientific Press, 2006

[16] Rensselaer Polytechnic Institute - Troy, NY USA, Chemistry Dept., Biotech-environment lecture notes http://www.rpi.edu/dept/chem-eng/Biotech-Environ/BIOSEN/enzbio.htm

[17] http://sst-web.tees.ac.uk/external/u0003076/BIOSENSORS_WEB/antibody/AGAB1.htm, Lecture notes, Rob Cumming, Microbiology, School of Science and Technology, Univ. of Teesside

[18] Moina C., Ybarra G., "Fundamentals and Applications of Immunosensors, Advances in Immunoassay Technology", Dr. Norman H. L. Chiu (Ed.), ISBN: 978-953-51-0440-7, InTech, (2012).

[19] K. Odenthal, J. Gooding, "An introduction to electrochemical DNA biosensors", Analyst, 2007, 132, 603–610

[20] A.M. Oliveira Brett, "DNA-based biosensors, Biosensors and Modern Biospecific Analytical Techniques", Ed. L. Gorton, ISBN: 978-0-444-50715-0, Pages 179-208

[21] Banerjee P., Bhunia A. K., "Mammalian cell-based biosensors for pathogens and toxins", Trends Biotechnol. 2009 Mar; 27(3):179-88.

[22] Betancourt T., Brannon-Peppas L., "Micro- and nanofabrication methods in nanotechnological medical and pharmaceutical devices", International Journal of Nanomedicine 2006:1(4) 483–495© 2006 Dove Medical Press Limited.

[23] Ziaie B., Antonio B., M. Z. Atashbar, "Introduction to Micro-/Nanofabrication", Springer Handbook of Nanotechnology, Editor: Prof. Bharat Bhushan, 2010, Springer-Verlag Berlin Heidelberg

[24] Pan T., Wang W., "From Cleanroom to Desktop: Emerging Micro-Nanofabrication Technology for Biomedical Applications", Annals of Biomedical Engineering, Vol. 39, No. 2, 2011 pp. 600–620

[25] Madou M. J., "Fundamentals of Microfabrication: The Science of Miniaturization", (2nd ed.). Boca Raton: CRC Press, 2002.

[26] Zhang G., Wang D., "Colloidal Lithography - The Art of Nanochemical Patterning", Chem. Asian J. 2009, 4, 236 – 245

[27] Yang, S. M., et al., "Nanomachining by colloidal lithography", Small, 2006. 2(4): p. 458-475.

[28] Colson P., "Nanostructuration induced by self-organization of polystyrene nanospheres as a template for the controlled growth of functional materials", University Of Liege, Thesis Ch. 1, 2011

[29] Kumar A., Whitesides G.M., "Features of gold having micrometer to centimeter dimensions can be formed through a combination of stamping with an elastomeric stamp and an alkanethiol "ink" followed by chemical etching", Appl. Phys. Lett. 63 (14), 4 October. 1993

[30] Xia Y., Tien J., Qin D., Whitesides G.M., "Non-photolithographic methods for fabrication of elastomeric stamps for use in microcontact printing", Langmuir Volume 12, No. 16, p 4033-4038

[31] Wilbur J.L., Kim E., Xia Y., G.M. Whitesides, "Lithographic Molding: A Convenient Route to Structures with Sub-Micrometer Dimensions", Adv. Mater. 1995, Volume 7, No. 7

[32] Clarson S.J., Semlyen J.A., "Siloxane Polymers". Englewood Cliffs, NJ: Prentice Hall 1993.

[33] Xia Y. and Whitesides G. M., "Soft Lithography", Annu. Rev. Mater. Sci. 1998. 28:153–84

[34] Xia Y., Whitesides G. M., "Soft lithography", Angewandte Chemie, International Edition 37, 550–575 (1998).

[35] Quist A. P., Pavlovic E., Oscarsson S., "Recent advances in microcontact printing", Anal. Bioanal. Chem. 381, 591–600 (2005).

[36] Weibel D. B. et al., "Bacterial printing press that regenerates its ink: Contact-printing bacteria using hydrogel stamps", Langmuir 21, 6436–6442 (2005).

[37] Delamarche E., "Microcontact printing of proteins", Nanobiotechnol. 31–52 (2004).

[38] Weibel D.B., DiLuzio W.R., Whitesides G.M., "Microfabrication meets microbiology", Nature reviews, Microbiology Volume 5, March 2007, 209.

[39] Wolfe D.B., Love J.C., Paul K.E., Chabinyc M.L., Whitesides G.M., "Fabrication of palladium-based microelectronic devices by microcontact printing", Appl. Phys. Lett. 80:2222–24, 2002.

[40] D. Losic, J. J. Gooding, J. G. Shapter, "Influence of Surface Topography on Alkanethiols SAMs Assembled from Solution and by Microcontact printing", Langmuir, 2001, 17, 3307-3316

[41] Gates B. D., Xu Q., Love J. C., Wolfe D. B., G. M. Whitesides, "Unconventional Nanofabrication", Annu. Rev. Mater. Res. 2004, 34:339–72

[42] Haverkorn von Rijsewijk H.C., Legierse P.E.J., Thomas G.E., "Manufacture of LaserVision video disks by a photopolymerization process", 1982. Philips Tech. Rev 40:287–97

[43] Wuff G., "Molecular Imprinting in Cross-Linked Materials with the Aid of Molecular Templates— A Way towards Artificial Antibodies", Angew. Chem. Int. Ed. Engl. 34:1812–32 1995.

[44] Rogers J.A., Paul K.E., Jackman R.J., Whitesides G.M., "Using an Elastomeric Phase Mask for sub-100 nm Photolithography in the Optical Near Field", Appl. Phys. Lett., 1997, 70, 2658-2660

[45] M. C. Hutley, "Diffraction Gratings", Academic Press (New York, 1982), p. 29

[46] M. Nakano, N. Nishida, "Holographic laser scanners using generalized zone plates", Appl. Opt., 18 (3073-3074) 1979

[47] Kiewit A., "Microtool fabrication by etch pit replication", Rev. Sci. Instrum. 44 (1741-1742) 1973

[48] Kim E., Xia Y., Whitesides G. M., "Micromolding in Capillaries: Applications in Materials Science", Nature 1995, 376, 581.

[49] Martin C. R., "Nanomaterials: a membrane-based synthetic approach", Science. 1994 Dec 23; 266(5193):1961-6.

[50] Pisignano D. I., Sariconi E., Mazzeo M., Gigli G., Cingolani R., "High-Temperature Microfluidic Lithography", Adv. Mater. 2002, 14, 1565

[51] Zhao X. M., Xia Y., Whitesides G. M., "Fabrication of Three-Dimensional Micro-Structures: Microtransfer Molding", Adv. Mater., 1996, 8, 837-840.

[52] Leung W. Y., Kang H., Constant K., Cann D., Kim C. H., Biswas R., Sigalas M. M. Ho K. M., "Fabrication of photonic band gap crystal using microtransfer molded templates", J. Appl. Phys. 2003, 93, 5866.

[53] Handbook of Microlithography, Micromachining and Microfabrication, Editor P.R. Choudhury, SPIE Press Monograph PM 39 (Chapter 2 Electron Beam Lithography, M.A. McCord, Stanford University and M.J. Rocks, Cornell University)

[54] Altissimo M., "E-beam lithography for micro-/nanofabrication", Biomicrofluidics 4, 026503, 2010 American Institute of Physics

[55] Handbook of thin-film deposition processes and techniques, Principles, Methods, Equipment and Applications, 2nd Edition, Krishna Seshan Intel Corporation Santa Clara, California, Noyes Publications, William Andrew Publishing, Norwich, New York, U.S.A. 2002

[56] Bunshah R. F., "Deposition Technologies for Films and Coatings: Developments and Applications", Noyes Publications, Park Ridge, NJ (1982)

[57] Ghandhi S. K., "VLSI Fabrication Principles", John Wiley & Sons, New York (1983)

[58] Maissel L. I., Clang R., (eds.), "Handbook of Thin Film Technology", Ch. 2, McGraw-Hill, New York (1970)

[59] Howard, R. E., W. J. Skocpol, et al. (1986). "Nanostructures" Annual Review of Materials Science 16(1): 441-466.

[60] H. Yoshimotoa, Y.M. Shina, H. Teraia, J.P. Vacantia, "A biodegradable nanofiber scaffold by electrospinning and its potential for bone tissue engineering", Biomaterials 24 (2003) 2077–2082

[61] Vasita R., Katti D. S., "Nanofibers and their applications in tissue engineering", International Journal of Nanomedicine 2006:1(1) 15–30

[62] Ji L., Zhang X., "Fabrication of porous carbon nanofibers and their application as anode materials for rechargeable lithium-ion batteries", Nanotechnology 20 (2009) 155705 (7pp)

[63] L. Zhang, A. Aboagye, A. Kelkar, C. Lai, H. Fong, "A review: carbon nanofibers from electrospun polyacrylonitrile and their applications", J Mater Sci (2014) 49:463–480

[64] Bogart L. et al., "Nanoparticles for Imaging, Sensing and Therapeutic Intervention", ACS Nano, VOL. 8, NO. 4, 3107–3122, 2014

[65] S. Chapman et al., "Nanoparticles for cancer imaging: The good, the bad, and the promise", Nano Today (2013) 8, 454—460

[66] K. S. Soppimatha et al., "Biodegradable polymeric nanoparticles as drug delivery devices", Journal of Controlled Release 70 (2001) 1–20

[67] K. Cho, X. Wang, S. Nie, et al., "Therapeutic Nanoparticles for Drug Delivery in Cancer", Clin. Cancer Res. 2008;14:1310-1316.

[68] W. Li, D. Xu, Y. Hu, K. Cai, Y. Lin, "Surface modification of titanium substrates with silver nanoparticles embedded sulfhydrylate chitosan/gelatin polyelectrolyte multilayer films for antibacterial application", J Mater Sci: Mater Med (2014) 25:1435–1448

[69] D. Bera, L. Qian, T. Tseng, P. H. Holloway, "Quantum Dots and Their Multimodal Applications: A Review", Materials 2010, 3, 2260-2345;

[70] S. Iijima, "Helical microtubules of graphitic carbon", Letters to Nature, Volume 354, November 1991

[71] M. Meo, M. Rossi, "Prediction of Young's modulus of single wall carbon nanotubes by molecular-mechanics based finite element modeling", Composites Science and Technology 66 (2006) 1597–1605

[72] S. J. Tanders, "Individual Single Wall Carbon Nanotubes As Quantum Wires", Letters to Nature, Volume 386, April 1997

[73] R. B. Weisman, "Optical Spectroscopy of Single-Walled Carbon Nanotubes", Contemporary Concepts of Condensed Matter Science, Carbon Nanotubes: Quantum Cylinders of Graphene, 3 2008: 109-133

[74] S. Berber, Y. Kwon, D. Tománek, "Unusually High Thermal Conductivity of Carbon Nanotubes", Physical Review Letters, Volume 84, Number 20, 2000

[75] Y. Ando, X. Zhao, "Synthesis of Carbon Nanotubes by Arc-Discharge Method", New Diamond and Frontier Carbon Technology, Vol. 16, No. 3 2006

[76] A. M. Morales, C. M. Lieber, "A Laser Ablation Method for the Synthesis of Crystalline Semiconductor Nanowires", Science, Vol. 279, 9 January 1998

[77] M. Kumar, Y. Ando, "Chemical Vapor Deposition of Carbon Nanotubes: A Review on Growth Mechanism and Mass Production", Journal of Nanoscience and Nanotechnology, Vol. 10, 3739–3758, 2010

[78] G. Che, B. B. Lakshmi, C. R. Martin, E. R. Fisher, "Chemical Vapor Deposition Based Synthesis of Carbon Nanotubes and Nanofibers Using Template Method", Chem. Mater. 1998, 10, 260-267

[79] A. Szabó et al., "Synthesis Methods of Carbon Nanotubes and Related Materials", Materials 2010, 3, 3092-3140

[80] Wu, W., D. Dey, et al. (2008). "A Novel Self-aligned and Maskless Process for Formation of Highly Uniform Arrays of Nanoholes and Nanopillars." Nanoscale Research Letters 3(3): 123 - 127.

[81] Schröper, F., D. Brüggemann, et al. (2008). "Analyzing the electroactive surface of gold nanopillars by electrochemical methods for electrode miniaturization." Electrochimica Acta 53(21): 6265-6272.

[82] Palacios, R., P. Formentin, et al. (2011). "Beta-Phase Morphology in Ordered Poly(9,9-dioctylfluorene) Nanopillars by Template Wetting Method." Nanoscale Res Lett 6(1): 35.

[83] Shin, C. S., W.; Hong, H.G. (2007). " Electrochemical fabrication and electrocatalytic characteristics studies of gold nanopillar array electrode (AuNPE) for development of a novel electrochemical sensor. ." Electrochim. Acta 2007, (53, 720-728).

[84] Santos, A., P. Formentín, et al. (2010). "Fabrication and characterization of high-density arrays of P3HT nanopillars on ITO/glass substrates." Solar Energy Materials and Solar Cells 94(7): 1247-1253.

[85] Stranz, A., Ü. Sökmen, et al. (2010). "Fabrication and Characterization of Nanopillars for Silicon-Based Thermoelectrics." Journal of Electronic Materials 39(9): 2013-2016.

[86] Nomura, S., H. Kojima, et al. (2006). "Nanopillar sheets as a new type of cell culture dish: detailed study of HeLa cells cultured on nanopillar sheets." Journal of Artificial Organs 9(2): 90-96.

[87] G. Panaitov, S. T., B. Hofmann, A. Offenhäusser. 2011. Fabrication of gold micro-spine structures for improvement of cell/device adhesion. Microelectron. Eng. 88, 8 (August 2011), 1840-1844.

[88] Chang, Y. F., Q. R. Chou, et al. (2007). "Fabrication of high-aspect-ratio silicon nanopillar arrays with the conventional reactive ion etching technique." Applied Physics A 86(2): 193-196.

[89] Wolfrum, B., Y. Mourzina, et al. (2006). "Fabrication of Large-Scale Patterned Gold-Nanopillar Arrays on a Silicon Substrate Using Imprinted Porous Alumina Templates." Small 2(11): 1256-1260.

[90] Cheung, C. L., R. J. Nikolić, et al. (2006). "Fabrication of nanopillars by nanosphere lithography." Nanotechnology 17(5): 1339.

[91] Sanetra, N., V. Feig, et al. (2011). "Low impedance surface coatings via nanopillars and conductive polymers." physica status solidi (a) 208(6): 1284-1289.

[92] Hu, W., A. S. Crouch, et al. (2010). "Inhibited cell spreading on polystyrene nanopillars fabricated by nanoimprinting and in situ elongation." Nanotechnology 21(38).

[93] Kouklin, N. A. and J. Liang (2006). "Ultradense GaN nanopillar and nanopore arrays by self-assembly nanopatterning." Journal of Electronic Materials 35(5): 1133-1137.

[94] Hsu, C.-M., S. T. Connor, et al. (2008). "Wafer-scale silicon nanopillars and nanocones by Langmuir--Blodgett assembly and etching." Applied Physics Letters 93(13): 133109-133103.

[95] Kuo, C.-W., J.-Y. Shiu, et al. (2010). "Polymeric nanopillar arrays for cell traction force measurements." ELECTROPHORESIS 31(18): 3152-3158.

[96] K. C. Cheung, Y. K. Choi, T. Kubow, and L. P. Lee, "Nanostructured electrodes for improved neural recording," in Proc. Mater. Res. Soc., 2002, pp. 191–196.

[97] Brüggemann, D., B. Wolfrum, et al. (2011). "Nanostructured gold microelectrodes for extracellular recording from electrogenic cells." Nanotechnology 22(26): 265104.

[98] Hanson, L., C. Xie, et al. (2011). "Vertical Nanopillars for Biointerface: Cell Interactions with Inorganic Nanostructures." Biophysical Journal 100(3, Supplement 1): 473a.

[99] Haq F, Venkatramani A, Keith C, Zhang G., "Neurite development in PC12 cells cultured on nanopillars and nanopores with sizes comparable with filopodia", Int J Nanomed. 2007; 2(1):107–115.

[100] Arnold, M., E. A. Cavalcanti-Adam, et al. (2004). "Activation of Integrin Function by Nanopatterned Adhesive Interfaces." ChemPhysChem 5(3): 383-388.

[101] Sjöström, T., G. Lalev, et al. (2011). "Initial attachment and spreading of MG63 cells on nanopatterned titanium surfaces via through-mask anodization." Applied Surface Science 257(10): 4552-4558.

[102] Brammer, K. S., C. Choi, et al. (2011). "Hydrophobic nanopillars initiate mesenchymal stem cell aggregation and osteo-differentiation." Acta Biomaterialia 7(2): 683-690.

[103] Fozdar DY., L. Jae Young, et al. (2010). "Hippocampal neurons respond uniquely to topographies of various sizes and shapes." Biofabrication 2(3): 035005.

[104] Venkataramani Anandan, Yeswanth L Rao, Guigen Zhang (2006). "Nanopillar array structures for enhancing biosensing performance" Int J Nanomedicine. March; 1(1): 73–79.

[105] Rajan, G., A. Venkataramani, et al. (2008). "Optimizing the functionalization process for nanopillar enhanced electrodes with GOx/PPY for glucose detection." Nanotechnology 19(39): 395501.

[106] Anandan, V., X. Yang, et al. (2007). "Role of reaction kinetics and mass transport in glucose sensing with nanopillar array electrodes." Journal of Biological Engineering 1(1): 5.

[107] Murthy, B. R., J. K. K. Ng, et al. (2008). "Silicon nanopillar substrates for enhancing signal intensity in DNA microarrays." Biosensors and Bioelectronics 24(4): 723-728.

[108] Wang, S., H. Wang, et al. (2009). "Three-Dimensional Nanostructured Substrates toward Efficient Capture of Circulating Tumor Cells." Angewandte Chemie International Edition 48(47): 8970-8973.

[109] Xie, C., L. Hanson, et al. (2011). "Vertical nanopillars for highly localized fluorescence imaging." Proceedings of the National Academy of Sciences 108(10): 3894-3899.

[110] Fan, Z., D. Ruebusch, et al. (2009). "Challenges and prospects of nanopillar-based solar cells." Nano Research 2(11): 829-843.

[111] Wong, S. M., H. Y. Yu, et al. (2011). "Si Nanopillar Array Surface-Textured Thin-Film Solar Cell with Radial p-n Junction." Electron Device Letters, IEEE 32(2): 176-178.

[112] Ryder DA, Tucker RT, et al. (2011). "Indium tin oxide nanopillar electrodes in polymer/fullerene solar cells." Nanotechnology 22(8): 085706.

[113] Mariani, G., P.-S. Wong, et al. (2011). "Patterned Radial GaAs Nanopillar Solar Cells." Nano Letters 11(6): 2490-2494.

[114] Kapadia, R., Z. Fan, et al. (2012). "Nanopillar photovoltaics: Materials, processes, and devices." Nano Energy 1(1): 132-144.

[115] Fan, Z., H. Razavi, et al. (2009). "Three-dimensional nanopillar-array photovoltaics on low-cost and flexible substrates." Nat Mater 8(8): 648-653.

[116] Kubo, W. and S. Fujikawa (2010). "Au Double Nanopillars with Nanogap for Plasmonic Sensor." Nano Letters 11(1): 8-15

[117] Manimaran, M., P. R. Vaya, et al. (2000). "Electroluminescent device based on AlxGa1xAs-GaAs quantum well nanostructures." Optical and Quantum Electronics 32(10): 1191-1199.

[118] Tang, Y.-H., M.-J. Huang, et al. (2011). "Fabrication of silicon nanopillar arrays and application on direct methanol fuel cell." Microelectronic Engineering 88(8): 2580-2583.

[119] Chang, S.-w., J. Oh, et al. (2010). "Fabrication of silicon nanopillar-based nanocapacitor arrays." Applied Physics Letters 96(15): 153108-153103.

[120] Ji, L., Z. Tan, et al. (2011). "Multilayer nanoassembly of Sn-nanopillar arrays sandwiched between graphene layers for high-capacity lithium storage." Energy & Environmental Science 4(9): 3611-3616.

[121] Xie, C., L. Hanson, et al. (2010). "Noninvasive Neuron Pinning with Nanopillar Arrays." Nano Letters 10(10): 4020-4024

[122] Bucaro, M. A., Y. Vasquez, et al. (2012). "Fine-Tuning the Degree of Stem Cell Polarization and Alignment on Ordered Arrays of High-Aspect-Ratio Nanopillars." ACS Nano.

[123] Choi, C. K., A. E. English, et al. (2007). "An endothelial cell compatible biosensor fabricated using optically thin indium tin oxide silicon nitride electrodes." Biosensors and Bioelectronics 22(11): 2585-2590.

[124] Purwanto, A., H. Widiyandari, et al. (2009). "Facile Method for the Fabrication of Vertically Aligned ITO Nanopillars with Excellent Properties." Chemistry of Materials 21(18): 4087-4089.

[125] Ghassemi S., O. Rossier, et al. (2009), Gold-tipped elastomeric pillars for cellular mechanotransduction, AVS.

[126] Kim D., H. Lee, et al. (2007). "Replication of high-aspect-ratio nanopillar array for biomimetic gecko foot-hair prototype by UV nano embossing with anodic aluminum oxide mold." Microsystem Technologies 13(5-6): 601-606.

[127] Feng J.-J., Y.-H. Lu, et al. (2010). "Electrosynthesis of SER-Active Silver Nanopillar Electrode Arrays" The Journal of Physical Chemistry C 114(16): 7280-7284.

[128] Kaji, N., Y. Tezuka, et al. (2003). "Separation of Long DNA Molecules by Quartz Nanopillar Chips under a Direct Current Electric Field." Analytical Chemistry 76(1): 15-22.

[129] Dr. Rabbani Armaan M., Online presentation "Cell-based assay and CHO cells", Author stream.com (arsh29), October 2011

[130] Oxoid Microbiology Products, Technical support, Formulation of culture Media, development and manufacture, oxoid.com

[131] Davis J.M., "Animal cell culture essential methods", p91-151, Ed. Wiley-Blackwell, Chichester 2011

[132] William H. Heidcamp, "Cell Biology Laboratory Manual", Gustavus Adolphus College, Saint Peter, Minnesota, USA

[133] Liu Q. et al., "Cell-Based Biosensors and Their Application in Biomedicine", Chem. Rev. 2014, 114, 6423−6461

[134] Hu N., Wu C., Ha D., Wang T., Liu Q., Wang P., "A novel microphysiometer based on high sensitivity LAPS and microfluidic system for cellular metabolism study and rapid drug screening", Biosensors and Bioelectronics, Vol. 40, Iss. 1, 2013, P. 167–173

[135] Hafner F., "Cytosensor Microphysiometer: Technology and recent applications", Biosensors and Bioelectronics, 2000; Vol. 15: 149–58.

[136] P. Wang et al., "Cell-based biosensors and its application in biomedicine" Sensors and Actuators B 108 (2005) 576–584

[137] C. Ziegler**, "**Cell-based biosensors", Fresenius J Anal. Chem. (2000) 366 :552–559

[138] Chen P.H., Zhang W., Zhou J., Wang P., Xiao L.D., Yang M., "Development of planar patch clamp technology and its application in the analysis of cellular electrophysiology". Progress in Natural Science, 19(2), 153-160 (2009)

[139] Py C., Denhoff M. W., Martina M., Monette R., Comas, T., Ahuja T., Martinez, D., Wingar S., Caballero J., Laframboise S., "A novel silicon patch-clamp chip permits high-fidelity recording of ion channel activity from functionally defined neurons", Biotechnology and Bioengineering 2010, 107, 593.

[140] Fertig N., Klau M., George M., Blick R. H., Behrends J. C., "Activity of single ion channel proteins detected with a planar microstructure", Applied Physics Letters 2002, 81, 4865.

[141] Klemic K. G., Klemic J. F., Reed M., Sigworth F. J., "Micromolded PDMS planar electrode allows patch clamp electrical recordings from cells", Biosensors and Bioelectronics, Vol. 17, Iss. 6–7, 2002, P. 597–604

[142] Mayer M., Kriebel J. K., Tosteson M. T., Whitesides G. M., "Microfabricated teflon membranes for low-noise recordings of ion channels in planar lipid bilayers", Biophys. J. 2003, 85, 2684.

[143] P. Wang, Q. Liu, "Cell-Based Biosensors, Principles and Applications", Artech House, London, 2010

[144] Kim H. et al., "Large Area Two-Dimensional B Cell Arrays for Sensing and Cell-Sorting Applications", Biomacromolecules, Vol. 5, 2004, pp. 822–827.

[145] Giaever I., Keese C.R., "Use of electric fields to monitor the dynamical aspect of cell behavior in tissue culture", Biomedical Engineering, IEEE Transactions on BME-33 (2), (1986) 242-247.

[146] Ehret R., Baumann W., Brischwein M., Schwinde A., Stegbauer K., Wolf B., "Monitoring of cellular behaviour by impedance measurements on interdigitated electrode structures", Biosensors and Bioelectronics, 12(1):29-41 (1997).

[147] X. Huang, D.W. Greve, D. D.Nguyen, M.M. Domach, "Impedance Based Biosensor Array for Monitoring Mammalian Cell Behavior", Sensors, 2003, Proceedings of IEEE, 304 - 309 Vol.1

[148] L. Ceriotti et al., **"**Online monitoring of BALB/3T3 metabolism and adhesion with multiparametric chip-based system", Analytical Biochemistry 371 (2007) 92–104

[149] Giaever I., Keese C.R., **"**Use of Electric Fields to Monitor the Dynamical Aspect of Cell Behavior in Tissue Culture", IEEE Transactions on biomedical engineering, Vol. BME-33, No. 2, February 1986

[150] J. Wegener, M. Sieber, H. J. Galla, "Impedance analysis of epithelial and endothelial cell monolayers cultured on gold surfaces", J. Biochem. Biophys. Methods 32 (1996) 151-170

[151] Giaever I., Keese C.R., "Micromotion of mammalian cells measured electrically", Proc. Natl. Acad. Sci. USA Vol. 88, pp. 78%-7900, September 1991

[152] N. Eisei et al., **"**Podokinesis in endothelial cell migration: role of nitric oxide", *Am. J. Physiol.* 274 (*Cell Physiol.* 43): C236–C244, 1998

[153] Keese C.R., Giaever I., "A Biosensor that Monitors Cell Morphology with Electrical Fields", IEEE Engineering in medicine and biology, July 1994

[154] S. Arndt et al., "Bioelectrical impedance assay to monitor changes in cell shape during apoptosis", Biosensors and Bioelectronics 19 (2004) 583–594

[155] C. Xiao, J. H.T. Luong, "Assessment of cytotoxicity by emerging impedance spectroscopy", Toxicology and Applied Pharmacology 206 (2005) 102– 112

[156] J.H. Yeon, J.K. Park, "Cytotoxicity test based on electrochemical impedance measurement of HepG2 cultured in microfabricated cell chip", Analytical Biochemistry 341 (2005) 308–315

[157] E. Moore, O. Rawley, T. Wood, P. Galvin, "Monitoring of cell growth *in vitro* using biochips packaged with indium tin oxide sensors", Sensors and Actuators B 139 (2009) 187–193

[158] Cuvelier D. et al., "The Universal Dynamics of Cell Spreading," Curr. Biol., Vol. 17, No. 8, 2007, pp. 694–699.

[159] Noiri E. et al., "Permissive Role of Nitric Oxide in Endothelin-Induced Migration of Endothelial Cells", J. Biol. Chem., Vol. 272, No. 3, 1997, pp. 1747–1752.

[160] C. R. Keese et al., "Electrical wound-healing assay for cells in vitro", PNAS, February 10, 2004, vol. 101 no. 6

[161] L. Ceriotti et al., "Assessment of cytotoxicity by impedance spectroscopy", Biosensors and Bioelectronics 22 (2007) 3057–3063

[162] Autolab Application Note EIS06, Electrochemical Impedance Spectroscopy (EIS) Part 6 – Measuring raw signals in EIS

[163] D. Strik et al., "Feasibility Study on Electrochemical Impedance Spectroscopy for Microbial Fuel Cells: Measurement Modes & Data Validation", ECS Transactions, 13 (21) 27-41 (2008)

[164] E. Barsoukov, J.R. Macdonald, eds., "Impedance Spectroscopy; Theory, Experiment, and Applications", 2nd ed., Wiley Interscience Publications, 2005

[165] A.J. Bard, L.R. Faulkner, "Electrochemical Methods; Fundamentals and Applications", Wiley Interscience Publications 2000.

[166] Dr. Burak Ulgut, Webinar "Electrochemical Impedance Spectroscopy and Its Applications to Battery Analysis", Gamry Instrument, February, 2014

[167] Lectures at International Workshop on Impedance Spectroscopy 2014 (European Edition), Castellón (Spain) June 2014. Chaired by Prof. Francisco Fabregat Santiago from Universitat Jaume I, Spain, ISSchool-CS14 Conference.

[168] Application notes for Metrohm Autolab, http://www.ecochemie.nl/Applications/

[169] Giaever I., Keese C.R., "Monitoring fibroblast behavior in tissue culture with an applied electric field", Proc. Natl. Acad. Sci. USA, Vol. 81, pp. 3761-3764, June 1984

[170] K. Benson, S. Cramer HJ Galla, "Impedance-based cell monitoring: barrier properties and beyond", Fluids and Barriers of the CNS 2013, 10:5

[171] W.G. Jiang (Ed.), "Electric Cell-Substrate Impedance Sensing and Cancer Metastasis
Series: Cancer Metastasis - Biology and Treatment", Vol. 17, Springer

[172] Giaever I., Keese C.R., "Toxic? Cells can tell", Chemtech, 116-125 (Feb. 1992).

[173] Keese C. R., Karra N., Dillon B., Goldberg A. M., Giaever I., "Cell-Substratum Interactions as a Predictor of Cytotoxicity", In vitro and molecular toxicology; 11, 2; 183-192

[174] F. Asphahani et al., "Single-cell bioelectrical impedance platform for monitoring cellular response to drug treatment", Phys. Biol. 8 (2011) 015006 (11pp)

[175] F. Asphahani et al., "Influence of cell adhesion and spreading on impedance characteristics of cell-based sensors", Biosensors and Bioelectronics 23 (2008) 1307–1313

[176] A. Rub et al., "A micro-electrode array biosensor for impedance spectroscopy of human umbilical vein endothelial cells", Sensors and Actuators B: Chemical, Volume 118, Issues 1–2, 25 October 2006, Pages 115-120,

[177] Y. Qiu et al., "Real-Time Monitoring Primary Cardiomyocyte Adhesion Based on Electrochemical Impedance Spectroscopy and Electrical Cell−Substrate Impedance Sensing", Analytical Chemistry 2008 80 (4), 990-996

[178] A. Rub et al., "A Detailed Model for High-Frequency Impedance Characterization of Ovarian Cancer Epithelial Cell Layer Using ECIS Electrodes", IEEE TRANSACTIONS ON BIOMEDICAL ENGINEERING, VOL. 56, NO. 2, FEBRUARY 2009 485

[179] P. Wolf et al., "Microelectrode chip based real time monitoring of vital MCF-7 mamma carcinoma cells by impedance spectroscopy", Biosensors and Bioelectronics, Volume 24, Issue 2, 15 October 2008, Pages 253-259, ISSN 0956-5663,

[180] L. Yang, "Electrical impedance spectroscopy for detection of bacterial cells in suspensions using interdigitated microelectrodes", Talanta, Volume 74, Issue 5, 15 February 2008, Pages 1621-1629, ISSN 0039-9140,

[181] L. Ceriotti et al., "Assessment of cytotoxicity by impedance spectroscopy, Biosensors and Bioelectronics", Volume 22, Issue 12, 15 June 2007, Pages 3057-3063, ISSN 0956-5663

[182] L. Wang et al., "Real-time, label-free monitoring of the cell cycle with a cellular impedance sensing chip", Biosensors and Bioelectronics, Volume 25, Issue 5, 15 January 2010, Pages 990-995, ISSN 0956-5663

[183] M. Varshney et al., "A label-free, microfluidics and interdigitated array microelectrode-based impedance biosensor in combination with nanoparticles immunoseparation for detection of Escherichia coli O157:H7 in food samples", Sensors and Actuators B: Chemical, Volume 128, Issue 1, 12 December 2007, Pages 99-107, ISSN 0925-4005

[184] S. Reitinger et al., "Electric impedance sensing in cell-substrates for rapid and selective multipotential differentiation capacity monitoring of human mesenchymal stem cells", Biosensors and Bioelectronics, Volume 34, Issue 1, 15 April 2012, Pages 63-69, ISSN 0956-5663

[185] D. Opp et al., "Use of electric cell–substrate impedance sensing to assess in vitro cytotoxicity", Biosensors and Bioelectronics, Volume 24, Issue 8, 15 April 2009, Pages 2625-2629, ISSN 0956-5663

[186] E. Urcan et al., "Real-time xCELLigence impedance analysis of the cytotoxicity of dental composite components on human gingival fibroblasts", Dental Materials, Volume 26, Issue 1, January 2010, Pages 51-58, ISSN 0109-5641

[187] M. Guo et al., "Monitoring of cell growth and assessment of cytotoxicity using electrochemical impedance spectroscopy", Biochimica et Biophysica Acta (BBA) - General Subjects, Volume 1760, Issue 3, March 2006, Pages 432-439, ISSN 0304-4165

[188] K. B. Male et al., "Assessment of Cytotoxicity of Quantum Dots and Gold Nanoparticles Using Cell-Based Impedance Spectroscopy", Analytical Chemistry 2008 80 (14), 5487-5493

[189] F. David et al., "Viability and Membrane Potential Analysis of Bacillus megaterium Cells by Impedance Flow Cytometry", Biotechnology and Bioengineering, Vol. 109, No. 2, February, 2012

[190] K. Heileman et al., "Dielectric spectroscopy as a viable biosensing tool for cell and tissue Characterization and analysis", Biosensors and Bioelectronics 49(2013)348–359

[191] Q. Liu et al., "Impedance studies of bio-behaviour and chemosensitivity of cancer cells by micro-electrode arrays", Biosensors and Bioelectronics 24 (2009) 1305–1310

[192] J. J. Yu et al., "CHK2 and ERCC1 in the DNA Adduct Repair Pathway that Mediates Acquired Cisplatin Resistance", Platinum and Other Heavy Metal Compounds in Cancer Chemotherapy Cancer Drug Discovery and Development 2009, pp 189-194

[193] T Schwarzenberger et al., "Impedance sensor technology for cell-based assays in the framework of a high-content screening system", Physiol. Meas. 32 (2011) 977–993

[194] F. Xie et al., "Use of cellular electrical impedance sensing to assess in vitro cytotoxicity of anticancer drugs in a human kidney cell nephrotoxicity model", Analyst, 2012, 137, 1343

[195] C. Xiao et al., "A simple mathematical model for electric cell-substrate impedance sensing with extended applications", Biosensors and Bioelectronics, Volume 25, Issue 7, 15 March 2010, Pages 1774-1780,

[196] S. Ostrovidov et al., "Integration of a pump and an electrical sensor into a membrane-based PDMS microbioreactor for cell culture and drug testing", Biomedical Microdevices October 2011, Volume 13, Issue 5, pp 847-864

[197] Omori T. et al., "Validation study on five cytotoxicity assays by JSAAE II", Statistical analysis. Altern. Anim. Test. Exp. 1998, 5, 39–58.

[198] Botham, P., "Acute systemic toxicity", ILAR J. 2002, 43, 27–30.

[199] Botham, P., "Acute systemic toxicity: Prospects for tiered testing strategies", Toxicol. in vitro 2004, 18, 227–230.

[200] Xing J. Z. et al., "Dynamic monitoring of cytotoxicity on microelectronic sensors", Chem. Res. Toxicol. 2005, 18, 154–161

[201] Keese, C., Karra, N., Dillon, B., Goldberg, A., Giaever, I., "Cell-Substratum Interactions as a Predictor of Cytotoxixity." In Vitro & Molecular Toxicology 11 (2), (1998)

[202] C. Xiao et al., "On-Line Monitoring of Cell Growth and Cytotoxicity Using Electric Cell-Substrate Impedance Sensing (ECIS)", Biotechnol. Prog. 2003, 19, 1000-1005

[203] J. Z. Xing et al., "Microelectronic cell sensor assay for detection of cytotoxicity and prediction of acute toxicity", Toxicology in Vitro 20 (2006) 995–1004

[204] Patterson, R. "Bioelectric Impedance Measurements", The Biomedical Engineering Handbook: Second Edition, Ch. 73, Ed. Joseph D. Bronzino, CRC Press LLC, 2000

[205] David S. Holder, "Electrical Impedance Tomography: Methods, History and Applications", IOP publishing ltd. 2005

[206] B. H. Brown, "Electrical impedance tomography (EIT): a review", Journal of Medical Engineering & Technology, Volume 27, Number 3, (May/June 2003), pages 97–108

[207] Kennelly, A.E., Impedance. Proceedings of the Ieee, 1984. 72(4): p. 463-492.

[208] Grimnes, S.M.O.G., Bioimpedance, in Wiley Enccyclopedia of Biomedical Engineering. 2006, John Wiley & Sons.

[209] Zou, Y. and Z. Guo, A review of electrical impedance techniques for breast cancer detection. Med Eng Phys, 2003. 25(2): p. 79-90.

[210] Maxfield, C.B., J.; Williams, T.; Kester, W.; Bensky, D., Electrical engineering - know it all. 2008: Elsevier.

[211] Dean, D.A., et al., Electrical Impedance Spectroscopy Study of Biological Tissues. J Electrostat, 2008. 66(3-4): p. 165-177.

[212] Miklavcicˇ, D., N.a. Pavselj, F.X. Hart, Electrical properties of tissues, in Wiley Encyclopedia of Biomedical Engineering, M. Akay, Editor. 2006, John Wiley & Sons: Hoboken, New Jersey.

[213] Gitter, A.H., M. Fromm, and J.D. Schulzke, Impedance analysis for the determination of epithelial and subepithelial resistance in intestinal tissues. J Biochem Biophys Methods, 1998. 37(1-2): p. 35-46.

[214] Schwan H.P., Linear and nonlinear electrode polarization and biological materials. Ann Biomed Eng, 1992. 20(3): p. 269-88.

[215] Riu, P.J., Preface. Annals of the New York Academy of Sciences, 1999. 873(1): p. xi-xi.

[216] Brown, B.H., Electrical impedance tomography (EIT): a review. J Med Eng Technol, 2003. 27(3): p. 97-108.

[217] Holder, D.S. Electrical Impedance Tomography of brain function. in Automation Congress, 2008. WAC 2008. World. 2008.

[218] Hope, T.A. and S.E. Iles, Technology review: the use of electrical impedance scanning in the detection of breast cancer. Breast Cancer Res, 2004. 6(2): p. 69-74.

[219] Stojadinovic, A., et al., Electrical Impedance Scanning for the Early Detection of Breast Cancer in Young Women: Preliminary Results of a Multicenter

Prospective Clinical Trial. Journal of Clinical Oncology, 2005. 23(12): p. 2703-2715.

[220] Riedel, T. and I. Frerichs, Electrical Impedance Tomography, in Paediatric Lung Function, U. Frey and P.J.F.M. Merkus, Editors. 2010, Euroean Respiratory Society: Plymouth, UK.

[221] Muders, T., H. Luepschen, and C. Putensen, Impedance tomography as a new monitoring technique. Curr Opin Crit Care, 2010. 16(3): p. 269-75.

[222] Frerichs, I., Electrical impedance tomography (EIT) in applications related to lung and ventilation: a review of experimental and clinical activities. Physiol Meas, 2000. 21(2): p. R1-21.

[223] Kun, S., et al., Algorithm for tissue ischemia estimation based on electrical impedance spectroscopy. Biomedical Engineering, IEEE Transactions on, 2003. 50(12): p. 1352-1359.

[224] Baxter, A.J., et al., Evaluation of applied potential tomography as a new non-invasive gastric secretion test. Gut, 1988. 29(12): p. 1730-1735.

[225] Mangnall, Y.F., et al., Applied potential tomography: a new non-invasive technique for assessing gastric function. Clin Phys Physiol Meas, 1987. 8 Suppl A: p. 119-29.

[226] Avill, R., et al., Applied potential tomography. A new noninvasive technique for measuring gastric emptying. Gastroenterology, 1987. 92(4): p. 1019-26.

[227] Soulsby, C.T., et al., Measurements of gastric emptying during continuous nasogastric infusion of liquid feed: Electric impedance tomography versus gamma scintigraphy. Clinical Nutrition, 2006. 25(4): p. 671-680.

[228] Lukaski, H.C., Requirements for Clinical Use of Bioelectrical Impedance Analysis (BIA)a. Annals of the New York Academy of Sciences, 1999. 873(1): p. 72-76.

[229] Hoffer, E.C., C.K. Meador, and D.C. Simpson, A RELATIONSHIP BETWEEN WHOLE BODY IMPEDANCE AND TOTAL BODY WATER VOLUME*. Annals of the New York Academy of Sciences, 1970. 170(2): p. 452-461.

[230] Dua, R., et al., Detection of basal cell carcinoma using electrical impedance and neural networks. Biomedical Engineering, IEEE Transactions on, 2004. 51(1): p. 66-71.

[231] Emtestam, L., et al., Electrical Impedance of Nodular Basal Cell Carcinoma: A Pilot Study. Dermatology, 1998. 197(4): p. 313-316.

[232] Aberg, P., et al., Skin cancer identification using multifrequency electrical impedance-a potential screening tool. Biomedical Engineering, IEEE Transactions on, 2004. 51(12): p. 2097-2102.

[233] Aberg, P., et al., Non-invasive and microinvasive electrical impedance spectra of skin cancer - a comparison between two techniques. Skin Res Technol, 2005. 11(4): p. 281-6.

[234] Beetner, D.G., et al., Differentiation among basal cell carcinoma, benign lesions, and normal skin using electric impedance. Biomedical Engineering, IEEE Transactions on, 2003. 50(8): p. 1020-1025.

[235] Aberg, P., I. Nicancer, and S. Ollmar. Minimally invasive electrical impedance spectroscopy of skin exemplified by skin cancer assessments. in Engineering in Medicine and Biology Society, 2003. Proceedings of the 25th Annual International Conference of the IEEE. 2003.

[236] Nyren, M., N. Kuzmina, and L. Emtestam, Electrical impedance as a potential tool to distinguish between allergic and irritant contact dermatitis. J Am Acad Dermatol, 2003. 48(3): p. 394-400.

[237] Nicander, I., et al., Allergic contact reactions in the skin assessed by electrical impedance – a pilot study. Skin Research and Technology, 1997. 3(2): p. 121-125.

[238] Lindholm-Sethson, B., et al., Multivariate analysis of skin impedance data in long-term type 1 diabetic patients. Chemometrics and Intelligent Laboratory Systems, 1998. 44(1-2): p. 381-394.

[239] Nicander, I., P. Aberg, and S. Ollmar, The use of different concentrations of betaine as a reducing irritation agent in soaps monitored visually and non-invasively. Skin Res Technol, 2003. 9(1): p. 43-9.

[240] Nicander, I., et al., The ability of betaine to reduce the irritating effects of detergents assessed visually, histologically and by bioengineering methods. Skin Res Technol, 2003. 9(1): p. 50-8.

[241] Blichmann, C.W. and J. Serup, Assessment of skin moisture. Measurement of electrical conductance, capacitance and transepidermal water loss. Acta Derm Venereol, 1988. 68(4): p. 284-90.

[242] Van De Water, J.M., et al., Impedance Cardiography*. Chest, 2003. 123(6): p. 2028-2033.

[243] Fellahi, J.-L., et al., Noninvasive Assessment of Cardiac Index in Healthy Volunteers: A Comparison Between Thoracic Impedance Cardiography and Doppler Echocardiography. Anesthesia & Analgesia, 2009. 108(5): p. 1553-1559.

[244] Durney, C.H., H. Massoudi, and M.F. Iskander, Radiofrequency Radiation Dosimetry Handbook 4ed. 1986: Armstrong Laboratory (AFMC), Brooks Air Force Base, TX 78235-5301 330.

[245] Gabriel, C., S. Gabriel, and E. Corthout, The dielectric properties of biological tissues: I. Literature survey. Phys Med Biol, 1996. 41(11): p. 2231-49.

[246] Rajewsky, B., The Biophysical Basis of Ultra-Short Wave Therapy. Radiology, 1938. 31(6): p. 697-706.

[247] Kalvoy, H., et al., Electrical Impedance of Stainless Steel Needle Electrodes. Annals of Biomedical Engineering, 2010. 38(7): p. 2371-2382.

[248] England, T.S., Dielectric Properties of the Human Body for Wave-lengths in the 1-10 cm. Range. Nature, 1950. 166(4220): p. 480-481.

[249] Schwan, H.P. and K. Li, Capacity and Conductivity of Body Tissues at Ultra-High Frequencies. Proceedings of the Institute of Radio Engineers, 1953. 41(3): p. 422-422.

[250] Cook, H.F., The Dielectric Behaviour of Some Types of Human Tissues at Microwave Frequencies. British Journal of Applied Physics, 1951. 2(Oct): p. 295-300.

[251] Broggi, G. and A. Franzini, Value of serial stereotactic biopsies and impedance monitoring in the treatment of deep brain tumours. Journal of Neurology, Neurosurgery & Psychiatry, 1981. 44(5): p. 397-401.

[252] Broggi, G., et al., Treatment of deep brain abscesses by stereotactic implantation of an intracavitary device for evacuation and local application of antibiotics. Acta Neurochirurgica, 1985. 76(3): p. 94-98.

[253] Kalvoy, H., et al., Impedance-based tissue discrimination for needle guidance. Physiological Measurement, 2009. 30(2): p. 129-40.

[254] Lee, B.R., et al., Bioimpedance: novel use of a minimally invasive technique for cancer localization in the intact prostate. Prostate, 1999. 39(3): p. 213-8.

[255] Halter, R.J., et al., Passive bioelectrical properties for assessing high- and low-grade prostate adenocarcinoma. Prostate, 2011. 71(16): p. 1759-67.

[256] Tsui, B.C., et al., Atlas of Ultrasound- and Nerve Stimulation-Guided Regional Anesthesia. 2008, New York: Springer Verlag. 302.

[257] Kimura, S., et al., Application of electrical impedance analysis for diagnosis of a pulmonary mass. Chest, 1994. 105(6): p. 1679-82.

[258] SparkNotes Editors, "SparkNote on Introduction to Electrochemistry." SparkNotes.com. SparkNotes LLC. n.d.. Web. 20 Oct. 2014.

[259] A. Tuteja, "Fundamentals of Physical Chemistry", Discovery Publishing Pvt. Ltd., 2010

[260] Randles, J.E.B, "A cathode ray polarography", Trans. Faraday Soc 44 (1948) p. 322 – 338

[261] Nicholson R.S., "Theory and Application of Cyclic Voltammetry for Measurement of Electrode Reaction Kinetics", Anal. Chem. Vol, 36 (1964) p. 1351

[262] P. Kissinger, W.R. Heineman, "Laboratory Techniques in Electroanalytical Chemistry", Marcel Dekker, Inc., New York, 1996.

[263] J. Wang, "Analytical Electrochemistry", John Wiley & Sons, New York, 2006.

[264] Zoski C.G., "Handbook of Electrochemistry", Elsevier Science, 2007

[265] Compton R. G., Banks C. E., "Understanding Voltammetry", Imperial College Press, London, 2011

[266] Heinz J., "Cyclic Voltammetry-Electrochemical Spectroscopy", New Analytical Methods vol. 23 no. 11 (1984) p. 831.

[267] Bard A.J, Faulkner L.R, "Electrochemical Methods, Fundamentals and Applications", John Wiley & Sons, Inc., 1980.

[268] Brett C.M.A, Brett A.M.O, "Electrochemistry: Principles, Methods and Applications", Oxford University Press (1993).

[269] A.J. Bard, G. Inzelt, F. Scholz, "Electrochemical Dictionary", Springer, 2012

Chapter 2

2 SENSOR AND DEVICE DEVELOPMENT AND CHARACTERISATION

2.1 INTRODUCTION

The fabrication methods of interdigitated electrodes, for different detection techniques, have been extensively reported in literature. Many approaches have been used for fabricating this kind of devices, as mentioned earlier in chapter 1. In the majority of papers, it has been reported that the interdigitated structures have been achieved mainly through UV photolithography as Iwasaki and Kamath [1, 2] have described in their work as well as many others. Many steps and the use of special equipment are required to complete this process. Therefore, in the last few years there have been a few efforts to try to simplify the fabrication process for IDEs. For example, Kim et al. [3] used a laser printing technology with silver ink on a glass substrate. By adjusting printing parameters, the authors were able to produce IDEs having width between 6 and 28 μm and thickness below 1 μm. Screen printing was another technique adopted to fabricate usable IDEs for various sensor applications [4, 5]. On the other hand, Tseng et al. [6] used ink jet printing to first print Pd colloids, followed by electro-less plating of Ni on polyethylene terephthalate (PET) substrate. Successful patterns could be obtained when the line width was above 30 μm. However, they have to perform a gold displacement process afterwards to improve the electrical conductivity of the interdigitated sensors. Other methods, like micro-molding have been reported by Chou [7] as well as many others [8 – 11]. Another method quite widely used is the e-beam lithography combined with standard photolithography as in [12, 13].

In literature, many articles described applications in the biosensing field [14, 15]. Electrochemical biosensors [16 – 22], often referred to as amperometric, potentiometric, conductimetric, or impedimetric [23], are advantageous as they are highly sensitive, rapid, inexpensive, and suitable for designing integrated microsystems [24, 25]. Very frequently, this design was used for impedimetric measurements on living mammalian cells to monitor their viability and cytotoxicity effects of certain compounds [26 – 29], following the pioneering work done by Giaever and Keese in 1986 [30]. Other papers reported similar application for bacteria and viruses using again impedance based detection techniques [31, 32].

2.2 SCOPE

The original idea for the impedance sensors that are described in this thesis stemmed from an FP6 project called Toxichip. The project was concerned with the fabrication of interdigitated impedance electrodes used to monitor the cytotoxicity of certain compounds on cells immobilized on the electrodes surface [33]. Those electrodes were quite big in terms of surface area which did not allow a good reproducibility in the results. In this thesis work it was decided to improve the Toxichip electrodes by reducing the electrodes active area and modifying the surface area of the electrode, hoping that this would lead to an increased sensitivity of the assay. In this chapter there will be a description on how the electrodes used in this project have been designed, fabricated and tested. The results and the methodologies used for the fabrication of holders, connectors and the PMMA blocks will also be described in this part together with the testing and the cleaning protocols used prior to the use with the cell cultures.

This type of technology would potentially help to provide an in-depth knowledge of various cellular responses occurring as a result of toxicity and would have major beneficial implications in applications such as neurology, cytotoxicity and pharmacology.

2.3 OBJECTIVES

- Fabrication of gold interdigitated impedance electrodes on a Pyrex substrate
- Fabrication of Nanopillars with different height and layout on the each finger of the electrodes
- Investigation of potential use of ITO as electrode material
- Fabrication of an integrated Ag/AgCl reference electrode for electrochemical measurements
- Characterization of the electrodes
- Creation of a cleaning procedure for first and subsequent use with cell cultures
- Creation of a packaging procedure of chip
- Design and fabrication of holders to obtain measurement data with the fabricated electrodes

2.4 FABRICATION MATERIALS AND INSTRUMENTS

2.4.1 Reagents and materials

MicroChem LOR3A lift-off resist, MicroChem S1805 imaging resist, Microposit MF319 developer, Microposit R1165 resist stripper and Silicon Nitride were purchased from Shipley Ltd, Coventry, UK. ZEP 520A Resist, ZEP-A Thinner and ZED N50 were purchased from Zeon Chemicals, Chiyoda-ku, Tokyo, Japan; gold powders were purchased from Pi-Kem Ltd, Staffordshire, UK; indium tin oxide (ITO), titanium and silver were purchased from Umicore, Brussels, Belgium; ferric chloride pellets were purchased from Sigma Aldrich, Dublin, Ireland; Pyrex wafers (100mm diameter x 0.5mm thickness wafer with semi-standard flat (32.5mm), BullenTech, OH, USA); biocompatible double-sided pressure sensitive adhesive tape of medical grade (Orabond 1397PP, Orafol, Germany); laser-sintered powder PA 2200 (Beta Layout Ltd, Shannon, Co. Clare, Ireland); Harwin Probe spring-loaded contact 2.54mm pitch (Farnell Ireland, Dublin); biocompatible Plexiglas sheets (Farnell Ireland, Dublin); Loadpoint thermal-release dicing film (Loadpoint Ltd., Swindon, UK).

2.4.2 Instruments

STS PECVD and STS RIE (Surface Technology Systems plc, Newport, UK); Temescal FC-2000 Evaporator (Temescal, Livermore, CA, USA); Karl Suss Mask Aligner 1006 (Suss Microtec AG, Garching, Germany); Jeol 6000 FS/E Electron Lithography System (Jeol, Akishima, Tokyo, Japan); DISCO DAD3350 Automatic dicing machine (DISCO Corp. Ota-ku, Tokyo Japan); Atomic Force Microscope MFP-3D (Asylum Research, Santa Barbara, CA, USA); FEI FEG Scanning Electron Microscope (FEI Corp., Hillsboro, Oregon, USA); Contact Angle System OCA (DataPhysics Instruments GmbH, Filderstadt, Germany)

2.5 DESIGN

2.5.1 Electrode design

The impedance electrodes for this part of the research have been designed with an interdigitated structure comprising of ten fingers electrodes (five for each branch). The width of the fingers is 40 μm as well as the spacing between each of them. Their length is 500 μm although in the fabrication mask they have been designed to be 520 μm long as they overlap by 20 μm onto the track connecting it to the pads for the signal collection to ensure electrical continuity in the system (see figure 2.1 below). Several masks have been designed to allow the fabrication of each part of the electrode. In particular, it has been chosen to divide the fingers in two different masks containing five in each to allow making them in different materials if needed (for example Au and Pt). There are in fact different layers for the fingers (red and purple), reference electrode (light blue), tracks (yellow), pads (yellow), passivation layer (grey) and alignment marks (not shown here).

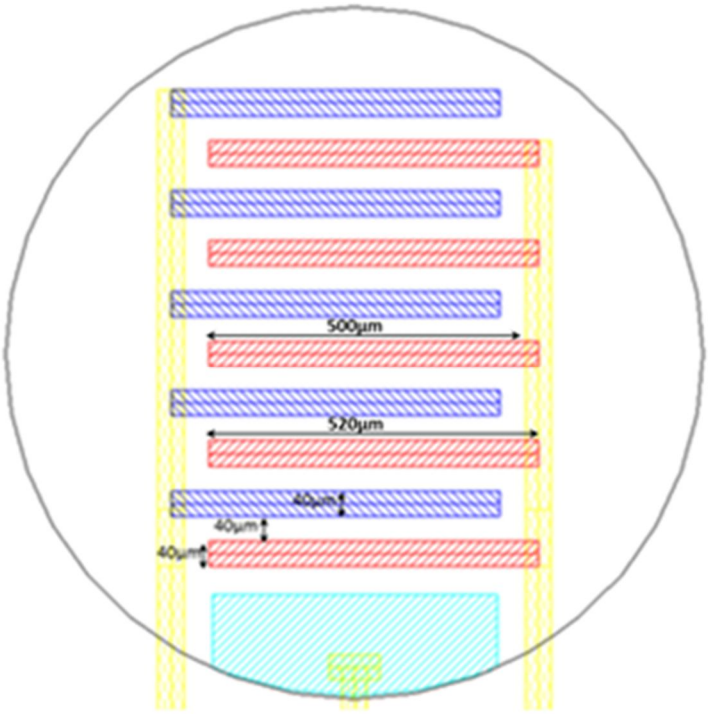

Figure 2.1: Schematic of the fabricated device with the interdigitated electrode dimensions

The nanopillars fabricated on the interdigitated electrodes have a diameter of 150nm, a pitch of 500nm fixed by the prepared mask and a variable height depending on the thickness of the resist deposited during the fabrication. We used mostly nanopillars 60nm or 100nm tall.

The choice of this electrode's dimensions come from an earlier study done in Tyndall in a similar project and published in [26]. This paper shows a research conducted in order to determine the best interdigitated impedance electrode configuration (in terms of width and spacing of the fingers) for cell culture analyses to differentiate between live and dead cells. Specifically in this case, the A549 cell line was used for the experiments, which was also used in this PhD research project. The experiments published in this paper and continued in following studies (also using BALBc 3T3 cells, which were not published because the student carrying on the project had to leave her PhD position) showed that A549 cells gave the best results using two interdigitated electrodes configurations, one with 60 m finger width and 20 m finger gap and the other with

40 m finger width and 40 m finger gap. In the experiments using the BALB cell lines it was found that the best configuration was 40 m finger width and 40 m finger gap. In general a small gap between the electrodes, in this kind of technique, helps to increase the sensitivity of the experiments [34].

2.5.2 Electrode holder design

In order to obtain the electric impedance measurements, connectors with a related holder have been designed and fabricated. Two different types of electrode holders were fabricated for different applications. The first one was a custom-made holder designed using Solidworks, solid modelling CAD (computer-aided design) software (figure 2.2).

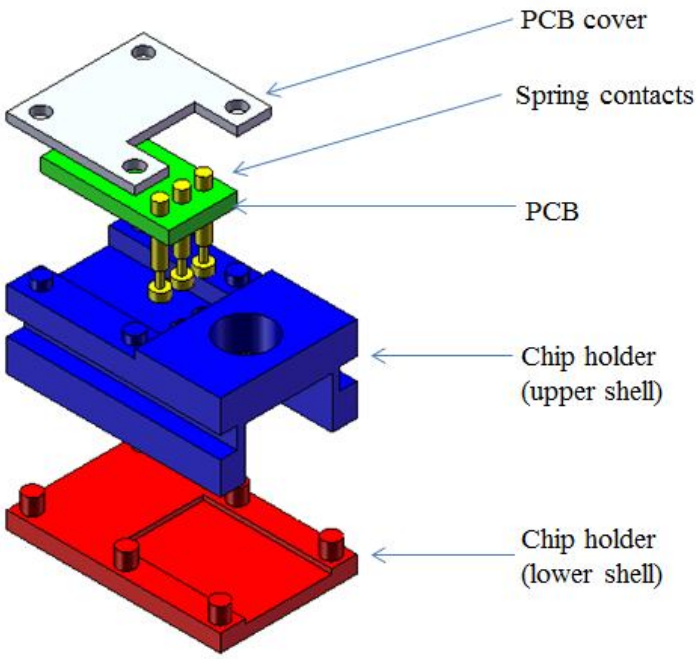

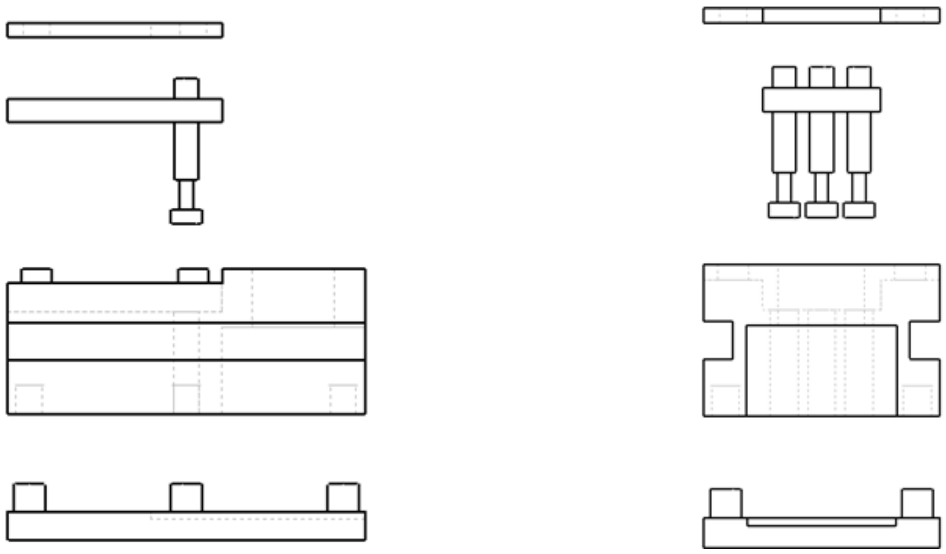

Figure 2.2: Drawings made using Solidworks for the device custom-made holder

These parts (figure 2.3) were fabricated by Beta Layout Ltd (Shannon, Co. Clare, Ireland) using a rapid prototyping machine (EOSINT P 760). They were made of laser-sintered powder PA 2200 on the basis of polyamide 12 which possess excellent properties: high strength and stiffness, good chemical resistance, excellent long-term constant behaviour, high selectivity and detail resolution, various finishing possibilities, biocompatibility (according to EN ISO 10993-1 and USP/level VI/121 °C), approved for food contact in compliance with the EU Plastics Directive 2002/72/EC.

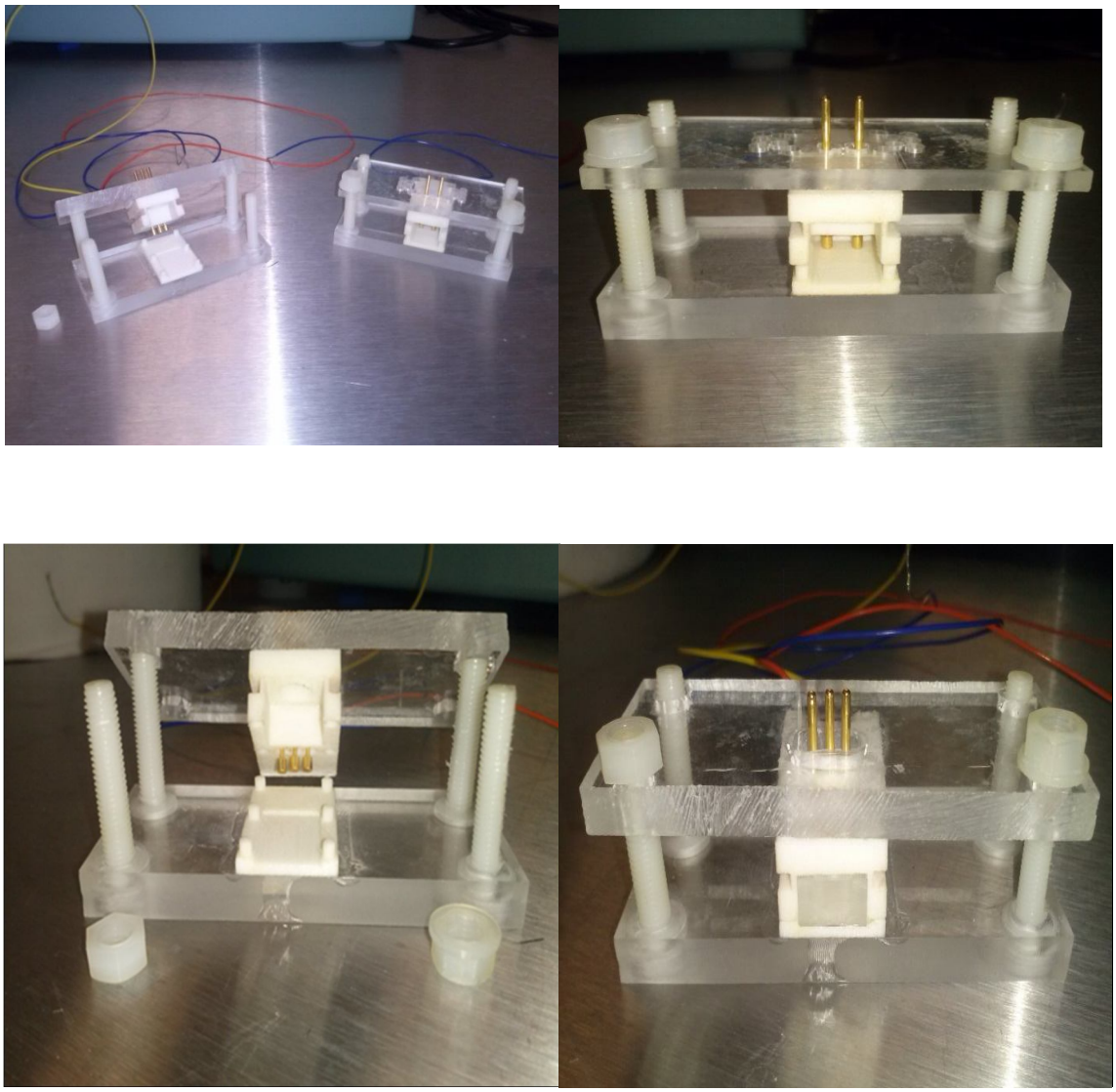

Figure 2.3: Fabricated holder device using the rapid prototyping technique

Spring-loaded contacts with flat heads were used to guarantee an electrical connection between the electrode pads and the impedance analyser. To achieve a better stability of the system, the polymeric shells were glued to a Plexiglas structure, conveniently spaced with four plastic screws. This holder was used to perform the experiments done on the cell cultures. The packaged devices sit into the designated slot formed by the upper and lower shell represented in figure 2.2

The second type of holder was fabricated using card edge connectors from Samtec UK (Cumbernauld, Scotland) represented in figure 2.4. These card edge connectors were suitable for cards with 500 μm thickness, the same as a Pyrex wafer. Then wires were soldered at the right connectors on the opposite side of the receptacle to get them connected to the impedance analyser. The guides on both sides of the connectors were removed to make the device easier to use. Also, the side with the electrical connections was cut and shortened to match the width of the diced electrodes (~10mm). This holder was used in the electrochemical measurements as it was smaller compared to the first type and fitted into the small 5ml beakers in which the experiments were carried out.

Figure 2.4: Card edge connectors used for the electrodes fabricated on a Pyrex substrate 500μm thick

2.6 CONTACT ANGLE PROCEDURE

The electrodes were placed carefully under the needle of a syringe (loaded in the previous stage) delivering the water droplet. The syringe was filled with 100 ml of deionised water (18.2 MΩ.cm-1) taken from a Milli-Q (Millipore, Bedford, MA) water purification system. A droplet of 200 μl was delivered on the area covered by the interdigitated gold electrode using a syringe controlled with the dedicated software of the contact angle machine. Then the system, through the use of a camera, detected the drop of water on the substrate. The system automatically recognised the baseline (the red line in the pictures shown in paragraph 2.10.5) and defined the shape of the droplet calculating finally the CA (contact angle) on the left and on the right side of the water drop.

2.7 FABRICATION PROCEDURE

The fabrication of the interdigitated electrodes on Pyrex wafers (100mm diameter x 0.5mm thickness wafer with semi-standard flat (32.5mm), BullenTech, OH, USA), was done as follows:

The contact metal deposition was done by the standard lift-off process. Pyrex wafers are first dipped in 5:1 BOE solution for 5 seconds to clean and promote resist adhesion. HMDS adhesion promoter was then spun on at 3000 rpm for 50 seconds. The same procedure was then adopted for the lift-off resist MicroChem LOR3A before baking the wafers on the hot plate at 150°C for 3 minutes. MicroChem S1805 imaging resist was spun on at 3000 rpm for 50 seconds and wafers were hot-plate baked again at a temperature of 115°C for 2 minutes. They were then aligned with their mask and exposed to UV in a Karl Suss MA1006 mask-aligner with an exposing dose of 40mW/cm^2. The wafers were subsequently developed in Microposit MF319 developer for 60 seconds and rinsed in DI and then oven baked at 90°C for 30 minutes. They were then loaded in Temescal FC2000 e-beam evaporator and the chamber was evacuated to $<5x10^{-7}$ Torr and Ti:Au (10:200nm) was evaporated onto the wafers. Surplus Ti:Au and photoresist were lifted off in Microposit R1165 resist stripper, leaving the desired metal contact pattern on the Pyrex wafers.

To fabricate the nanopillars on the fingers of these electrodes (which will be from now on referred to as “flat” to differentiate them from the nanostructured ones), a 60 nm thick layer of Silicon Nitride was deposited on the wafers in the STS PECVD (Plasma Enhanced Chemical Vapour Deposition) system. This thickness will determine the height of the nanopillars. E-beam lithography (Jeol 6000FS/E Electron Lithography System) was then employed to define the nanopillars pattern on top of the Silicon Nitride overlying the metal fingers. The wafers were prepared for this step with a coating of a layer of 1:1 ratio mix of ZEP 520A Resist with ZEP-A Thinner which was spun first at 500 rpm for 10 seconds and increased to 3000 rpm for 60 seconds. To allow better alignment and thus reducing error with the e-beam process, it was necessary to evaporate a layer of 200nm of ITO on the opposite side of the wafers to reduce the high transparency typical of the Pyrex material. Next, the beam drew the desired patterns

(which have been previously designed on dedicated software and recalled at the moment of the procedure) on the interdigitated finger electrode. After this step, the wafers were dipped in ZED N50 developing solution for 30 seconds, then immersed in IPA for further 30 seconds and finally dried using a nitrogen gun. The Silicon Nitride was etched through the metal fingers in the STS RIE (Reactive Ion Etching) system where the nanopillars patterns were defined by using the e-beam photoresist as a mask. Wafers were then again loaded in to the Temescal evaporator and evaporated with Ti:Au (5:65nm) to fill the holes created with the RIE. The excess metal and the photoresist were removed using again the Microposit R1165 resist stripper leaving nanopillars of, approximately, 60 nm in height. To fabricate a taller version of these nanopillars it was simply necessary to increase the thickness of the resist of Silicon Nitride before the e-beam patterning (figure 2.5 and 2.6).

The reference electrode for the three-electrode system was made in Ag/AgCl. The procedure for its fabrication was the same followed for the step of Gold deposition except that Ti:Ag was evaporated instead of Ti:Au and the lift-off was done after the Ti:Ag layer had been treated with the FeCl3 solution. This treatment was done by preparing a ferric chloride ($FeCl_3$) solution 0.05M. Pellets of $FeCl_3$ (0.811 g) were diluted in 100 ml of hot water; this solution was then poured in a plastic Petri dish and placed on a Rotamax 120 shaker (Heidolph Instruments, UK). The wafer was positioned then into the solution with the metal facing up. The shaker was then set at 50 rpm and the wafer was let to react in the solution for 50 seconds. After this, the wafer was removed from the $FeCl_3$, rinsed with DI water and dried with a nitrogen gun.

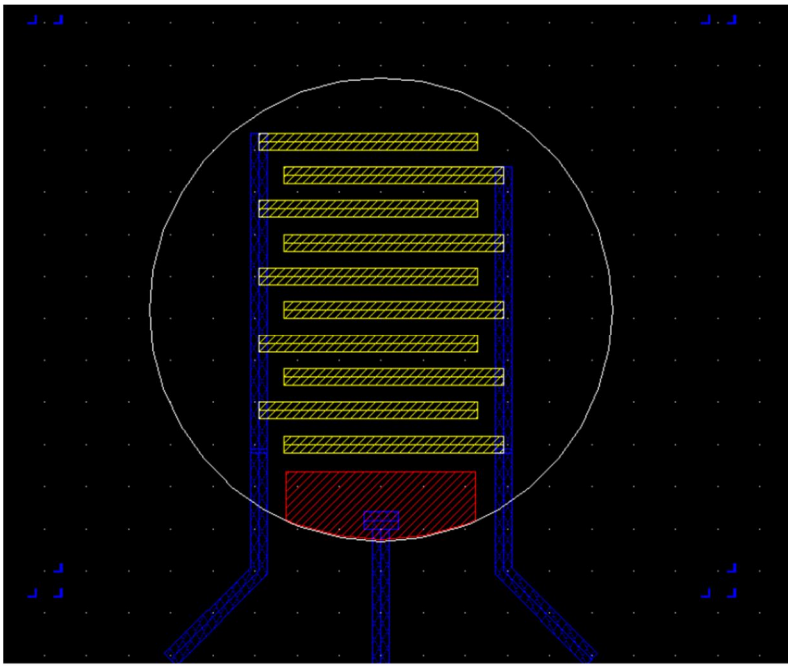

Figure 2.5: Gds file of the devices with the reference Ag/AgCl electrode

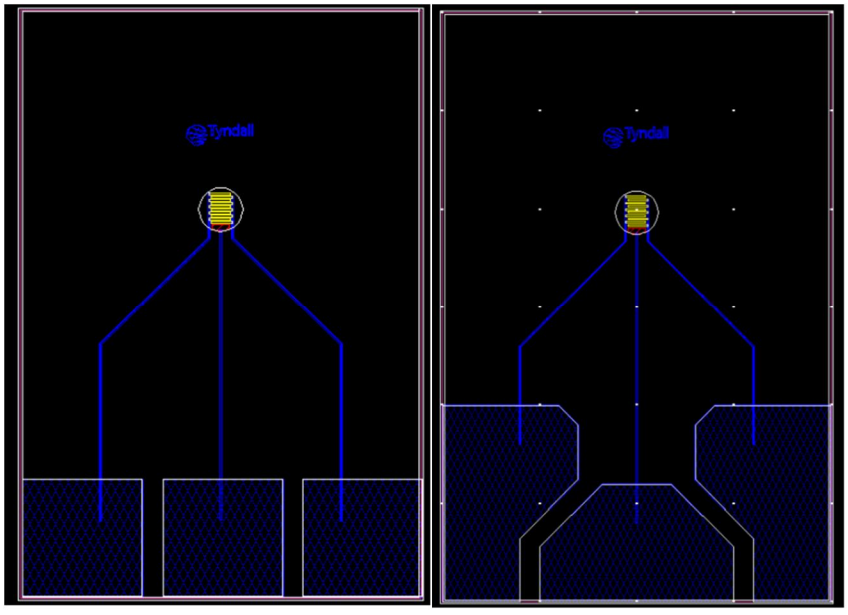

Figure 2.6: Gds file of the two device configurations with the reference Ag/AgCl electrode

This kind of fabrication technique for the reference electrodes on the wafers of different materials has been used numerous times in our research group giving always good

results. These reference electrodes were then tested several times in different experiments showing always an acceptable level of stability as confirmed by the studies done by Moujahid in 2011 [35]. The stability of the reference electrode was characterised by measuring the open-circuit potential and cyclic voltammetry relative to the commercially available Ag/AgCl reference electrode giving always good results.

2.8 CLEANING PROCEDURE

Right after the fabrication process, the devices were covered with a protective layer of Shipley S1813 resist to avoid the glass cracking or the electrodes to be scratched during the dicing procedure. To remove this resist it was necessary to soak the electrodes for five minutes in pure warm acetone (~ 40 °C) and rinse it afterward with deionised water.

In order to use the interdigitated electrodes devices for tissue culture applications it was necessary to soak the devices in vials containing IPA and put them in a sonicator for 15 minutes. Same thing has to be repeated substituting the IPA with deionised water. If the chips have been used previously and need a thorough cleaning, the sonication step with IPA and deionised water can be repeated several times. Then the chips are plasma treated for 15-20 minutes and then stored under sterile conditions in the tissue culture laboratory.

2.9 PACKAGING PROCEDURE

PMMA block were used to package the fabricated devices. These polymeric pieces were attached to the Pyres substrate using a biocompatible double-sided pressure sensitive adhesive tape of medical grade (Orabond 1397PP, Orafol, Germany). To promote the adhesion between the electrode substrate and the Plexiglas material, the Pyrex chips were heated up on a hotplate for 5 minutes at 120 °C before applying the PMMA block on which the tape was applied beforehand. The central part of the adhesive put on the plastic material was cut off precisely with a scalpel in the middle not to cover the electrode area once the two parts were bonded together.

2.10 RESULTS

2.10.1 Preliminary tests for the achievement of the nanopillar fabrication and troubleshooting

Before getting the final protocol for the nanopillars fabrication, many tests have been performed to optimize this procedure.

The very first attempts were done on a plain Pyrex wafer with no electrodes on it, in order to study the possible layout of the nanostructures. A square area with ITO deposited on the substrate was divided in 16 different square smaller areas with different diameter and pitch figures for the nanopillar layout. In figure 2.7 it is possible to see the how the first test was planned:

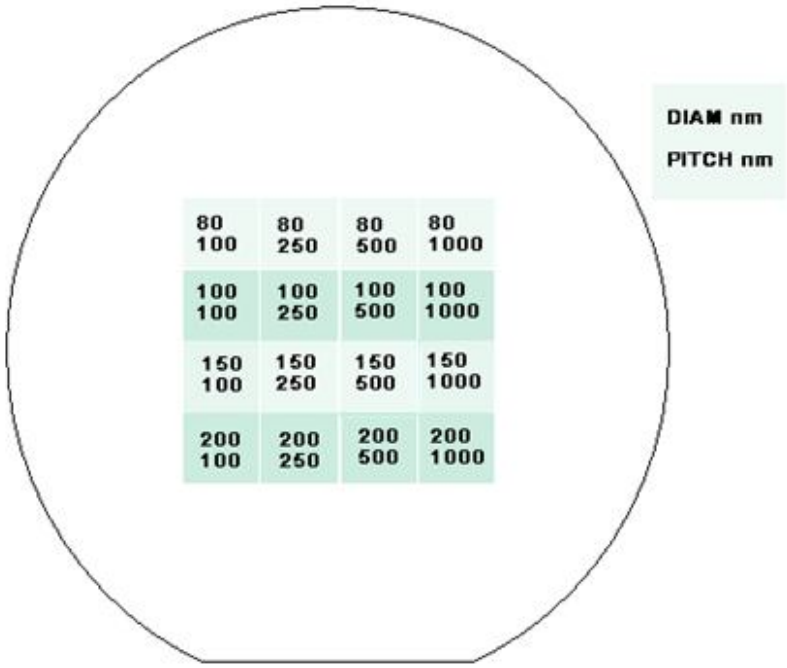

Figure 2.7: Schematic of the test areas for the nanopillars fabrication

All the 16 small square were imaged using the scanning electron microscope in Tyndall before and after the deposition of ITO in the hollow part created with the e-beam process (figure 2.8 and 2.9), but unfortunately the first thing that was evident was the

fact that the ITO was too brittle for this purpose. Most of the nanostructures were damaged or in some case did not appear at all as it is possible to see in figure 2.10.

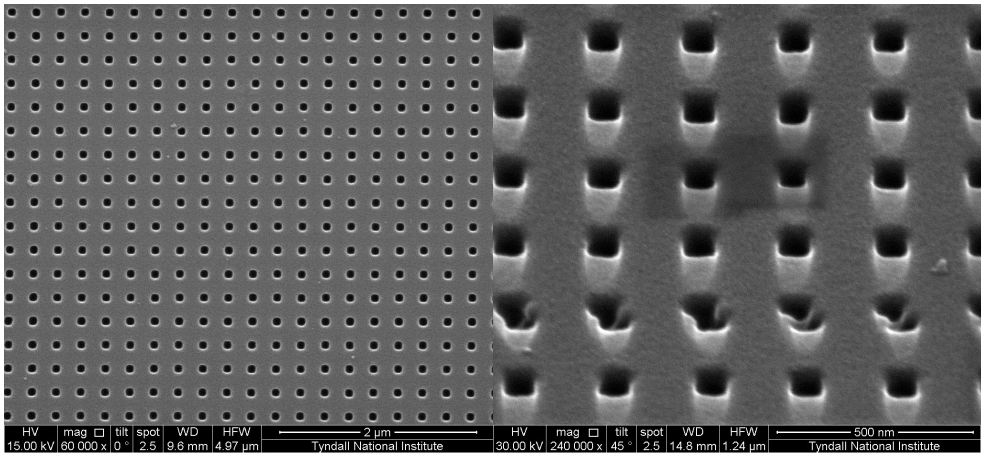

Figure 2.8: Preliminary test for the nanopillars linear layout

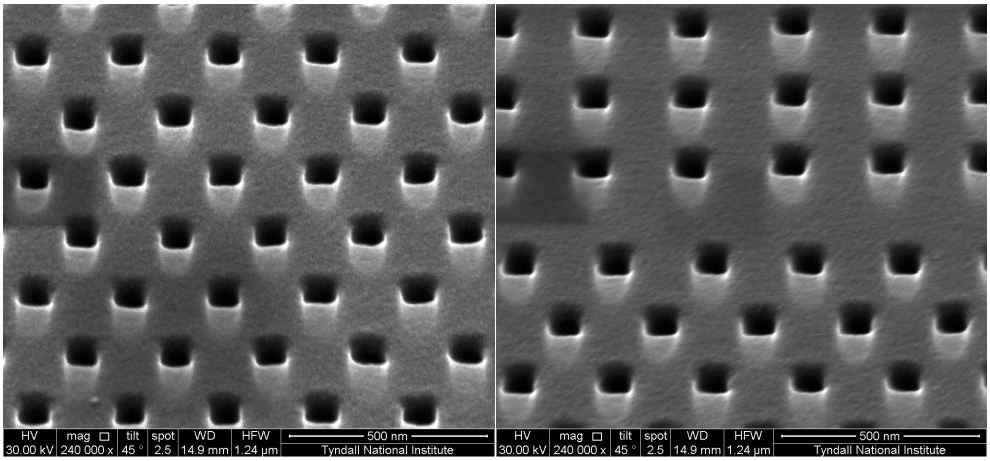

Figure 2.9: Preliminary test for the nanopillars linear and honeycomb layouts

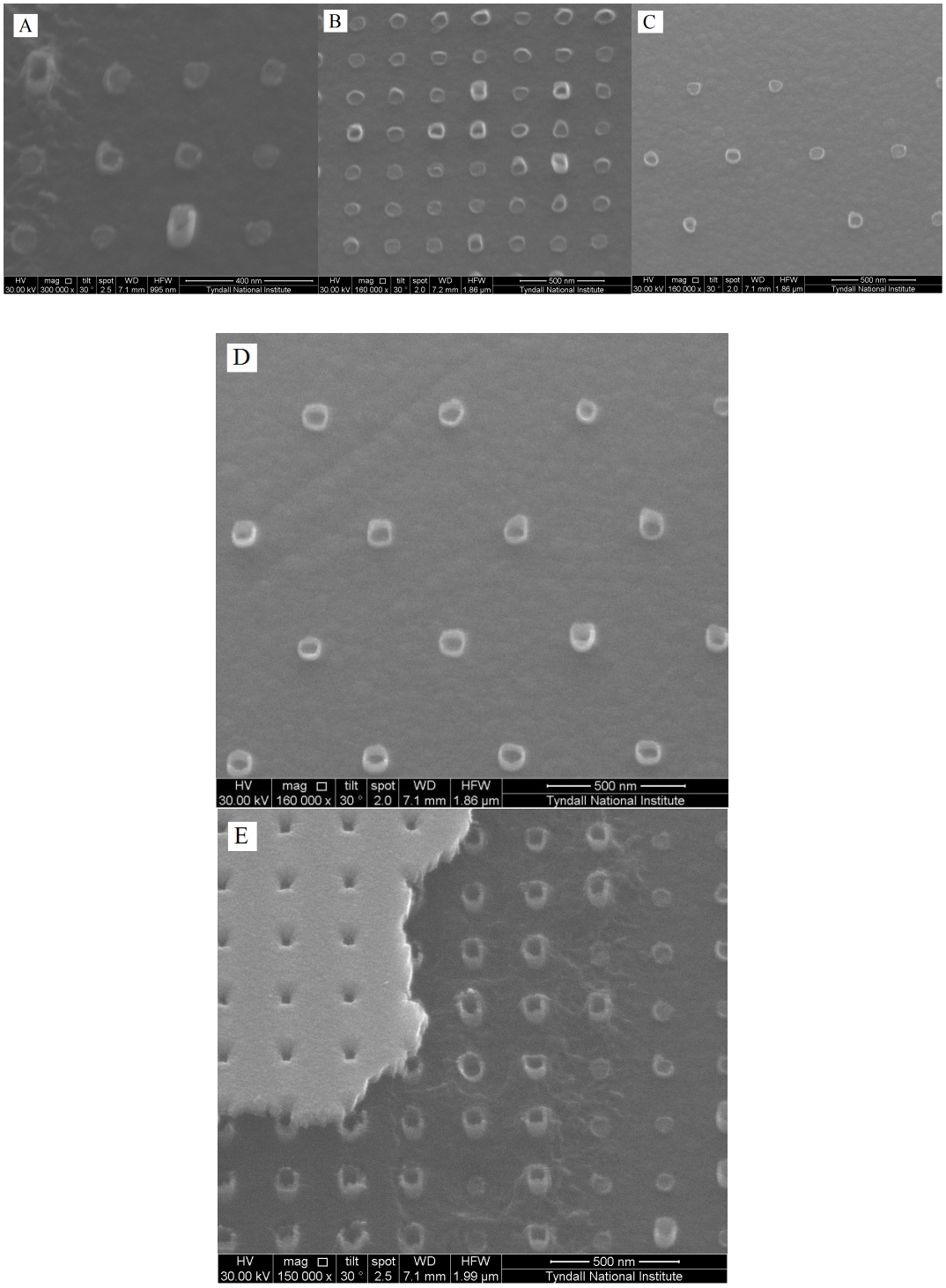

Figure 2.10: Preliminary test for the nanopillars linear and honeycomb layouts on ITO finger electrodes; A, B, C and D show the imperfections in the fabrication, while E shows the unsuccesful resist strip-off process on the linear layout

After a few more test run it was proven that fabricating the ITO nanopillars on an ITO finger electrode was unlikely to happen. Stripping-off the excess metal and resist also proved to be challenging and most of the times did not work after few "washings" as it is possible to see in picture 2.10 (E). Some investigations were also done using Silicon as substrate, but the results were as bad as the earlier tests and in this way the transparency would have been completely compromised.

The ITO was deposited by an e-beam evaporation followed by the lift-off technique. The patterned wafers were loaded in the Leybold Syrus-Pro 710 e-beam evaporation system and pumped down to $<5x10^{-6}$ mbar. The ITO was then evaporated from pellets and deposited with an ion- assisted deposition (IAD). That was done with the substrate surface continually bombarded with oxygen ions generated from the system's APS1000 plasma system. The IAD resulted in a denser, more transparent film when compared with unassisted evaporations. After the evaporation process, the photoresist used to pattern the substrates was removed in Microposit R1165 resist stripper. Substrates were then rinsed in running DI, leaving the ITO nanopillars remaining.

It was then decided to switch metal from ITO to gold although in this way the electrode transparency was lost completely. It was decided to proceed anyway as the area not covered by the electrode would have been relatively large and the cell culture could have been checked easily around the electrode area; the dimensions of the fingers (length and width) would have been also smaller compared to those of the Toxichip version.

Few more tests carried out with a Silicon substrate covered by a thin layer of gold gave better results compared to those obtained with ITO but still were not great (figure 2.11). They were not done on Pyrex because there were no more wafers available in-house while there were plenty of Silicon wafers that helped to troubleshoot some issues (reduced costs during the troubleshooting part). In fact, many problems arose during the fabrication especially from the e-beam side.

The very first issue (which actually happened also with the tests using ITO), was the shape of the nanopillars itself. The perfect circular shape of the cylinder was a problem

for the e-beam as it is not equipped with a rotational stage and can only execute quantized movements on the X and Y axis. When using a circle in the drawing file, the system was forced to achieve that geometry but often incurred in errors that were reported after the machine stopped. This problem was solved by drawing a polygon with many sides, although, after many attempts, it was noticed that an octagon was more than enough to achieve a very good approximation of a circumference.

While trying to simulate a possible fabrication scenario, it was noticed that the writing time for the machine would have been very long to pattern one wafer (10-12 hours) especially with layouts that featured small diameters and pitches (the smaller the dimensions, the higher the number of nanopillars to be printed by the e-beam). For this reason, it was decided to choose a diameter of 150 nm and a pitch of 500 nm. These figures for the nanopillars dimensions were not too small to cause the system to crash and not too large and far apart, possibly compatible for the cell growth.

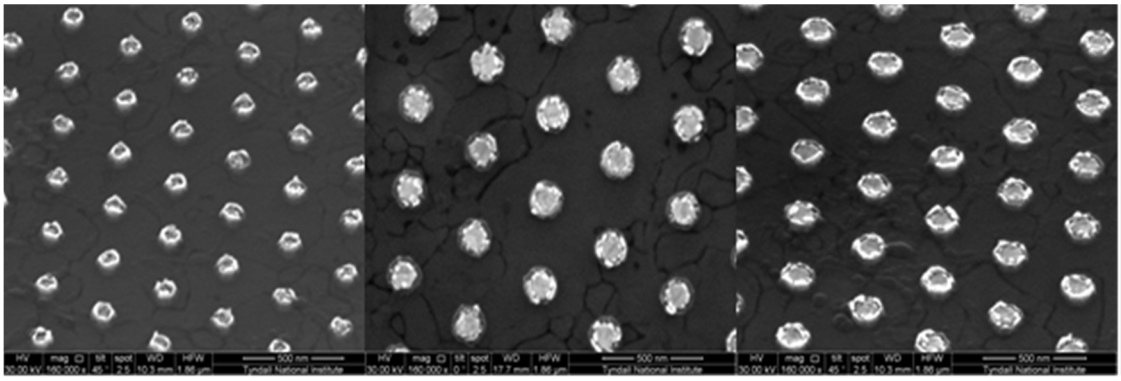

Figure 2.11: Preliminary test for the nanopillars fabrication on a silicon wafer, some examples of the honeycomb layout using gold on Silicon.

The major issue to solve was represented by the alignment of the nanostructures with the fingers of the interdigitated electrodes. At first, together with the fabrication technicians, it was decided to use the "flat" of the wafer, which is a 32 mm (~ 1 ¼ inch) linear part cut off from a 10 cm (~ 4 inch) wafer to aid the alignment with the mask. But unfortunately it could not work because the flat of the wafer, for as precise as it could have been, it always introduced a minimum systematic error due to fabrication of the wafer. If the flat was in fact longer, shorter or tilted of few nanometers than the nominal

dimensions, it would have introduced errors that propagated to the mask patterning resulting in the nanopillars being printed outside the area of the interdigitated electrode. As this traditional method could not be used, a few alignment marks were drawn in two different areas of the wafer. These marks were scanned by the e-beam system prior to the patterning allowing a precise fabrication. Despite this expedient, the alignment was still far from being acceptable. After a few additional tests it was found that, due to the transparency of the Pyrex substrate, the e-beam was scattered or reflected at times and thus not able to align precisely with the marks. In order to solve this issue, or at least limit these inconvenient effects, a thin layer (~ 50 nm) of ITO was deposited on the opposite side of the wafer used for the electrode fabrication. This impacted positively on the procedure giving great results for the pillars alignment. As it is possible to see in figure 2.12, a precision of ± 5 µm was achieved

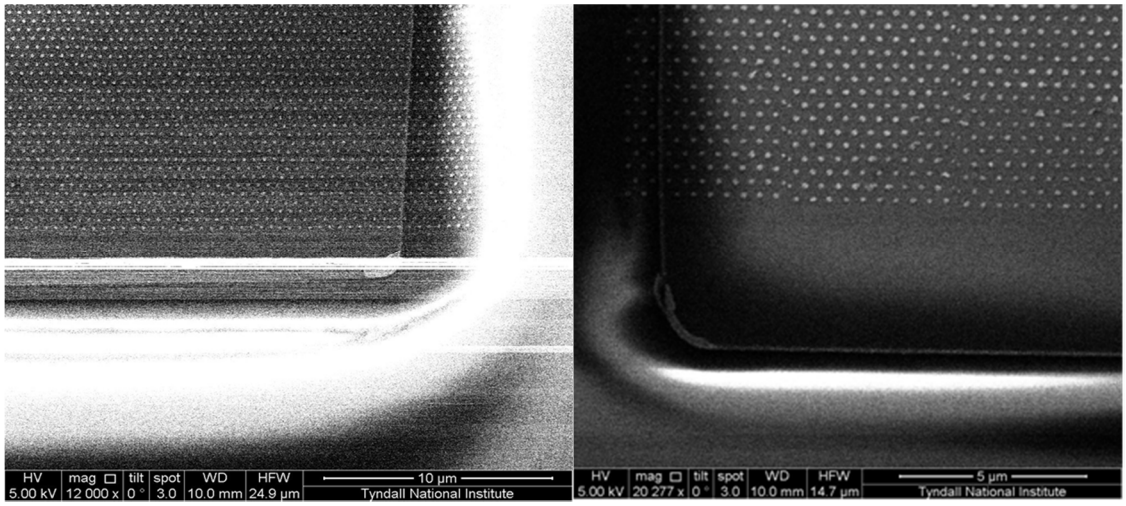

Figure 2.12: misalignment of nanopillars fabricated on the finger electrode

The chips were fabricated then following the same "style" used for the Toxichip project as in figure 2.13

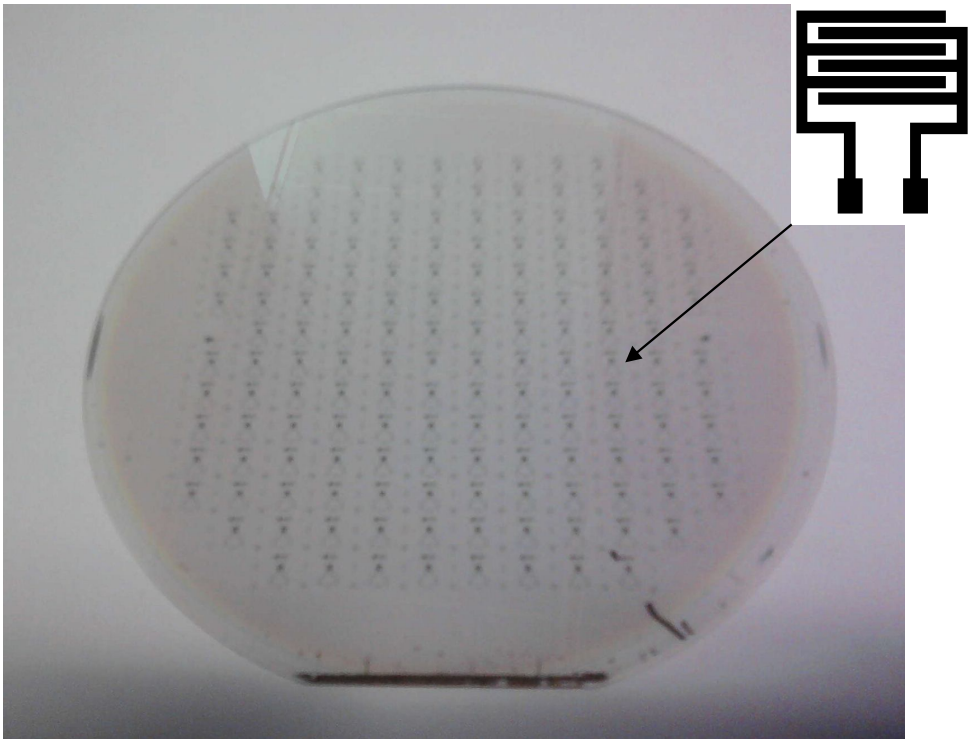

Figure 2.13: First generation of impedance electrodes fabricated with a mask used in a previous project

In this way it was possible to use the same PCBs used in the older project (figure 2.14), but in the longer run this seemed to be too expensive in terms of consumables and also quite long as for the flip-chip technique used to package such devices there would have been a person specifically working on that (which proved to be quite costly too).

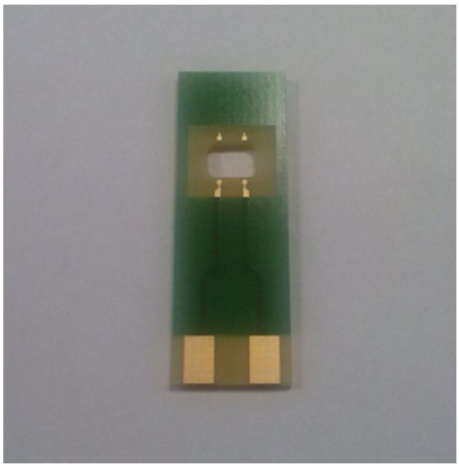

Figure 2.14: PCB used for packaging the first generation electrodes

It was decided then to change completely approach and redesign of the whole device as this solution would have allowed only a small volume of liquid in the culture chamber (in the other project the device worked in a continuous microfluidic environment).

The idea of this new approach was to use a bigger area around the interdigitated electrode which remained the same, in terms of dimensions and fabrications process, as the ones described in the earlier stage of the project. Bigger pads were then used to allow both the soldering of wires on them, the use of clips of the "crocodile" type or spring contacts (figure 2.15).

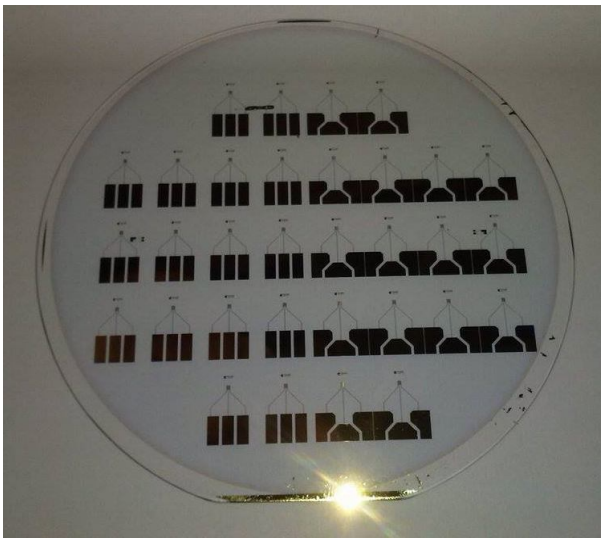

Figure 2.15: Pyrex wafer with the current device version

2.10.2 SEM Analysis

Once all the parameters were finalized (as for the procedure listed in paragraph 2.1.1) it was possible to obtain the nanostructures on the finger electrodes that can be seen in figures 2.16 and 2.17:

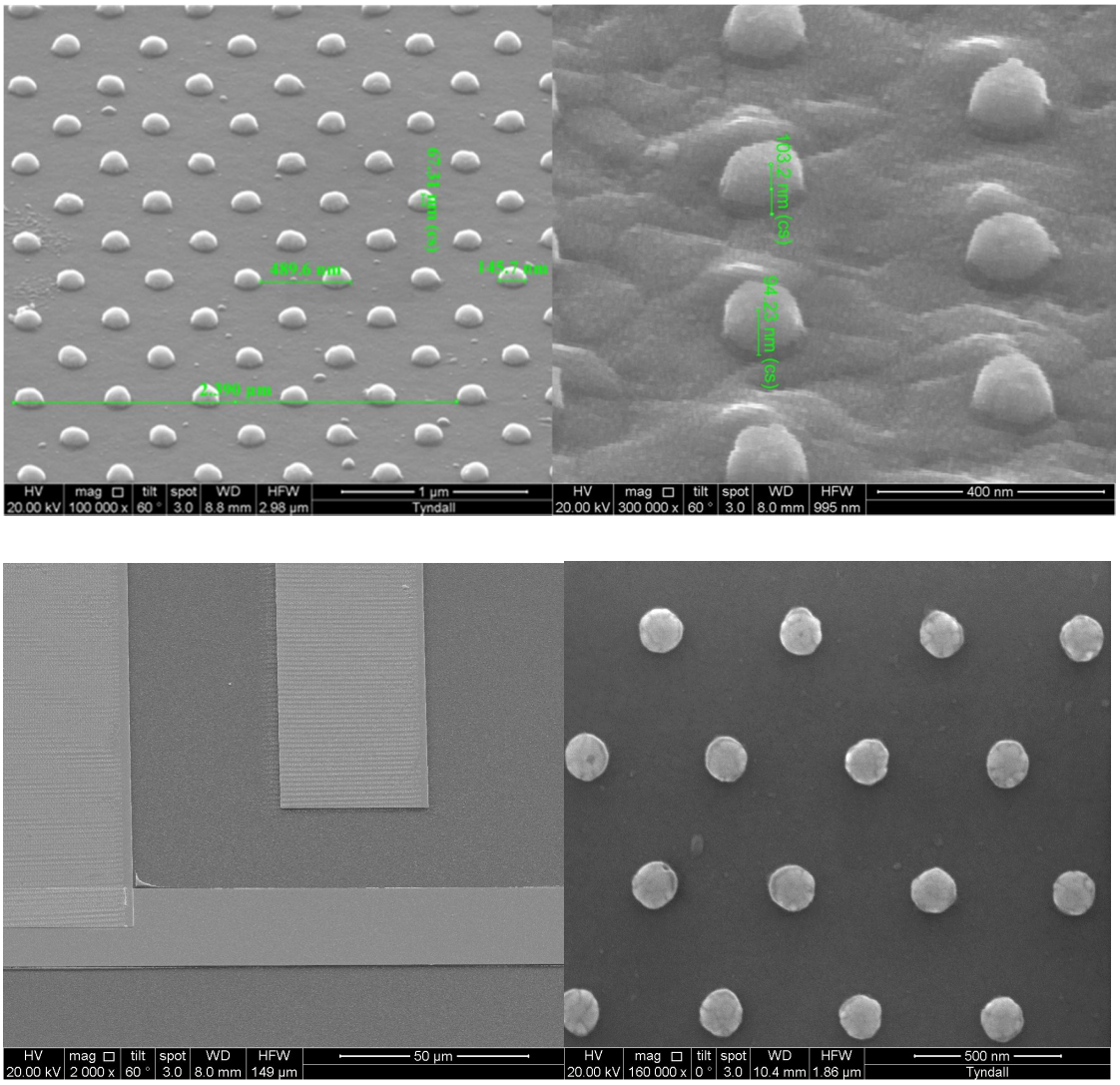

Figure 2.16: SEM images of the nanopillars fabricated on the interdigitated impedance electrodes

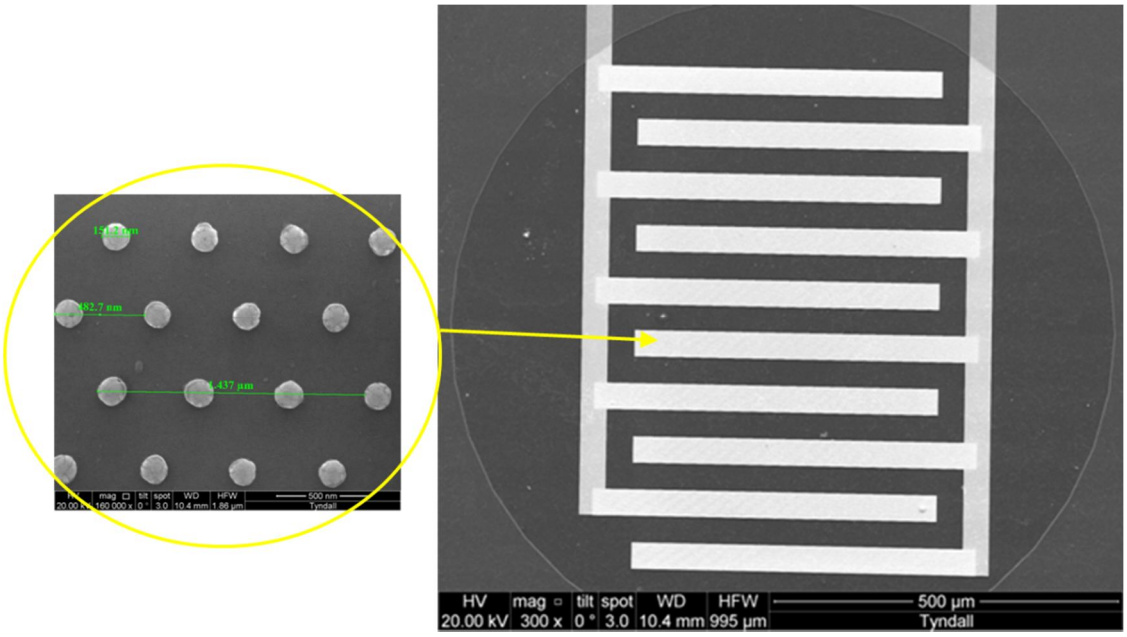

Figure 2.17: SEM images of the nanopillars located on the interdigitated structure

The images were taken using the FEI scanning electron microscope at the Tyndall National Institute and illustrate well the successful fabrication of the nanostructures on top of the fingers of the impedance interdigitated electrodes.

2.10.3 AFM Analysis

Imaging with an Atomic Force Microscope (AFM) have been also carried out in Tyndall National Institute to characterize the surface featuring the nanostructures which was useful to have a better insight on what the nanopillars looked like on the gold interdigitated fingers. A commercial atomic force microscope (MFP-3D, Asylum Research) in AC (alternating current) mode (intermittent contact mode) was used for topography mapping of the films. Olympus AC160TS silicon cantilevers (Al reflex coated, ~70/300 kHz resonant frequency, respectively) were used for imaging.

Atomic force microscopy (AFM) serves to visualise sample surface topography and demonstrates resolution at the nanometre scale. The principle of AFM is based on measuring the various strengths of interaction (forces) between a probe (with radius of

~10 nm) fixed at the end of a cantilever and the atoms of the surface of a material. Forces that can be measured include mechanical contact forces, van der Waals forces, capillary forces, chemical bonding, electrostatic forces, piezoresponses, magnetic forces etc. When the tip is brought into proximity of a sample surface, forces between the tip and the sample lead to a deflection of the cantilever according to Hooke's law. The deflection of the cantilever is followed by positioning a laser beam on the superior face of the cantilever, the beam is reflected about a mirror into an array of photodiodes which register the light signal and convert deflection changes into a topography map of the sample surface.

AC160TS probes were used for this analysis.

The details of the scan parameters used in the measurement were as follows:

Table 2.1: AFM scan parameters

Scan rate	Scan angle	Set point	Integral gain	Drive amplitude	Drive frequency	No. of scan points/lines
0.75 Hz	90°	200 mV	8	40 mV	363 kHz	512

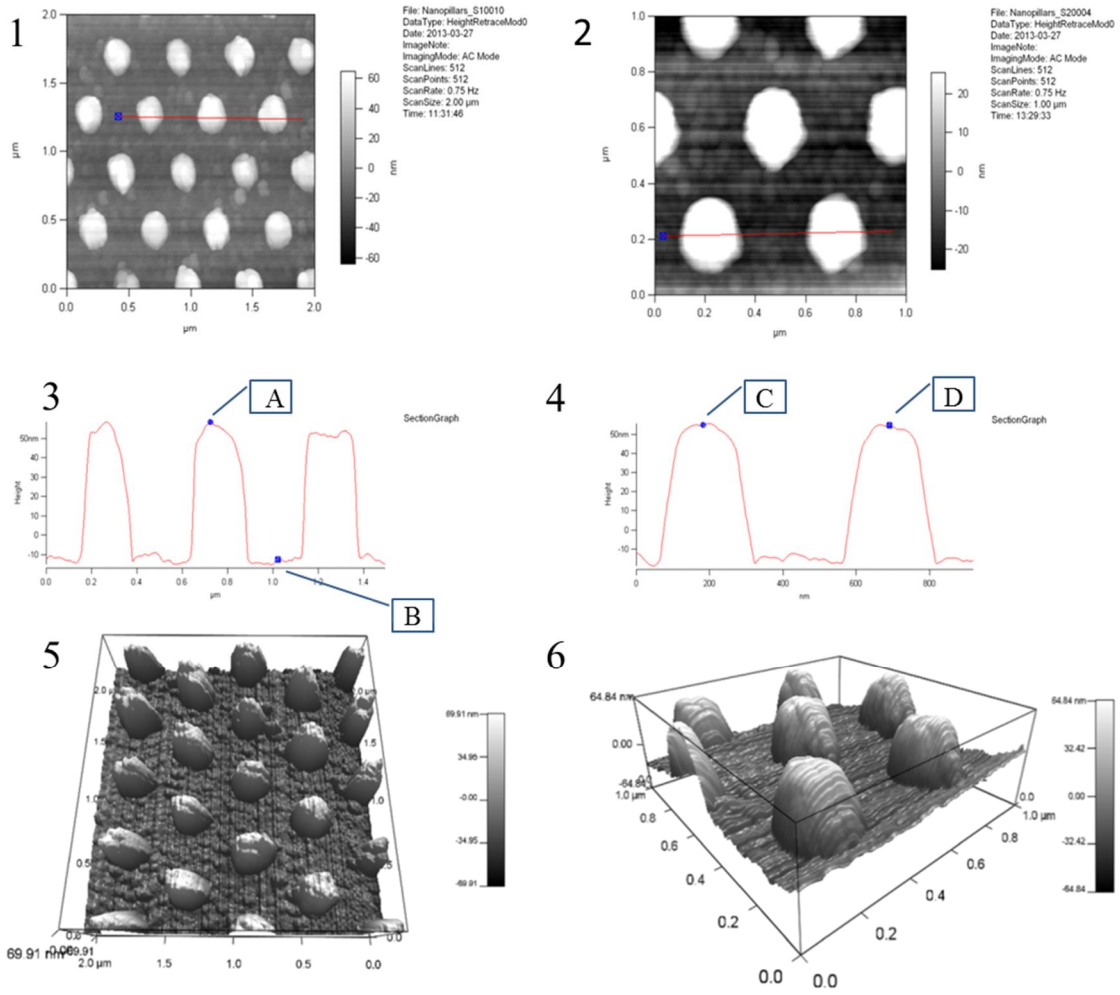

Figure 2.18: AFM pictures giving information about the nanopillars fabricated on the electrode surface

Since this was a qualitative measurement (not quantitative), the calibration of the probe (tip) was not performed on that day using the inverse optical lever sensitivity technique. However, the instrument was routinely calibrated every 6 months (following the manufacturer calibration standards). The AFM was used as an additional technique to confirm that the fabrication steps were successful and estimate the goodness of the pillars topography. With this measurement it was possible to analyse the structure of our nanostructured surface and observe with a good approximation the shape of the nanopillars fabricated on the gold substrate of the impedance electrodes. Figure 2.18 shows a few images of the nanopillars taken with the AFM. Image 1 and image 2 show a representation of the topography and the height of the nanopillars. The area scanned is 2x2 μm^2 for image 1 and 1x1 μm^2 for image 2. In 3 it is represented (in 2D) the line

profile across the nanopillars in the position indicated by the red line in image 1. The height of the nanostructures is approximately 65 nm as can be seen in the graph. Image 4 represents (in 2D) the line profile across the nanopillars in the position indicated by the red line in image 2 and the pitch is approximately 500 nm. Image 5 and 6 show a 3D reconstruction calculated by the AFM software from, respectively, image 1 and 2.

This analysis provided us with information about the topography of the fabricated structures like their shape, pitch, height, etc. In this way also the lateral profile was mapped which could have been rather difficult to inspect using the SEM technique only.

2.10.4 Packaging

The chips fabricated on the Pyrex wafer were then diced using DISCO DAD3350 Automatic dicing machine (Blade Type: Kulicke & Soffa S2040, diamond coated resin, width = 47um; blade speed: 30,000 rpm; cut rate: 0.1 mm/sec) carried out on Loadpoint thermal-release dicing film ("Blue film"). The devices were cut in a rectangular shape of 10 mm in width and 15 mm in length (figure 2.19). During this process they were covered with a protective layer of Shipley S1813 resist to avoid any cracking in the glass. The resist, before packaging, was removed by soaking the devices in warm acetone (~ 40 °C) for 5 minutes, rinsed with DI water and then dried with a nitrogen gun.

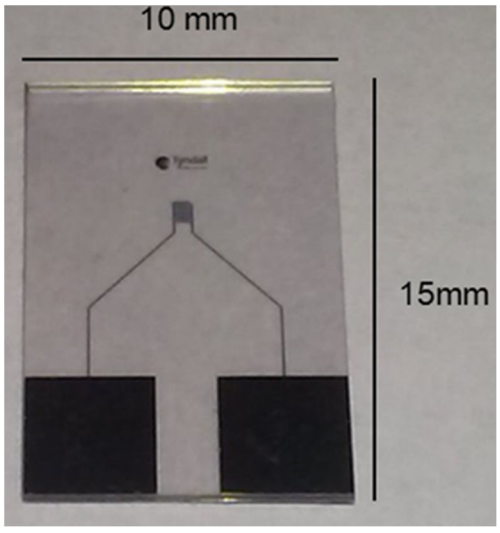

Figure 2.19: Diced device with the impedance electrode

The creation of a well in which to grow the cell culture was done using a parallelepiped-shaped Plexiglas (PMMA) block with a circular hole in its centre (figure 2.20). The plastic block was then glued to the chip through a biocompatible double-sided pressure sensitive adhesive tape of medical grade (Orabond 1397PP, Orafol, Germany). This method proved to be more efficient than any other method tried beforehand like the use of UV-cured glue 68NOA - biocompatible by Norland) or Masterbond EP3HTMED Epoxy by Masterbond which failed after the cleaning process with IPA for use with cells. These were in fact not able to guarantee a lasting seal between the PMMA block and the Pyrex substrate even if that was declared as possible in each datasheet of these products. The devices packaged with these two methods either came apart right after the first wash or leaked once the tissue culture procedure was running wasting a lot of work and time.

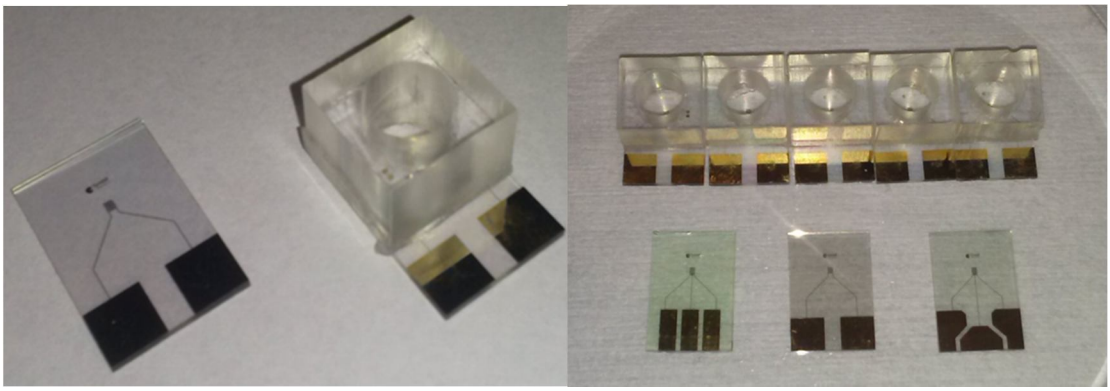

Figure 2.20: Devices after the dicing procedure and packaged with the Plexiglas (PMMA) block to create a volume in which is possible to culture the cells for the cytotoxicity analysis

2.10.5 Contact angle measurement

A contact angle machine was used to test the hydrophobicity and hydrophilicity of the electrode surface (Contact Angle System OCA, DataPhysics Instruments,). Using the sessile drop method (part of the SCA202 software installed on the system) the following results were obtained and they are represented in table 2.2, 2.3, 2.4 and 2.5 for the nanostructured electrodes, the flat electrode and the bare Pyrex substrate. The snapshots

in figure 2.21, 2.22 and 2.23 give an idea of the differences in the droplet shape on the different substrates.

Table 2.2: Contact angle results on the nanostructured electrode (100nm)

Nano 100nm	
CA left	CA right
66.6	66.3
66.7	67.8
67.4	70.2
70.2	70.9
67.2	66.9
67.62	68.42

Table 2.3: Contact angle results on the nanostructured electrode

Nano 60nm	
CA left	CA right
44.2	42.4
49.7	47.8
45.7	48.3
46.4	50.1
49.1	51.6
47.02	48.04

Table 2.4: Contact angle results on the flat electrode

Flat	
CA left	CA right
41.7	40.9
42.2	43.3
43.4	40.8
45.0	44.0
43.3	43.3
43.12	42.46

Table 2.5: Contact angle results on the bare Pyrex substrate

Bare substrate	
CA left	CA right
39.2	38.8
40.7	36.9
42.8	40.3
41.6	39.7
36.6	36.6
40.18	38.46

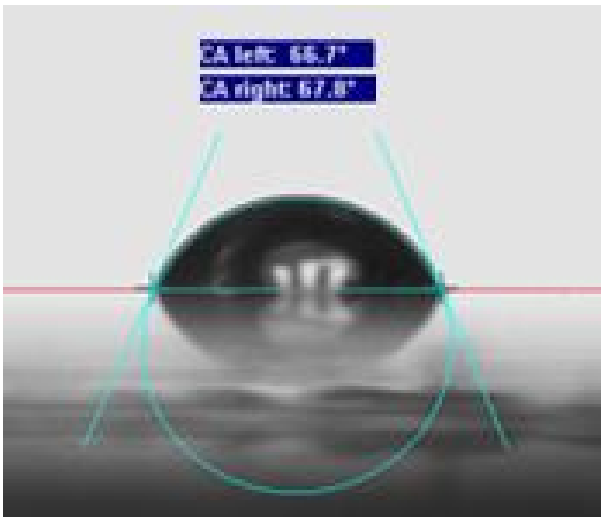

Figure 2.21: Contact angle measurement on the nanostructured electrode (100nm)

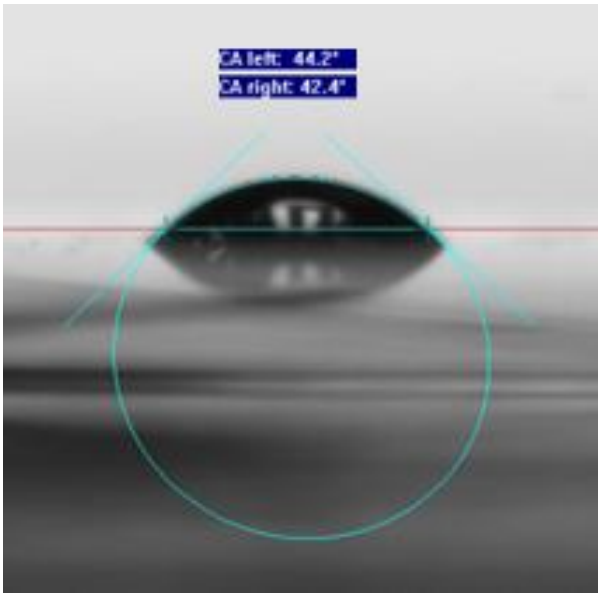

Figure 2.22: Contact angle measurement on the nanostructured electrode (50nm)

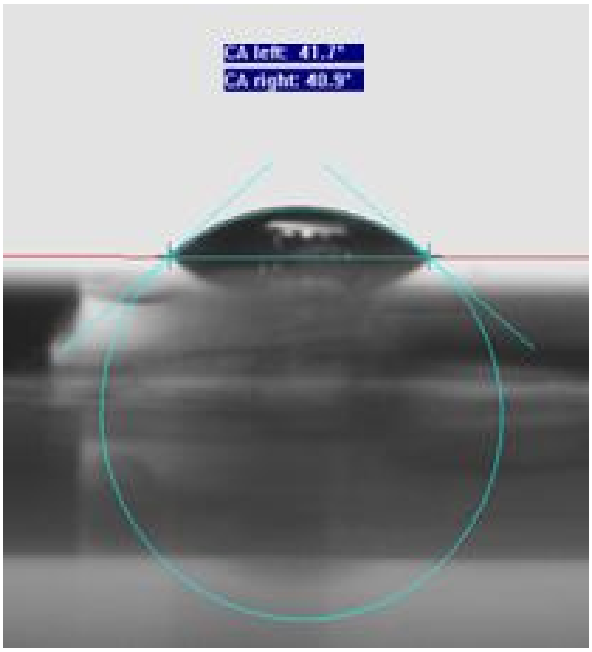

Figure 2.23: Contact angle measurement on the flat electrode

These contact angle figures suggested that the presence of the nanostructures on the electrode surface introduced a small increase in hydrophobicity of the device. Both the average angles for the surfaces were well below the threshold of 90°, over which would define them as hydrophobic surfaces. The difference between the angles measured for the two samples was not high but it showed that the flat surface was slightly more hydrophilic, as expected.

2.11 DISCUSSION

Interdigitated impedance electrodes are very important in biosensing and for measurements on mammalian cells for monitoring their viability and the cytotoxicity of certain drugs and chemical compounds [14, 15].

The electrodes designed in this research comprised of 10 finger electrodes (5 on each branch of the interdigitated electrode) with a spacing and width of 40μm and a length of 500μm. By varying the thickness of the e-beam resist used during the fabrication process, it was possible to obtain nanopillars 60nm or 100nm tall. Many research groups have so far fabricated nanopillars on different substrates for many different uses [36, 37], but no one has yet combined the nanopillars with an impedance detection system.

The material used for both the finger electrodes and the nanopillars was gold. The first choice material, ITO, that would have allowed a complete transparency to the whole system, was not suitable for this kind of fabrication. Some electrodes were fabricated including an Ag/AgCl reference electrode in order to allow electrochemical measurements without using a cumbersome external reference electrode.

Holders and connectors for the devices were designed and fabricated for connecting the electrodes to the impedance detection systems, which were a Zahner IM6e and an Autolab electrochemical workstations.

The devices were fabricated using a combination of UV lithography, metal lift-off, evaporation and e-beam lithography techniques. The electrodes were then packaged using a pressure sensitive, medical grade double-sided adhesive tape.

Analysis using the AFM and SEM confirmed the success of the fabrication processes showing the nanopillars fabricated with the correct layout and dimensions. It was noticed that there was an error that could occur during the fabrication of the pillars on the finger electrodes. Due to misalignment (because of scattering or reflection of the electron beam on the Pyrex substrate) the nanostructures can be shifted of a maximum of ±5μm off the finger electrode area.

A cleaning procedure of the devices was also performed before the use with cell cultures or any other biological compounds to be eventually tested.

The fabrication procedure created a lot of problems at the start of this project and lot of work and time was dedicated to the troubleshooting. Once all the parameters and procedure were defined and finalised, the fabrication proved to be a relatively easy and fast process but still quite expensive. It has been estimated that the total cost was ~20-22 € per device including the labour and all the consumables used. Hopefully in future the fabrication costs might decrease making this technique more economically appealing for the fabrication of nanopillars.

2.12 FUTURE WORK

Further optimisation is envisaged in the fabrication process of the nanopillars to reduce the misalignment on the finger electrodes. New layouts of the electrodes will be experimented for other applications as well as taller nanopillars created by modifying the thickness of the resist. New materials will be also used to try to fabricate both the nanopillars and the electrodes, especially ITO will be tried again as it would be very beneficial in terms of cell imaging under the microscope. The opportunity of having the electrodes working in an array format will be also explored to be embedded in a fluidic system.

2.13 REFERENCES

[1] Y. Iwasaki, M. Morita, "Electrochemical Measurements with Interdigitated Array Microelectrodes", Current Separations 14:1 (1995)

[2] R. R. Kamath, M. J. Madou, "Three-Dimensional Carbon Interdigitated Electrode Arrays for Redox-Amplification", Anal. Chem. 2014, 86, 2963−2971

[3] C. Lee, C. Chiang, Y. Wang, and R. Ma, "A self-heating gas sensor with integrated NiO thin-film for formaldehyde detection," Sensors and Actuators, B: Chemical, vol. 122, no. 2, pp. 503–510, 2007.

[4] C. Park, T. Kwon, B. Kim et al., "Front-side metal electrode optimization using fine line double screen printing and nickel plating for large area crystalline silicon solar cells," Materials Research Bulletin, vol. 47, no. 10, pp. 3027–3031, 2012.

[5] A. Geupel, D. Schonauer, U. Roder-Roith et al., "Integrating nitrogen oxide sensor: a novel concept for measuring low concentrations in the exhaust gas," Sensors and Actuators B: Chemical, vol. 145, no. 2, pp. 756–761, 2010.

[6] C. Tseng, Y. Chou, T. Hsieh, M. Wang, Y. Shu, and M. Ger, "Interdigitated electrode fabricated by integration of ink-jet printing with electroless plating and its application in gas sensor," Colloids and Surfaces A: Physicochemical and Engineering Aspects, vol. 402, pp. 45–52, 2012.

[7] K.S. Chou, C.H. Lee, "Fabrication of Silver Interdigitated Electrode by a Stamp Method", Advances in Materials Science and Engineering, Volume 2014, Article ID 514508, 5 pages

[8] T. N. Ki, R. Wartena, P. J. Yoo et al., "Stamped microbattery electrodes based on self assembledM13 viruses," Proceedings of the National Academy of Sciences of the United States of America, vol. 105, no. 35, pp. 17227–17231, 2008.

[9] L. Montelius, B. Heidari, M. Graczyk, I. Maximov, E.-L. Sarwe, T. G. I. Ling, "Nanoimprint and UV lithography: mix & match process for fabrication of interdigitated nanobiosensors," Microelectronic Engineering, vol. 53, no. 1–4, pp. 521–524, 2000.

[10] T. Burgin, V. Choong, G.Maracas, "Large area submicrometer contact printing using a contact aligner", Langmuir, vol. 16, no. 12, pp. 5371–5375, 2000.

[11] M. Cavallini, D. Gentili, P. Greco, F. Valle, F. Biscarini, "Micro- and nanopatterning by lithographically controlled wetting," Nature Protocols, vol. 7, no. 9, pp. 1668–1676, 2012.

[12] M. M. Islam, K. Ueno, S. Juodkazis, Y. Yokota, H. Misawa, "Development of Interdigitated Array Electrodes with Surface-enhanced Raman Scattering Functionality", Analytical Sciences, 2010, 26(1), 13.

[13] L.H.D. Skjolding, C. Spegel, A. Ribayrol, J. Emneus, L. Montelius, "Characterisation of nano-interdigitated electrodes", Journal of Physics: Conference Series 100 (2008) 052045

[14] P. Van Gerwen et al., "Nanoscaled interdigitated electrode arrays for biochemical sensors", Sensors and Actuators B 49 (1998) 73–80

[15] H. Wang et al., "Electrochemical Biosensor Based on Interdigitated Electrodes for Determination of Thyroid Stimulating Hormone", Int. J. Electrochem. Sci., 9 (2014) 12 – 21

[16] S.K. Kima et al., "Fabrication of comb interdigitated electrodes array (IDA) for a microbead-based electrochemical assay system", Biosensors and Bioelectronics 20 (2004) 887–894

[17] C. E. Chidsey, B. J. Feldman, C. Lundgren, and R.W. Murray, "Micrometer-Spaced Platinum Interdigitated Array Electrode: Fabrication, Theory, and Initial Use", Anal. Chem. 1986, 58, 601-607

[18] A. E. Cohen, R. R. Kunz, "Large-area interdigitated array microelectrodes for electrochemical sensing", Sensors and Actuators B, 62, 2000. 23–29

[19] S. Rana, R. H. Page, C. J. McNeil, "Comparison of Planar and 3-D Interdigitated Electrodes as Electrochemical Impedance Biosensors", Electroanalysis 2011, 23, No. 10, 2485 – 2490

[20] K. Aoki, "Quantitative analysis of reversible diffusion-controlled currents of redox soluble species at interdigitated array electrodes under steady-state conditions", J. Electroanal. Chem., 256 (1988) 269-282

[21] R. Kostecki, X. Song, and K. Kinoshita, "Electrochemical Analysis of Carbon Interdigitated Microelectrodes", Electrochemical and Solid-State Letters, 2 (9) 465-467 (1999)

[22] X. Zhu, C. H. Ahn, "Electrochemical Determination of Reversible Redox Species at Interdigitated Array Micro/Nanoelectrodes Using Charge Injection Method", IEEE Transactions on Nanobioscience, Vol. 4, No 2, June 2005

[23] Z. Zou et al., "Functionalized nano interdigitated electrodes arrays on polymer with integrated microfluidics for direct bio-affinity sensing using impedimetric measurement", Sensors and Actuators A 136 (2007) 518–526

[24] S. M. Radke, E. C. Alocilja, "A high density microelectrode array biosensor for detection of E. coli O157:H7", Biosensors and Bioelectronics 20 (2005) 1662–1667

[25] E. Bakker, Y. Qin, "Electrochemical Sensors", Anal. Chem. 2006, 78, 3965

[26] A. Paschero, E. McLoughlin, E. Moore, "Continuous non-destructive monitoring of cell health using impedance based interdigitated electrode structured sensors", Proceedings of the 5th BioNanoTox and Applications International Research Conference, Little Rock, Arkansas, 4–5 November 2010. AIP, pp. 100-105.

[27] K. F. Lei, "Review on Impedance Detection of Cellular Responses in Micro/Nano Environment", Micromachines 2014, 5, 1-12

[28] R. Ehret et al., "Monitoring of cellular behaviour by impedance measurements on interdigitated electrode structures", Biosensors & Bioelectronics Vol. 12, No. 1, pp. 2941, 1997

[29] X. Huang, D.W. Greve, D. D.Nguyen, M.M. Domach, "Impedance Based Biosensor Array for Monitoring Mammalian Cell Behavior", Sensors, 2003. Proceedings of IEEE Vol. 1, pp 304 – 309

[30] I. Giaever, C.R. Keese, "Use of Electric Fields to Monitor the Dynamical Aspect of Cell Behavior in Tissue Culture", IEEE Transactions on biomedical engineering, Vol. BME-33, No. 2, February 1986

[31] M. Varshney, Y. Li, B. Srinivasan, S. Tung, "A label-free, microfluidics and interdigitated array microelectrode-based impedance biosensor in combination

with nanoparticles immunoseparation for detection of Escherichia coli O157:H7 in food samples", Sensors and Actuators B 128 (2007) 99–107

[32] Y. Fu et al., "Exploiting Enzyme Catalysis in Ultra-Low Ion Strength Media for Impedance Biosensing of Avian Influenza Virus Using a Bare Interdigitated Electrode", Anal. Chem. 2014, 86, 1965−1971

[33] E. Moore, O. Rawley, T. Wood, P. Galvin, "Monitoring of cell growth in vitro using biochips packaged with indium tin oxide sensors", Sensors and Actuators B 139 (2009) 187–193

[34] F. Alexander Jr., D. T. Price, S. Bhansali, Optimization of interdigitated electrode (IDE) arrays for impedance based evaluation of Hs 578T cancer cells, Journal of Physics: Conference Series 224 (2010) 012134

[35] W. L. Moujahid, Electrochemical detection of marine pollution A thesis submitted for the degree of Master of Science to the National University of Ireland, Cork Tyndall National Institute, Cork. July 2011

[36] N.N. Li, N.L. Zhu , Y.F. Zhang , Y.H. Sun and J. Chen , High throughput fabrication of titanium nanopillars by maskless plasma etching, 18th International Conference on Miniaturized Systems for Chemistry and Life Sciences October 26-30, 2014, San Antonio, Texas, USA

[37] S. Sakuma et al, Fabrication of Nanopillar Micropatterns by Hybrid Mask Lithography for Surface-Directed Liquid Flow, Micromachines 2013, 4, 232-242

Chapter 3

3 APPLICATION OF SENSORS FOR CYTOTOXICITY MONITORING AND DRUG SCREENING

3.1 INTRODUCTION

The interaction of mammalian cells with artificial surfaces is interesting for both scientific and medical reasons [1]. Processes like tumor metastasis, wound healing, or cell migration are focused in general on the stationary and dynamic interactions of cells cultured in vitro with a specific substrate [2, 3].

Assays performed on cells in tissue culture have been considered as one of the established areas of in vitro assays that involve measurements of cytotoxicity (the ability of cytotoxic compounds to inflict damage and often kill cells). There is a critical need for determination of the cytotoxic potential danger of chemicals in environmental and medical research and in the food, cosmetic, and pharmaceutical industries [4]. Cytotoxicity can be measured by following the cellular metabolic rate (e.g., tetrazolium salt cleavage), [5] the activity of cytoplasmic enzymes (e.g., lactate dehydrogenase), [6] or the release of particular artificial labels, radioactive or nonradioactive [7]. The two principal methodologies for testing cytotoxicity, the neutral red uptake assay (NR) [8] and the total cellular protein assay [9]. Although useful and widespread, are not suitable for continuous, automated and real-time analysis. Cytotoxicity assays based on the loss of membrane integrity may come across serious limitations since the initial sites of damage of many cytotoxic agents and compounds are intracellular. Therefore, cells can be irreversibly damaged or killed while their membranes are still intact [10]. Other cytotoxicity methods consist of the measurement of pH changes with a microphysiometer [11] and the measurement of the barrier function of a cell layer

(transcellular resistance) upon exposure to test compounds [12]. Both of these noninvasive methods present quantitative data but require cell layers grown on membrane inserts. There have been attempts to study cytotoxic effects by monitoring intracellular motion of small vesicles or organelles in cultured cells using optical analysis [13] and video-enhanced microscopy [14]. The procedures, however, are complex as they require extensive data processing and only provide semiquantitative results. Among all the methods currently in use, particular interest is dedicated to the development of electric cell-substrate impedance sensing (ECIS) as a tool for in vitro toxicity testing. This technique uses a small gold electrode deposited on the bottom of tissue culture wells and immersed in culture medium. Inoculated cells attach to the electrode surface to form a confluent layer. The attached and spread cells act as an insulator because their plasma membranes interfere with the free space above the electrode for current flow. Consequently, a drastic change in the measured impedance due to the cell attachment and spreading can be measured [15 – 17]. Nevertheless, attached and spread neuronal cells were reported to be electrically transparent until tetrodotoxin, a highly specific sodium channel blocker, was added [18]. ECIS is able to provide quantitative information with respect to cell morphological changes, cell movements, and alteration in cellular function in cultures exposed to various drugs, chemicals, and biochemical treatments [19 – 21]. Since cells are sensitive to pollutants, drugs, and toxins, this type of biosensor has been proven as a reliable predictor of cytotoxicity to represent the general cell response resulting from a variety of inhibition mechanisms [22]. ECIS is a versatile and noninvasive tool and is capable to provide quantitative information with respect to cell morphological changes, cell micromotion and alteration in cellular function under various drug, chemical, and biochemical treatments [15, 16, 23- 26].

3.1.1 Electric cell substrate impedance sensing (ECIS)

In ECIS, cells spread onto an electrode and, due to their insulating properties, they impede the flow of current from the electrode to the surrounding media. An alternating current is applied on the electrodes and the voltage is monitored using a lock-in amplifier. In absence of cells cultured on the conductive surface, electric current can flow freely from the surface to the electrodes [27]. Cells growing on the electrode hinder

the current flow and thus increase the resistance of the system (measured in ohms) because cell membrane acts as an insulator. The magnitude and time course of the rise of impedance value is more marked when the cell density approaches the confluence status. Electrodes without any cells show a minimal 'base-line' resistance. The addition of analytes that either kill the cell monolayer or cause disturbances leads to changes in impedance [27]. In confluent cell layers, the current must travel through the cell/electrode gap and then through the intercellular space to reach the surrounding media. The respective resistances of these gaps and spaces affect the current. These resistances are determined by the gaps or tight junctions between cells and various cell-electrode adhesion molecules. At higher frequencies, the current can take a transcellular pathway, revealing information about the plasma membrane and cytoplasm. For single frequency impedance measurements (over time analysis), a preliminary examination of the impedance spectra allows for the selection of a suitable operating frequency. To improve experimental resolution, the working frequency is typically selected in the region with the greatest variations in impedance vs. changing experimental conditions [28].

Typically, two different electrode structures are used in impedance sensing: the monopolar [24, 29] and the interdigitated [30, 31]. With the monopolar structure, the area around the working electrode is relatively large, only a few cells on the relatively small working electrode contribute to the measured impedance, which results in fluctuations among different sets experiments. Moreover, this design involves the fabrication of counter electrode significantly larger than the working which hinders further miniaturization, essential in a high-throughput screening (HTS) system. On the other hand, the interdigitated structure shows improved performance as the current flows in the vicinity of the electrodes surface. A much higher sensitivity to impedance change is demonstrated compared with the conventional design [32]. However, no preference can be given to these two prototypes without considering their specific applications.

3.2 OBJECTIVES

Literature has showed a new trend in tissue cultures for the manipulation of cells with the use of 3D structured dishes. Many have reported a different appearance of the cells cultured on such substrates [33-35]; cells in fact do not look anymore flat and spread like in the standard tissue cultures dishes but they appear more rounded and closer in appearance to what they would look like in a normal in-vivo tissue [36]. The objectives are

- Study whether the nanopillars allow a good growth of the cells on them
- Study if with electrical impedance measurements for cytotoxicity monitoring it is possible to achieve better sensitivity in the assay compared to the same type of flat electrodes.
- Test three different cell lines for on the nanostructured electrodes exposed to two different chemicals to determine their cytotoxicity on A549, Balb c3T3 and HeLa cell lines. The chemicals used are an extract of Antrodia Camphorata and Nicotine.
- Take images of different cell lines immobilized on the flat and nanostructured surfaces to compare their morphology and observe how the surface topography influences the attachment of cell.

Low aspect ratio of the nanopillars was adopted to avoid a too low focal contact of the cells with the substrate [37-39].

3.3 EXPERIMENTAL DETAILS

3.3.1 Materials - Cell lines

Three different cell lines were used in these impedance measurement experiments: A549 (Human epithelial cells from lung carcinoma), BALB/c 3T3 (Clone 31, fibroblasts from mouse embryo) and HeLa (Human epithelial cells from cervical carcinoma). The tissue culture work was carried out entirely in the Tyndall National Institute laboratories.

3.3.1.1 A549 cell line

A549 are human epithelial cells from lung carcinoma and this line was initiated in 1972 by D.J. Giard, et al. [40] through explant culture of lung carcinomatous tissue from a 58-year-old Caucasian male (CCL-185, American Type Culture Collection, Manassas, VA, USA). A549 cells are grown as a monolayer. For this cell line it was necessary a decomplemented serum and that the media was changed 2-3 times weekly. Their doubling time was approximately 22 hours. The protocol for subculturing A549 cell in T75cm^2 flask was as follows: the old media was removed and discarded; then the flask was gently rinsed with 10mls of warmed HBSS (Hank's Balanced Salt Solution) which was then discarded. Subsequently, 3 ml of warmed trypsin-EDTA (ethylene diamine tetra acetic) acid were added to ensure that the base of the flask was coated. Then the flask was incubated for 5mins at 37^{o}C. To ensure cells have lifted, the flask was gently tapped and checked using the microscope. An excess of warmed routine media (7mls) was added and the solution was transferred to a universal container (or tube) which was then centrifuged at 1000rpm for 5 minutes. The supernatant was removed and discarded. The pellet was re-suspended in routine media and transferred to a new flask (subcultivation ratio of 1/3 to 1/8 as recommended by manufacturer). The cultures were maintained at a cell concentration between 6 X 10^3 and 6 X 10^4 cell / cm^2. Finally the flask was topped up with fresh warmed routine media. A final volume of 15mls with an extra 5mls added per each extra day as recommended (e.g. Friday to Monday would require a volume of 25mls.)

3.3.1.2 BALBc 3T3 cell line

The BALBc 3T3 (clone A31) is one of several cell lines developed by S.A. Aaronson and G.T. Todaro in 1968 [41] from disaggregated 14- to 17-day-old BALB/c mouse embryos (CCL-163, American Type Culture Collection, Manassas, VA, USA). BALB/c 3T3 cells are routinely grown as a monolayer and they are extremely sensitive to contact inhibition. For this reason, the users should never allow cultures to become fully confluent before passaging. At subconfluence cells are elongated and very much fibroblast-like. If the cells are allowed to grow up to a 100% confluence level and remain in this condition for any length of time, the cells take on a more flattened, epithelial-like morphology; cells then become extremely granulated and stop dividing.

NBCS must be used as FBS can interfere with contact inhibition. Decomplemented serum, unlike the A549 cells, is not necessary for this cell line. Media must be changed twice a week.

The protocol for subculturing BALBc 3T3 cell in T75cm^2 flask was as follows: the old media was removed and discarded; then the flask was gently rinsed with 10 ml of warmed HBSS (Hank's Balanced Salt Solution) which was then discarded. Subsequently, 4 ml of warmed trypsin-EDTA (ethylene diamine tetra acetic) acid were added to ensure that the base of the flask was coated. Then the flask was incubated for 5 minutes at 37^{o}C. To ensure cells have lifted, the flask was gently tapped and checked using the microscope. An excess of warmed routine media (6 ml) was added and the solution was transferred to a universal container (or tube) which was then centrifuged at 1000rpm for 5 minutes. The supernatant was removed and discarded. The pellet was re-suspended in routine media and transferred to a new flask (subcultivation ratio of 1/3 to 1/5 as recommended by manufacturer). Finally the flask was topped up with fresh warmed routine media. A final volume of 15mls with an extra 5mls added per each extra day as recommended (e.g. Friday to Monday would require a volume of 25ml).

3.3.1.3 HeLa cell line

HeLa are Human epithelial cells from cervical carcinoma and it is the oldest and most commonly used human cell line [42]. The line was derived from cervical cancer cells taken by researcher George Gey on February 8, 1951 [43], from Henrietta Lacks, a patient who eventually died of her cancer on October 4, 1951. This cell line was extraordinarily durable and prolific even if contaminated with many other cell lines used in research. Before this, cells cultured from other cells had a life span of just a few days. Cells from Lacks's tumour sample, however, behaved differently from the others. Gey was able to isolate a single cell, multiply it, and start the cell line. The sample was named HeLa after the initial letters of Henrietta Lacks' name. As the first human cells grown in a lab that were "immortal" (they do not die after a few cell divisions), they could be used for conducting many experiments. HeLa cells are grown as a monolayer. Their doubling time is 24 hours and their media must be refreshed 2-3 times a week

The protocol for sub culturing HeLa cell in T75cm^2 flask was as follows: the old media was removed and discarded; then the flask was gently rinsed with 10 ml of warmed HBSS (Hank's Balanced Salt Solution) which was then discarded. Subsequently, 2 ml of warmed trypsin-EDTA (ethylene diamine tetra acetic) acid were added to ensure that the base of the flask was coated. Then the flask was incubated for 2 minutes at 37^{o}C. To ensure cells have lifted, the flask was gently tapped and checked using the microscope. An excess of warmed routine media (8 ml) was added and the solution was transferred to a universal container (or tube) which was then centrifuged at 1000rpm for 5 minutes. The supernatant was removed and discarded. The pellet was re-suspended in routine media and transferred to a new flask (subcultivation ratio of 1/3 to 1/5 as recommended by manufacturer). Finally the flask was topped up with fresh warmed routine media. A final volume of 12-15mls with an extra 5mls added per each extra day as recommended (e.g. Friday to Monday would require a volume of 25ml).

3.3.1.4 Antrodia Camphorata

Antrodia Camphorata is a unique mushroom of Taiwan, which has been used as a traditional medicine for protection of diverse health-related conditions. Antrodia Camphorata is a fungal parasite on the inner cavity of the endemic species Cinnamomum kanehirae (Bull camphor tree) Hayata (Lauraceae). The host plant is a large evergreen broad-leaved tree, which only grows in Taiwan, and is distributed over broad-leaved forests at an altitude of 2000m. Being a local species, A. Camphorata was historically used in Taiwan by the aborigines as a traditional prescription for the discomforts caused by alcohol drinking or exhaustion. Furthermore, the regular consumption is believed to preserve human vitality and promote longevity [44]. The preparations from fruiting bodies have been used for the prevention, or treatment, of numerous diseases including liver diseases, food and drug intoxication, diarrhea, abdominal pain, hypertension, itchy skin and tumorigenic diseases [45, 46]. Both the fruiting bodies and mycelium of *A. Camphorata* have potent anti-proliferative activity against various cancers *in vitro* and *in vivo*. It was indicated that there were multiple potent mechanisms underlying the anti-cancerous effects of *A. Camphorata*. The crude $CHCl_3$/MeOH extract from fruiting bodies of *A. Camphorata* exhibited significant cytotoxic activity against P 388 murine leukemia cells [47]. The ethylacetate extract

from fruiting bodies of *A. Camphorata* (EAC) exhibited apoptotic effects in two human liver cancer cell lines, Hep G2 and PLC/PRF/5 in a dose dependent manner [48]. In another study, the ethanolic extract from solid-state cultivated mycelia of *A. Camphorata* showed potent anti-proliferation effect in human non-small cell lung carcinoma A549 cells but not primary human fetal lung fibroblast MRC- 5 cells [49].

3.3.1.5 Nicotine

Nicotine, an organic compound found in all tobacco leaves, is the quintessential compound responsible for a smoker's dependence on cigarettes [50]. On average, each cigarette contains 10 to 14 mg of nicotine. Smokers can vary their nicotine intake levels by modulating the frequency and volumes of puffs; however, approximately 1 mg of nicotine is actually absorbed systemically. A weak base, nicotine is absorbed more readily in basic conditions as opposed to acidic conditions. The slightly basic conditions and large surface area of the lungs, therefore, provide one of the most optimal conditions for nicotine absorption following inhalation. Once in the bloodstream, nicotine is quickly exposed to all organs through cardiovascular circulation. Average blood nicotine levels in chronic smokers have been shown to reach 19.0 +/- 11.3 ng per ml after the first cigarette and 22.9 +/- 11.2 ng per ml after the second cigarette [51], correlating to 0.117 +/- 0.070 μM and 0.141 +/- 0.069 μM, respectively. The effects of nicotine exposure are highly dependent on the dose of nicotine administered [52]. As a result, positive and negative effects of nicotine are common. Nicotine treatments have been shown to improve diseases such as ulcerative colitis [53], Alzheimer's [54] and Parkinson's [55]. On the other hand, nicotine has been shown to adversely affect embryonic stem cell development [56], as well as delay skeletal healing following traumatic injury [57].

3.3.1.6 Reagents

For the culture of the A549 cells these reagents were used: DMEM, FBS (cat. F9665), HEPES buffer (Sigma cat. H0887), HBSS w/o calcium and magnesium (Sigma cat. H6648), Trypsin EDTA (Gibco cat. 25300-062). The routine media was made of DMEM supplemented with FBS (10%), and L-glutamine (1%) freeze media: Routine media + 5% DMSO (Dimethyl Sulfoxide). For the culture of BALBc 3T3 cells these

reagents were used: DMEM with 4.5 g/L glucose and glutamax (Gibco cat. 31966-021), Newborn Calf Serum (not FBS Gibco cat. 26010-074), HBSS w/o calcium and magnesium (Sigma cat. H6648), Trypsin EDTA (Gibco cat. 25300-062). The routine media was made of 450mls DMEM + 50mls NBCS (No antibiotics). The freeze media was made of routine media + 5% DMSO. For the culture of HeLa cells these reagents were used: Reagents Used: MEME sigma, FBS (Sigma cat. F9665), Penicillin/Streptomycin (Sigma cat. P4333), HBSS w/o calcium and magnesium (Sigma cat. H6648), Trypsin EDTA (Gibco cat. 25300-062). The routine media was made of: DMEM (500mls), FBS (50mls, 10%), Penicillin/Streptomycin (2.5mls, 5mM). The freeze media was made of routine media + 5% DMSO. Liquinox (Alconox, NY, USA), IPA (Isopropyl Alcohol, Sigma), Resazurin sodium salt (powder, BioReagent, Sigma), Trypan blue (powder, BioReagent, Sigma)

All the above reagents were purchased from Sigma Aldrich, Dublin, Ireland. DMEM + glutamax (Gibco) was purchased from Gibco Biosciences, Dublin, Ireland.

A. Camphorata was collected from the Yuli, Hualien County, Taiwan, in December 2006. A voucher specimen (YMT 6002) was deposited in the Herbarium of the Institute of Biochemical Sciences and Technology, Chaoyang University of Technology, Taiwan, ROC. It was then given to us by Professor John Luong, Biotechnology Research Institute, National Research Council Canada, Montreal, Quebec. Nicotine was purchased from VWR International Ltd. (VWR International, Northern Ireland Ltd.).

3.3.2 Apparatus

Zahner IM6e Electrochemical workstation (ZAHNER-elektrik GmbH & Co. KG, Kronach, Germany); CO_2 incubator Panasonic MCO-18AC-PE (Panasonic Biomedical, Leicestershire, UK); Hettich Centrifuge Universal 320 (Andreas Hettich GmbH, Tuttlingen, Germany); Optical Microscope Olympus CKH41SF (Olympus Life Science Europe, Hamburg, Germany)

3.4 PROCEDURES

3.4.1 Cell count-Trypan blue exclusion assay

The trypan blue (TB) method is a very common assay for evaluating cytotoxicity in experimental investigations where dead cells absorb TB into the cytoplasm because of loss of membrane selectivity, whereas live cells remain unstained. The Trypan blue exclusion test was used, in our case, to check the percentage of viable cells present in a cell suspension. After exposure to TB, live cells appear white and dead cells appear blue upon microscopic examination [58]. Equal volumes of Trypan blue stain and cell suspension were mixed before cells were examined and counted with a hemocytomer. This is used to determine the quality of the cell suspension prior to use in an experiment. Cell suspensions used in our cytotoxicity experiments showed a cell viability of ≥95%.

3.4.2 Resazurin assay

The resazurin assay performed here measures the reduction of blue non-fluorescent 1,2,3 Resazurin dye (7-hydroxy-3H-phenoxazin-3-one10-oxide) to pink fluorescent resorufin by metabolically active cells indicating cell viability. Cell health can be monitored by numerous methods. Plasma membrane integrity, DNA synthesis, DNA content, enzyme activity, presence of ATP, and cellular reducing conditions are known indicators of cell viability and cell death. Resazurin assays are used as cell health indicator by using the reducing power of living cells to quantitatively measure the proliferation of various human and animal cell lines, bacteria, plant, and fungi allowing also establishing relative cytotoxicity of agents within various chemical classes. [59] When cells are alive they maintain a reducing environment within the cytosol of the cell. Resazurin is a non-toxic, cell permeable compound that is blue in colour and non-fluorescent. Upon entering cells, resazurin is reduced to resorufin, a compound that is red in colour and highly fluorescent. Living cells continuously convert resazurin to resorufin, increasing the overall fluorescence and colour of the media surrounding cells. The reduction of resazurin correlates with the number of live mammalian cells presents [60]. The level of reduction was quantified through measurements with a spectrophotometer at 445nm and at 590nm emission frequencies.

Resazurin was dissolved in HBSS at a final concentration of 440µM.

MW= 251.17g/L

440µM = 251.17g x 440 x 10-6 =0.110515g/L

Resazurin (440µM) was sterile filtered using a syringe with 0.45nm pores prior to use in cell culture.

Resazurin (440µM) was diluted in routine media at 10% giving 44µM concentration to be added to cells.

3.4.3 Impedance measurement setup

Impedance measurements have been performed with a Zahner IM6e electrochemical workstation and impedance analyser (Zahner-elektrik GmbH, Kronach – Germany). This instrument allowed to perform both time and frequency analysis on the in-house fabricated electrodes described in Chapter 2. The cables connected to the instrument were kept at the minimum length possible in order to avoid any external noise and the "antenna" effect when working at higher frequencies, even though the range of those used for our tests would require cables of few meters in length to show this undesired behaviour. The instrument came in with its own dedicated Thales software in which it was possible to select different kind of tests. EIS program was used for the frequency tests and the C/E measurement option was selected for the time analysis (fixed frequency over time). In the picture below it is possible to see that the instrument had to be located on a trolley as the measurements on the tissue culture needed to be performed in sterile fume hoods to avoid the culture contamination and the risk of biological hazards for the laboratory users and then removed from the laboratory to comply with the strict guidelines that tissue culture facilities have to follow. The instrument comprises of two parts: the communication box (the smaller device under the laptop in figure 3.1) and the impedance measurement unit. The smaller box works as an interface to eventually connect several different units to same computer. They both communicate with the laptop via USB connection.

Figure 3.1: Zahner impedance analyser setup near the fume hood for cytotoxicity measurements

The system has four channels for taking the impedance measurements and would offer several other configurations also for non-impedance related tests. In this case, since impedance electrode had a two-pad configuration, it was necessary to short-circuit the reference and counter electrode probes (green and red respectively) and the sense and test (working) electrode probes together (blue and black respectively) as in figure 3.2. In order to make this connection more stable, a little bar of copper was soldered on one clip of each couple and to which the other one was then attached before the experiment (figure 3.3). In case of disconnection of one of these clips, the system stops the measurement warning the user of the interruption of the potentiostatic loop.

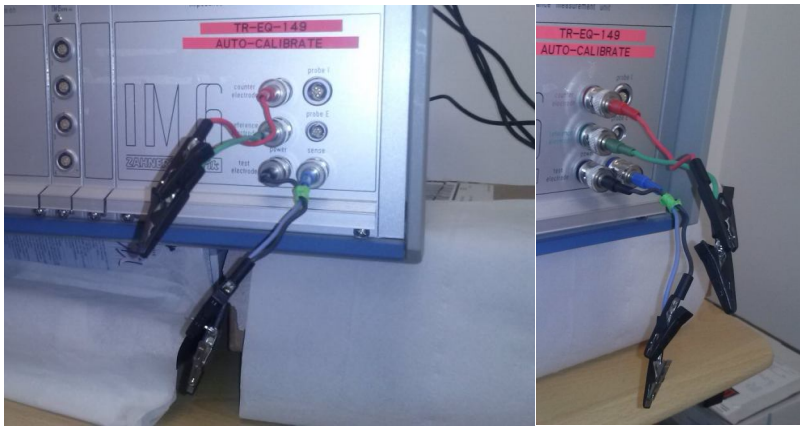

Figure 3.2: (Left) the four different probes of the impedance analyser (reference: green; counter: red; working: black; sense: blue).
Figure 3.3: (Right) Probes short-circuited for measurements

In the screenshots below it is possible to notice that the Thales software offers two options for the impedance experiments: a frequency analysis and a time analysis. To use the first one it was necessary to select the EIS program. In the following menu it was possible to choose the range of operating frequencies and the amount of samples to be collected under and above 66Hz and how many sine waves should be used for measuring each data point. The frequency analysis was useful to establish a frequency to use during the time analysis. To operate a time analysis it was necessary instead to select the C/E menu and click on the measurement icon. In the following menu it was possible to choose different options; in this case the time box was selected. Under the "linear scan" menu it was possible to select the parameters of the measurement which were the duration and the delay between samples. For both the EIS and the C/E, prior to start the measurement, it was necessary to open the potentiostats menu. Here the potentiostat can be turned on allowing the user to select the desired signal amplitude and the frequency to use during an analysis over time (figure 3.4).

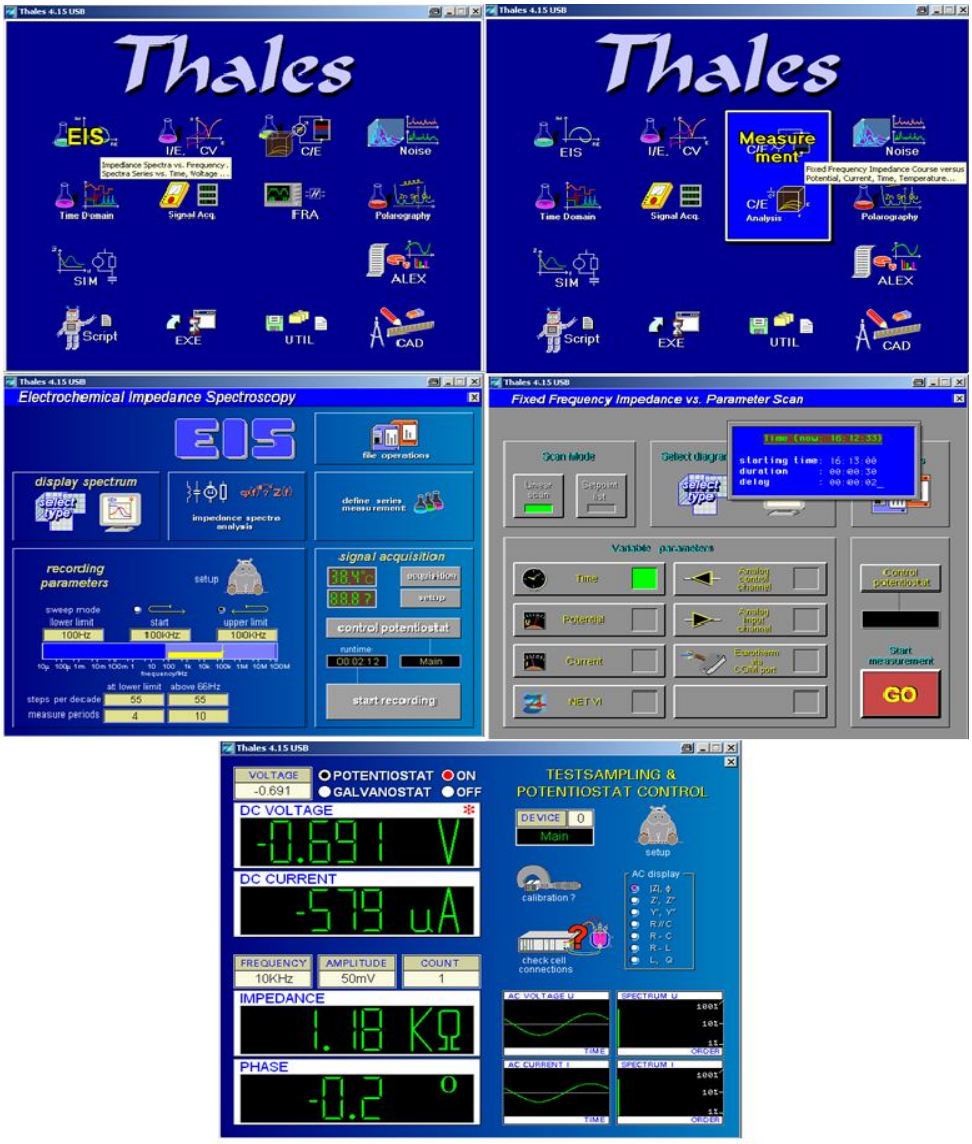

Figure 3.4: Thales software screenshots. On the left is shown the menu for setting up a frequency measurement on the right the time analysis. Both can access the same Potentiostat menu

3.4.4 Impedance measurement protocol

The parameters for impedance measurement were selected in the software described above. For the frequency analysis a range going from 100Hz to 100MHz with 55 samples taken per decade (in a logarithmic scale), 10 sine waves per each sample and signal amplitude 50mV was used. In the time analysis the experiments lasted 30 seconds with a delay of 2 seconds between each sample, frequency 10 kHz, signal amplitude 50mV. The electrodes with the cultured cells were inserted in the holder fabricated in-house described in chapter 2. The holder was kept inside the fume hood to avoid sample

contaminations and connected through short wires to the impedance analyser cables. As described before, reference and counter were short-circuited as well as the test and sense cable. In order to avoid any possible contact of the metal clips with the metallic surface of the fume hood, the clips were placed on a thick paper tissue scotch-taped to the fume hood surface.

3.4.5 Cytotoxicity testing

ECIS technique was used to evaluate the cytotoxicity effect of the chemicals on the cultured cells. An extract of Antrodia Camphorata and Nicotine were tested on A549 immortalized cell line using five flat electrodes and five nanostructured electrodes. Of these, one was used as a positive control, one as a negative control and the remaining three as test electrodes with the drugs. The cells were cultured for 24h and impedance figures at a frequency of 10 kHz (with a signal amplitude of 50mV) were recorded for each electrode in tests lasting 30 seconds each with a data sampling of 2 seconds (15 data points for each measurement) repeated for 3 times. The chemicals were then added to the cells cultured on the three test electrodes while the negative controls were exposed to a drop of Liquinox detergent (used to clean bio samples). The positive control was tested in the same way but no chemical was added. Impedance was then recorded again at 48 hours to evaluate the cytotoxic effect over the following 24 hours in the same way as described above.

The impedance analyser was transported for every test in the tissue culture facility as every test had to be carried out in the fume hood to avoid any kind of contamination. Cables long enough to reach the inner part of the fume hood were selected keeping in account their length, which could have affected the measurement outcome.

For each measurement, the sealed Petri dishes containing the devices with the cultured cells were removed from the CO_2 incubator and placed in the fume hood for as short time as possible to avoid contaminations and thermal shocks to the cells which could have died as a direct consequence. After every set of measurements the cells were placed back again in the incubator.

3.4.6 Cell fixing procedure for SEM imaging

After the cells were cultured on the impedance electrodes at the desired confluence level, they were fixed for an evaluation under the SEM microscope. The cell media was removed and substituted with a primary fixative solution containing Glutaraldehyde, Paraformaldehyde in 0.1M Sodium Cacodylate/HCl buffer pH 7.2. After the cells have been immersed in the fixative for 90 minutes, they have been washed with an SEM buffer for 30 minutes before being immersed for 120 minutes in Osmium Tetroxide. After this the samples are soaked again in SEM buffer overnight. The dehydration process is constituted of several consecutive washes with a solution containing an increased concentration of Acetone (as it can be seen in the table 3.1 below).

Table 3.1: Protocol for fixing the cells for SEM imaging

Fixation	**Day 1**
Primary Fixative	90 mins
Buffer Wash	30 mins
Osmium Tetroxide (OsO_4)	120 mins
Buffer	Held overnight

Dehydration	**Day 2**
25% Acetone	15 mins
50% Acetone	15 mins
75% Acetone	15 mins
100% Acetone	15 mins
100% Acetone	15 mins
100% Acetone	15 mins
100% Acetone	15 mins

Once the Acetone sequence was completed, the cells were transferred into tetramethylsilane (TMS) solution for 15 minutes and then air-dried from TMS in fume hood. Samples were then mounted on the metal stubs using double-sided carbon tape

and sputter coated with ~5 nm layer of gold using Quorum Q150 RES Sputter Coating System.

Samples were held in a desiccator until they were examined using Jeol JSM 5510 Scanning Electron Microscope.

3.5 RESULTS

3.5.1 Optical analysis

Both flat and nanostructured electrodes were inoculated with the same amount of cells, cultured and maintained at 37°C +5% CO_2 and analysed under an optical microscope. The cells on both electrodes were analysed and compared in terms of confluency. They looked quite similar in terms of spreading and confluence, however, the cells growing on the flat electrode had a larger surface area if analysed singularly compared to those growing on the other device. This showed that the nanostructures did not inhibit the growth of cells on the culturing surface. It was however necessary to analyse further the cells closely with the aid of a scanning electron microscope. Different numbers of cells seeded at 24 hours of incubation were examined on both kinds of devices giving always similar results. As follows, there are a few examples of pictures obtained with an optical microscope with A549 (figure 3.5 and 3.6) and BALBc 3T3 cells (figure 3.7 and 3.8).

In figure 3.5 are represented confluent layers of A549 cells growing on a flat electrode (left) and on a nanostructured electrode (right). The initial amount of cells placed on the device was 30000. It is possible to note, after 24 hours growth, how slightly bigger the cells on the left picture are compared to those on the right. Same observations can be made for figure 3.6, were the initial number of cells was 50000.

A similar situation was observed using BALBc 3T3. In figure 3.7 are shown confluent layers of cells grown for 24 hours (from an initial number of 30000) on a flat electrode (left) and on a nanostructured electrode (right). Same procedure was followed for the cells shown in figure 3.8 which had a starting quantity of 50000. It is possible to notice that, in both cases, the cells growing on the flat electrode (shown on left in both cases) had a higher surface area compared to those on the nanostructured electrode

(The cells to be observed are those close to the fingers of the interdigitated electrodes as those are the ones potentially influenced by the presence of the nanopillars)

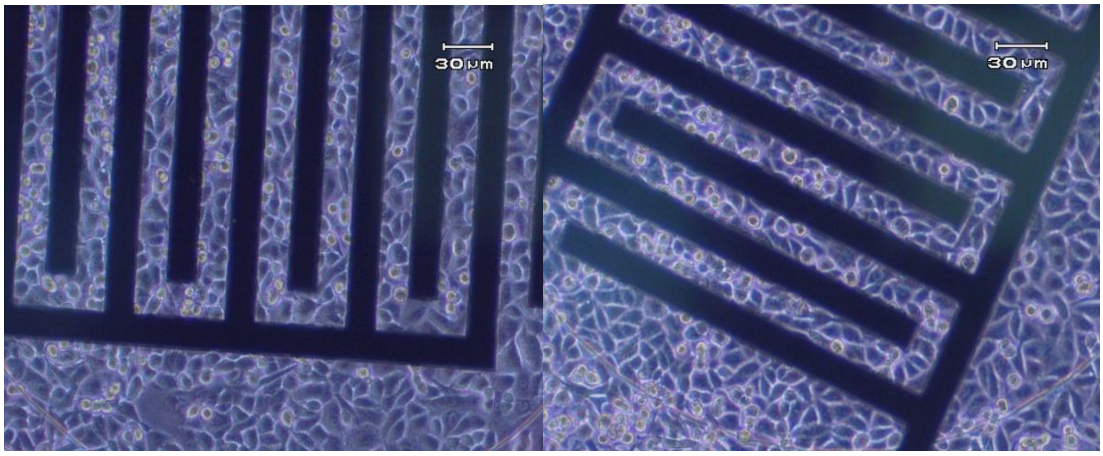

Figure 3.5: 30000 A549 cells on a flat electrode (left) and on the nanostructured electrode (right) after 24 hours

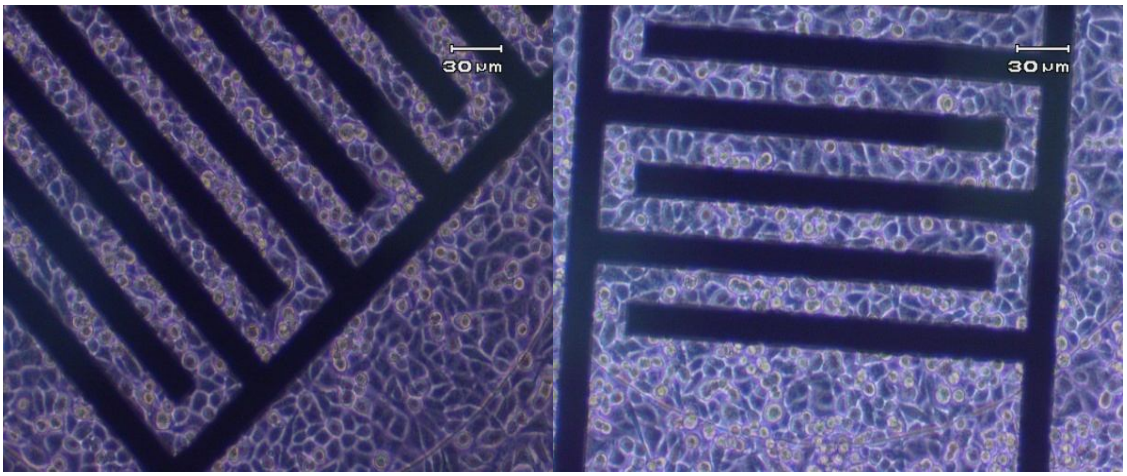

Figure 3.6: 50000 A549 cells on a flat electrode (left) and on the nanostructured electrode (right) after 24 hours

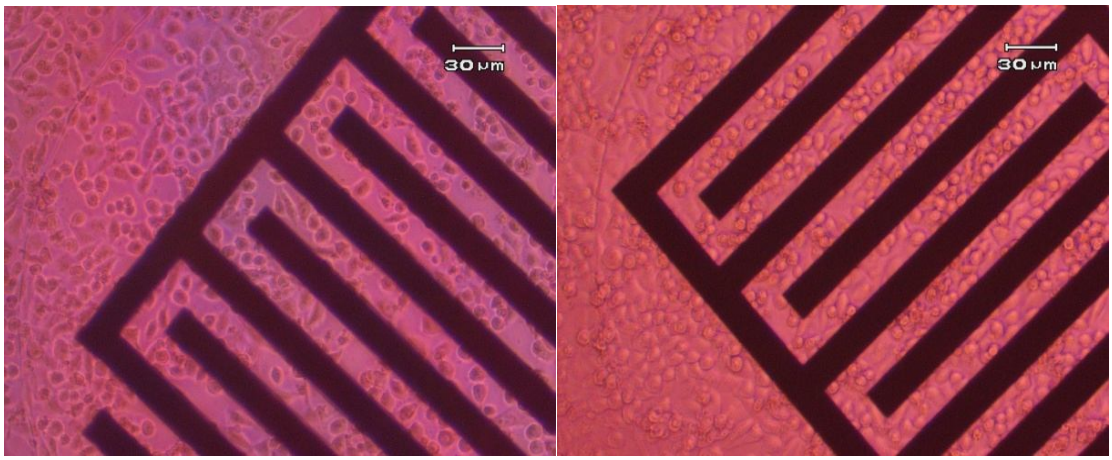

Figure 3.7: 30000 BALB cells on a flat electrode (left) and on the nanostructured electrode (right) after 24 hours

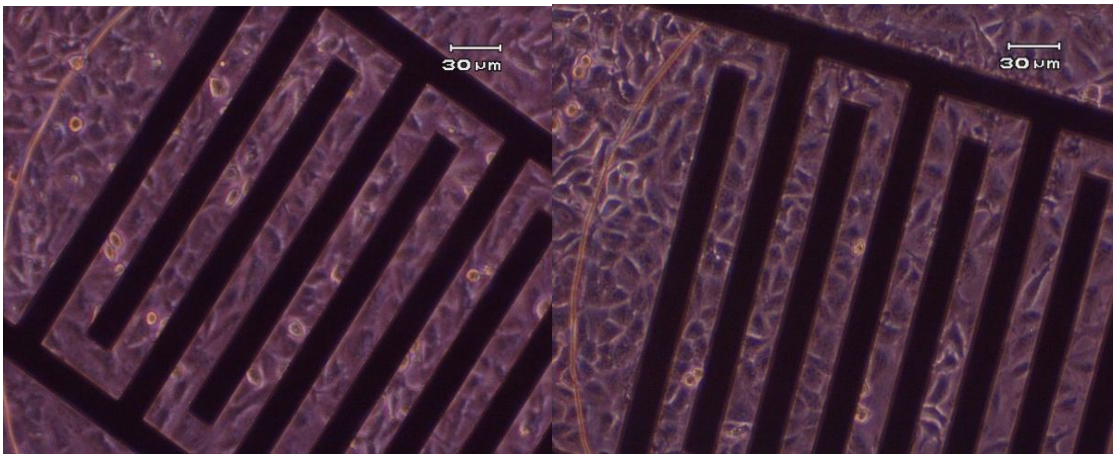

Figure 3.8: 50000 BALB cells on a flat electrode (left) and on the nanostructured electrode (right) after 24 hours

3.5.2 SEM analysis

The three cell lines used in this research were analysed under the scanning electron microscope (SEM) to have a better insight on their morphology since the analysis with the optical microscope could not give enough information on their shape and spreading. The cells were cultured for 24 hours before being fixed following the procedure explained in paragraph 3.4.6.

The HeLa cell line showed some differences when cultured on the flat and on the nanostructured electrode. The cells immobilised on the flat electrode looked, as expected, very flat and well spread with very long filopodia. Those growing on the nanostructures instead showed a lower surface area and looked more three-dimensional compared to the ones growing on the flat electrodes; the differences however are not very marked. It was quite clear at least that the cells growing on the flat electrode had a very close focal contact with the substrate, while the cells attached to the surface with nanopillar showed a bigger gap between the electrode and the basal membrane of the cell. This should, in theory, have increased the resistive and capacitive contribution to the impedance measurement during the ECIS analysis. Also, the intercellular gaps seemed to be quite tight for both the cases.

Same differences could be observed on the A549 cell line. These cells looked very three-dimensional when attached to the nanostructured gold substrate showing again none or very small cell protrusions.

A little or no differences were noticed on the Balb cells growing on the two different electrode surfaces.

For example figure 3.9 shows HeLa cells growing on a nanostructured surface which caused the formation of quite wide gaps between the basal membrane and the substrate. In the yellow circle it is possible to see a portion of the nanopillars fabricated outside the electrode area which still affected the cell morphology making it appear very three-dimensional. In the red circles are highlighted the gaps formed between the basal membrane and the substrate; it was also possible to notice how small and short the filopodia looked on the nanostructures. Figure 3.10 shows a single HeLa cell on a flat electrode; contrarily to what happens in figure 3.11, the cell looked well spread on the substrate and showed very long filopodia (highlighted in the blue circles), while in the other picture the same kind of cell looked more round with very few filopodia visible and a surface area smaller than the one in figure 3.10. In figure 3.12 it can be clearly observed the small single focal adhesion points that the cell had with the nanostructured surface and the big gaps formed between the basal membrane and the electrode. Figure 3.13 and 3.14 both show images of an A549 cell. In both the cases, it is visible that they had a very limited number of very short protrusions and the cells looked very three-

dimensional, especially the one in figure 3.14 which looked almost like a sphere growing on the nanopillars. The BALB cells, as shown in figure 3.15, did not show any relevant differences when cultured on the flat or on the nanostructured surface.

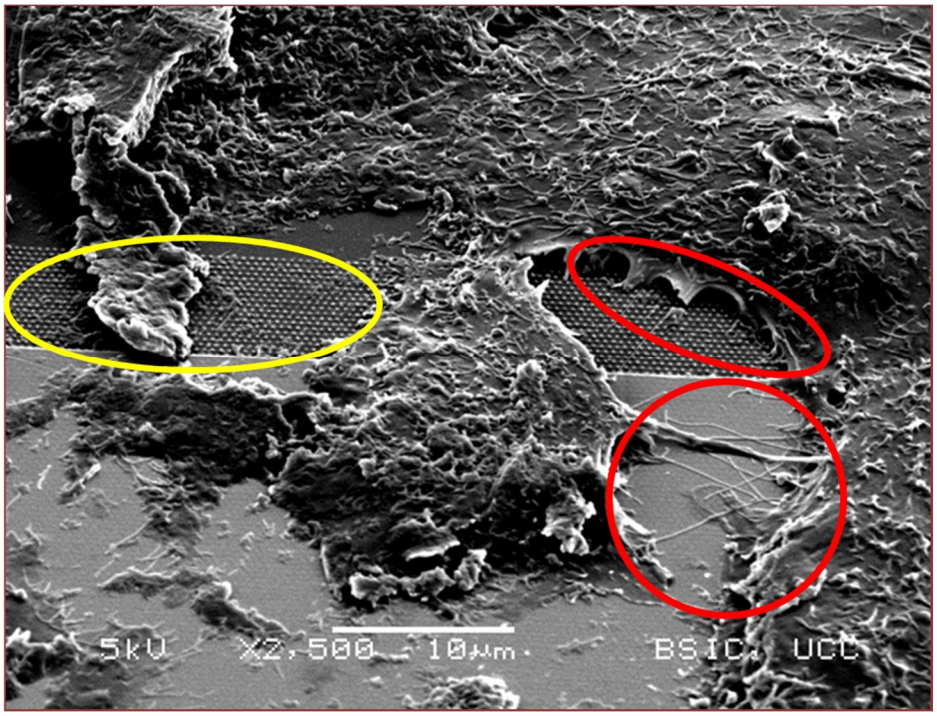

Figure 3.9: HeLa cells, SEM tilted image x2500, influence of nanopillars for the creation of gap between the basal membrane and the substrate

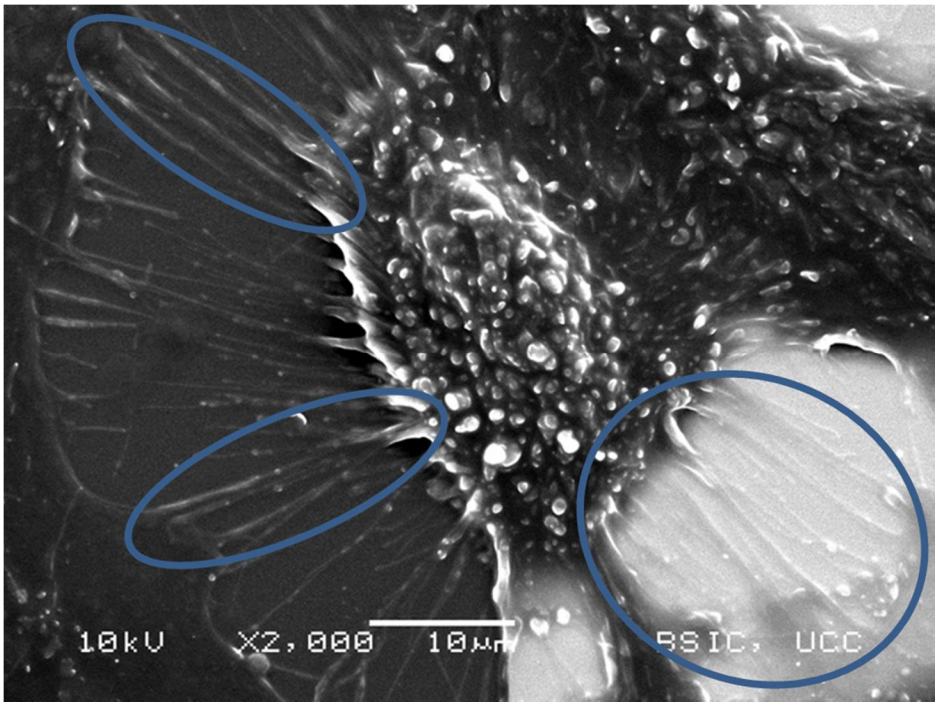

Figure 3.10: HeLa This single cell is well spread and attached to a flat electrode and shows very long filopodia

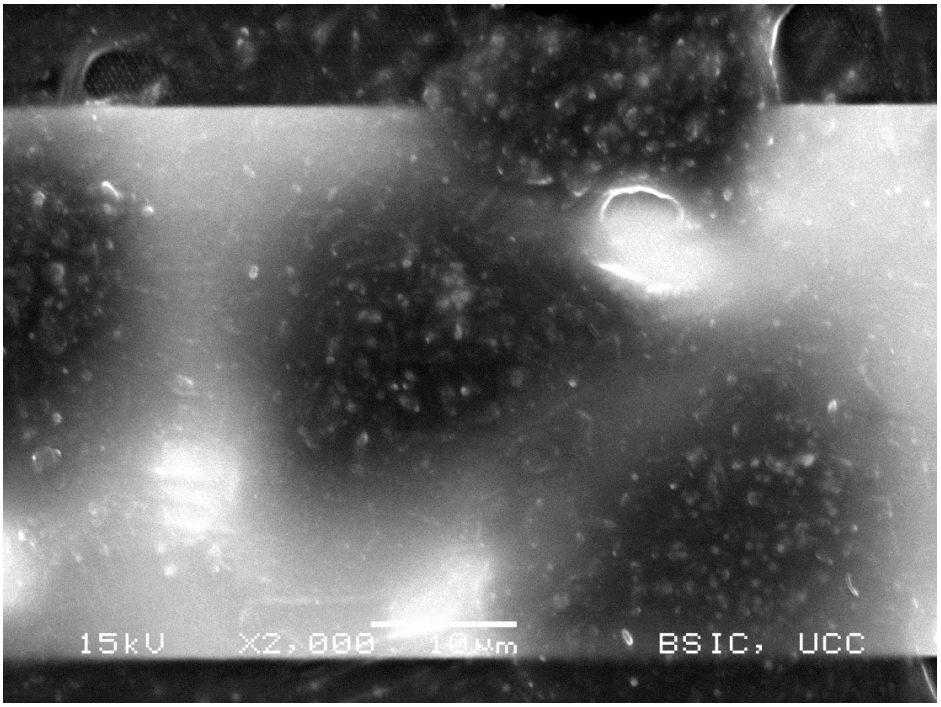

Figure 3.11: HeLa cells on a nanostructured electrode look quite smaller and round with no or very short filopodia visible.

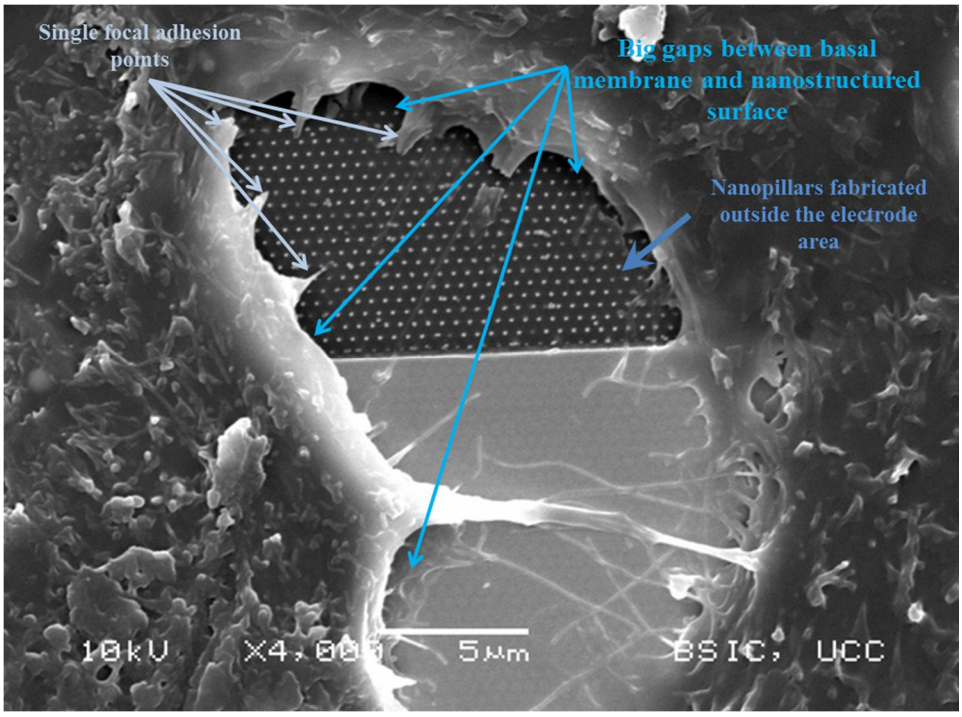

Figure 3.12: HeLa cells big gaps between cells' basal membrane and nanostructured surface (tilted image)

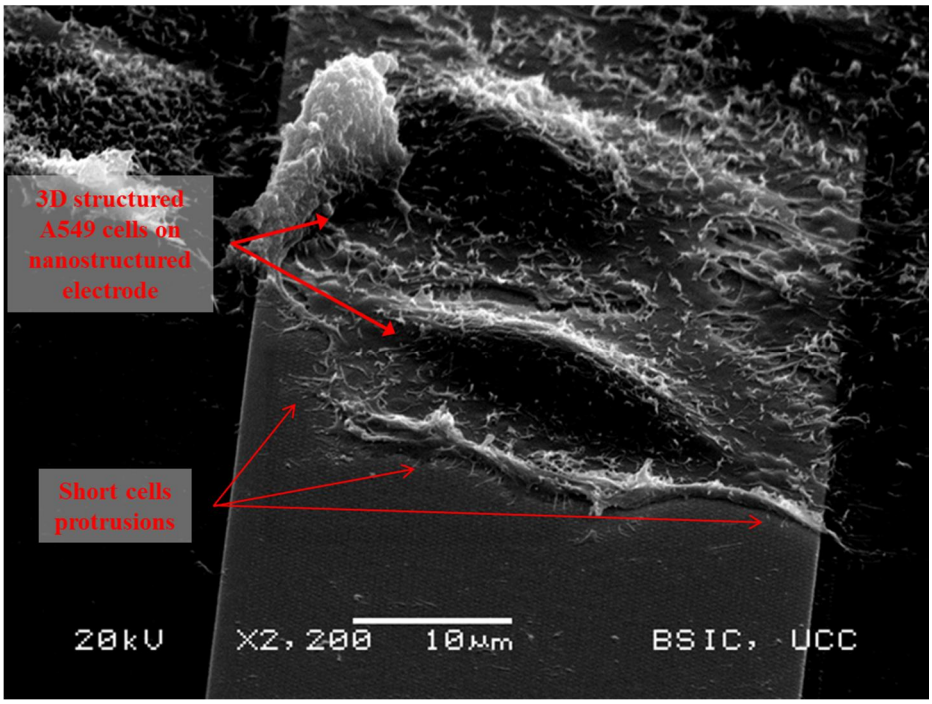

Figure 3.13: Tilted image of A549 cells growing on a surface with nanopillars

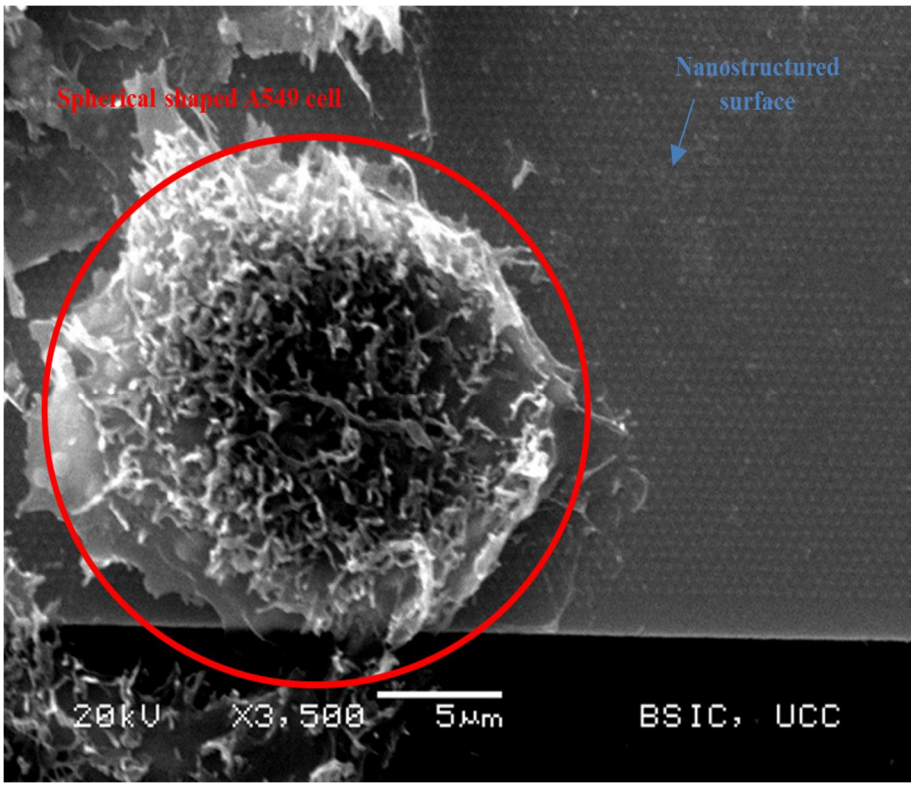

Figure 3.14: A549 single cell growing on a nanostructured electrode with a clear spherical shape

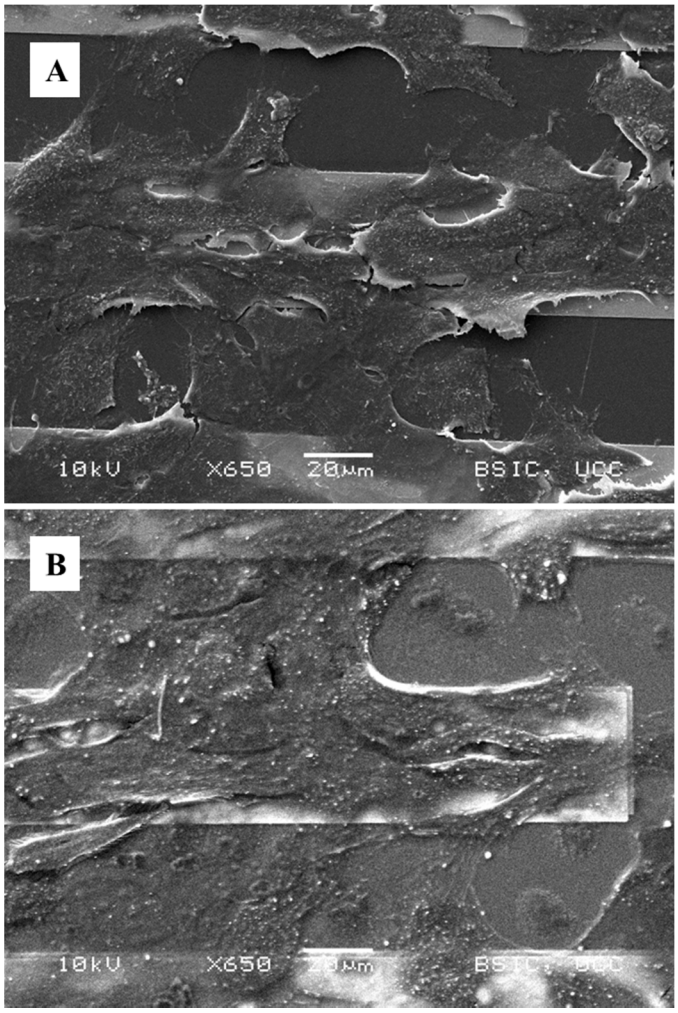

Figure 3.15: BALB cells do not show much differences between flat (A) and nanopillars (B)

3.5.3 Impedance analysis

Both kinds of electrodes were tested with A549 cell line using an extract of Antrodia Camphorata and Nicotine at different concentrations following the procedure explained earlier in paragraph 3.4.5. The results did not match what expected as no increase in sensitivity in this kind of test was noticed. The results however, showed the expected trends in terms of impedance values (lower figures where the cells were dead and higher where the cells were still alive).

The main cause for not improving the sensitivity of the assay had to do with the fact that the inoculation of the cells was performed manually and the fact that the cell attachment

to the substrate followed a completely random process. Even following an automated procedure for the inoculation of the cells on the impedance electrode would not give an absolute certainty that the same amount of cells would attach on the electrode's fingers in the same way and at the same time.

An increase of sensitivity was noticed only in the experiments carried out on A549 cells exposed to Nicotine, but more statistical evidences will be needed to prove these results with an absolute confidence.

In the following graphs are reported tests done with a single concentration (500 μM) of A. Camphorata (figure 3.16 and 3.19), various concentrations (250 μM, 500 μM and 1mM) (figure 3.17 and 3.20) of the same extract and various concentrations (1 mM, 3mM and 5 mM) of Nicotine (figure 3.18).

Data in the graphs were labelled in the same way for every set of experiment. Red was the negative control, blue was the positive control, green, purple and orange represented the test electrodes. The data for each electrode were represented with two columns of the same colour: on the left was represented the value recorded at 24 hours of incubation before the chemical injection and on the right was the impedance measurement recorded at 48 hours.

Each column in the graph represented an averaged value of 3 sets of 15 data points each.

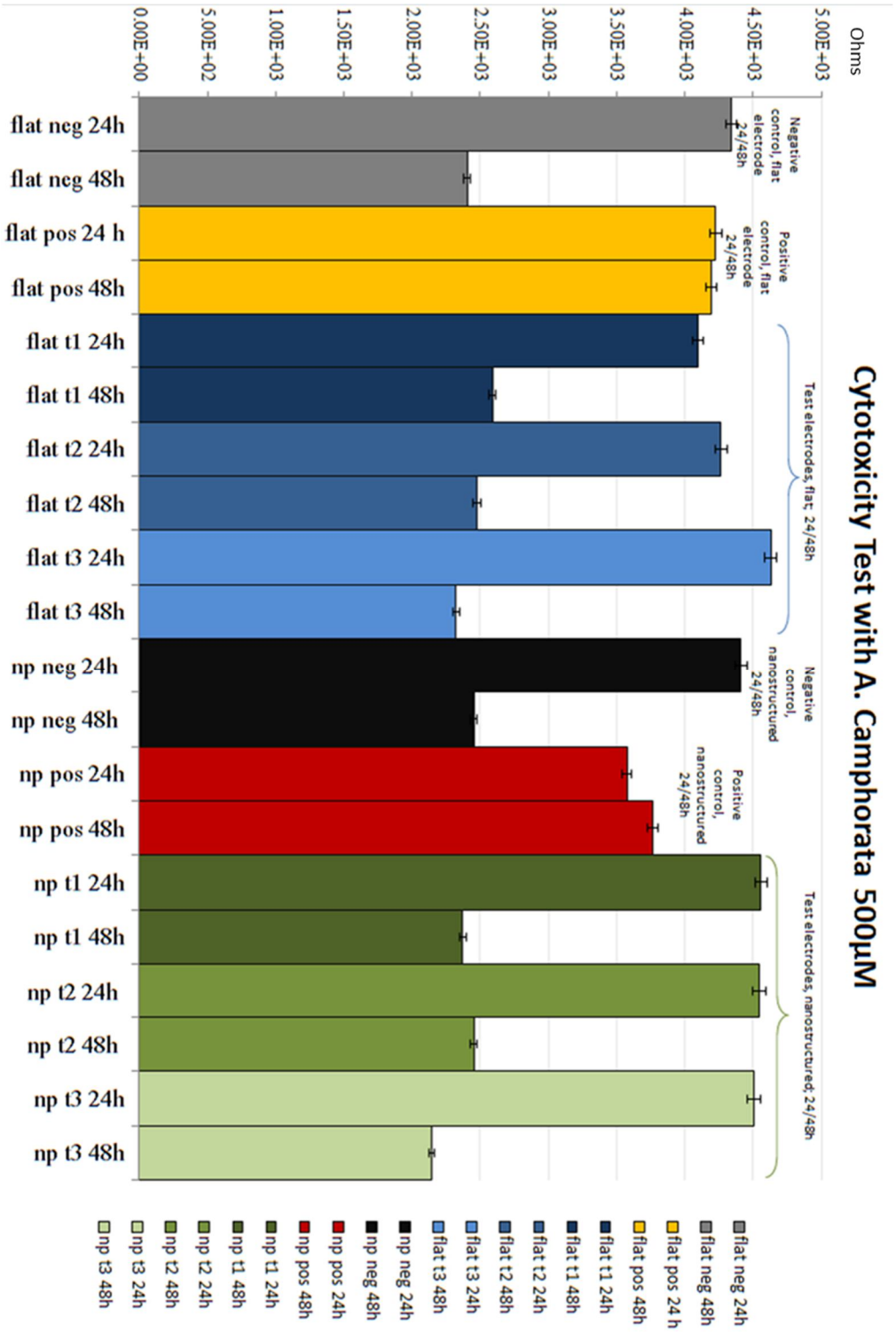

Figure 3.16: impedance test done with a single concentration (500 µM) of A. Camphorata

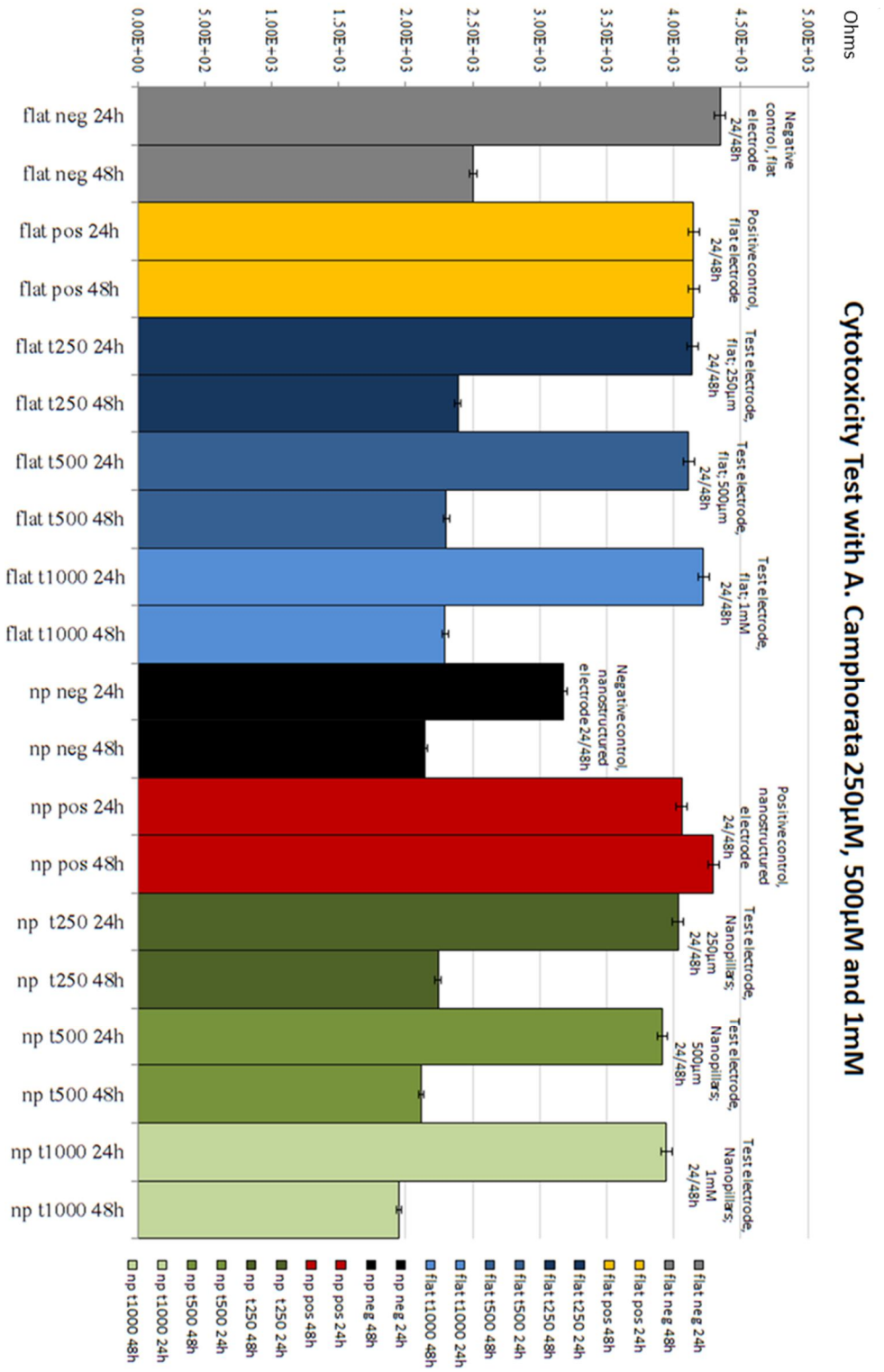

Figure 3.17: impedance test done with various concentrations (250 µM, 500 µM and 1mM) of A. Camphorata

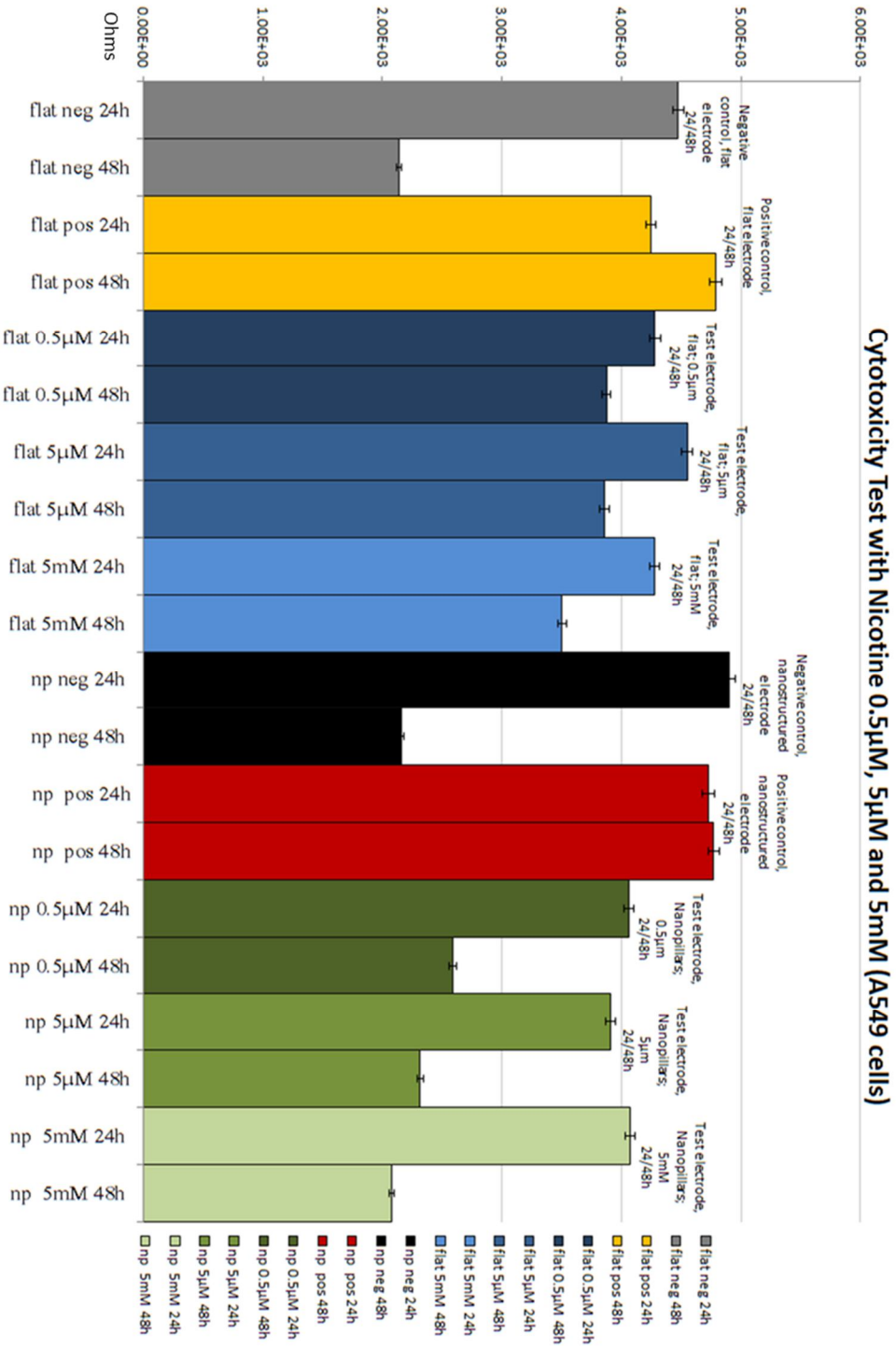

Figure 3.18: impedance test done with various concentrations (0.5 µM, 5 µM and 5mM) of Nicotine

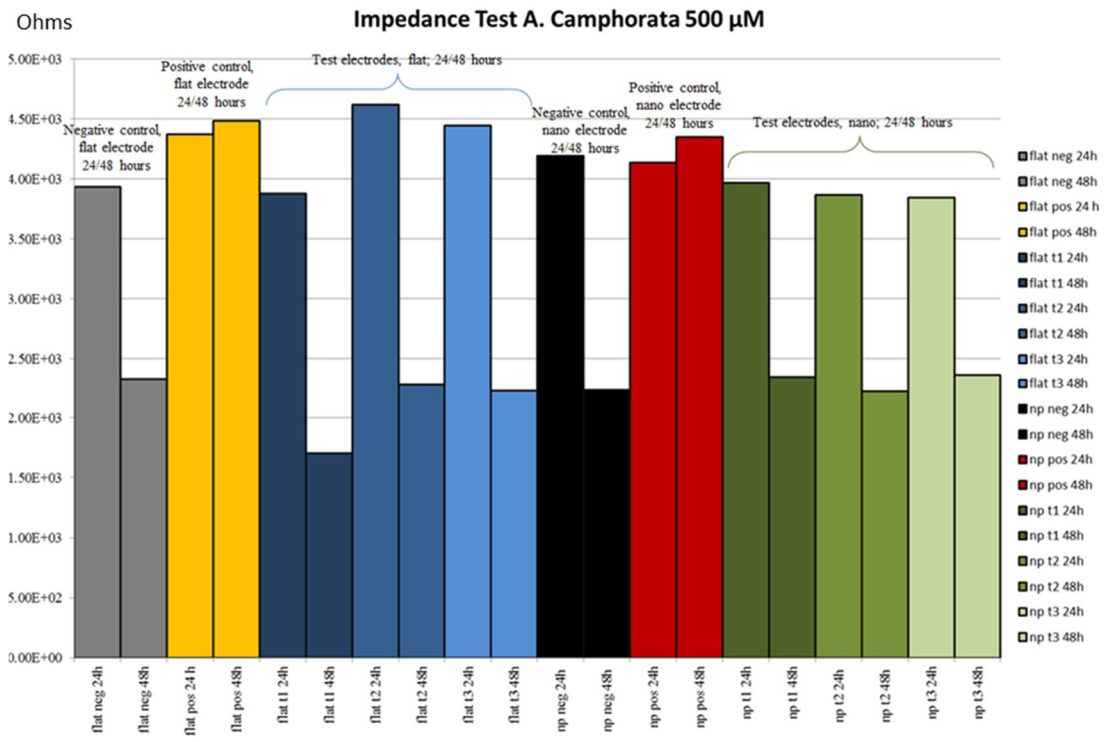

Figure 3.19: impedance test done with a single concentration (500 µM) of A. Camphorata

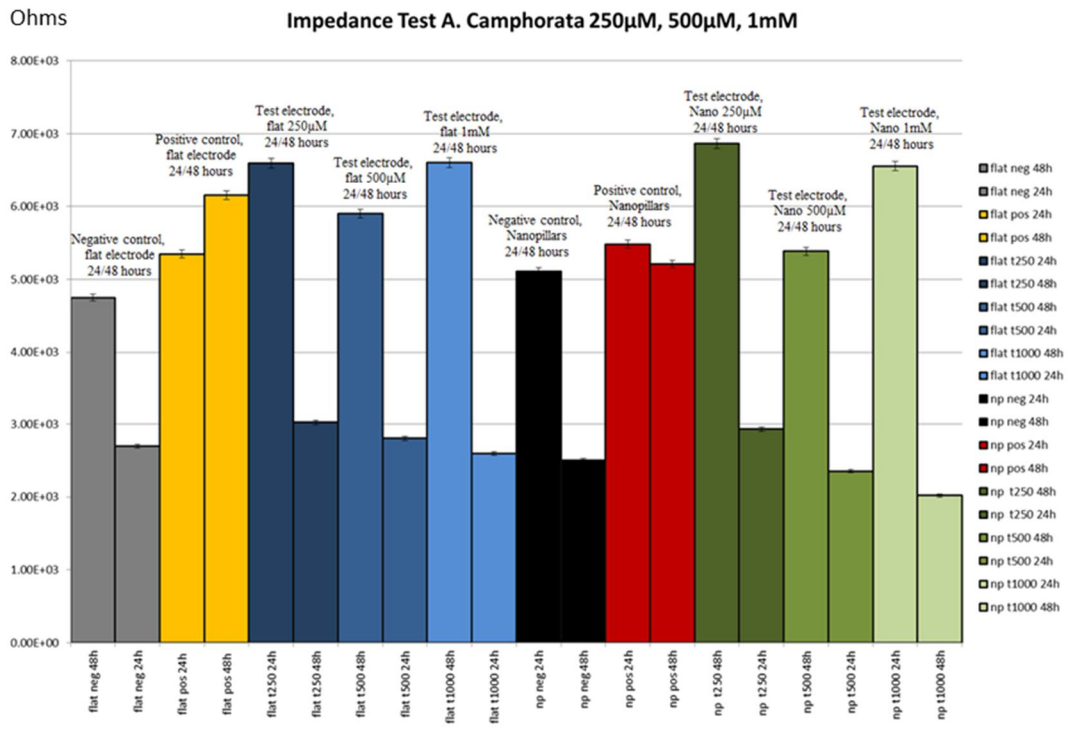

Figure 3.20: impedance test done with various concentrations (250 µM, 500 µM and 1mM) of A. Camphorata

3.6 DISCUSSION

Three different cell lines (HeLa, A549, BALBc 3T3) have been imaged using an optical microscope and a scanning electron microscope. When comparing the cells cultured on the flat and nanostructured electrodes it was found that the cells appeared very similar in terms of spreading and confluence. However, the cells growing on the standard electrode had a slightly larger surface area compared to those growing on the nanostructured device [1]. This finding confirmed that the nanostructures did not prevent the cells from growing on the culturing surface even if the morphology of the cells growing on the nanostructured electrodes was different from the standard morphology of cells cultured on flat substrates [3]. In order to obtain better information about the cells it was necessary to further analyse the cells with the aid of a scanning electron microscope (SEM).

All the cell lines available for the experiments were immobilised on the substrate following the same procedure. Expected results were observed through the images obtained with the aid of a scanning electron microscope. HeLa cells cultured on the nanopillars formed few and small contact points with the surface leading to wide gaps at the interface with the basal membrane. They also had a smaller surface area compared to those growing on the flat electrode. On the non-modified electrodes it was very evident how flat the cells were compared to those on the nanostructured electrodes. The filopodia appeared to be very different in the two circumstances: on the flat electrodes in fact there were many protrusions which extended for a few microns (usually more than 10-15µm), while on the devices with the nanopillars their number and length was very limited (<5µm).

The A549 cells (as well as the HeLa) appeared very round and had a smaller surface area when growing on the nanopillars. Their appearance was very three-dimensional compared to those imaged on the flat surface electrodes. Figure 3.14, for example, shows an almost spherical shaped cell; however, confluent layers of cells were achieved on the modified electrodes similar to those formed in the same conditions on the standard electrode.

The BALBc 3T3 cells however did not show any differences between those grown on the flat and nanostructured electrode.

The large gaps between the basal membrane of the cell and the impedance electrode surface, on the nanostructured electrodes, should in theory have showed differences in the impedance figures collected during the analysis over time with a fixed frequency of 10 kHz [8].

The mechanism and the behaviour of cells on nanostructures is not yet fully understood [62-64] but this thesis also aims to give additional information to future researches and further studies in the field of cell adhesion to nanostructured surfaces.

Impedance measurements obtained with the dead cells on the negative control electrodes or the test electrodes with the drugs can be compared to those done on the electrodes containing just media in the tested volume (as no cells are attached and cover the electrode surface). The impedance figures recorded on these devices were between 1.5 kΩ and 2.5 kΩ, while the figures recorded on confluent cell layers range between 4 kΩ and 5.5 kΩ with peaks of almost 7 kΩ if there was more than one layer of cells growing on each other. There was then a very clear separation between the values of living cell compared to the dead ones which was almost 2.5 – 3 kΩ. In this way it was very easy to determine whether the drugs affected the cells normal life cycle or not.

However, little or no differences were noticed in the impedance analysis carried out on the two different kinds of electrodes using cultured cells. The main reason for this negative result resided in the fact that the cells were placed manually on the electrodes and the attachment to the substrate always happened in a different way and did not follow a precise and repeatable process. A manual inoculation of the cells onto the electrodes could never give an absolute certainty that the same amount of cells would attach on the electrode in the same way each time. Even if there was an automated procedure for seeding the cells, this would not lead to the exact same conditions to provide a good comparison between the two kinds of electrodes as the attachment of the cells onto the substrate would be still a naturally random process.

Nevertheless, the results obtained showed that the impedance electrodes fabricated in-house worked correctly. The impedance values measured from the cell cultured on the interdigitated devices increased or decreased according to the ECIS theory. This means that when the cells died after 48 hours (like in the case of the negative controls) the impedance figures decreased dramatically from the starting values reported after 24 hours. When the cell were grown and maintained alive (positive controls) the impedance figures were recorded to be higher (or at least constant) during the experiments. In the cases of the tests performed using the Antrodia extract and Nicotine, the impedance values decreased considerably and were very similar to those reported for the tests on the negative controls.

An increase of sensitivity was noticed only in the experiments carried out on A549 cells growing on the nanostructured electrodes and exposed to different concentration of a solution containing Nicotine. More experiments to achieve a higher level of statistical significance will be needed to prove these findings with absolute confidence.

3.7 FUTURE WORK

Future work on this assay will be carried out confirm these findings on the other cell lines. Different electrode layouts combined with different nanopillar configurations will be fabricated to determine whether the presence of the nanostructures could potentially improve the sensitivity of this assay.

Future projects will give us the chance to test several other types of cell lines with different potential drugs or toxic substances.

3.8 REFERENCES

[1] J. Wegener et al., "Electric Cell–Substrate Impedance Sensing (ECIS) as a Noninvasive Means to Monitor the Kinetics of Cell Spreading to Artificial Surfaces", Experimental Cell Research 259, 158–166 (2000)

[2] D. A. Lauffenburger, A. Horwitz, "Cell Migration: A Physically Integrated Molecular Process" Cell, Vol. 84, 359–369, February 9, 1996

[3] Horwitz, A., Parsons, J. T. (1999). Cell migration—Movin' on. Science 286, 1102–1103.

[4] C. Xiao et al., "Assessment of Cytotoxicity Using Electric Cell-Substrate Impedance Sensing: Concentration and Time Response Function Approach", Anal. Chem. 2002, 74, 5748-5753

[5] M. V. Berridge et al., "The Biochemical and Cellular Basis of Cell Proliferation Assays That Use Tetrazolium Salts", Biochemica No. 4 1996

[6] A. de Luca et al., "TGF-b-Induced Apoptosis of Cerebellar Granule Neurons Is Prevented by Depolarization", The Journal of Neuroscience, July 1, 1996, 16(13):4174 – 4185

[7] K. Lappalainen et al., "Comparison of Cell Proliferation and Toxicity Assays Using Two Cationic Liposomes", Pharmaceutical Research August 1994, Volume 11, Issue 8, pp 1127-1131

[8] E. Borenfreund et al., "A simple quantitative procedure using monolayer cultures for cytotoxicity assays (HTD/NR-90)", Journal of tissue culture methods 1985, Volume 9, Issue 1, pp 7-9

[9] P. Knox et al., "The frame multicentre project on In vitro cytotoxicology", Food and Chemical Toxicology, Volume 24, Issues 6–7, June–July 1986, Pages 457-463

[10] Wyllie A. et al., "Apoptosis and Cell Proliferation", 2nd ed., Boehringer Mannheim, Biochemica: Mannheim, Germany, 1998

[11] J.W. Parce et al., "Detection of cell-affecting agents with a silicon biosensor", Science 13 October 1989: 246 (4927), 243-247

[12] Pasternak A. S. et al., "Measurement of trans-epithelial electrical resistance in perfusion: potential application for in vitro ocular toxicity testing", Biotechnol Bioeng. 1996 Jun 5;50(5):568-79.

[13] Maile W. et al., "New methods for cytotoxicity testing: quantitative video microscopy of intracellular motion and mitochondria-specific fluorescence", Molecular Toxicology [1987, 1(4):427-437]

[14] Weiss D.G., "Videomicroscopic measurements in living cells: dynamic determination of multiple end points for in vitro toxicology", Molecular Toxicology [1987, 1(4):465-488]

[15] Giaever I., Keese C.R., "Toxic? Cells can tell", Chemtech, 116-125 (Feb. 1992).

[16] Keese C.R., Giaever I., "A Biosensor that Monitors Cell Morphology with Electrical Fields", IEEE Engineering in medicine and biology, July 1994

[17] Giaever I., Keese C. R., "A morphological biosensor for mammalian cells", Nature 366, 591-592 (9 December 1993)

[18] Borkholder, D.A., DeBusschere, B.D., and Kovacs, G.T.A., "An Approach to the Classification of Unknown Biological Agents with Cell-based Sensors," Technical digest of the 1998 Solid-State Sensor and Actuator Workshop, Hilton Head Island, SC, 6/7-6/11, Transducer Research Foundation, Cleveland, pp. 178-82 (1998).

[19] Automated Real-Time Measurement of Chemotactic Cell Motility BioTechniques 31:1130-1138 (November 2001), Nacima Hadjout, Gary Laevsky, David A. Knecht and Michael A. Lynes

[20] Assessment of Rapid Morphological Changes Associated with Elevated cAMP Levels in Human Orbital Fibroblasts, Lavanya Reddy,* Hwai-Shi Wang,†,1 Charles R. Keese,* Ivar Giaever,* and Terry J. Smith, EXPERIMENTAL CELL RESEARCH 245, 360–367 (1998)

[21] Tiruppathi, C.; Malik, A. B.; Del Vecchio, P. J.; Keese, C. R.; Giaever, I. Proc. Natl. Acad. Sci. U.S.A. 1992, 89, 7919-7923. Electrical method for detection of endothelial cell shape change in real time: Assessment of endothelial barrier function

[22] C. Xiao et al., "On-Line Monitoring of Cell Growth and Cytotoxicity Using Electric Cell-Substrate Impedance Sensing (ECIS)", Biotechnol. Prog. 2003, 19, 1000-1005

[23] Keese, C., Karra, N., Dillon, B., Goldberg, A., Giaever, I., "Cell-Substratum Interactions as a Predictor of Cytotoxixity." In Vitro & Molecular Toxicology 11 (2), (1998)

[24] Xiao C., Lachance B., Sunahara G., Luong, J.H.T., "An in-depth analysis of electric cell substrate impedance sensing to study the attachment and spreading of mammalian cells", Anal. Chem. 2002, 74, 1333–1339.

[25] J. H. T. Luong et al., "Monitoring Motility, Spreading, and Mortality of Adherent Insect Cells Using an Impedance Sensor", Analytical Chemistry 2001 73 (8), 1844-1848

[26] Q. Liu et al., "Impedance studies of bio-behavior and chemosensitivity of cancer cells by micro-electrode arrays", Biosensors and Bioelectronics 24 (2009) 1305–1310

[27] J. Wang et al., "Microfabricated Electrochemical Cell-Based Biosensors for Analysis of Living Cells In Vitro", Biosensors 2012, 2, 127-170;

[28] K. Heileman et al., "Dielectric spectroscopy as a viable biosensing tool for cell and tissue Characterization and analysis", Biosensors andBioelectronics49(2013)348–359

[29] Wang, L.; Zhu, J.; Deng, C.; Xing, W.; Cheng, J. An automatic and quantitative on-chip cell migration assay using self-assembled monolayers combined with real-time cellular impedance sensing. Lab Chip 2008, 8, 872–878.

[30] Ehret, R.; Baumann, W.; Brischwein, M.; Schwinde, A.; Stegbauer, K.; Wolf, B. Monitoring of cellular behaviour by impedance measurements on interdigitated electrode structures. Biosens. Bioelectron. 1997, 12, 29–41.

[31] Chang, B.W.; Chen, C.H.; Ding, S.J.; Chen, D.C.H.; Chang, H.C. Impedimetric monitoring of cell attachment on interdigitated microelectrodes. Sens. Actuat. B: Chem. 2005, 105, 159–163.

[32] P. Wang, Q. Liu, "Cell-Based Biosensors, Principles and Applications", Artech House, London, 2010

[33] W. Hu et al., "Inhibited cell spreading on polystyrene nanopillars fabricated by nanoimprinting and in situ elongation", Nanotechnology 21 (2010) 385301

[34] R. Gangadharan, "Nanopillar based electrochemical biosensor for monitoring microfluidic based cell culture", PhD Thesis, Clemson University, 2012

[35] F. Haq et al., "Neurite development in PC12 cells cultured on nanopillars and nanopores with sizes comparable with filopodia", International Journal of Nanomedicine 2007:2(1) 107–115

[36] J. Lee et al., "Three-Dimensional Cell Culture Matrices: State of the Art", Tissue Engineering: Part B Volume 14, Number 1, 2008

[37] C. H. Choi, C. J. Kim, "Green Tribology: Biomimetics, Energy Conservation and Sustainability", Chapter 4, edited by Michael Nosonovsky, Bharat Bhushan, Springer-Verlag, Berlin Heidelberg 2012

[38] S. Nomura et al., "Nanopillar sheets as a new type of cell culture dish: detailed study of HeLa cells cultured on nanopillar sheets", J Artif Organs (2006) 9:90–96

[39] C. W. Kuo et al., "Polymeric nanopillar arrays for cell traction force measurements", Electrophoresis 2010, 31, 3152–3158

[40] Giard DJ et al., "In vitro cultivation of human tumors: establishment of cell lines derived from a series of solid tumors", J. Natl. Cancer Inst. 51: 1417-1423, 1973.

[41] Aaronson S.A. et al., "Development of 3T3-like lines from Balb-c mouse embryo cultures: transformation susceptibility to SV40", J Cell Physiol. 1968 Oct; 72(2):141-8.

[42] R. Rahbari, "A novel L1 retrotransposon marker for HeLa cell line identification", BioTechniques 46:277-284 (April 2009)

[43] Scherer W.F. et al., "Studies on the propagation in vitro of poliomyelitis viruses. IV. Viral multiplication in a stable strain of human malignant epithelial cells (strain HeLa) derived from an epidermoid carcinoma of the cervix". J. Exp. Med. 97 (5): 695–710

[44] M. Geethangili et al., "Review of Pharmacological Effects of Antrodia camphorata and Its Bioactive Compounds", Evidence-Based Complementary and Alternative Medicine Volume 2011, 17 pages

[45] Z. T. Tsai, S. L. Liaw, "The Use and the Effect of Ganoderma", San Yun Press, Taichung, Taiwan, 1985

[46] C. J. Chen et al., "Study on solid cultivation and bioactivity of Antrodia camphorata," Fungal Sciences, vol. 16, pp. 65–72, 2001.

[47] C. H. Chen, S. W. Yang, Y. C. Shen, "New steroid acids from Antrodia cinnamomea, a fungal parasite of Cinnamomum micranthum," Journal of Natural Products, vol. 58, no. 11, pp. 1655–1661, 1995.

[48] Y. L. Hsu et al., "Apoptotic effects of extract from Antrodia camphorata fruiting bodies in human hepatocellular carcinoma cell lines", Cancer Letters, vol. 221, no. 1, pp. 77–89, 2005.

[49] H. Wu et al., "Proteomic analysis of the effect of Antrodia camphorata extract on human lung cancer A549 cell", Proteomics, vol. 6, no. 3, pp. 826–835, 2006

[50] Benowitz N. L. et al., "Nicotine chemistry, metabolism, kinetics and biomarkers", Handbook of Experimental Pharmacology, 192, 29-60 (2009).

[51] Herning R. I., Jones R. T., Benowitz N. L., Mines, A. H., "How a cigarette is smoked determines blood nicotine levels", Clinical Pharmacology and Therapeutics, 33(1), 84-90 (1983).

[52] Gullihorn L., Karpman R., Lippiello L., "Differential effects of nicotine and smoke condensate on bone cell metabolic activity", Journal of Orthopaedic Trauma, 19(1), 17-22 (2005).

[53] Wu W., Cho C. H., "The pharmacological actions of nicotine on the gastrointestinal tract", Journal of Pharmacological Sciences, 94(4), 348-358 (2004).

[54] Chan A., Chien Y. W., Jin Lin S., "Transdermal delivery of treatment for alzheimer's disease: Development, clinical performance and future prospects", Drugs and Aging, 25(9), 761-775 (2008).

[55] Takeuchi H. et al., "Nicotinic receptor stimulation protects nigral dopaminergic neurons in rotenone-induced Parkinson's disease models", Journal of Neuroscience Research, 87(2), 576-585 (2009).

[56] Zdravkovic T. et al., "Human embryonic stem cells as a model system for studying the effects of smoke exposure on the embryo", Reproductive Toxicology, 26(2), 86-93 (2008).

[57] Ma L. et al., "Influence of low-dose nicotine on bone healing. Journal of Trauma - Injury, Infection and Critical Care", 70(6), E117-E121 (2011)

[58] B.A. Avelar-Freitas et al., "Trypan blue exclusion assay by flow cytometry", Braz J Med Biol Res. Apr 2014; 47(4): 307–3015.

[59] D. Shum et al., "A high density assay format for the detection of novel cytotoxic agents in large chemical libraries", Journal of Enzyme Inhibition and Medicinal Chemistry 2008 23: 6, 931-945

[60] S. L. Voytik-Harbin et al., "Application and evaluation of the alamarblue assay for cell growth and survival of fibroblasts", In Vitro Cellular & Developmental Biology – Animal March 1998, Volume 34, Issue 3, pp 239-246

[61] C. W. Kuo, D. Chueh and P. Chen, Investigation of size–dependent cell adhesion on nanostructured interfaces, Journal of Nanobiotechnology 2014, 12:54

[62] Chien FC, Kuo CW, Yang ZH, Chueh DY, Chen P: Exploring the formation of focal adhesions on patterned surfaces using super-resolution imaging. Small 2011, 7:2906–2913.

[63] Tan JL, Tien J, Pirone DM, Gray DS, Bhadriraju K, Chen CS: Cells lying on a bed of microneedles: An approach to isolate mechanical force, Proc Natl Acad Sci USA 2003, 100:1484–1489.

Chapter 4

4 APPLICATION OF NANOSTRUCTURED ELECTRODES AS ELECTROCHEMICAL SENSOR

4.1 INTRODUCTION

4.1.1 Background

A chemical sensor is a device able to transform chemical information, ranging from the concentration of a specific sample component to total composition analysis, into analytically useful signals. The chemical information could originate from a chemical reaction of a certain analyte or from a specific physical property of the system under investigation. A chemical sensor is a crucial component of an analyser. In addition to the sensor itself, the analyser may contain devices that could perform several different functions like sampling, sample transport, signal processing, data processing. Chemical sensors, like almost any other sensors, contain two elementary functional components: a receptor part and a transducer part. Some sensors may also comprise a separator which is, for example, a membrane. In the receptor part of a sensor the chemical information is transformed into a specific form of energy which the transducer must be able to measure. The transducer part is a device capable of converting the energy carrying the chemical information about the sample into a useful analytical signal. The transducer as such does not show selectivity. The receptor part of chemical sensors may be based upon various principles [1]:

- physical, where no chemical reaction takes place. Typical examples are those based upon measurement of absorbance, refractive index, conductivity, temperature or mass change;

- chemical, in which a chemical reaction with participation of the analyte gives rise to the analytical signal;
- biochemical, in which a biochemical process is the source of the analytical signal. Typical examples are microbial potentiometric sensors or immunosensors. They may be regarded as a subgroup of the chemical ones. Such sensors are called biosensors.

In some cases it is not possible to decide unequivocally whether a sensor operates on a chemical or on a physical principle as they could be confused quite easily. This is, for example, the case when the signal is due to an adsorption process. Sensors are normally designed to operate under well-defined conditions for specific analytes in certain sample types. Therefore, it is not always necessary that a sensor responds specifically to a certain analyte [1]. Under carefully controlled operating conditions, the analyte signal may be independent of other sample components, thus allowing the determination of the analyte without any major preliminary treatment of the sample. Otherwise unspecific but satisfactory reproducible sensors can be used in series for multicomponent analysis using multivariate calibration software and signal processing. Such systems for multicomponent analysis are called sensor arrays.

Electrochemical devices transform the effect of the electrochemical interaction analyte – electrode into a useful signal [2]. Such effects may be stimulated electrically or may result in a spontaneous interaction at the zero-current condition. The following subgroups may be distinguished:

a) voltammetric sensors, including amperometric devices, in which current is measured in the DC or AC mode. This subcategory includes sensors based on chemically inert electrodes, chemically active electrodes and modified electrodes [3, 4]. In this group also includes sensors with and without external current source (galvanic sensors).

b) potentiometric sensors, in which the potential of the electrode is measured against a reference electrode [5, 6].

c) chemically sensitized field effect transistor (ChemFET) in which the effect of the interaction between the analyte and the active coating is converted into a change of the source-drain current. The interactions between the analyte and the coating are, from a

chemical point of view, similar to those found in potentiometric ion-selective sensors [7].

d) potentiometric solid electrolyte gas sensors, different from the 'b' subgroup because they usually work in a high temperature environment with solid electrolytes and are usually applied for gas sensing measurements [8, 9].

4.1.2 Dopamine

Dopamine (DA), as a simple organic chemical in the catecholamine family, is a monoamine neurotransmitter that plays a critical role in the function of the mammalian central nervous, hormonal, and cardiovascular systems [10, 11]. Since its discovery, DA has attracted a great deal of attention in clinical fields because its abnormal levels indicate various diseases, such as Parkinson's disease, senile dementia, Huntington's disease and schizophrenia [12, 13]. DA is currently the subject of intense research focus to neuroscientists and chemists and it is essential to develop rapid and simple methods for its determination. Over the past several decades, tremendous effort has been made and various techniques have been developed, such as fluorimetry, chemiluminescence, capillary electrophoresis, and ion chromatography [14]. The common instrumental techniques like high performance liquid chromatography (HPLC) have been widely used for the determination of DA [15]. However, such methods of detection are often complicated and very expensive. The electrochemical oxidation of DA has been studied and the results show that the electrochemical oxidation is a two-electron process with transfer of two protons [16]. Various inorganic and organic materials [17], Langmuir-Blodgett (LB) film [18], microfluidics system [19], sol-gel material based electrodes [20], enzyme-less biosensor [21], enzyme amplification system [22] and voltammetric electrodes [23] have all been reported for the oxidation of DA.

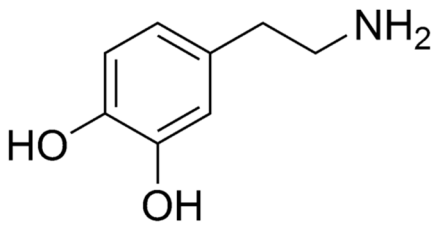

Figure 4.1: Chemical structure of Dopamine

4.1.3 Uric acid

Uric acid (UA) is the primary end-product of purine metabolism in the human body and excreted in the urine [24]. It is derived from purines arising from the catabolism of dietary and endogenous nucleic acid stem from increased catabolism dysfunction of one of the shunt pathways which leads to increased urate production [25]. The assay of uric acid in body fluids (e.g: serum and urine) is a clinically valuable diagnostic indicator. The concentration levels of UA in men is 200-430 μM and for women is 140-360 μM in serum for normal, healthy humans [26]. Monitoring UA continuously is necessary as it has been shown that extreme abnormalities of UA levels are symptoms of several diseases such as gout, hyperuricemia, and Lesch-Nyhan syndrome [27]. Similarly, elevated uric acid levels are related to other conditions including increased alcohol consumption, obesity, diabetes, high cholesterol, kidney disease, and heart diseases. Many epidemiological studies have suggested that serum uric acid is also a risk factor for cardiovascular disease [28]. It is therefore essential to develop rapid methods, preferably simple and inexpensive, for the determination of UA in routine analysis. UA exists as an anion beyond pH 5.4 in the alkaline range (pKa of UA is 5.4). Although there are several techniques available for the determination of UA including spectrophotometry [29] and chromatography [30], electrochemical detection of UA has received much interest due to its biological importance and easy oxidation property [31].

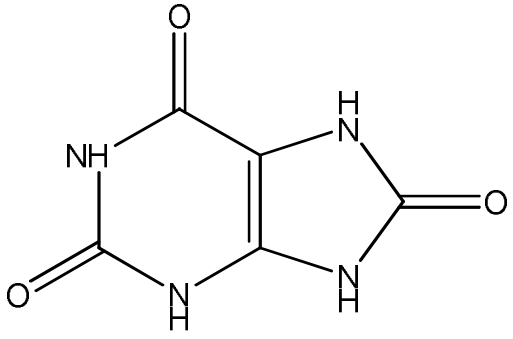

Figure 4.2: Chemical structure of Uric Acid

About 70% of daily uric acid disposal in humans occurs via the kidneys, and in 5-25% of humans, impaired renal excretion leading to increased levels of UA causing

hyperuricemia. However, impaired renal excretion is not the only cause of high levels of UA, there can be any number of reasons including hereditary reasons, diet – high intake of dietary purine and fasting or rapid weight loss. High levels of UA can lead to a number of serious illnesses including Gout, Lesch-Nyhan syndrome, cardiovascular disease, type II diabetes and metabolic syndrome [32].

Low levels of UA can also lead to number of serious illnesses which include multiple sclerosis and oxidative stress which can lead to stroke and atherosclerosis. Thus it is crucial to develop rapid methods for the determination of UA in routine analysis.

4.1.4 Detection of DA and UA methods

Several human diseases and neurological disorders such as Schizophrenia, and Parkinson's disease can be caused by abnormalities in DA concentration [13], which makes the determination of DA concentration in body fluids important in diagnosing related diseases. Thus, there is a continuing interest in the development of a simple, sensitive and reliable method for the determination of DA. Various methods have been developed for the determination of DA, such as high performance liquid chromatography [30], gas chromatography–mass spectrometry [33], microdialysis [34], chemiluminescence [35] and electrochemistry [36], but due to the great clinical significance, many researchers are still striving for better methods. Among the reported methods, electrochemistry has attracted wide attention due to its convenience, speed, high sensitivity, selectivity and reproducibility. However, a major problem encountered in the determination of DA is the interference of EP (Epinephrine), UA and AA (Ascorbic Acid) which coexist with DA in body fluids and have close oxidation potentials at bare electrodes. Although the selective detection of DA using modified electrodes has been reported a number of times [37, 38], all these reported methods considered only some of the EP, UA and AA interferents. So it is essential to develop a convenient method that can detect DA concentration in the presence of EP, UA and AA [39]. Ascorbic acid (AA) is well known for its antioxidant property and usually coexists with DA in biological samples. Since the concentration of AA is generally much higher than that of DA (100–1000 times) in biological samples, the development of a simple

and rapid method for the determination of DA with high selectivity and sensitivity is desirable for diagnostic applications [40, 41].

There are many standard analytical methods that have been reported in the literatures for uric acid determination. The levels of uric acid in different biological matrices such as urine and serum have been determined by numerous standard analytical methods such as reversed-phase liquid chromatography [42], potentiometric enzyme electrode [43] and flow injection analysis system with tubular amperometric detector [44]. All the analytical methods are well established and exhibit a large range of advantages. However, these methods also have weaknesses such as being still under development, time-consuming and expensive; they cannot be performed easily outside the laboratory and need very highly skilled technicians. On the other hand, early-warning systems are needed for scientists to react in case of contamination or pollution. Biosensor technology is a powerful alternative to conventional analytical techniques, harnessing the specificity and sensitivity of biological systems in small and low cost devices. Biosensors are defined as measurement devices that utilize chemical or biological reactions to detect and quantify a specific analyte. Biosensors consist of an analyte-specific bioreceptor (enzyme, antibody, nucleic acid, tissue, cell or microorganism) and a physical transducer element (electrode, optical, mass, or quartz) which converts the change in the receptor to a detectable signal [45]. In enzyme-based determination, the enzyme reacts selectively with its substrate associated with or integrated within physico-chemical transducers which may be optical, electrochemical, thermometric, piezoelectric or magnetic [33]. Recently, a few reports on spectrophotometric determination of uric acid using different approaches have been reported [46, 47]. Among the current methods used to determine blood UA levels, electrochemical analysis conveniently yields a rapid response, is highly sensitive, and is low in cost [48, 49], however electrochemical analysis techniques are plagued by interference from ascorbic acid (AA). The oxidation potentials of UA and AA overlap on unmodified electrodes [50 – 52].

4.2 OBJECTIVES

This chapter originates from a short collaboration to another project carried out in UCC where the determination of several biological substances was performed with electrodes different from those used in this project. These electrodes were used for a quick comparison test but it was found out that these interdigitated impedance electrodes could be as well used (following a proper optimization of their design) for electrochemical testing (cyclic voltammetry). This work would need further future improvements, however, it was worth mentioning it in this thesis as an additional possible application of this kind of nanostructured electrodes.

The objectives of the studies reported in this chapter were

- To characterize the in-house fabricated electrodes with electrochemical techniques
- To compare the electrochemical behavior between flat and nanostructured electrodes during the simultaneous detection of Dopamine and Uric Acid in a sample

In this chapter it is shown that the nanostructured interdigitated impedance electrodes have a higher sensitivity and better electron transfer properties compared to the flat version of the same electrode in the electrochemical detection of dopamine (DA) and uric acid (UA) in a solution.

4.3 EXPERIMENTAL

4.3.1 Apparatus

The electrochemical experiments were performed with a CHI1040A electrochemical workstationat room temperature. Magnetic stirring was performed during the amperometric determination of this experiment, solutions pH was controlled with Orion 520A pH meter (Figure 4.3).

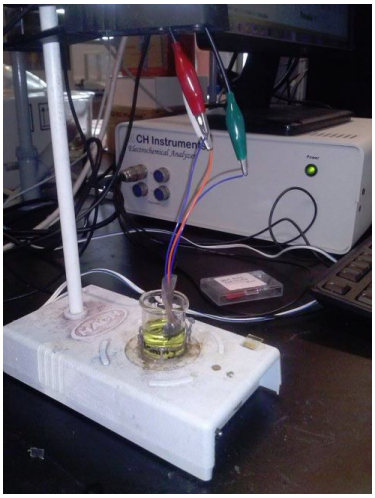

Figure 4.3: Setup for electrochemical measurement done with CH Instrument 1040A

4.3.2 Reagents

All the chemicals used were of analytical grade with highest purity and aqueous solutions were prepared with deionised water (18.2 MΩ.cm-1) using a Milli-Q (Millipore, Bedford, MA) water purification system. NaH_2PO_4, Na_2HPO_4, H_3PO_4, $[Fe(CN)_6]^{3-/4-}$, uric acid and dopamine were purchased from Sigma - Aldrich (Dublin, Ireland).

Stock solution of DA (10 mM) was prepared daily by dissolving a suitable amount of the reagent in water and was kept in the dark before use. UA solution (50 mM) was prepared by first dissolving it in a small volume of 0.1 M NaOH solution and diluted with water.

Phosphate-buffers of desired pH values were prepared by mixing solutions of 0.1 M NaH_2PO_4 and 0.1 M Na_2HPO_4 at different ratios. The pH values were adjusted by H_3PO_4 solution. Buffers and samples were sonicated for 5 minutes before use.

4.3.3 Procedure

4.3.3.1 Buffers and solutions

Solutions were prepared daily for these experiments.

3.90025g of sodium phosphate monobasic dehydrate were used to make up H_2NaPO_4 (100mM) in 250ml of deionised water;

3.549g of sodium phosphate dibasic were used to make up HNa_2PO_4 (100mM) in 250ml of deionised water;

0.0558g of potassium hexacyanoferrate(II) trihydrate [$C_6FeK_4N_63(H_2O)$] (0.25mM) plus 0.0413g of potassium hexacyanoferrate(III) [$C_6FeK_3N_6$] (0.25mM) plus 0.372g of potassium chloride KCl (0.1M) were dissolved in 50ml of deionised water to prepare ferrocyanide $[Fe(CN)_6]^{3-/4-}$solution (5mM).

0.1M UA in solution was prepared dissolving 0.504g of UA powder in 30 ml of deionised water;

20mM DA in solution was prepared dissolving 0.038g of DA powder in 10 ml of deionised water;

0.1 M Phosphoric acid (H_3PO_4), to adjust the solutions pH, was prepared from an already made solution at 85% of initial concentration (14.8M) by bringing it first down to 1M and then diluting it further down to 0.1M. 6.75ml of H_3PO_4 were diluted in 100ml of deionised water to bring it down to 1M. 10ml of this solution were further diluted using 90ml of deionised water to get the 0.1M solution.

All the solutions have been analysed in a 10 ml beaker and mixed with a magnetic stirrer before every single measurement.

4.3.3.2 Cyclic voltammetry

The electrodes were rinsed before every measurement taken and attached to a card edge connector (as described in chapter 2). The system was then connected to the CHI 1040A for the analysis. The scan rate varied from 100mV/s to 400mV/s (with increasing steps of 20mV/s), the potential window for the experiments monitoring the scan rate was between -0.4V and 0.4V while, during the detection of DA and UA it was considered between -0.4V and 1.2V. Before every experiment the electrodes were "cleaned" by doing 20 cycles of voltammetry in buffer solutions with a high scan rate (500mV/s). These parameters were selected in the start menu of the dedicated software. All experiments were conducted at room temperature and all the solutions analysed were mixed using a magnetic stirrer. All the analyses were repeated three times each to ensure correct readings from the instrument.

4.4 RESULTS

4.4.1 Electrochemical behaviour

Ferrocyanide $[Fe(CN)_6]^{3-/4-}$ was employed as a redox probe to investigate the electrochemical behaviour of both the flat and the nanostructured interdigitated electrodes. As it can be seen in the figure reported below (Figure 4.4), the electrode with the nanopillars (red line) showed better electron transfer properties in terms of peak potential difference and higher peak currents compared to the those of its flat counterpart (black line).

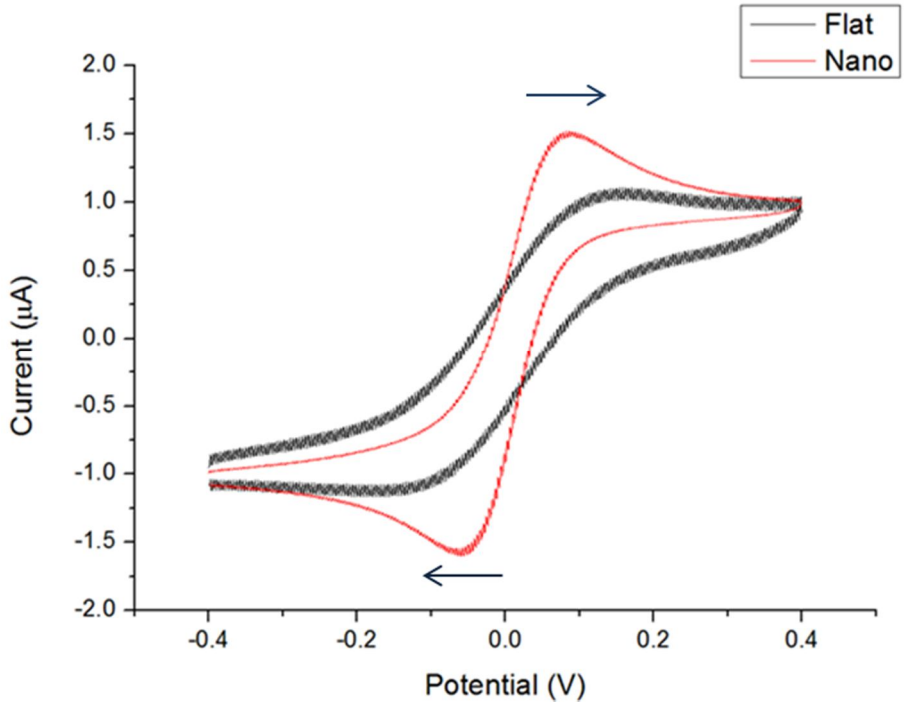

Figure 4.4: Cyclic voltammograms of a flat and nanopillar electrode in 5mM $[Fe(CN)_6]^{3-/4-}$ in 0.1 M KCl with a scan rate of 200mV/s (pH4).

Normally, the electrode reaction during a scan from, for example, +600 mV to 0.0 mV is

$$Fe^{III}(CN)_6^{3-} + e^- \rightarrow Fe^{II}(CN)_6^{4-} \quad (1)$$

The electrode potential, E, is thermodynamically determined by the Nernst relationship

$$E = E^{o} + (0.0591/n) \log (a_{ox}/a_{R}) \qquad (2)$$

where a_{ox} is the activity of the oxidized species, ferricyanide in this case, and a_R is the activity of the reduced species, ferrocyanide. Experimentally, the activity is affected by the presence of other ions. For practicality, we therefore define a "formal potential" that uses concentration in mole/L rather than activity, which we do not know. The Nernst equation becomes

$$E = E^{o'} + (0.0591/n) \log [C_{ox}/C_{R}] \qquad (3)$$

The "formal" potential, $E^{o'}$, depends on the nature of electrolytes in the solution. For ferri/ferrocyanide in aqueous solutions at 25ºC:

$$Fe(CN)_6^{3-} + e- = Fe(CN)_6^{4-} \qquad (4)$$

Experiments were also conducted at different scan rates and the peak currents increased in correspondence with the increase of the scan rate values which indicated that it was a surface controlled by diffusion processes (Figure 4.5).

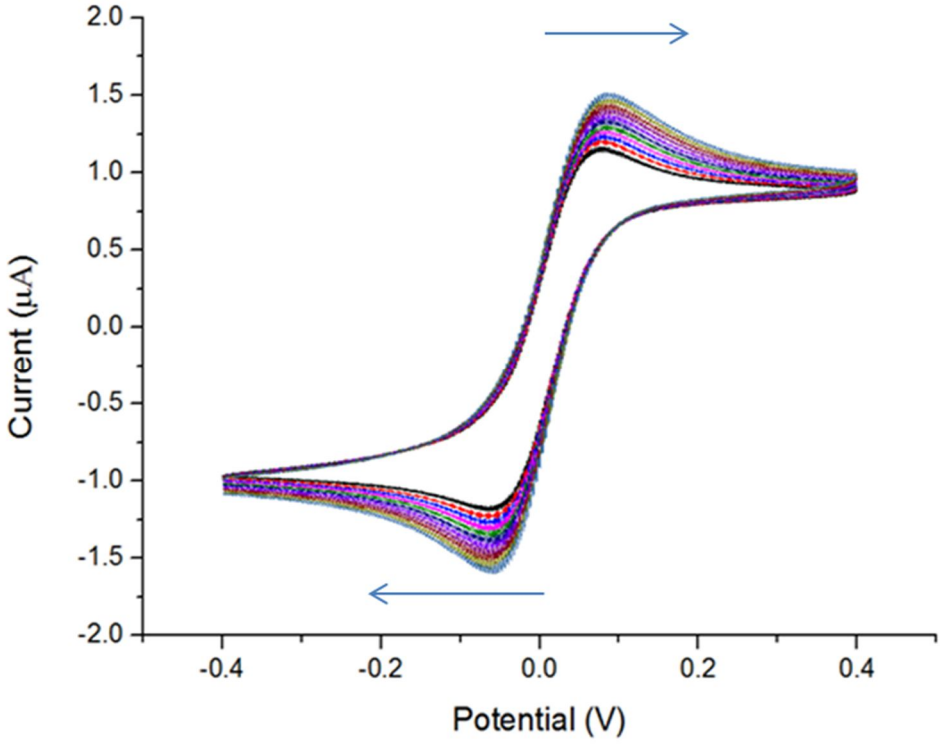

Figure 4.5: Cyclic voltammograms of a nanopillar electrode in 5mM $[Fe(CN)_6]^{3-/4-}$ in 0.1 M KCl with a varying scan rate of 100-400mV/s.

4.4.2 Simultaneous detection of DA and UA

The following figure displays the binary cyclic voltammogram of DA and UA obtained with both nanostructured (red line) and flat (black line) electrodes in 0.1mol/l PBS solution at a scan rate of 50mV/s (Figure 4.6). It can be seen that the voltammetric peaks of DA and UA were quite broad for the flat electrode with potential peaks located respectively at 0.18mV and 0.52mV, while two well-defined peaks of DA and UA, located at 0.12mV and 0.44mV, were observed on the cyclic voltammetry carried out with the electrode with the nanopillars which also showed much enlarged peak currents. These results indicated that the nanostructured electrode exhibited enhanced sensitivity due to the increased active surface area available for the reaction.

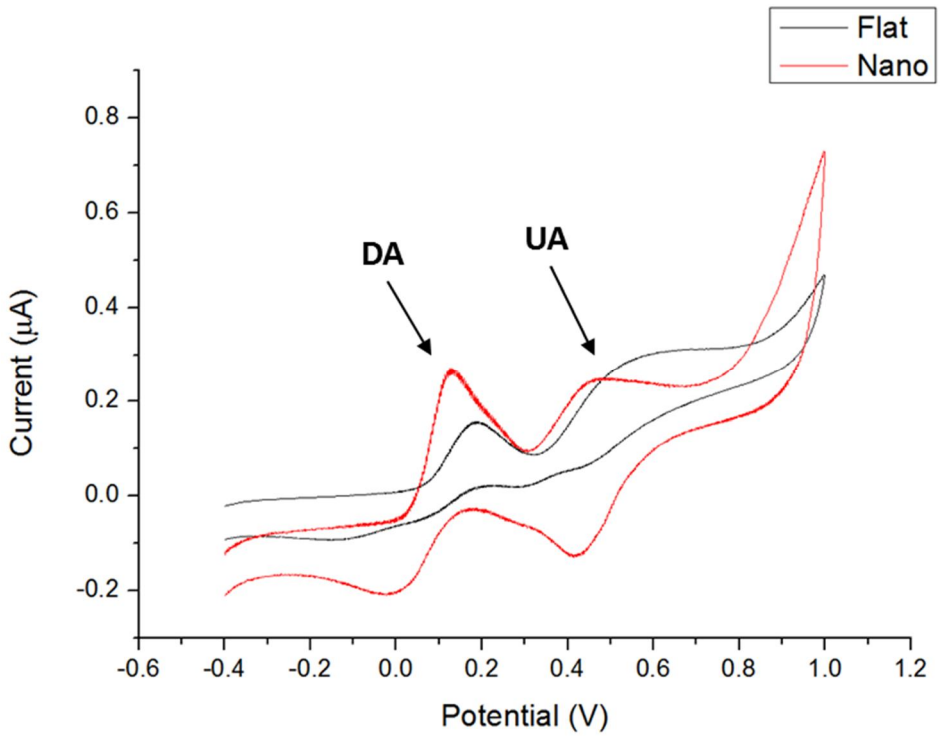

Figure 4.6: CV's of 0.14mM DA and 1.17mM UA obtained with nano and flat electrodes in 0.1mol/l PBS solution, scan rate 50mV/s

4.4.3 Calibration curves with DA and UA

Simultaneous detection of DA and UA in a concentration range of 0.98mM to 2.1mM UA and 0.01mM to 0.33mM DA was carried out with a flat electrode (Figure 4.7). The electrochemical oxidation peak currents for both DA and UA increased with increases in their concentrations. The peak potentials kept steady and the calibration curves were linear for both the analytes (Figure 4.8).

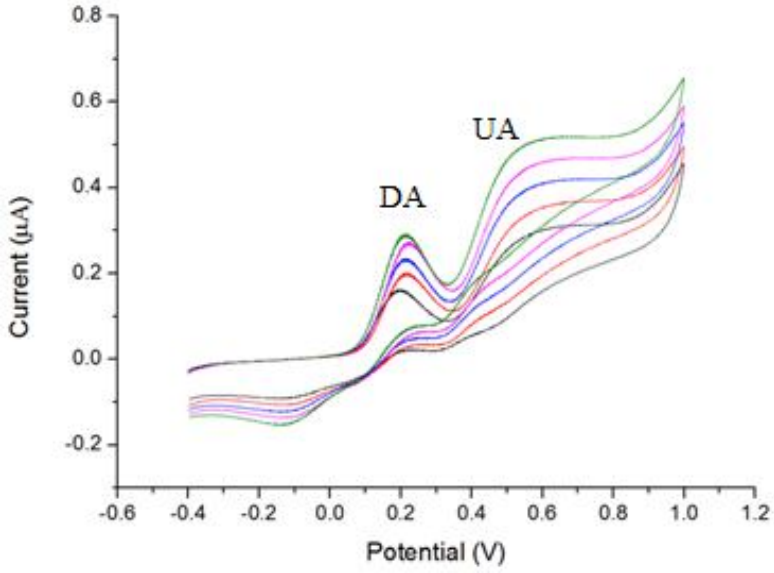

Figure 4.7: CV's of various DA and UA concentrations at the flat electrode in 0.1 M PBS solution, pH 4. Concentrations of analytes range from 0.98 mM to 2.1 mM UA and 0.01mM to 0.33mM DA.

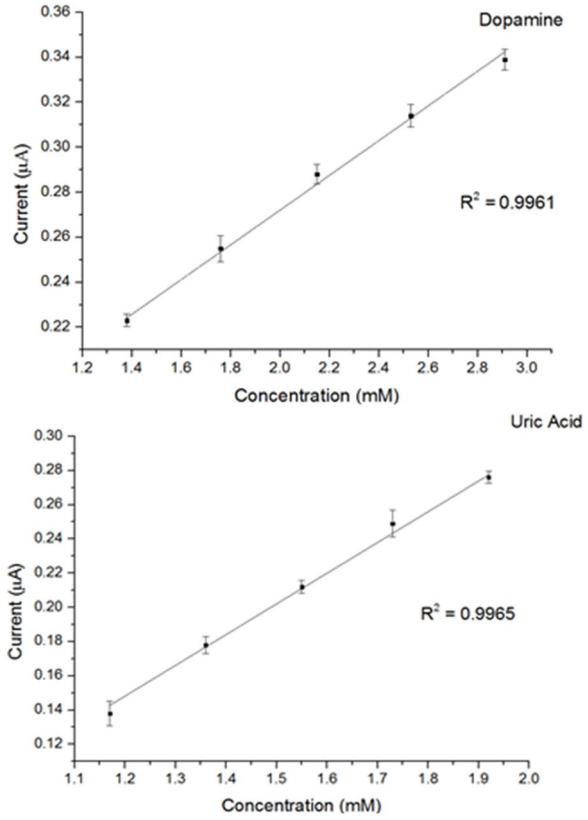

Figure 4.8: (left) Calibration plot for DA obtained from the CV's recording shown in figure 4.7; (right) Calibration plot for UA obtained from the CV's recording shown in figure 4.7

Simultaneous detection of DA and UA in a concentration range of 0.98mM to 2.1mM UA and 0.01mM to 0.33mM DA was repeated using a nanostructured electrode (Figure 4.9). The electrochemical oxidation peak currents for both DA and UA increased with increases in their concentrations. The peak potentials kept steady and the calibration curves were linear for both the analytes (Figure 4.10).

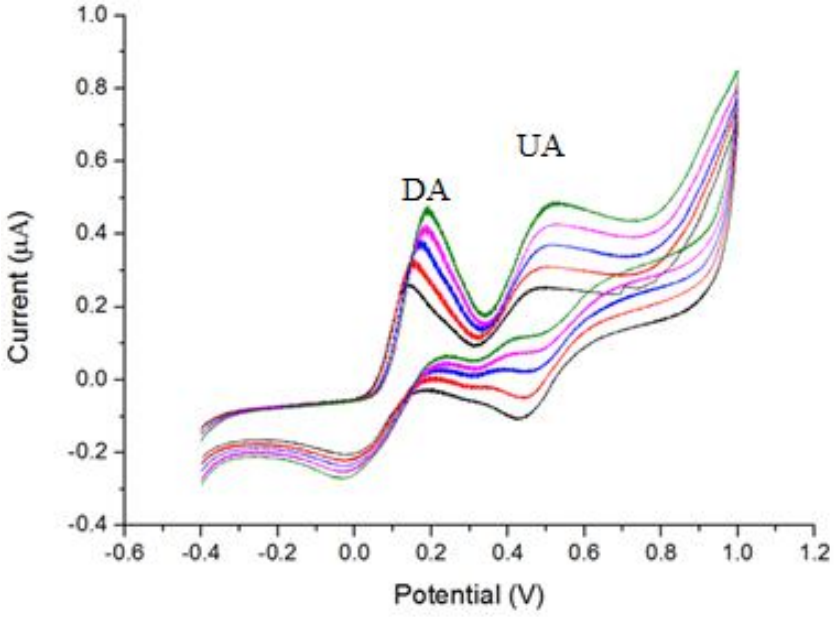

Figure 4.9: CV's of various DA and UA concentrations at the nano electrode in 0.1 M PBS solution, pH 4. Concentrations of analytes range from 0.98 mM to 2.1 mM UA and 0.01mM to 0.33mM DA.

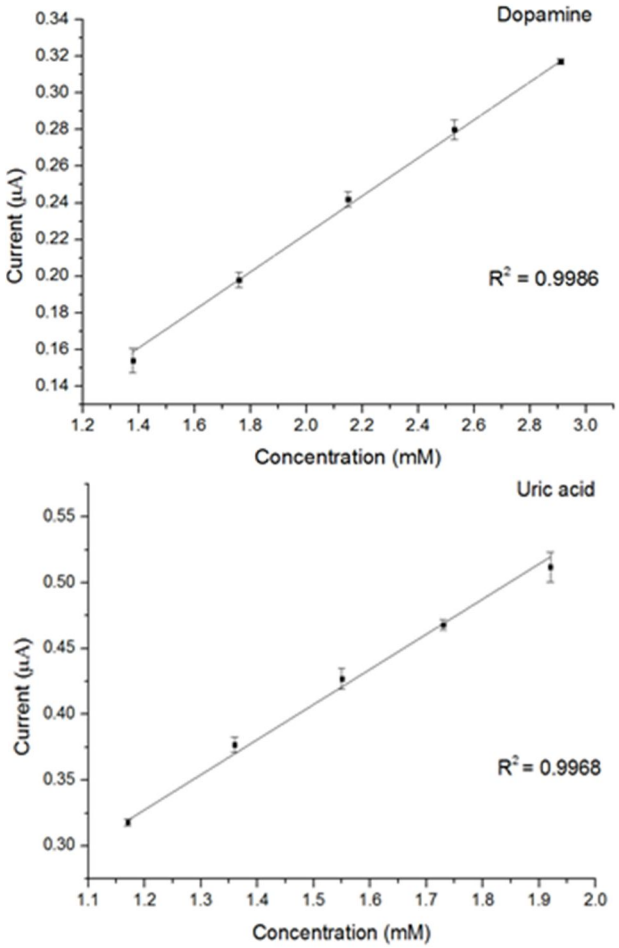

Figure 4.10: (left) Calibration plot for DA obtained from the CV's recording shown in figure 4.9; (right) Calibration plot for UA obtained from the CV's recording shown in figure 4.9

The analytes were added to the buffer solution in small amounts at each measurement. For the tests with DA, 50µl were initially added to the buffer. Then another quantity of 50µl was added to reach 100µl. From this amount, 20µl of analytes were added at each step during the experiment until reaching a total of 500µl, where no improvements in the detection were noticed. The same process was followed for UA, until reaching a maximum of 300µl.

4.5 DISCUSSION

The performances of the interdigitated electrodes with nanopillars were compared to those of their flat counterpart toward the simultaneous detection of dopamine and uric acid. The nanostructured ones showed greater sensitivity and the peaks in the voltammograms reported were higher and better defined when compared to smaller and broader ones of the flat electrodes. This was due to the fact that the nanostructured electrodes had a larger surface area; for this reason the nanopillars fabricated on the interdigitated electrodes enhanced the electron transfer property of the flat version of this electrode as it was also demonstrated by Shin [53].

The shift which can be noted along the x-axis in figures 4.6, 4.7 and 4.9 were due to the fact that each device had their own reference electrode embedded in the system. Small differences occurred in each electrode due to fabrications imperfections which were likely to determine these small differences in the measurements. Reference electrodes are generally expected to maintain constant electrode potentials throughout their operational lifetime, but many different processes can compromise proper reference electrode potential, and numerous studies have been performed towards minimizing these effects [54]. In the case of the Ag/AgCl electrode, dissolution of AgCl changes the activity of the ions in the electrolyte, which affects the potential. This problem becomes much worse if the volume of the filling solution is small. Additionally, as the electrode operates, there is continuous dissolution of the AgCl layer, and once it is used up, the electrode potential changes dramatically, since AgCl is no longer available for cathodic operation. Quasi-reference electrodes (like they could be considered in this case) do not have an internal electrolyte, and their potential can therefore be severely affected with variations in the test solution. However, the absence of a separating membrane makes the design much simpler, and allows lower drifts due to convective mixing [54].

The peaks measured with the nanostructured electrodes had a closer peak to peak separation which showed a better diffusion process. The coefficient of determination, R^2, indicates how well the data fit the linear statistical model. In this case the value was very close to 1 which shows a good reproducibility and repeatability when increasing the concentration and potential in a linear way.

The methodology used to achieve these results was the same used in the paper [55] and it was successful to characterise in-house fabricated screen-printed electrode (SPE) with their surface modified with gold nanoparticles. This inexpensive device was used for the simultaneous determination of dopamine (DA) and uric acid (UA). In this detection, the electrochemical potential of DA and UA were resolved into two peaks at +330 mV and +526 mV, respectively. Under optimum conditions, the oxidation current peak current was linearly dependant on DA and UA concentration in the range of 0.03 mM to 0.2 mM and 0.1 mM to 1.17 mM respectively. The SPE modified with gold nanoparticles showed good sensitivity and reproducibility. This paper was to the best of our knowledge the first reporting of a SPE modified in situ with electroplated gold (Au) nanoparticles for the simultaneous determination of DA and UA.

4.6 FUTURE WORK

These experiments outlined encouraging results for the use of these electrodes as electrochemical sensors. However, more experiments and characterization will be needed in the future to confirm the feasibility of this route.

Experiments are currently being carried out to investigate the effect of different nanopillar configurations, in terms of pillar dimensions and spacing to optimize the detection of DA and UA.

More electrodes with different configurations will be fabricated to further investigate the effect of the presence of the nanostructures used to modify the electrode surface.

4.7 REFERENCES

[1] A. Hulanicki et al., "Chemical sensors definitions and classification", Pure & Appl. Chem., Vol. 63, No 9, 1247-1250, 1991.

[2] J. R. Stetter et al., "Sensors, Chemical Sensors, Electrochemical Sensors, and ECS", Journal of The Electrochemical Society, 150 (2) S11-S16 (2003)

[3] C.C. Liu, "Electrochemical sensors", The biomedical engineering handbook. 1 ed. Joseph D. Bronzino, 2000.

[4] J. Tvrdikova et al., "Voltammetric and amperometric determination of selected dinitronaphthalenes using single crystal silver amalgam based sensors", Electrochimica Acta 73 (2012) 23– 30

[5] E. Bakker, K. Chumbimuni-Torres, "Modern Directions for Potentiometric Sensors", J. Braz. Chem. Soc., Vol. 19, No. 4, 621-629, 2008.

[6] E. Bakker, E. Pretsch, "Potentiometric sensors for trace-level analysis", Trends Analyt Chem. 2005 March; 24(3): 199–207.

[7] D. M. Wilson et al., "Chemical Sensors for Portable, Handheld Field Instruments", IEEE Sensors Journal, Vol. 1, No. 4, December 2001

[8] G. Jasinski, P. Jasinski, "Solid electrolyte gas sensors based on cyclic voltammetry with one active electrode", IOP Conf. Series: Materials Science and Engineering 18 (2011) 212007

[9] I. Hasegawa, Solid electrolyte type nitrogen monoxide gas sensor operating at intermediate temperature region Sensors and Actuators B 108 (2005) 314–318

[10] D. Levesque, C. Rouillard, "Nur77 and retinoid X receptors: crucial factors in dopamine-related neuroadaptation", Trends in Neurosciences Vol.30 No.1

[11] M. Heien et al., "Real-time measurement of dopamine fluctuations after cocaine in the brain of behaving rats", PNAS, July 19 2005, vol. 102, no. 29, 10023–10028

[12] J. J. Mateos et al., "Decreased striatal dopamine transporter binding assessed with [123I] FP-CIT in first-episode schizophrenic patients with and without short-term antipsychotic-induced parkinsonism", Psychopharmacology (2005) 181: 401–406

[13] J. Smythies, "The Neurotoxicity of Glutamate, Dopamine, Iron and Reactive Oxygen Species: Functional Interrelationships in Health and Disease: A Review – Discussion", Neurotoxicity Research, Vol. 1, pp. 27-39

[14] Z. Guo et al., "Sensitive and selective electrochemical detection of dopamine using an electrode modified with carboxylated carbonaceous spheres", Analyst, 2013, 138, 2683

[15] R. P. H. Nikolajsen, "Analytical methods for determining urinary catecholamines in healthy subjects", Analytica Chimica Acta 449 (2001) 1–15

[16] H. R. Zare et al., "Voltammetric studies of an oracet blue modified glassy carbon electrode and its application for the simultaneous determination of dopamine, ascorbic acid and uric acid", Journal of Electroanalytical Chemistry 589 (2006) 60–69

[17] G. P. Jin et al., "Novel choline and acetylcholine modified glassy carbon electrodes for simultaneous determination of dopamine, serotonin and ascorbic acid", Journal of Electroanalytical Chemistry 569 (2004) 135–142

[18] M. Ferreira et al., "Langmuir–Blodgett films from polyaniline/ruthenium complexes as modified electrodes for detection of dopamine", Thin Solid Films 446 (2004) 301–306

[19] Katsuyoshi Hayashi et al., "On-line microfluidic sensor integrated with a micro array electrode and enzyme-modified pre-reactor for the real-time monitoring of blood catecholamine", Electrochemistry Communications 5 (2003) 1037–1042

[20] D. R. Shankaran et al., "Sol–gel derived metal dispersed ceramic graphite composite electrode for amperometric determination of dopamine", Analytica Chimica Acta 478 (2003) 321–327

[21] M. Sotomayor et al., "Development of an enzymeless biosensor for the determination of phenolic compounds", Analytica Chimica Acta 455 (2002) 215–223

[22] F. Lisdat et al., "Catecholamine detection using enzymatic amplification" Biosensors & Bioelectronics Vol. 12. No. 12, pp. 1199-121 I, 1997

[23] M.A. Dayton, A.G. Ewing, R.M. Wightman, "Diffusion processes measured at microvoltammetric electrodes in brain tissue", Journal of Electroanalytical Chemistry 146 (1983) 189

[24] Y. Li, X. Lin, "Simultaneous electroanalysis of dopamine, ascorbic acid and uric acid by poly (vinyl alcohol) covalently modified glassy carbon electrode", Sensors and Actuators B 115 (2006) 134–139

[25] E. Akyilmaz et al., "A biosensor based on urate oxidase_/peroxidise coupled enzyme system for uric acid determination in urine", Talanta 61 (2003) 73_/79

[26] W. S. Waring et al., "Uric acid as a risk factor for cardiovascular disease", QJMed 2000, 93, 707-713

[27] W. L. Nyhan, "Behaviour in the Lesch-Nyhan syndrome", Journal of autism and childhood schizophrenia September 1976, Volume 6, Issue 3, pp 235-252

[28] I. Grabowska et al., "Uric acid determination in a miniaturized flow system with dual optical detection", Sensors and Actuators B 130 (2008) 508–513

[29] W. J. Pudelkiewicz, M. W. Stutz, L. D. Matterson, "Determination of Uric Acid in Avian Excreta by the Use of Uricase and Differential Spectrophotometry", Poultry Science 1968) 47 (4): 1274-1277

[30] Y. Yue-Dong, "Simultaneous Determination of Creatine, Uric Acid, Creatinine and Hippuric Acid in Urine by High Performance Liquid Chromatography", Biomedical chromatography Vol. 12, 47–49 (1998)

[31] Elena Popa et al., "Selective Voltammetric and Amperometric Detection of Uric Acid with Oxidized Diamond Film Electrodes", Anal. Chem. 2000, 72, 1724-1727

[32] Veronique Vitart et al., "SLC2A9 is a newly identified urate transporter influencing serum urate concentration, urate excretion and gout", Nature Genetics Vol. 40, No. 4, April 2008

[33] H. H. Hamzah et al., "Spectrophotometric Determination of Uric Acid in Urine Based-Enzymatic Method Uricase with 4-Aminodiphenylamine Diazonium Sulfate (Variamine Blue RT Salt)", J Anal Bioanal Tech 2013, S7

[34] T. Horn, L. Bauce, R. Landgraf, Q. J. Pittman, "Microdialysis with High NaCl Causes Central Release of Amino Acids and Dopamine", J. Neurochem., 1995, 64, 1632.

[35] N. T. Deftereos, N. Grekas and A. C. Calokerinos, "Flow injection chemiluminometric determination of albumin", Analytica Chimica Acta, 2000, 403, 137-143.

[36] D. P. Quan et al., "Electrochemically selective determination of dopamine in the presence of ascorbic and uric acids on the surface of the modified Nafion/single wall carbon nanotube/poly(3-methylthiophene) glassy carbon electrodes", Colloids and Surfaces B: Biointerfaces 88 (2011) 764– 770

[37] X. Lin et al., "Electrocatalytic oxidation and determination of dopamine in the presence of ascorbic acid and uric acid at a poly (*p*-nitrobenzenazo resorcinol) modified glassy carbon electrode", Sensors and Actuators B 122 (2007) 309–314

[38] Abolanle S. Adekunle et al., "Electrochemical Response and Impedimetric Behaviour of Dopamine and Epinephrine at Platinum Electrode Modified with Carbon Nanotubes-Gold Nanocomposite" Int. J. Electrochem. Sci., 6 (2011) 2826 - 2844

[39] X. Ma et al., "Electrochemical detection of dopamine in the presence of epinephrine, uric acid and ascorbic acid using a graphene-modified electrode", Anal. Methods, 2012, 4, 1687

[40] X. Xiao et al., "Simultaneous Detection of Dopamine, Ascorbic Acid and Uric Acid at Lithographically-Defined 3D Graphene Electrodes", Electroanalysis 2014, 26, 52 – 56

[41] Y.R. Kim et al., "Electrochemical detection of dopamine in the presence of ascorbic acid using graphene modified electrodes", Biosensors and Bioelectronics 25 (2010) 2366–2369

[42] Arno Hausen et al., "Quantitation of Urinary Uric Acid by Reversed-Phase Liquid Chromatography", Clin. Chem. 27/8, 1455-1456 (1981)

[43] T. Kawashima, G. A. Rechnitz, "Potentiometric enzyme electrode for uric acid", Anal Chim Acta. 1976 May;83(1):9-17.

[44] M. B. Garcia et al., "Automatic Determination of Uric Acid in Urine in a FIA System with a Tubular Amperometric Detector" Portugaliae Electrochimica Acta 22 (2004) 249-262

[45] E. S. Gil, G. R. Melo, "Electrochemical biosensors in pharmaceutical analysis" Brazilian Journal of Pharmaceutical Sciences vol. 46, n. 3, jul./set 2010.

[46] M. R. Moghadam et al., "Chemometric-assisted kinetic–spectrophotometric method for simultaneous determination of ascorbic acid, uric acid, and dopamine", Analytical Biochemistry 410 (2011) 289–295

[47] V. Sanz, S. Marcos, J. Galba, "Uric acid determination using uricase and the autotransducer molecular absorption properties of peroxidase", Analytica Chimica Acta 607 (2008) 211–218

[48] Y. Liu and W. Wei, "Detection of Cytochrome *c* at Biocompatible Nanostructured Au-lipid Bilayer-modified Electrode", Analytical Sciences 2008, Vol. 24 1431

[49] P. Wang et al., "Fabrication of layer-by-layer modified multilayer films containing choline and gold nanoparticles and its sensing application for electrochemical determination of dopamine and uric acid" Talanta 73 (2007) 431–437

[50] A. L. Liu et al., "Simultaneous voltammetric determination of norepinephrine, ascorbic acid and uric acid on polycalconcarboxylic acid modified glassy carbon electrode", Biosensors and Bioelectronics 23 (2008) 1488–1495

[51] J. M. Zen et al., "Selective voltammetric method for uric acid detection using pre-anodized Nafion-coated glassy carbon electrodes", Analyst, June 1998, Vol. 123 (1345–1350)

[52] M. Khan et al., "Electrochemical determination of uric acid in the presence of ascorbic acid on electrochemically reduced graphene oxide modified electrode", Journal of Electroanalytical Chemistry 700 (2013) 54–59

[53] C. Shin, W. Shin, H. Hong, Electrochemical fabrication and electrocatalytic characteristics studies of gold nanopillar array electrode (AuNPE) for development of a novel electrochemical sensor, Electrochimica Acta 53 (2007) 720–728

[54] M. W. Shinwari et al., Microfabricated Reference Electrodes and their Biosensing Applications, Sensors 2010, 10, 1679-1715

[55] Una B. Crowley, Walter Messina, Miloslav Pravda, Jeremy D. Glennon and Eric Moore (2014) 'Electrochemical property of screen printed electrode modified with gold nanoparticles for the simultaneous determination of Dopamine and Uric acid'. Journal of Electroanalytical Chemistry,

Chapter 5

5 BIOIMPEDANCE SENSOR APPLICATION: SMART NEEDLE PROJECT

5.1 INTRODUCTION

Bioelectrical impedance measurement is a widely used, simple, quick, and non-invasive method for estimating body composition. It is currently in used in many different settings, including private clinicians' offices, health clubs, and hospitals. The most common and probably most well-known use of the bioimpedance technique is body fat analysis where an electrical impedance measurement of body tissues provides an estimate of total body water from which fat-free mass and body fat (adiposity) can be deduced. This concept can be then applied to differentiate several tissues from the nerve tissue. In the preliminary studies reported in this chapter, bioimpedance measurements were used in combination with techniques used in the field of anaesthesia (and more specifically to ultrasound guided peripheral nerve block), and it was possible to distinguish (using meat samples) muscle, fat, bone, connective tissues and eventually nerve tissue by constructing two needles into an impedance sensor. The results obtained in this preliminary study led to a project for the fabrication of an impedance sensor on the tip of a commercially available needle to improve the safety of the peripheral nerve block procedure.

5.1.1 Peripheral nerve block background

Preoperative nerve injuries represent the highest percentage in anaesthesia related injuries which can happen for several different reasons [1, 2]. nerves can be mainly damaged in chemical and mechanical way and may be often related to poor regional anaesthetic delivery [3]. In relation to regional anaesthesia, a successful peripheral nerve

block requires a placement of the drug in the direct proximity of the nerve. This, of course, constitutes a potential risk of touching the nerve with the needle tip which could also potentially lead to an unwanted intraneural injection. The direct contact of the needle with neural structure, however, doesn't necessarily lead to nerve injuries [4, 5]. Steinfeldt et al have shown that a minimal penetration of the nerve with the needle tip does not cause serious nerve damage [6] while other studies have shown that instead the intraneural injection of the anaesthetic could heavily damage the nerve. This is caused by the chemical interaction of the delivered neurotoxic drug on one hand [7] and the mechanical damages caused by the injection pressure on the other [7, 8].

To understand how the mechanical damage can occur, it is necessary to know deeply the nerve structure: it is made up of several fascicles which contain the nerve fibres. Each fascicle is walled by the perineurium, a tough and resistant tissue hard to penetrate and which is able to regulate the passage of different molecules from the surrounding tissue [7]. Clusters of fascicles together make up a nerve trunk. These contain also blood vessels and are surrounded by a membrane called epineurium (figure 5.1).

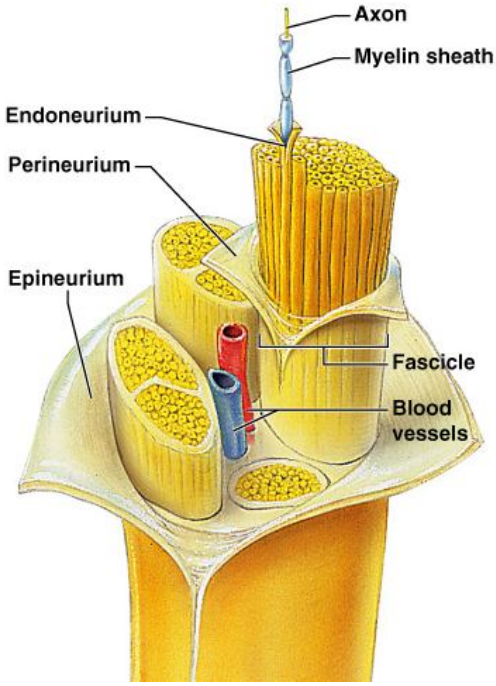

Figure 5.1: general structure of a nerve

A mechanical damage to the outer membrane does not affect the nerve fibres itself [6] but the injection of the anaesthetic around the perineurium disturbs the nerve function. In addition, as mentioned above earlier, the injection pressure can cause direct damage to the nerve or damage it indirectly by interacting with the blood flow through the vessels inside the epineurium [7].

It is then obvious that it is imperative to avoid needle to nerve contact during anaesthetic nerve blocks and, if this should unfortunately happen, to detect it before the anaesthetic is injected. In the past, the peripheral nerve block techniques were based on the placing the needle on 'anatomical landmarks' improved then by the electrical nerve stimulation and by ultrasound guidance, making it a relatively safe and successful procedure [4], but there is still a lot of room for improvement.

5.1.2 State of the art

Localization of nerves for regional anaesthesia relies in general on two different principles: electrical nerve stimulation (ENS) and ultrasonic needle guidance (USG). ENS is based on the natural neural functionality, while USG uses anatomical relationships to distinguish the endpoint of the needle insertion [9]. Both the options offer certain advantages and have to deal with some technical limitations. Therefore, often they are combined for the purpose.

5.1.3 Electrical nerve stimulation

To localize the nerve of interest with ENS, a short electrical pulse is used to induce a flow of ions through the neuronal cell membrane. This depolarizes the neuronal membrane which causes (depending on the nerve fibre of interest) either a paresthesia or a muscle contraction [10]. According to Coulomb's law (equation 1), the current needed to stimulate the nerve is proportionally inverse to the distance between needle and nerve [9]. This observation of the effects of the electrical stimuli on the patient helps the clinician to roughly establish where the needle is in respect to nerve bundle.

$$E = KQ/r^2 \quad (1)$$

Where: E = required stimulating current; K = constant; Q = minimal required stimulating current; r = distance between electrode and nerve

An oscillating square wave current generator is usually needed for stimulating the nerve; this generator provides a continuous stream of electrical pulses at given times and frequencies. A stainless steel needle is connected to its cathode and leads the electrical impulse to the nerve [9, 11]. At the beginning, a relatively high current of 1–2 mA is used with pulse duration of 0.1-0.2 ms to stimulate the nerve from a distance of 1-2 cm. As soon as a response is recognized current is decreased and the needle is guided nearer to the nerve. A current between 0.20 and 0.50 mA marks the endpoint of needle insertion and the drug is injected [10]. In this way a three-dimensional needle-guidance is possible and the anaesthesiologist can be sure to block exactly the nerve of interest [12].

Despite these advantages, there are some problems that limit the success of ENS. First of all, it shows a low sensitivity for detection of needle to nerve contact in comparison to paraesthesia or USG [13 - 15]. In addition, Sinha et al have shown that the current that is necessary to get a response after the placement of the needle with ENS could vary over a wide range without influencing the success of the nerve block [16], mainly because different nerves have different properties [15] or because the heterogeneous composition of the surrounding tissues, that have varied electrical properties, could channel the current away from or towards the nerve [12, 17].

5.1.4 Ultra-sound guidance

In ultrasonic needle guidance, both the needle and the nerve structures can be visualized by sound waves [18, 19]. The ultrasonic device is capable of emitting and receiving sound waves at the same time. The emitted waves are reflected or deflected by the connective tissue inside the nerve and the received sound waves are used to reconstruct a picture of the tissue with different contrasts [18, 20]. In addition, due to its watery

consistency the injected anaesthetic behaves like a contrast medium allowing to follow its distribution around the nerve during the injection [19].

For imaging a small nervous structure, it is necessary to use relatively high frequencies, as they provide high-resolution images. On the other hand, unfortunately, while increasing the frequency the penetration depth of the sound waves decreases. So, usually a frequency between 5 and 14 MHz is chosen to be used as a compromise [18].

For the performance of the nerve block with ultrasonic guidance there are a large number of different techniques according to the angle of needle insertion, the exact frequency, the geometry of the probe etc. [21]. All of them rely on the principle that it is not essential placing the needle at an exact point next to the nerve, but instead ensuring a uniform distribution of the drug around it [21, 22]. The possibility to observe this distribution allows to inject as little amounts of anaesthetic as possible and to increase success rates of nerve blocks in a pain-free way [21].

However, to use this technologies, good knowledge of human anatomy and a long practice are necessary [19].

5.1.5 Block success

Several randomized studies were made in the past to determine which technique was more reliable regarding to a successful block of the nerve of interest. They cover different kinds of nerve blocks and are resumed in table 5.1.

Table 5.1: randomized studies to compare success performed with help of ultrasound or nerve stimulation

Author/year	Type of block	Number of patients	Success rate	
			nerve stimulation	ultra sound
Marhofer /1997 [23]	Femoral	40	85%	95%
Marhofer/1998 [24]	Femoral	60	80%	95%
Macaire/2008 [25]	Median and Ulnar	60	93,3%	93,3%
Sauter/2008 [26]	Infra-clavicular	80	85%	95%
Casati/2007 [27]	Axillary	60	94%	97%
Perlas/2008 [28]	Popliteal sciatic	74	60,6%	89,2%
Chan/2007 [29]	Axillary	188	62,9%	82,8%
Sites/2006 [30]	Axillary	56	54%	82%
Kapral/2008 [31]	Interscalene	160	91%	99%
Liu/2005 [32]	Axillary	90	90%	90%
Williams/2003 [33]	Supraclavicular	80	78%	85%
Guerkan/2008 [34]	Infraclavicular	60	92,5%	95%
Taboada/2009 [35]	Intercavicular	70	91%	89%

With the only exception of Taboada et al [35], the data reported in the table shows a clear higher success rate of nerve blocks performed using the USG technique compared to the ENS one. But still these results are at the centre of critical discussion. In some of these studies the success rates is particularly very low. Sites et al for example got a success rate of 54% [30] and Chan et al got one of 63% [29] for an axillary plexus block using nerve stimulation while other literature reports a success rate of about 90% for this technique [36]. The reason for this discrepancy is most likely a different interpretation of the definition of a successful block and the fact that there many different ways of performing a nerve block with the ENS. There are certainly techniques more successful

than others and it is a strict responsibility of the anaesthetist to find the most suitable one for every different patient. But apart from this, ultra sound guidance seems to be the technique more effective in terms of success rate [37].

5.1.6 Safety/ Nerve contact

There is little existing data comparing the incidence of complications occurring during a nerve block performed with USG or ENS [38].

Some of the randomized studies comparing the success rate of these two guidance techniques consider their safety as well but they focus their attention on several other different aspects. Sauter et al mentioned that, in their study, suction of blood was noticed in 33% of the patients treated with ENS and in 5% treated with USG [26]. The rate of accidental vascular puncture for nerve blocks performed with ENS was 7.5% in the study of Gurkan et al [34], 15% in a study of Marhofer et al [23] while no vascular puncture was reported to have occurred in both studies when using USG. Lui et al observed adverse events in 20% of patients when ENS was used for needle guidance, while no adverse events occurred when USG was used [32]. Local bruising was observed by Chan et al in 13% of the cases when ENS was used and in 3% when USG was used [29]. During the research reported by Sauter et al, 2.5% of patients of the ENS-Group and 20% of the USG-Group experienced paresthesia during block performance [26] while Chan et al reported a 21% rate of patients experiencing paraesthesia for both the groups [29]. In another randomised study of ultrasound-guided femoral catheter placement, Fredrickson and Danesh-Clough did not observe any sign of central nervous system or cardiac toxicity in both the USG or ENS groups [39].

Abrahams et al reviewed and analysed all randomized controlled trials that have compared USG and ENS for nerve localization. They came to the conclusion, that there is no statistically significant difference between the USG and ENS groups regarding the experiencing of paresthesia during the nerve block or the incidence of neurological symptoms after the block's ending. To demonstrate the superiority of one of the techniques, additional studies and statistical data would be necessary [40].

The only study as of today, covering a large number of cases, was made by Fredrickson and Kilfoyle. They analysed 1000 USG peripheral nerve blocks and questioned the patients regarding neurological symptoms after 10 days, 1 month, 3 months and 6 months. As a result, they stated that the rate of neurologic complications of USG nerve blocks was very low and that the majority of complication occurring in their study was not related to the nerve block itself. [41] The frequency of complication observed was similar to the one reported in a comparable prospective study not using USG done by Borgeat et al [42]. But it was pointed out, however, that it is difficult to compare the safety of the two methods because of the high rate of complications caused by influences not related to the block technique itself [41].

The advantage of USG stands in the fact that nerves, vessels and the location of the needle in respect to these structures are visible. This helps preventing puncturing the vessels and avoiding needle to nerve contact which could lead to further complications [40], although, there are papers reporting cases of penetration of vessels or nerves as well as intravascular or intraneural injection during an USG nerve block [43-47]. In addition, there is a reported case of a pneumothorax related to a USG supraclavicular nerve block [48].

In a couple of cases, neural puncture or intraneural injection was noticed only by analysing the video of the needle insertion and not during the block performance [45, 46]. These cases demonstrate, that even if the use of USG has the potential to decrease the risk of intraneural injection compared to ENS, it does not totally avoid this kind of complication [49].

Regarding the ability to detect needle-to-nerve contact, Macfarlane et al examined several animal studies relating to indicators of needle-to-nerve contact and intraneural injection. They came to the conclusion, that neither ENS nor USG are sensitive enough to be completely reliable [15].

In conclusion, a definite and unequivocal statement to rank these techniques according to patient's safety during block performance cannot be made as of today. The American Society of Regional Anaesthesia and Pain Medicine (ASRA) summarize these findings in a Practice Advisory on Neurologic Complications with following statement: "No nerve localization or monitoring technique has been shown to be clearly superior in

terms of reducing the frequency of clinical injury" because "There are no animal or human data to support the superiority of one nerve localization technique — paresthesia, nerve stimulation, ultrasound — over another with regards to reducing the likelihood of nerve injury"[49].

5.1.7 Comparison

Till today, there is no common agreement about the use of ultrasound or needle guidance in regional anaesthesia. There are advantages and disadvantages for both techniques to perform the peripheral nerve block. As follows, the most relevant factors for a satisfying nerve block such as the block success, the safety of the nerve block and the ability for detecting needle to nerve contact are compared.

USG in regional anaesthesia offers many advantages in comparison to ENS. It is possible to visualize the needle, the nerve of interest and the surrounding structures like arteries, veins and other nerves. This helps avoiding accidental puncture or damage to these structures [50]. In addition, the possibility to observe the spreading of the anaesthetic around the nervous tissue helps to make sure that the drug reaches exactly its destination [19]. Another advantage is the fact that the needle insertion could be followed in real-time, which gives an exact impression of the position of the needle and helps to place it at the right place. Furthermore, the anatomy of nerves is varying in different patients. The visualization of the nerves helps to deal with this variability. All this could lead to a safer way of regional anaesthesia [50]. Some randomized studies have indicated a slightly better success rate of nerve blocks performed with US.

However, on the other hand some cases reported complications related to USG nerve block [43-48]. In addition, some papers reported difficulties about the handling of USG which may reduce the advantages of this technique. Hebl for example pointed out that it is difficult to visualize needle tip and nerve continuously during the block procedure [51]. All in all, the question if USG really is increasing the safety of nerve blocks cannot be answered till today. Experts are divided into three groups: the ones who see the USG as a great improvement of regional anaesthesia [18, 21, 37, 52, 53], the ones who consider NS as best practice for needle guidance [9] and those who require further data and more experience to make an objective evaluation [54 - 56]. One thing that makes it

difficult to define a superior technique is that regional anaesthesia is still an operator dependant procedure. Success and safety are determined not only by the technique itself but also by the skills of the anaesthetist. This brings up the problem of standardisation to generate objective data [47].

Borgeat pointed out that the number of patients necessary to show even a minimal advantage of one technique over the other, would be that large that it is possible that this could never be proven [42].

To achieve higher rates of success and safety the combination of the two techniques is usually recommended. In this way it would be possible to profit from the advantages of both [12, 36, 52].

However, even this could not hide the fact that both techniques, USG and ENS, are far from being completely risk-free. The final goal to reach a success rate of 100% without adverse events could not be reached till today. Still we cannot be totally sure to know the position of the needle or to find the right nerve and the risk of a permanent peripheral nerve injury is not completely eliminated [48, 49, 57-69].

Since neural puncture and intraneural injection is not preventable with neither ENS [4] nor USG [45, 46], a way to detect needle to nerve contact safely may lead development of nerve block performance into the right direction.

In this project we assume that the bioimpedance measurement of tissues could offer a new solution and a helpful tool to solve this current problem.

5.2 SCOPE

A few tests have been conducted to prove that a modified commercially available needle could be potentially used to determine the type of tissue it is in. The main preliminary work was done in collaboration with Dr Brian O'Donnell from the department of Anaesthesia of Cork University.

These studies originated from the need to determine the precise needle tip location prior to local anaesthetic injection during ultrasound-guided peripheral nerve block. This still remains a significant challenge, despite widespread availability of high resolution

ultrasound. Both Intraneural needle placement and intraneural local anaesthetic injection can harm the peripheral nerve. Sub-epineurial or intraneural needle placement can cause direct mechanical structural nerve injury [6, 60 – 62]. Furthermore, intraneural local anaesthetic injection can result in nerve injury due to increased intraneural pressure with resultant reduced neural blood flow and neural hypoxemia. Currently, despite the use of ultrasound guidance, intraneural needle placement may not be recognized, even by experienced clinicians, and can result in nerve injury with associated significant transient or permanent disability [63 – 65].

Bioimpedance, measured at the needle tip, may provide additional information as to needle tip location, thereby potentially facilitating detection of intraneural needle placement.

Bioimpedance measures the opposition of body tissues to the flow of a small alternating current which is usually no more than few hundreds nano amperes. Impedance is a function of two components (vectors): the resistance of the tissues themselves, and the additional opposition (reactance) due to the capacitance of membranes, tissue interfaces, and non-ionic tissues. Bioimpedance varies with frequency of the current used. Some applications may require the use of multi-frequency measurements or a frequency spectrum “sweep”.

5.3 OBJECTIVES

Bioimpedance, measured with a commercially available transcutaneous impedance circuit, has been used successfully to identify intraneural needle placement in an animal model. We hypothesized that bioimpedance measurements, taken directly from the needle tip would facilitate differentiation between muscles, fat and nerve.

The objectives of this series of studies were

- To create a macro prototype of the envisaged Smart Needle

- To determine whether bioimpedance within a cadaver animal could differentiate reliably between clinically relevant tissue types
- To determine the optimal current frequency range for this purpose.
- To collect characteristic impedance values for the different type of tissues in a continuos measurement (time analysis)
- To investigate possible methodologies to fabricate impedance sensors on a commercially available needle using different techniques

5.4 EXPERIMENTAL

5.4.1 Apparatus

Zahner IM6e electrochemical workstation and AutoLab electrochemical workstation (PGSTAT302N; Metrohm Autolab, Utrecht, The Netherlands) were used to measure the electrical bioimpedance on the meat ex-vivo samples. Commercially available needles Stimuplex A 50 (BBraun, Melsungen, Germany) used in anaesthesia for electrical nerve stimulation were used to fabricate the smart needle prototype. A syringe pump (KD scientific S200 Syringe pump) was used to perform the tests in a steady movement condition through the samples. The meat samples were kept at 37°C using an incubator (Thermo HybAid, Shake 'n' Stack HBSNS R240)

5.4.2 Procedure

Meat samples were obtained from local butchers and tested immediately after purchasing those (10-15 minutes from shop to laboratory). The samples were placed on a Plexiglas substrate covered with cling film. For the measurements done on the samples warmed at 37°C, the incubator was set at around 50°C before the samples was placed in it. After the meat was in the oven, the temperature was turned down to 37°C and the sample checked with a thermometer probe after 30 minutes. The samples were wrapped in cling film to avoid any drying processes.

The needle probe was placed in the desired tissues to be measured by simple visual inspection. In the experiments using a lamb carcass, dissection was needed to reveal the nerve bundles and it was performed by an expert anaesthesiologist to be sure to analyse the correct portions of nervous tissues

Impedance spectroscopy in ex-vivo sheep, beef and pig meat models was used to identify the optimal current and frequency range to differentiate between muscle, connective tissue and fat. Two meat models were used: refrigerated meat purchased from local suppliers; warm, freshly slaughtered meat from a local abattoir. Two proprietary regional anaesthesia needles (Stimuplex A 50, BBraun, Melsungen, Germany) were used. The needles were aligned in parallel and fixed one to the other using cyanoacrylate-based glue in a bipolar setup: one needle working as a source and the other as a detector. The spatial resolution of the "macro" prototype was 1.4mm as this was the maximum distance that occurred between the tips of the two needles (figure 5.2). The assembled needle array was next connected to the Autolab electrochemical workstation using shielded cables 25cm long to avoid any antenna-like behaviour (Autolab PGSTAT302N; Metrohm Autolab, Utrecht, The Netherlands) or to the Zahner IM6e Electrochemical workstation (ZAHNER-elektrik GmbH & Co. KG, Kronach, Germany); data were collected by the Frequency Response Analysis software for Autolab(used for the control of galvanostats and potentiostats in the performance of impedance measurements) and Thales software for the Zahner.

Frequency sweeps were performed to determine the optimum operating frequency range at which the largest magnitude of separation between tissue types occurs. The impedance analyser was set to measure impedance in a range between 100 Hz and 1MHz. To do this, the 'working' and 'sense' cables of the impedance analyser were short-circuited and the same was done for the 'reference' and 'counter' terminals of the IM6e. Thales software was used to operate the impedance analyser; to perform a frequency sweep the EIS program was used and here the frequency range and the signal amplitude were chosen. In order to have a reasonable experimental time (1.5 minute), it was chosen to obtain 55 impedance figures. Once the macro-needle was inserted into tissue, bioimpedance was recorded. The same tissue was analysed three times in total

before repeating the frequency sweep for the following tissue type. Pork, lamb and beef tissue samples, sourced from local butchers, were used and tested at two temperatures, 12° C and 37° C. Bioimpedance of muscle, fat and connective tissue was obtained. The reason why nerves could not be included in this preliminary study resided in the fact that these biostructures were reabsorbed in the tissue and disappeared naturally in a few hours after the animal was slaughtered.

Once the operating frequency was determined, it was possible to start monitoring the tissues bioimpedance along the time with the fixed frequency just like it would have happened in a real case scenario. For this, the C/E program on the Thales software was selected. For testing the meat samples it was decided that the data acquisition time frame was one minute with samples taken every two seconds (30 figures).

The results obtained in this preliminary study for the frequency sweep were represented using the Bode plot, while those obtained in the time analysis were represented in graphs where the impedance changes were plotted vs. time.

During each experimental bench test, currents of 10-25nA were applied at frequencies ranging from 100Hz to 1MHz. The bench experiments were conducted in the Life Science Interface laboratories, Tyndall National Institute, Cork, Ireland. Sheep, beef and pig meat samples were warmed to 37°C for the duration of each bench study. Three experimental bench test models were used. Firstly, the needle array was directed by hand using direct vision on sheep, beef and pig meat samples. The needle array was placed within muscle, fat and adjacent to bone. Secondly, the needle array was mounted on a driver and advanced through a block of meat with fat striations. The length of needle advancement through meat was correlated with the surface appearance of muscle or fat using an overlay scale. Impedance data was collected for a range of current amplitudes and frequencies under non-stationary needle conditions at 0.2mm/sec.

Based on what described in the paragraphs reported in the introductive chapter 1, it is indeed possible to identify specific tissues based on the characteristic electrical bioimpedance properties of the biomaterials. Bioimpedance data can provide information on tissue type and needle location. The idea of this project relied on the

design of a bipolar electrode system fabricated on a commercially available needle allowing for invasive impedance measurement only at the needle tip location (where the risk of damaging the nerves is obviously very high). The objective of this approach was to increase the safety of the nerve block procedure and allow for accurate determination of tissue type during real-time needle access in the patient's body. The addition of the bioimpedimetric tissue determination using the "smart needle" to the standard ultrasound imaging technique could be a possible solution to the limitations of USG peripheral nerve block. The feasibility of this technique for distinguishing the different kind of tissue was studied using a bipolar macro-needle-electrode made of two B/Braun Stimuplex A insulated needles, currently used in the clinical setting with the Stimuplex Dig RC and HNS 11/12 nerve stimulators. The two 22G x2" needles encapsulations were bent at 90° and glued together using cyanoacrylate based superglue as shown in figure 5.2. Only the "crown" area of the needle bevel is conductive (figure 5.3). This setup was used to measure impedance of different tissue types in different cuts of meat from different animal (beef, pork and lamb). The needle was connected to the Zahner IM6e impedance analyser (Zahner-elektrik GmbH, Kronach – Germany) for electrical impedance spectroscopy (EIS) to be performed.

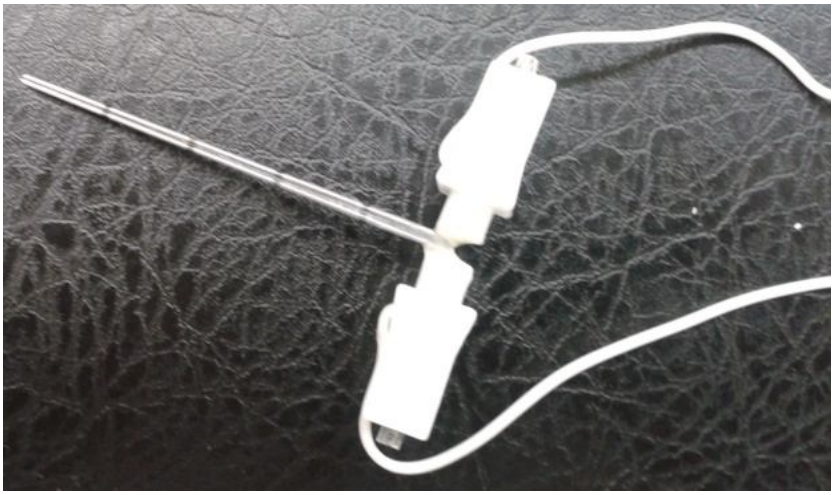

Figure 5.2: Macro needle prototype

Figure 5.3: Schematic of the "macro" needle

5.5 RESULTS

Based on other similar work done previously by Kalvoy and Kinouchi [66, 67] 30 kHz, 50 kHz and 70 kHz frequencies were deemed to be optimal for bioimpedance separation between our chosen types of tissues, so they were selected as the frequencies to be used for further testing. At frequencies above this range (hundreds of kHz or MHz) capacitive phenomena predominated while at lower frequencies (hundreds of Hz) a predominance of resistive effects were observed. Better differentiations of fat tissues were achieved at 70 kHz, while little difference was noticed in the analysis of lean tissue. A range of different signal amplitude between 0.1mV to 0.35mV was also investigated. On the basis of these observations, subsequent experiments were then conducted using 70 kHz and a signal amplitude of 0.3V (Figure 5.4).

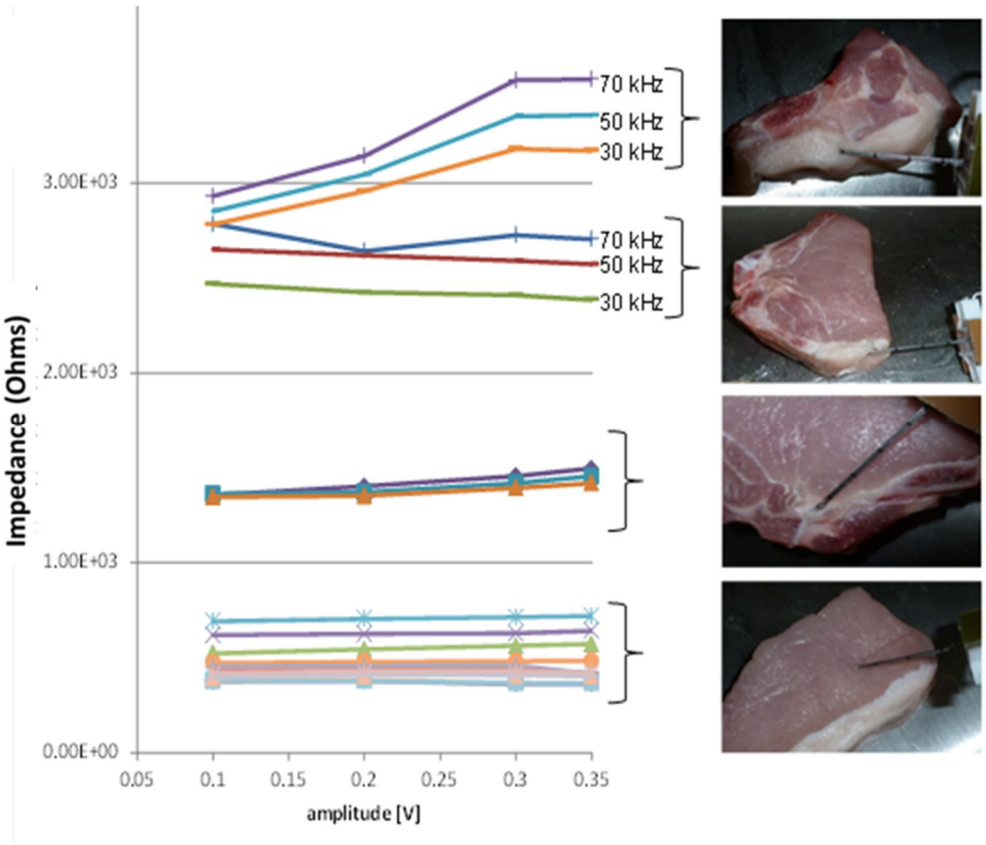

Figure 5.4: Examples of impedance values taken in different parts of meat samples with a change in signal amplitude

A freshly (less than one hour) slaughtered lamb carcass was obtained from a local abattoir. The hind quarters were removed, wrapped and superficially soaked in warmed saline solution (0.9% Sodium Chloride, isotonic solution) and transported to the laboratory. The temperature of the sample was maintained at 37°C. The anterior and posterior thighs of one hind quarter were dissected to reveal the musculature, blood vessels, nerves and bony structures (Figure 5.5). The needle array was advanced by hand using direct vision toward muscle, fat, nerve and bone. Bioimpedance measurements were obtained within the frequency and amplitude ranges previously described.

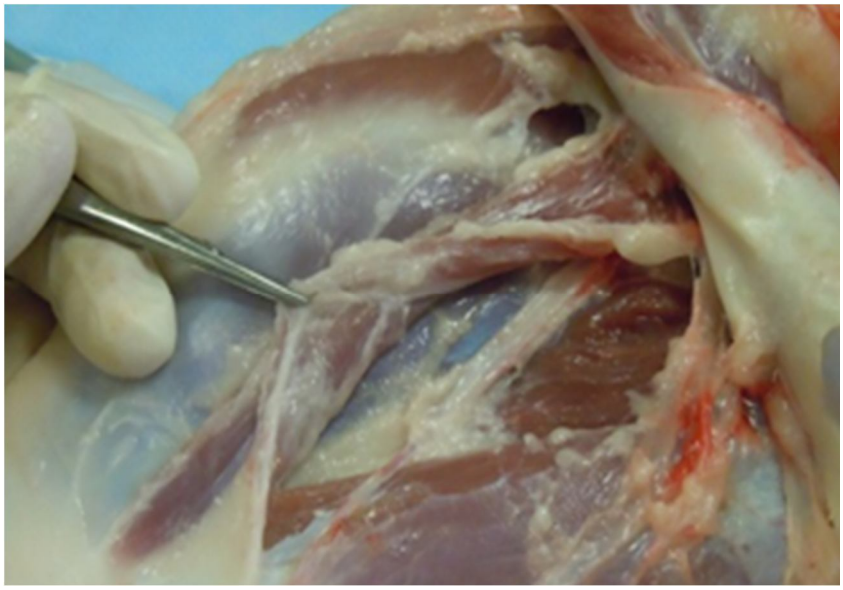

Figure 5.5: Freshly slaughtered lamb carcass, nerve structures still visible

The characteristic impedance figures measured for fat and muscle were significantly different in all samples tested. The greatest difference in tissue impedance between muscle and fat occurred between 30 kHz and 70 kHz. The signal amplitude of the sinusoidal current wave did not show to have any influence on the measured impedance. Greatest discrimination occurred at approximately 70 kHz. For this reason we chose to work with signals at 70 kHz, 0.3V amplitude and with a current variable between 25-40 nA which very clearly differentiated between muscle and fat, and distinguished nerve tissue from other tissues in the experiment on the lamb carcass.

Muscles have a characteristic impedance value that fluctuates between 1 kΩ and 5kΩ, while fat figures usually go well beyond 20-25 kΩ in the refrigerated samples. Bioimpedance values for fat and muscle in the lamb carcass were remarkably lower than those obtained in the refrigerated meat samples (Table 5.2 and 5.3, Figure 5.6).

Table 5.2: Impedance values in Ohm (Ω) recorded on the fresh lamb carcass

Muscle	Fat	Nerve
1317	17024	2830.4
1317.7	17003	3081
1317.9	16991	2937.7
1318.2	17061	2912.3
1318	16972	2894.7
1318.2	16887	2851.1
1318.6	17083	2836.3
1318.1	17065	2887.9
1317.1	17081	2898.3
1317.4	17011	3009.8

Table 5.3: Comparison of the average values in Ohm (Ω) of fresh and refrigerated lamb

	Muscle	Fat
Fresh	1317.82	17017.8
Refrigerated	3110.9	33977.33

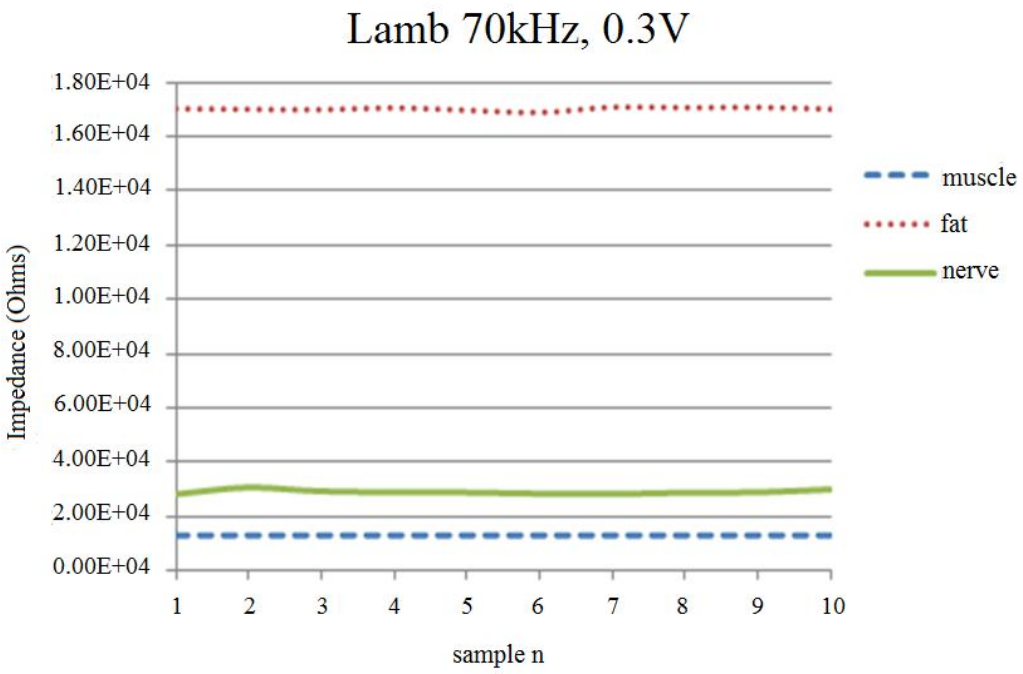

Figure 5.6: Impedance values obtained at a fixed frequency (70 kHz) on a freshly slaughtered lamb carcass (values from Table 5.2)

5.5.1 Frequency analysis

Different tissue types of pork, lamb and beef meat samples were analysed doing frequency sweeps from low to high frequencies. As the frequency increased the bioimpedance decreased showing that fat tissue in all meat samples and in all analyses had consistently higher bioimpedance than muscle. Bioimpedance values between those for fat and muscle were obtained for connective tissue (sometimes labelled in graphs as border tissue), which can be observed between the fat and the lean muscle. The same trend was observed when the frequency sweep was repeated when the meat was kept in an incubator in order to bring the meat at a temperature of 37°C (normal human temperature). The absolute values of bioimpedance for each tissue type recorded at 37°C was lower than those recorded at 12°C; however, the difference between fat and muscle bioimpedances at 37°C was still significant and remained undoubtedly differentiated from each other. An example is shown in the graphs below (figure 5.7) and shows the frequency analysis of pork chops in a frequency sweep at different temperatures. Same

trends with slightly higher values of bioimpedance were recorded measuring lamb and beef samples.

With the results obtained it was established that the biggest gap in bioimpedance value were in the frequency decade included between 10 and 100 kHz. It could be mistakenly thought that the a higher separation could be identified at very low frequency, but this should be avoided as at such low values there is a predominance of resistive effects (as already explained in chapter 1), while at higher frequencies it could be possible to incur in measuring a lot of external noise.

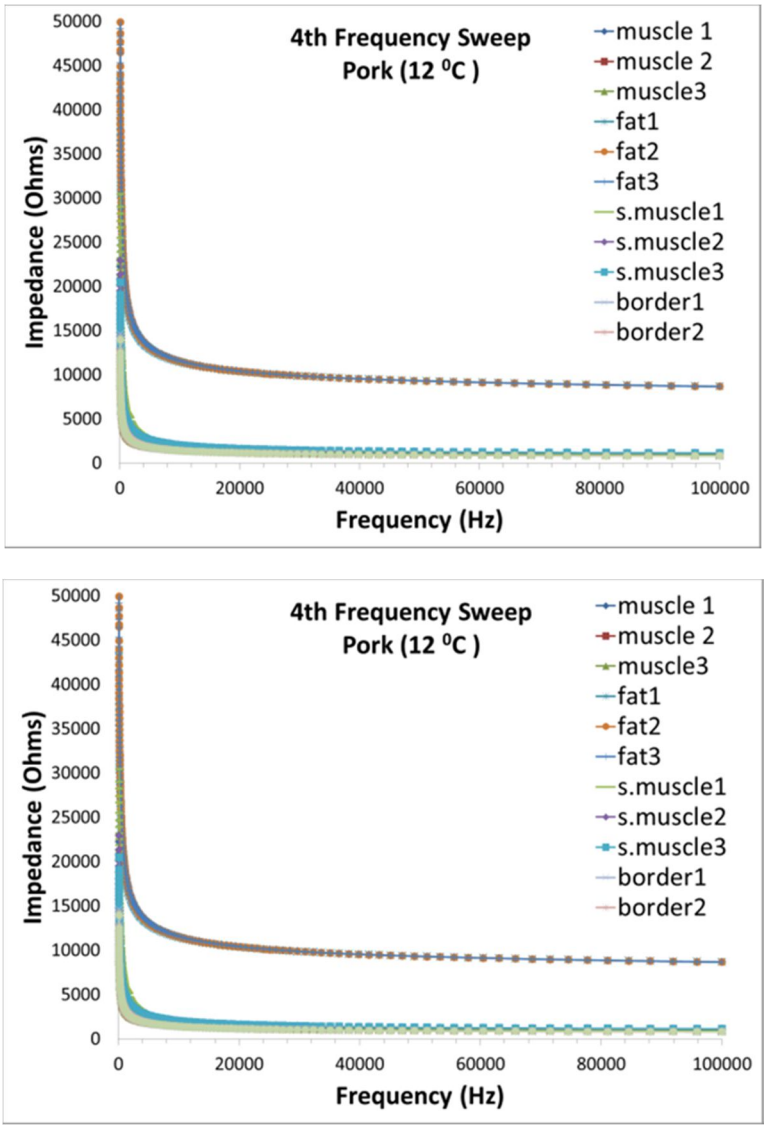

Figure 5.7: Frequency sweep on pork chops at 12°C and 37°C

The average bioimpedance figures obtained at 10, 30, 50 and 70 kHz through the frequency sweeps for each tissue type on each meat were calculated to demonstrate that within this range it was possible to find the optimum frequency for further tissue bioimpedance investigation. The following graphs show a significant bioimpedance separation between different lamb tissue types using this frequency range at different temperatures. The same trend was also obtained for pork and beef meat samples (figure 5.8).

Other examples of frequency sweeps on other meat samples are shown after (figure 5.9 and 5.10).

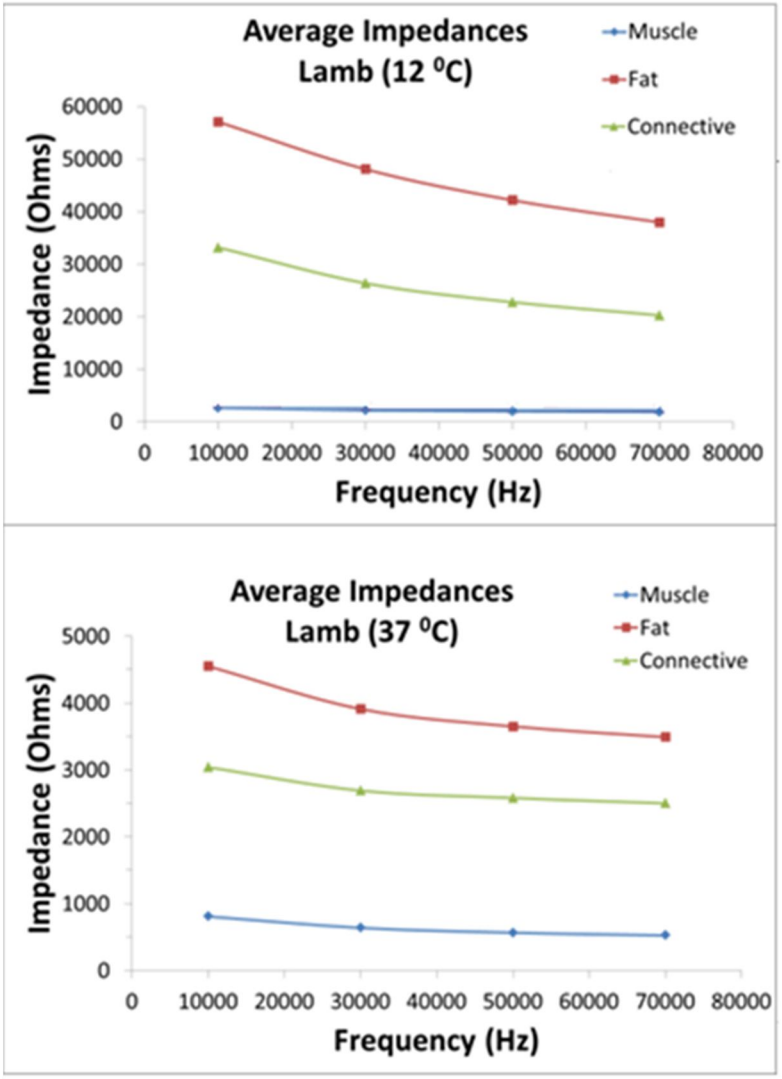

Figure 5.8: impedance values at different frequencies measured on lamb meat samples at 12°C and 37°C

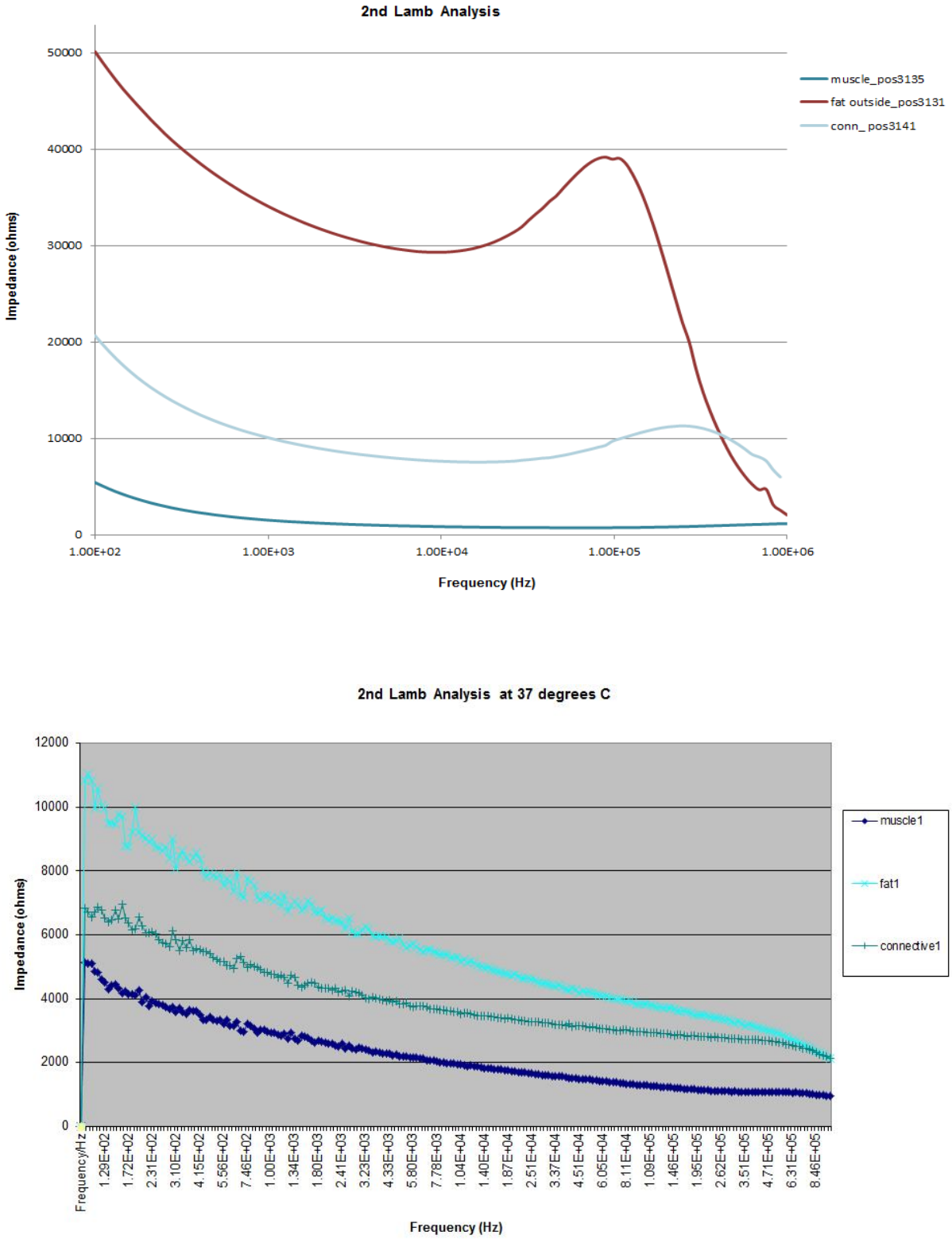

Figure 5.9: frequency sweep on lamb samples at 12°C and 37°C

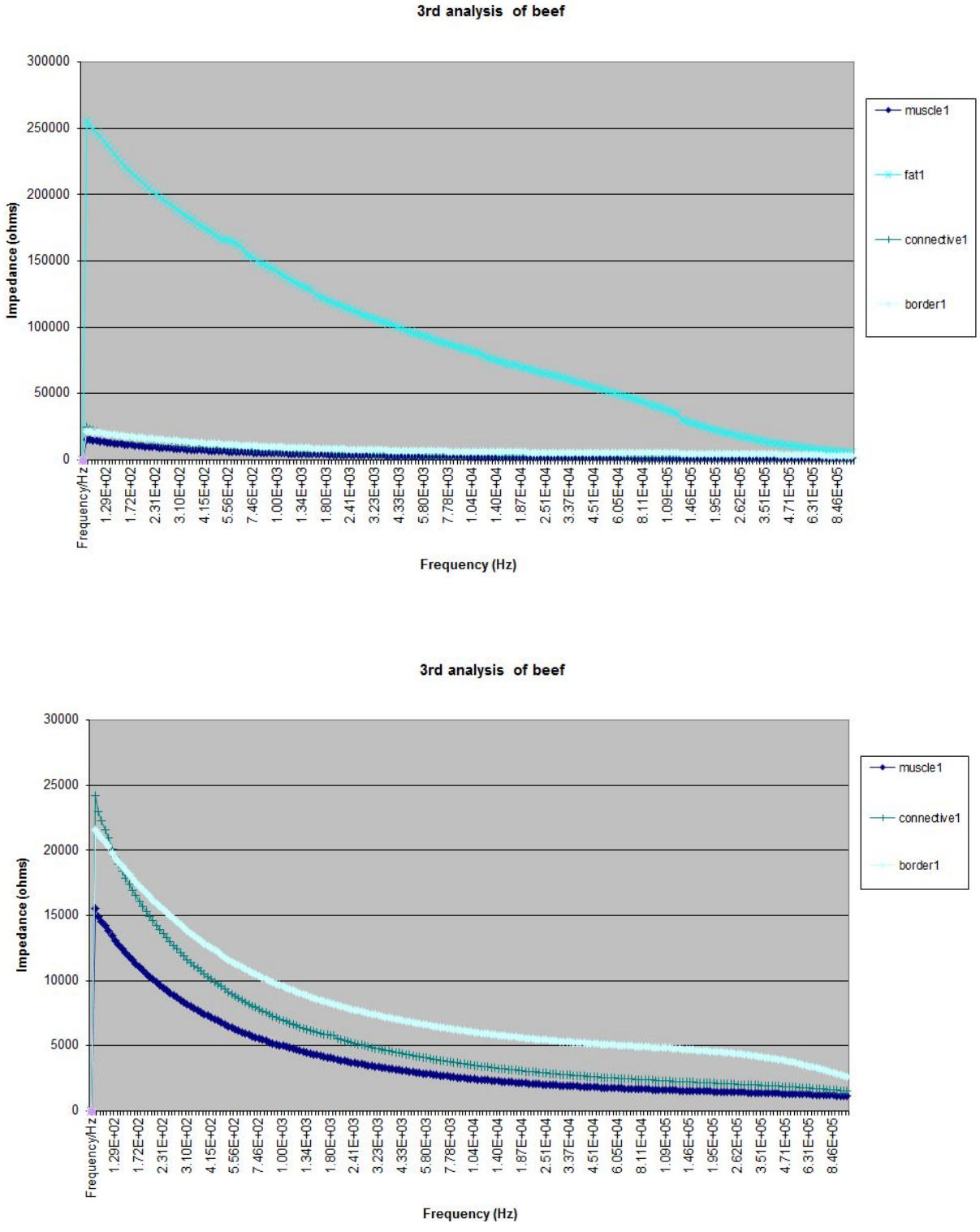

Figure 5.10: frequency sweep on beef samples at 12°C and 37°C

5.5.2 Time Analysis

5.5.2.1 Measurements at 12°C

Bioimpedance of different tissue types measured at 12°C plotted against the set of frequencies decided after the frequency sweeps experiments, revealed to be constant with the exception of some measurements of fat tissues of lamb samples, where bioimpedance values increased slightly over time. Bioimpedance recorded during the time analysis showed marked differences between tissue types. The median bioimpedance value was calculated for each tissue at 30, 50 and 70 kHz and these values (n=5) were used to calculate the average bioimpedance of each tissue type at each frequency. The approximate range for muscle bioimpedance was 203 – 616 Ω, the approximate bioimpedance range for fat was 5.02 - 17.8 kΩ and the approximate range for border tissue was 790 Ω – 1.55 kΩ. The results are illustrated in figure 5.11 are typical results obtained for time analysis of tissue bioimpedance.

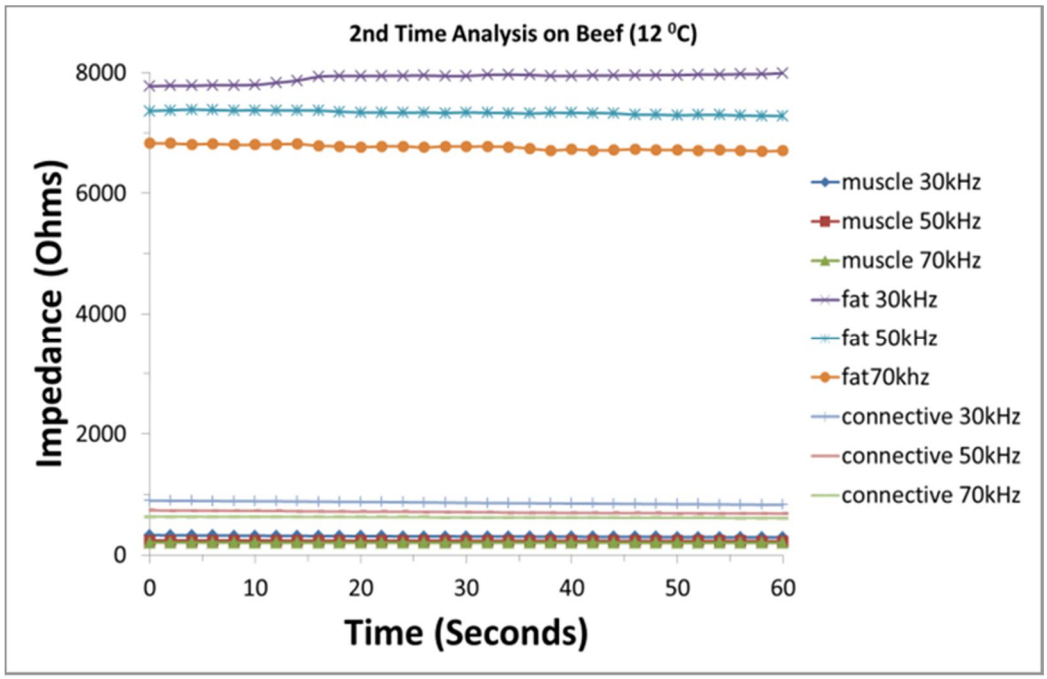

Figure 5.11: time analysis on beef sample at 12°C

5.5.2.2 Measurements at 37°C

When the meat samples were warmed up at 37°C to reproduce a similar case scenario of an in-vivo experiment, the bioimpedance values of different tissue types was found to be significantly reduced. Bioimpedance was plotted against time and the graphs of each repeated experiment showed a constant value (fairly straight line) at 30 kHz. However, when frequencies were increased to 50 and 70 kHz, fluctuations of bioimpedance in fat tissue were clearly observed. Despite these fluctuations of hundreds of Ohms, the separation between tissue types still remained clear (Fig. 5.12, 5.13 and 5.14). The median bioimpedance values were obtained for each tissue at 30, 50 and 70 kHz and these values (n=4) were used to calculate the average bioimpedance of each tissue type at each frequency. The approximate bioimpedance range for muscle, independent of species, was 100-175Ω. The approximate bioimpedance range of fat over the 3 meat types was 627 Ω - 3.2 kΩ and the range for border/connective tissue was 221-540Ω.

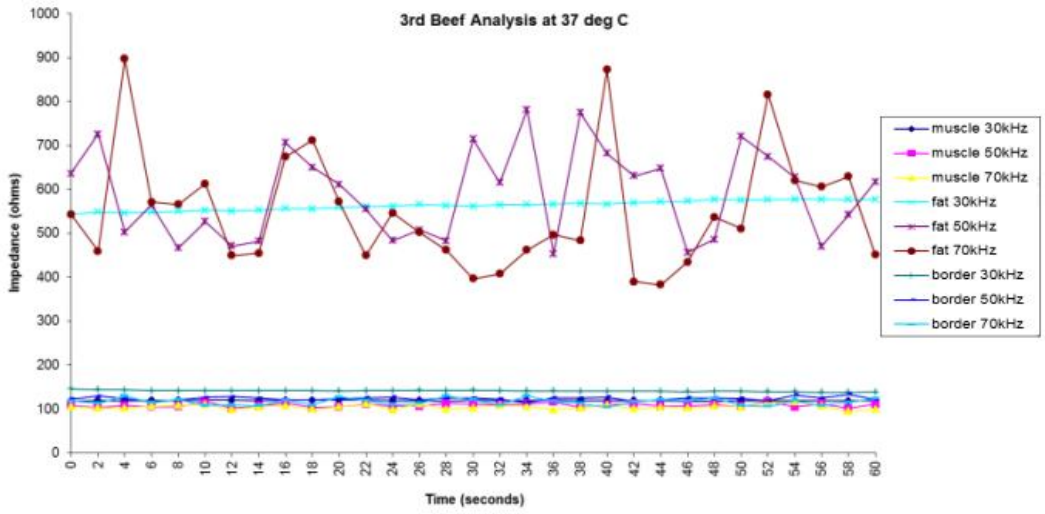

Figure 5.12: time analysis on beef sample at 37°C

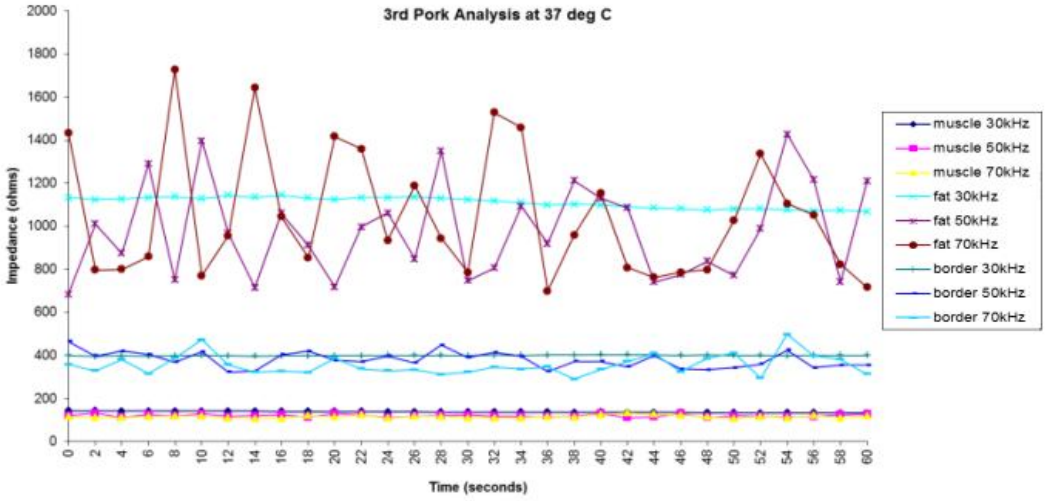

Figure 5.13: time analysis on pork sample at 37°C

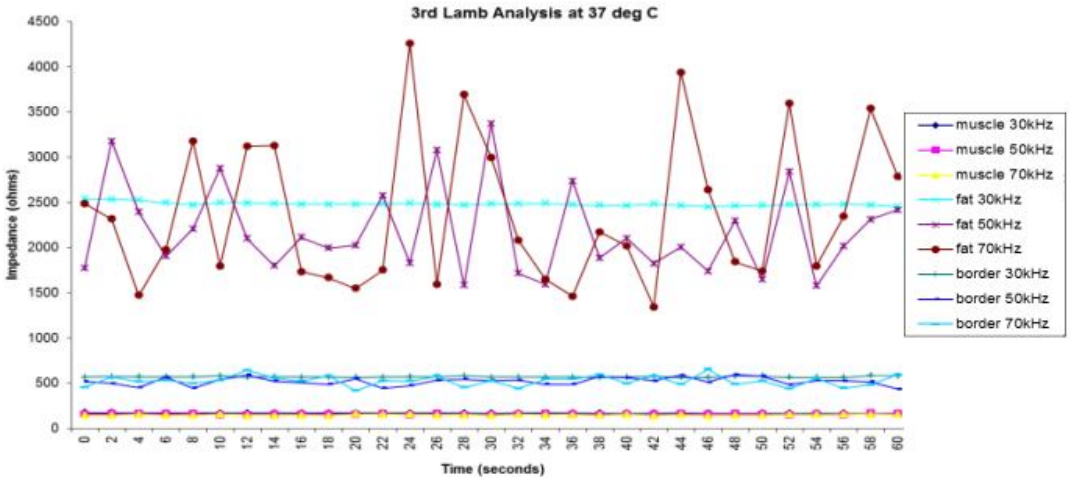

Figure 5.14: time analysis on lamb sample at 37°C

The large data scattering visible in the last three graphs were due to the fact that the meat, kept at 37°C in an oven, was slowly drying out. As described by [68] in these conditions there is an increase in intracellular Ca^{2+} level which likely determined these fluctuations during the impedance measurements.

5.5.3 Signal amplitude

Further tests were also performed to understand if the amplitude of the signal could have in some way changed or influenced the impedance measurements on the meat samples. For this reason bioimpedance values were obtained analysing pork chops at different frequencies of our range and different voltage amplitude, going from 100mV to 350mV. The pictures on the right show where the needle was inserted (figure 5.15 and 5.16).

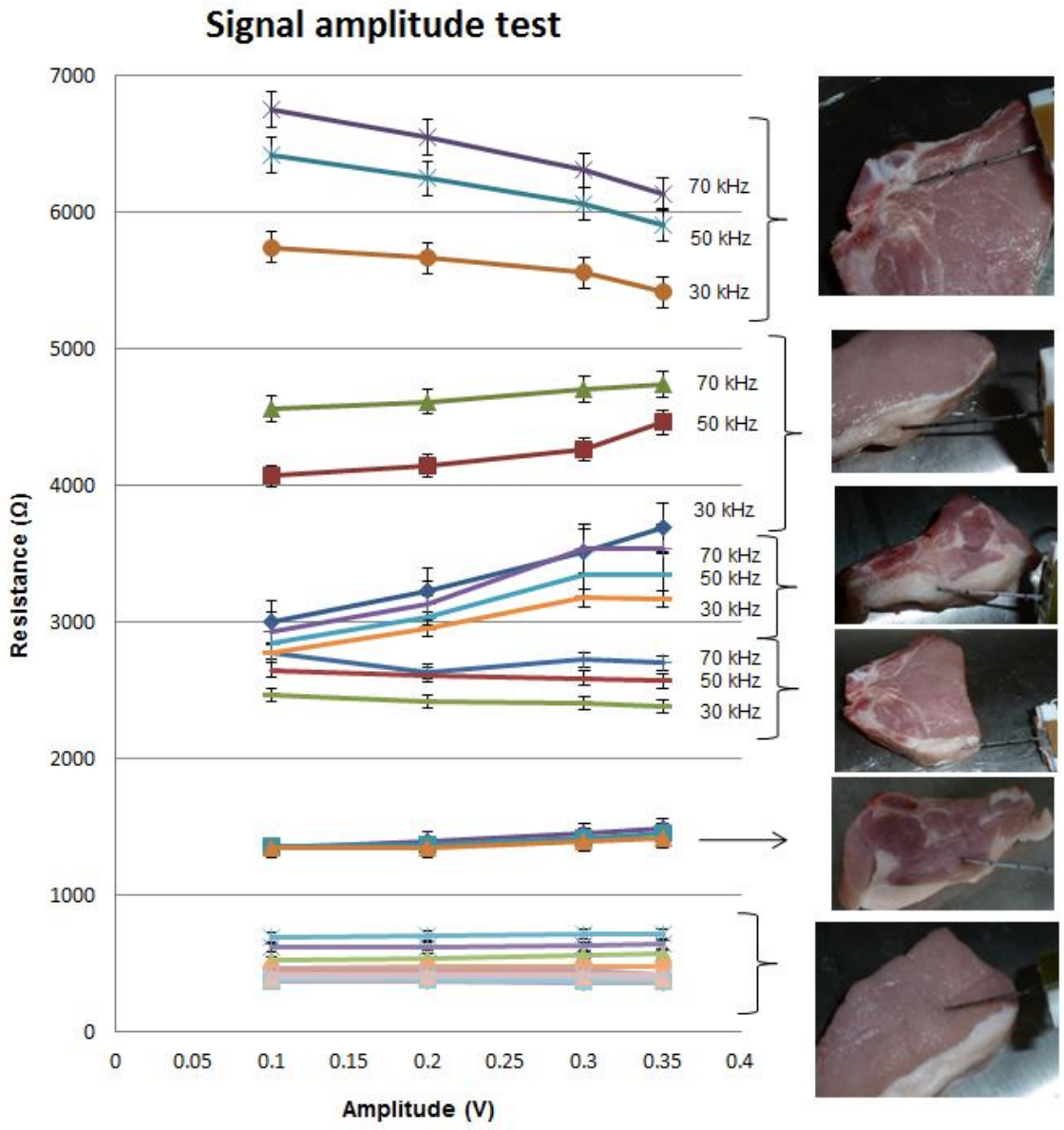

Figure 5.15: Impedance values measured in different kinds of tissues varying the signal amplitude

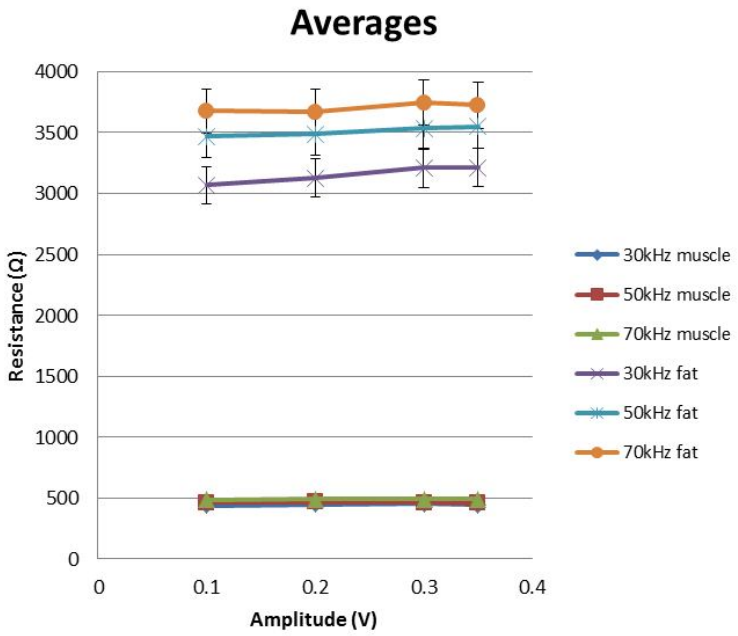

Figure 5.16: Measurements on muscle and fat varying the signal amplitude

Following these results and other obtained on the lamb and beef samples, it was decided that the variation of the signal amplitude did not have a marked effect on the results and there was no direct link with the frequency used in the experiment. For this reason all the experiments were then done at 100mV like those showed previously as the default amplitude value on the Zahner IM6e was used.

5.5.4 Steady movement through sample

Experiments with the needle going through the meat samples at a specific speed have also been performed with the aid of a syringe pump (KD scientific S200 Syringe pump) pushing the needle through a sample of bacon, trying to replicate a real case scenario where the clinician passes the needle subcutaneously through the tissues to the target location (figure 5.17). The meat was warmed up at 37°C and located in a transparent box (65L x 45W x 10H mm) with a hole to allow the passage of the needles from the shorter side. The impedance values were measured at a frequency of 70 kHz and amplitude of 0.1 V. Impedance data were acquired every second. The constant speed of the needle was set at 0.2 mm/sec; the depth of the needle was visualized thanks to a cm-

scale drawn on the top of the box giving information about its position in the meat (figure 5.18).

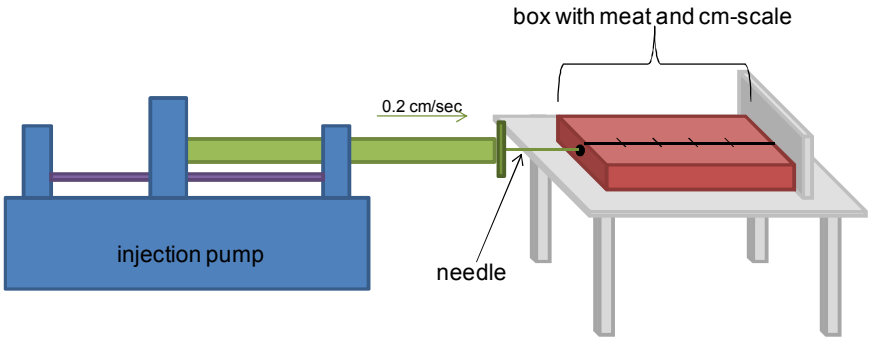

Figure 5.17: Setup of bioimpedance measurements using the syringe pump

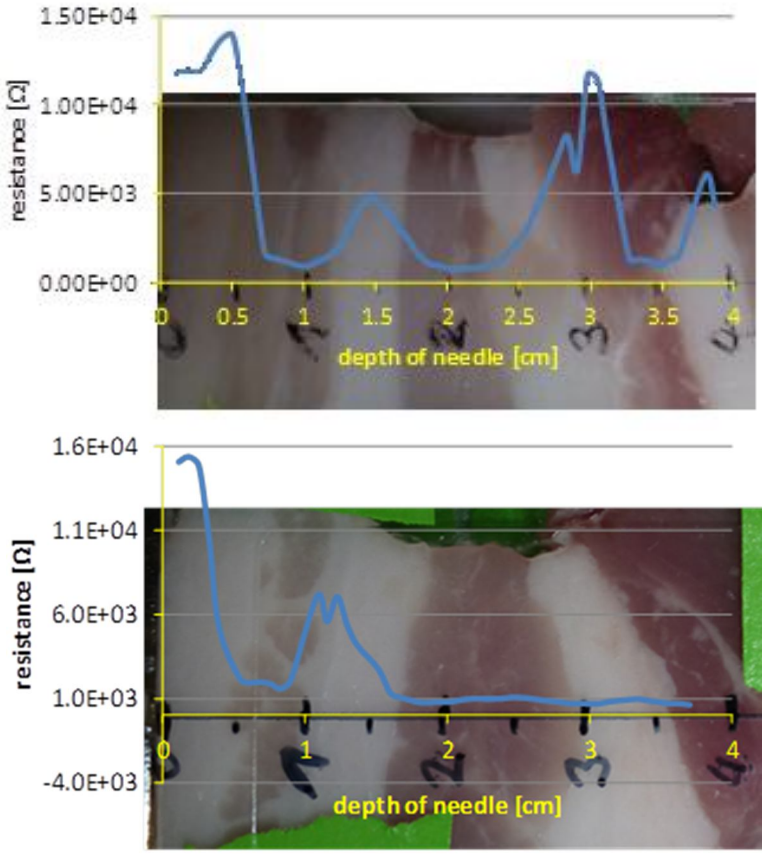

Figure 5.18: Resistance is changing while the needle is moving through the meat.

These figures showed that the resistance value changed while the needle went through the meat sample. The peaks shown in the graphs represented the number of layers of fat tissue in the bacon. However, these peaks appeared always a little later than expected according to the pictures. This happened because the needle compressed the raw meat on its way through the meat sample even if it was stored in a box which restricted its displacement on each side.

Often the different layers of tissue in a piece of bacon were not strictly parallel to each other. A meat sample with a cross-section like the one shown in the following figure (figure 5.19) may lead to a graph where the peaks can be shifted, along the time axis, and differ from what it would be expected to observe by seeing the surface of the sample itself.

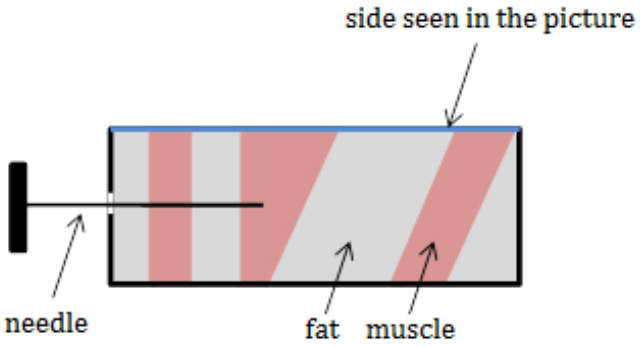

Figure 5.19: Layers of fat in the meat samples.

Also this set of experiment suggested that it would be feasible to use a needle to detect different kind of tissues and be applied as a sensor for peripheral nerve block procedures.

5.6 SENSOR FABRICATION ON THE NEEDLE

Miniaturisation of the two-electrode system was necessary in order to progress from the macro prototype made of two needles glued together to the actual 'smart' needle. The first objective, after confirming the feasibility of this concept, was to fabricate a two-pad impedance sensor onto a commercially available needle currently used by anaesthetists during standard procedures. The collaboration with Cork University Hospital (CUH) and consultant anaesthetist Dr Brian O'Donnell on this project, under the supervision of Prof George Shorten, provided access to an expert's opinion on which type of needle should be used as a substrate for the electrode fabrication to create the 'smart' needle. First of all, it was very important to use a needle familiar to the professionals in this area as PNB is a highly manual procedure requiring years of training and practice to become competent. Dr O'Donnell recommended two commercially available B Braun (B. Braun Melsungen AG, 34209 Melsungen, Germany) needles: Spinocan and Stimuplex A, which are currently used by anaesthetists in CUH.

The Spinocan needle was selected as it is a bare medical grade stainless steel, 22G (0.7mm diameter), 40mm long, needle; the fact that this needle is not coated with any insulation let a lot of space for experimenting with many different kind of materials, for both insulation and electrode fabrication. It is conventionally used for spinal anaesthesia; however it is not necessarily used for PNB. The Stimuplex A needle is, instead, an insulated needle with a conductive tip commonly used with a nerve stimulator and it is used for performing PNB by most anaesthetists in CUH. The Stimuplex A needle has similar dimensions to the Spinocan needle, 22G and 50mm long, however since the composition of the polymeric material insulating the needle is not completely known, some fabrication processes may be limited. For this reason the Spinocan needle was selected for the initial fabrication tests of the 'smart' needle. Other tests can be eventually conducted later on the Stimuplex A needle to see what kind of fabrication technique may be suitable on such substrate.

5.6.1 Photolithography

Photolithography is a process used in microfabrication to pattern specific layouts on a thin film material or directly on a substrate and it has been discussed in details in the first chapter of this thesis. Photolithography can print detailed features down to the nanometre scale, can be highly controlled and can print patterns over a large surface area in a cost-effective way. For these reasons this process was chosen to print electrodes directly onto a needle. As the aim of this project is to integrate the impedance sensor onto a commercially available needle, the substrate for the photolithography process was obviously not flat but round. This meant that a specific holder which could embed the needles had to be fabricated to ensure the needle surface was as flat as possible and flush with the holder surface.

Since the Spinocan needle was made of conductive stainless steel it had to be insulated in order to avoid the electrical continuity with the gold deposited to fabricate the impedance electrode onto its surface. For this reason the needle was coated with a 1µm layer of Silicon Nitride to prevent a short circuit between the electrodes and the needle surface. Photolithography was then used to pattern two gold tracks with pads at either end onto the needle to act as a two electrode system (as shown in fig. 5.20). A second passivation layer was then deposited over the electrodes tracks leaving only the pads at the tip and the top of the needle electrically conductive. The two smaller pads at the tip of the needle work as the actual impedance sensor while the bigger pads at the distal end of the needle allow wire bonding for connection to an impedance analyser and signal transmittance for processing.

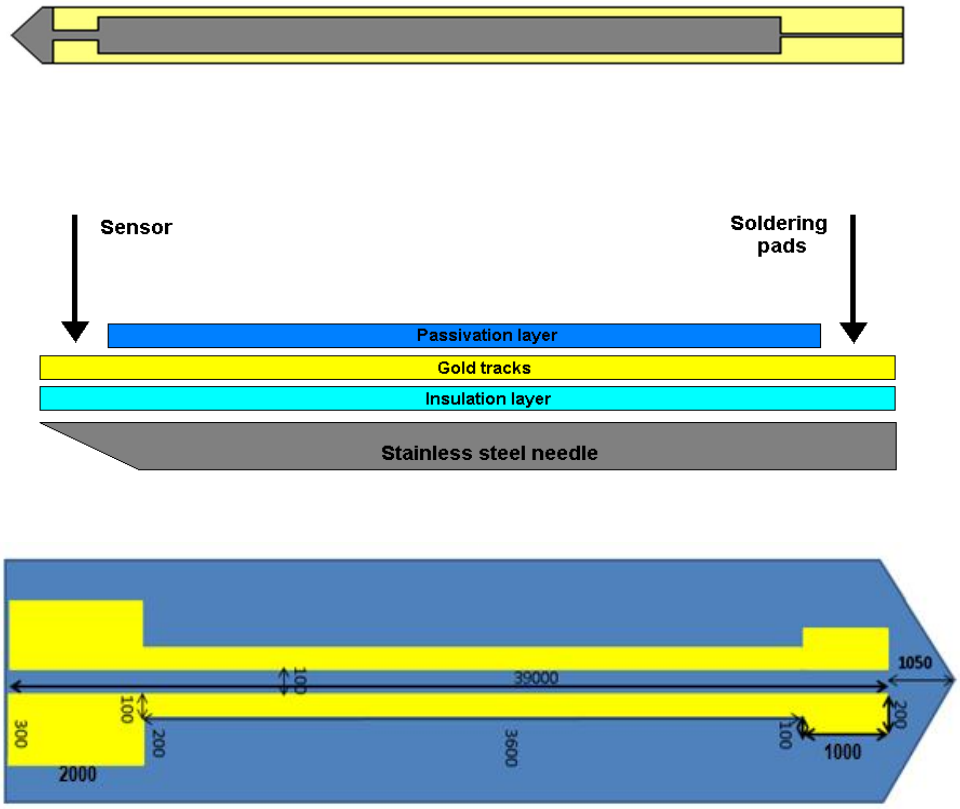

Figure 5.20: General schematic of the sensor fabricated on the needle with photolithography process and sensor dimensions (microns)

As mentioned above, a specific holder had to be fabricated to make the photolithography step. A standard 4 inches silicon wafer was etched to create grooves for the needles to be slotted in and kept in position. The substrate was then covered with 500nm of Si_3N_4 in a STS PECVD system. The wafers were patterned with Shipley S1813 photoresist and etched using Si_3N_4 in a STS ICP etch system. A mask was fabricated with the design of grooves where the needles would be allocated in (figure 5.21) and those parts were etched to a depth of ~350 um with KOH etchant to make grooves to fit unpackaged Spinocan needles.

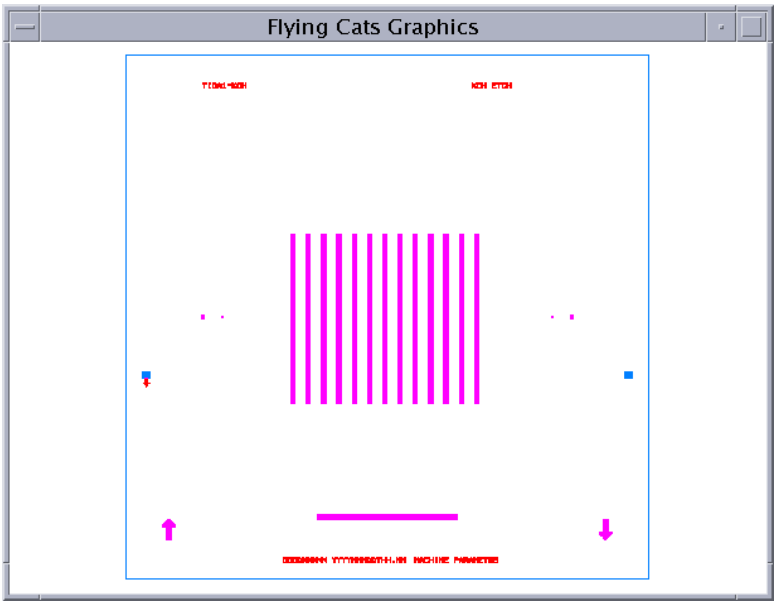

Figure 5.21: Mask with the design of grooves wHere the needles would be allocated in

The needles placed in the etched grooves were then coated with 1um of electrical dielectric, Si_3N_4, as above, using the STS PECVD system. The needles were rotated of 180° in the holder and again 1um of Si_3N_4 was deposited on the opposite side of the needles to make sure that the whole needle surface had been insulated.

To ensure that the needles would not get out of their place during the resist spinning, the empty needle holder was covered with a thick photoresist (MicroChem AZ9260). The insulated needles were subsequently placed into the grooves while the above mentioned photoresist was not completely cured so that it acted as an adhesive keeping the needles in place during the process. The needle filled wafer was thereafter baked in a convection oven at 90^{o}C for 3 hours to cure the photoresist.

The wafers with the needles in situ were coated with a layer of MicroChem PMGI SF11 lift-off resist and a layer of Shipley S1828 photoresist (among the many different resists and resist combinations tried in the fabrication facility in Tyndall, this one gave the best results). The needles were then exposed to the specifically designed electrode mask in a Karl Suss MA1006 mask aligner and developed in Microposit MF319 developer (figure 5.22).

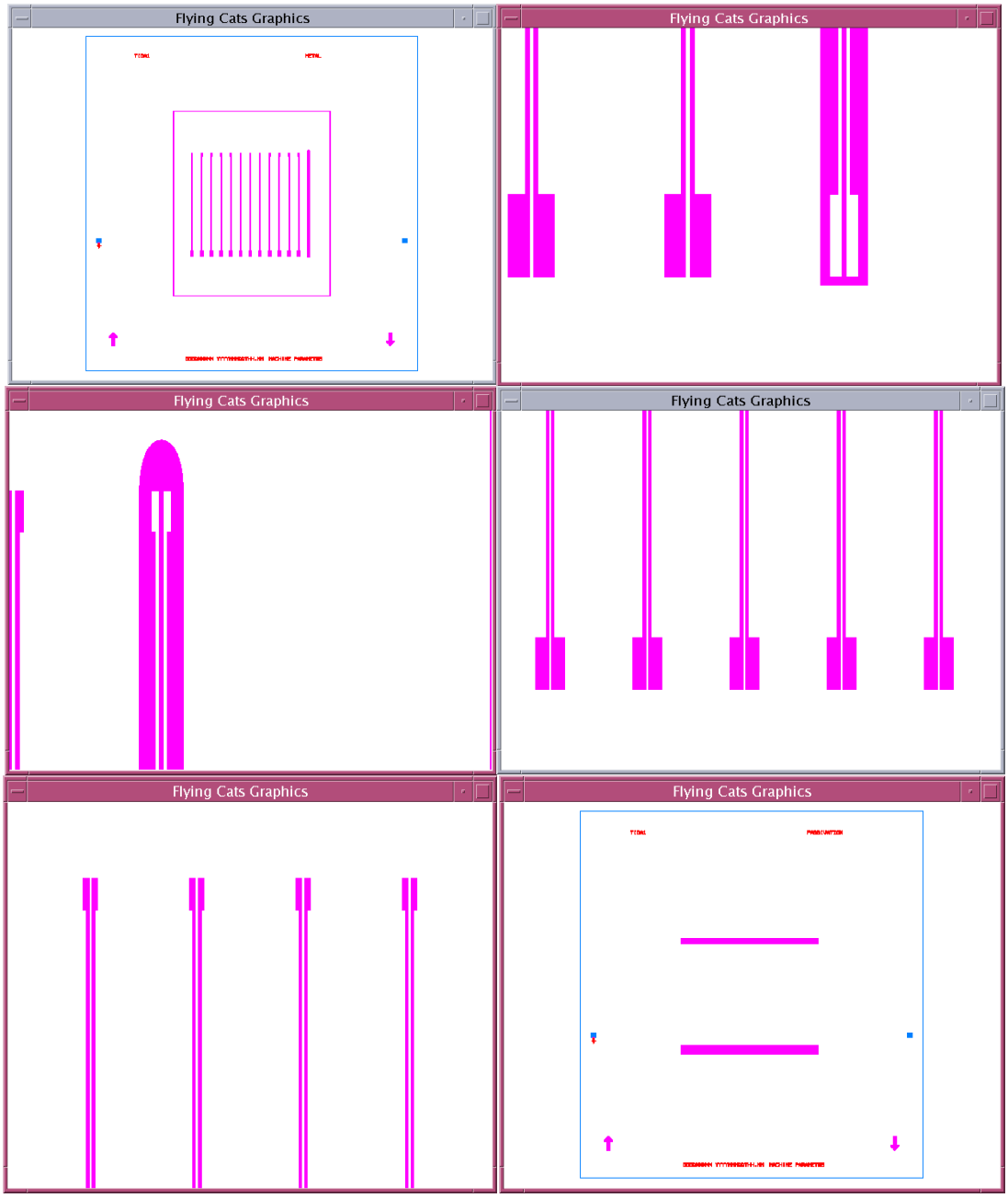

Figure 5.22: Snapshots of the mask designed for the photolithographic fabrication of the sensor on the needle

The electrode metal (Ti:Au, 20:200nm) was deposited onto the needles in a Temescal FC2000 e-beam evaporation system. The excess metal was "lifted-off" in Microposit R1165 resist stripper, which also removed the AZ9260 photoresist "glue" from the

wafers, allowing the needles with the electrode metal in place to be removed from the holders.

A 500nm passivation layer of Si_3N_4 was subsequently deposited onto the needles using the same method described for the needles insulation. The needles were again fixed in place in the etched Si wafers using the method described above and were patterned using Shipley S1828 photoresist to define contact openings in the Si_3N_4 passivation at both ends of the needles. The contact openings were etched in the Si_3N_4 using the STS ICP system. The remaining photoresist was removed in Microposit R1165 resist stripper which again also removed the photoresist "glue", allowing the needles to be removed from their Si carriers.

After the fabrication, an inspection under an optical microscope the needles was carried out revealing that the needles have discontinuous gold tracks and the gold was flaking off some needles (Figure 5.23 A-C).

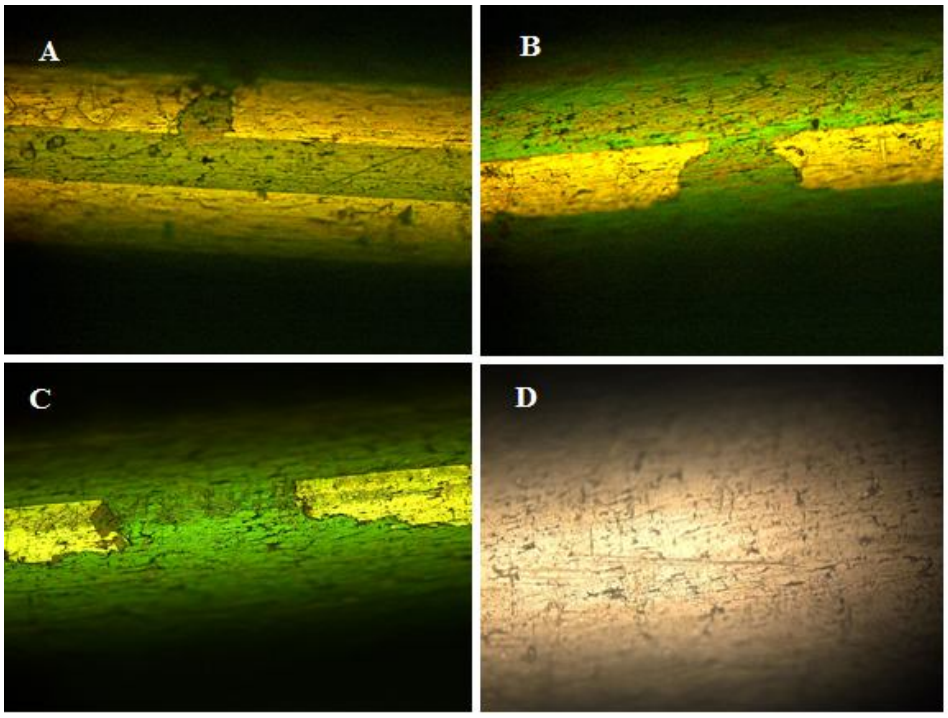

Figure 5.23: Gold electrodes on Spinocan needles post fabrication using photolithography. The top two images show the pads at the tip (A) and the top (B) of the needle, a discontinuous gold track can be seen in image C. Image D is a Spinocan needle as it comes from the manufacturer, under light microscope (objective x20).

During the optical inspection, it was noticed that the needles had a very rough surface (Figure 5.23 D). Subsequently the needles were analysed at the scanning electron microscope (SEM). Images can be seen below (figure 5.24).

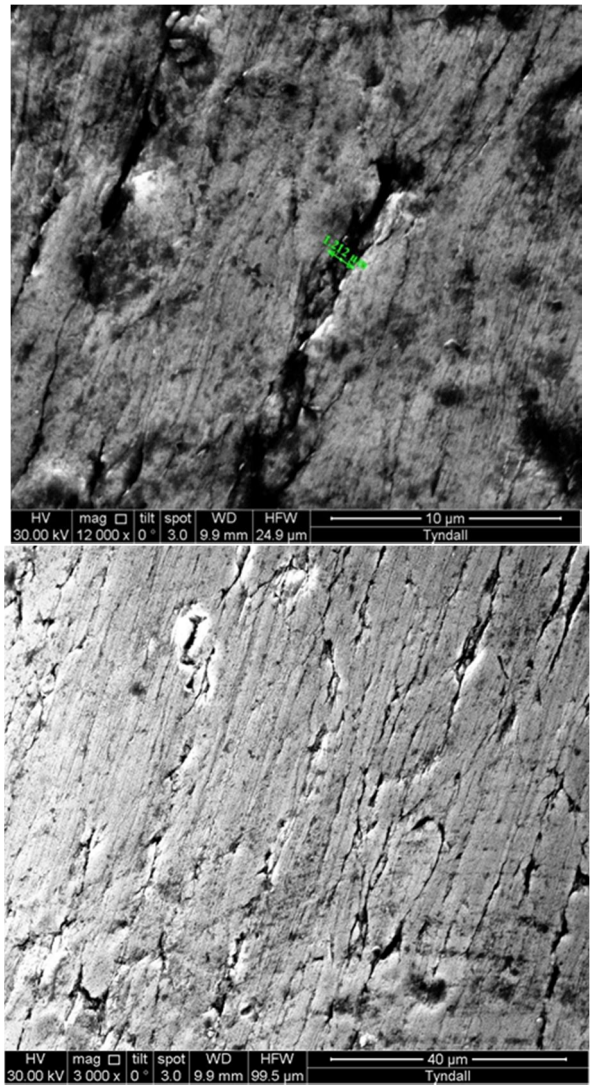

Figure 5.24: SEM images of bare needles

Electropolishing was identified as a possible pre-fabrication step based on the results achieved to try to have a smoother surface to work on. Electropolishing was first carried out by an external company, but since the costs were too high it was decided to setup a

system here at the Tyndall National Institute. The electrode fabrication was then repeated as described above with the electropolished needles. Fabrication of the electrodes onto these smoother surface needles appeared to be successful with continuous gold tracks seen on the needles using an optical microscope but unfortunately, post-packaging they resulted to be short circuiting with the needle body. Further fabrication runs using electropolished needles were performed; however after viewing them under the optical microscope the tracks revealed to be discontinuous and flaky just like the very first attempts done without a smooth surface (figure 5.23). The previous fabrication run was not reproducible and so other methods of fabricating gold electrodes onto a needle were investigated. In light of these results, it was concluded that photolithography was not a suitable fabrication method for the impedance gold electrodes on top of the needle tip; for this reason it was decided to look for other fabrication methods.

5.6.2 Laser Machining

Collaboration was on going with Professor Dermot Brabazon in Dublin City University for laser-machined microfluidic chips and for this reason it was decided to try to get the impedance electrode fabricated with the aid of a laser fabrication method. The principle was very simple: coating the needle with a passivation layer in the same way as it would have been done for the photolithography, coating then a 180° portion of the insulated needle through gold evaporation and then draw a line in the middle with the laser beam, separating, through ablation, two long rectangles which would have represented the two pads of the impedance electrode. Unfortunately several issues were found going through this method. The first was the lack of a suitable needle holder; in fact the needle could not be kept in the exact same place for the duration of the ablation process and the vibration of the machine caused it to rotate producing then a spiral around the needle instead of a straight line. The alignment of the laser also resulted to be problematic for the technician in DCU as the beam was partially reflected on the gold layer. The biggest issue however resided in the fact that the laser carried too much power during the ablation causing then the complete evaporation of the insulating layer underneath the evaporated gold and hence leading to a short circuit with the needle body.

5.6.3 Shadow masking

A few systems for the shadow masking technique were designed as this could be a potential solution for the fabrication issues. This technique, also called Niemeyer-Dolan technique or shadow evaporation technique, is a thin-film lithographic method to create nanometer-sized overlapping structures.

This technique uses an evaporation mask that is suspended above the substrate. The evaporation mask can be formed from two layers of resist. Depending on the evaporation angle, the shadow image of the mask is projected onto different positions on the substrate. By carefully choosing the angle for each material to be deposited, adjacent openings in the mask can be projected on the same spot, creating an overlay of two thin films with a well-defined geometry. One of the earliest devices fabricated for this project is the one represented in the picture below (figure 5.25):

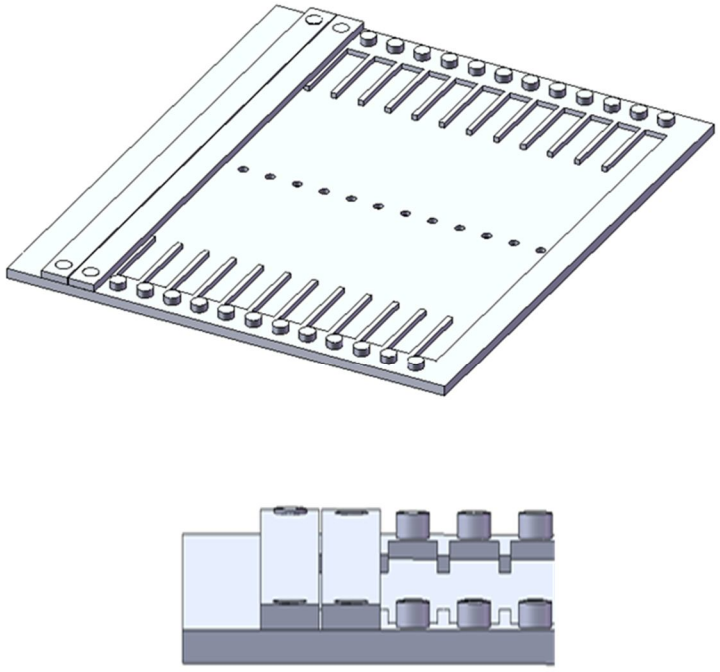

Figure 5.25: First generation shadow masking holder

The needles were slotted in the gaps created with the bars that fit in the holder; in this way only the desired portion of the needle was exposed to the gold deposition. Then an additional bar was applied on top of the assembly in order to mask a smaller portion of the same needle creating then a single rectangle of 100µm x 40mm. To create a second rectangle it would have been necessary to remove the needle for the slot, rotate it and repeat the same step again.

The fact that the needle had to be manually removed and placed again in the slot was one of the first issues that led to the failure of this method as there were too many chances to occur in manual handling errors. Another problem was due to the fact that the increased temperature inside of the machine for the fabrication caused a deformation of the thin metallic bars that held the needles precisely in place. The bars made the needles pop out leading to parts dispersed everywhere in the lab; also the fact that the bars had to be removable and not fixed caused them to literally fly away during processes that required the spinning of the holder.

So it was decided to change slightly approach by changing evaporating machine. This has the evaporation source placed on the lower part of the chamber with the evaporated material going towards the upper part of the evaporation chamber. A new shadow mask system was then designed following the requests of the lab technician. One base was designed to hold the needles in place and attached to the top of the evaporating chamber through one central screw (figure 5.26). The needles would remain attached to the base using the same idea of the photoresist working as glue. Then the mask was superimposed to the base and aligned with a system of four screws (figure 5.27). This mask had gaps of 200µm which would define the width of the gold tracks constituting the impedance electrodes. In order to make two of these tracks it was necessary just to flip the mask along one axis and realign with base as the mask gaps have been drawn to correspond to one external edge of the needle slot. In this way the two impedance electrodes should be spaced by a 300µm gap (as the needle diameter is 700µm) (figure 5.28).

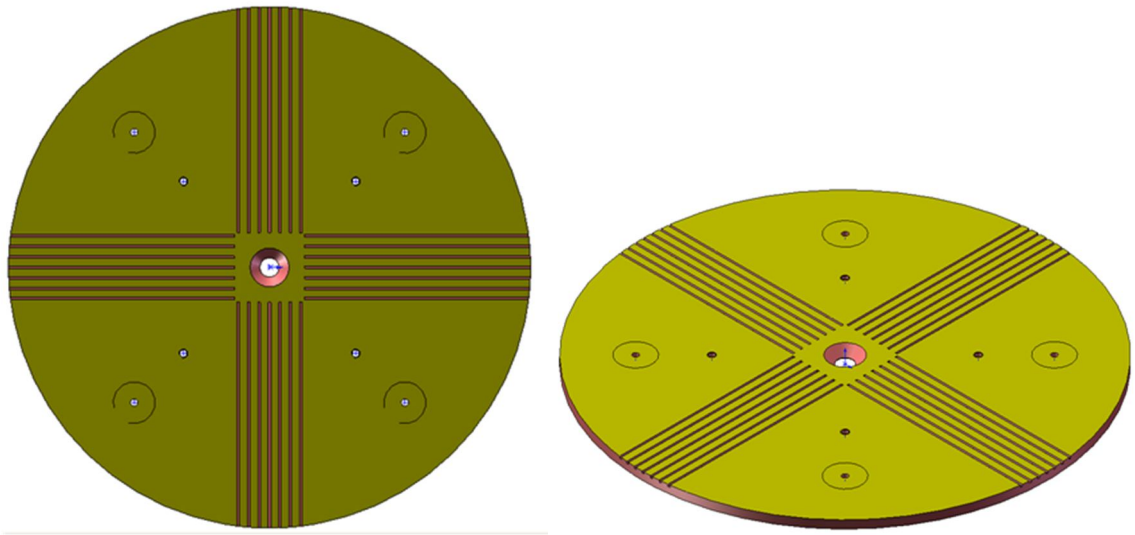

Figure 5.26: Base for shadow masking

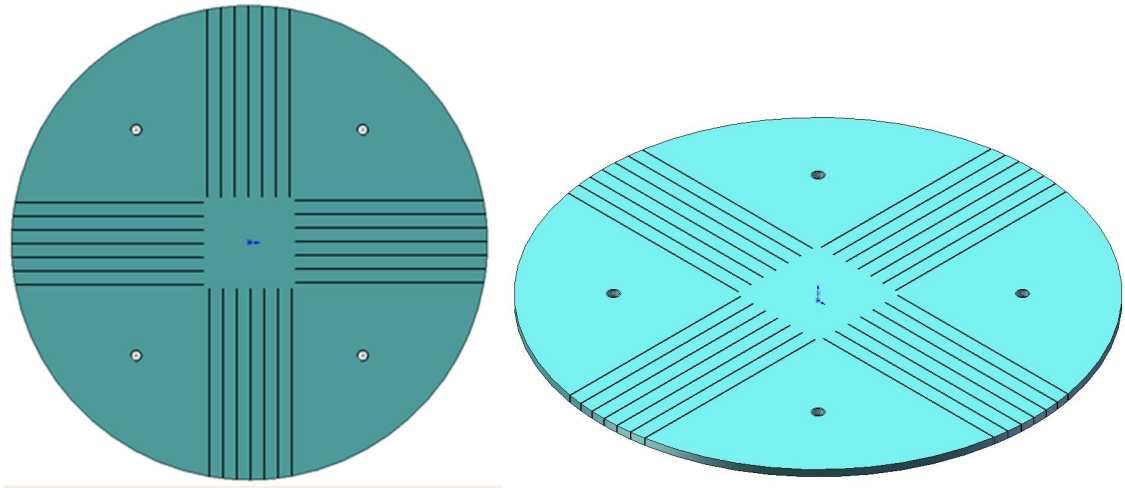

Figure 5.27: Mask used with the base in figure 5.26 for shadow masking

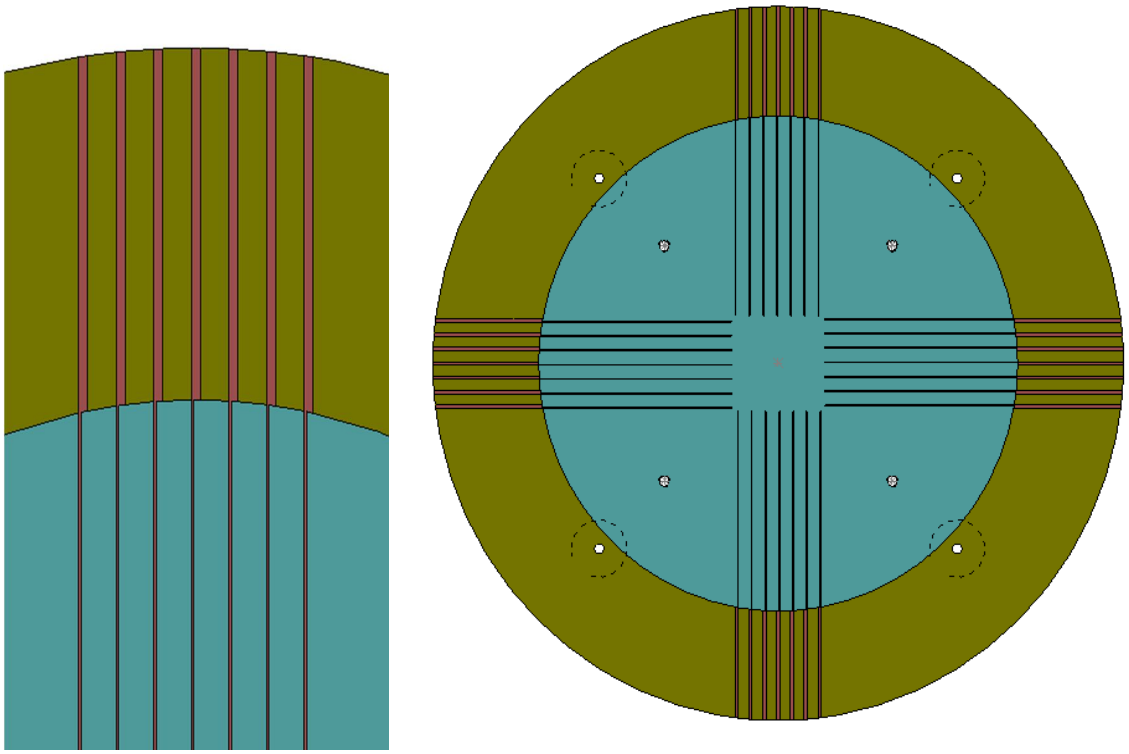

Figure 5.28: Mask superimposed on the base for shadow masking technique

The first attempts with this approach however did not lead to the expected results as the evaporated gold did not pass through the 200µm gaps of the mask, leaving the needle unfortunately blank.

So a modification to the masking technique was carried out by using a new mask (figure 5.29). With this method, nylon wires of a diameter of 250 µm (similar to those used for fishing rods) will be tightened into the grooves fabricated at the sides of the mask and kept in tight contact with the needle to mask its central part while gold will be evaporated on each side of the exposed portion of the needle (figure 5.30). At the moment the mask fabrication is still in progress in the workshop at Tyndall.

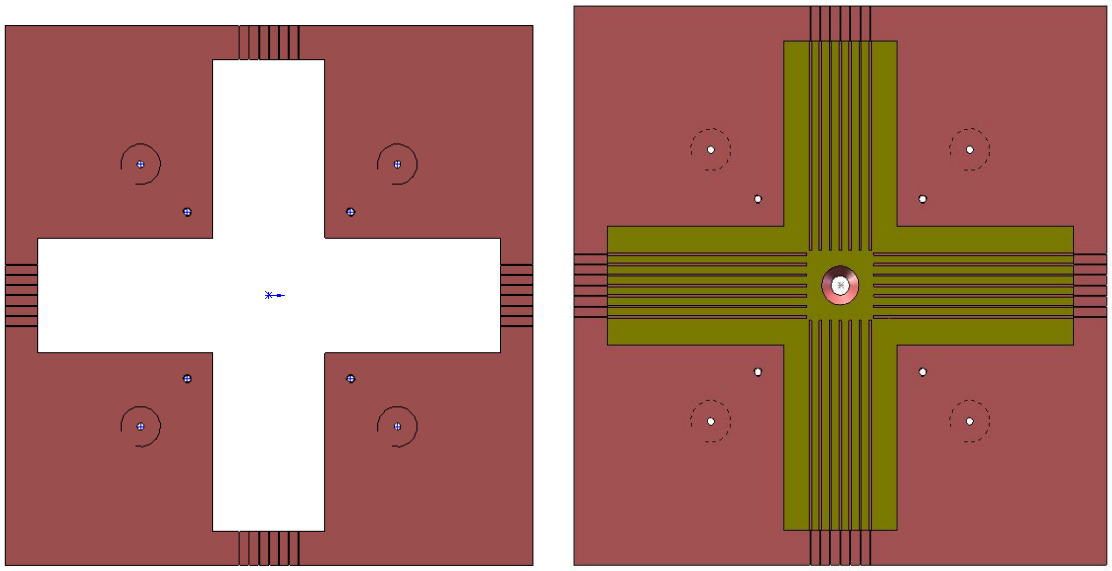

Figure 5.29: on the left is the new design of the mask, while on the right is a schematic of the mask on the base. The wires attached onto the mask will mask the evaporated gold creating the central gap of 250 µm

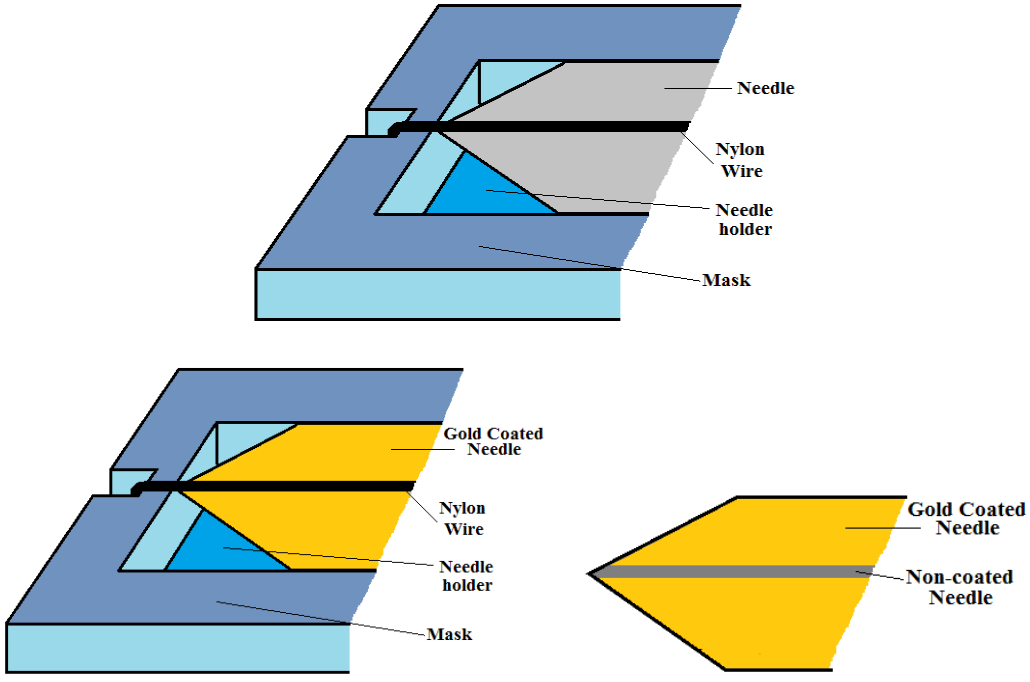

Figure 5.30: Shadow masking method combining a nylon wire with the mask

5.7 DISCUSSION

After reviewing the literature in relation to the peripheral nerve block technique, it is evident that both ENS and USG cover almost the entire range of methods used for this kind of procedure. It is also undeniable that these procedures are very safe and their rate of failure is quite low [4] and the potential injuries caused to the patients are usually minimal or can often be reversible. However, the smart needle project aims to further reduce the limitations of the previous techniques giving the clinicians an additional tool for correctly performing the peripheral nerve block procedure. Using the needle as a precision instrument and guidance tool may provide additional information as to the needle tip location and enhance safety in regional anaesthesia. Bioimpedance, as measured at the needle tip, provides additional information on needle tip location, thereby facilitating detection of intraneural needle placement.

These preliminary studies demonstrated the utility of bioimpedance measurement for tissue type identification and presented the optimum discriminatory frequency range which can be used to reliably differentiate between muscle, nerve and fat [66, 69, 70]. The evolution of ultrasound guided PNB must utilize available technology to overcome its current limitations.

The most reasonable explanation for the difference in values between fresh and refrigerated samples was that the lamb carcass, at the time of the experiment, was still warm and still rich of physiological fluid (blood, water, etc.). Unfortunately the nerve structures in the freshly slaughtered sample were reabsorbed and disappeared very quickly. For this reason multiple nerve bioimpedance measurements were unobtainable. The observation that bioimpedance values of the nerve tissue are quite different from muscle was still made but ultimately a significantly more in-depth study is still required to accurately determine the impedance characteristics of neural tissue. However, this study provided useful information to prove such a study is feasible.

The tests carried out with the macro needle showed that it is feasible to use an impedance electrode fabricated on the needle tip to differentiate several tissues from the

nerve tissue. In our preliminary studies to apply the use of bioimpedance in the field of anaesthesia and more specifically to ultrasound guided peripheral nerve block, we were able to distinguish, using meat samples, muscle, fat, bone, connective tissues and eventually nerve tissue [71].

The absolute values of bioimpedance for each tissue type recorded at 37°C were lower than those recorded at 12°C (one order of magnitude). However, the differences between fat and muscle bioimpedances at 37°C were still significant and remained clearly differentiated from each other. In the frequency analysis of pork, lamb and beef samples at different temperatures the same trends of values of bioimpedance were recorded during the measurements.

In the time analysis, with the frequency fixed at 10kHz and the samples kept at 12°C, the approximate range for muscle bioimpedance was 203 – 616 Ω, while the range for fat was 5.02 - 17.8 kΩ and for connective tissue was 790 Ω – 1.55 kΩ. When the samples were heated to 37°C and measured again at 10kHz, the approximate bioimpedance range for muscle was 100-175Ω. The approximate bioimpedance range of fat was 627 Ω - 3.2 kΩ and the range for connective tissue was 221-540Ω respectively.

In the experiments done on the fresh slaughtered lamb carcass, replicating a scenario close to the real application, the impedance values recorded for fat were around 17 kΩ, for muscle and lean tissue around 1.3 kΩ while the nervous structures had an impedance value of 2.9 kΩ.

Analysis performed with a needle moving steadily through an ex-vivo meat sample showed that the response to a different kind of biological tissue structure was instantaneous, which proves that this method could be used to monitor changes of impedance values in real-time and hence in a real surgery scenario.

It was possible to conclude from this data that measurements of bioimpedance at the needle tip location can give valuable information to the clinicians performing a peripheral nerve block procedure as the separation (in terms of impedance figures) was

very marked between the different type of tissues. More tests will be also carried out on other freshly slaughtered animal carcasses to get further information, especially about the nervous structures which are central in this research and difficult to measure in any other situation.

5.8 FUTURE WORK

Currently our group is working on integrating an impedance sensor to a commercially available anaesthetic needle that will help us to better understand the impedance characteristics of the different tissues in both ex-vivo and, eventually, in-vivo samples. Several techniques for the fabrication of the impedance electrode have been explored and the fabrication is still ongoing at the moment, with the technique of shadow masking likely to be the most successful one.

The main problem for the shadow masking technique appears to be the alignment of the needles in the mask itself and for this reason several different types of masks will be considered before obtaining a solution to the problem.

5.9 REFERENCES

[1] Cheney, F.W., et al., Nerve Injury Associated with Anesthesia: A Closed Claims Analysis. Anesthesiology, 1999. 90(4): p. 1062-1069.

[2] Kroll, D.A., et al., Nerve Injury Associated with Anesthesia. Anesthesiology, 1990. 73(2): p. 202-207.

[3] Chambers, W.A., Peripheral nerve damage and regional anaesthesia. Br J Anaesth, 1992. 69(5): p. 429-30.

[4] Jeng, C.L. and M.A. Rosenblatt, Intraneural injections and regional anesthesia: the known and the unknown. Minerva Anestesiol, 2011. 77(1): p. 54-8.

[5] Bigeleisen, P.E., Nerve puncture and apparent intraneural injection during ultrasound-guided axillary block does not invariably result in neurologic injury. Anesthesiology, 2006. 105(4): p. 779-83.

[6] Steinfeldt, T., et al., Histological Analysis After Peripheral Nerve Puncture with Pencil-Point or Tuohy Needletip. Anesthesia and Analgesia, 2011. 112(2): p. 465-470.

[7] Hogan, Q.H., Pathophysiology of peripheral nerve injury during regional anesthesia. Reg Anesth Pain Med, 2008. 33(5): p. 435-41.

[8] Selander, D. and J. Sjostrand, Longitudinal Spread of Intraneurally Injected Local-Anesthetics - Experimental-Study of Initial Neural Distribution Following Intraneural Injections. Acta Anaesthesiologica Scandinavica, 1978. 22(6): p. 622-634.

[9] Urmey, W.F., Electrical stimulation and ultrasound in regional anesthesia. European Journal of Pain Supplements, 2010. 4(4): p. 319-322.

[10] Tsui, B.C., et al., Atlas of Ultrasound- and Nerve Stimulation-Guided Regional nesthesia. 2008, New York: Springer Verlag. 302.

[11] Urmey, W.F., Percutaneous electrode guidance of the block needle for peripheral or plexus neural blockade. Techniques in Regional Anesthesia and Pain Management, 2002. 6(4): p. 145-149.

[12] Gebhard, R.E., Modalities of Nerve Block Performance-Is there a Silver Bullet?, in Dual Guidance-A Multimodal Approach to Nerve Location. 2008, B. Braun Medical Inc.: Bethlehem, Pennsylvania. p. 2 - 10.

[13] Urmey, W.F. and J. Stanton, Inability to consistently elicit a motor response following sensory paresthesia during interscalene block administration. Anesthesiology, 2002. 96(3): p. 552-554.

[14] Choyce, A., et al., What is the relationship between paresthesia and nerve stimulation for axillary brachial plexus block? Reg Anesth Pain Med, 2001. 26(2): p. 100-4.

[15] Macfarlane, A.J., A. Bhatia, and R. Brull, Needle to nerve proximity: what do the animal studies tell us? Reg Anesth Pain Med, 2011. 36(3): p. 290-302.

[16] Sinha, S.K., J.H. Abrams, and R.S. Weller, Ultrasound-Guided Interscalene Needle Placement Produces Successful Anesthesia Regardless of Motor Stimulation Above or Below 0.5 mA. Anesthesia & Analgesia, 2007. 105(3): p. 848-852.

[17] Ben-David, B. and J.E. Chelly, Current Channeling: A Theory of Nerve Stimulator Failure. Anesthesia & Analgesia, 2003. 96(5): p. 1531-1532.

[18] Marhofer, P., M. Greher, and S. Kapral, Ultrasound guidance in regional anaesthesia. British Journal of Anaesthesia, 2005. 94(1): p. 7-17.

[19] Kapral, S., P. Marhofer, and T. Grau, [Ultrasound in local anaesthesia. Part I: technical developments and background]. Anaesthesist, 2002. 51(11): p. 931-7.

[20] Kossoff, G., Basic physics and imaging characteristics of ultrasound. World Journal of Surgery, 2000. 24(2): p. 134-142.

[21] Steiner, E. and C. Nasel, Sonography of peripheral nerves: Basic principles. Acta Anaesthesiologica Scandinavica, 1998. 42: p. 46-48.

[22] Marhofer, P., et al., Fifteen years of ultrasound guidance in regional anaesthesia: Part 1. British Journal of Anaesthesia, 2010. 104(5): p. 538-546.

[23] Marhofer, P., et al., Ultrasonographic guidance improves sensory block and onset time of three-in-one blocks. Anesthesia and Analgesia, 1997. 85(4): p. 854-7.

[24] Marhofer, P., et al., Ultrasonographic guidance reduces the amount of local anesthetic for 3-in-1 blocks. Reg Anesth Pain Med, 1998. 23(6): p. 584-8.

[25] Macaire, P., et al., Ultrasound- or nerve stimulation-guided wrist blocks for carpal tunnel release: a randomized prospective comparative study. Reg Anesth Pain Med, 2008. 33(4): p. 363-8.

[26] Sauter, A.R., et al., Electrical Nerve Stimulation or Ultrasound Guidance for Lateral Sagittal Infraclavicular Blocks: A Randomized, Controlled, Observer-Blinded, Comparative Study. Anesthesia & Analgesia, 2008. 106(6): p. 1910-1915.

[27] Casati, A., et al., A Prospective, Randomized Comparison between Ultrasound and Nerve Stimulation Guidance for Multiple Injection Axillary Brachial Plexus Block. Anesthesiology, 2007. 106(5): p. 992-996 10.1097/01.anes.0000265159.55179.e1.

[28] Perlas, A., et al., Ultrasound Guidance Improves the Success of Sciatic Nerve Block at the Popliteal Fossa. Regional Anesthesia and Pain Medicine, 2008. 33(3): p. 259-265.

[29] Chan, V.W., et al., Ultrasound guidance improves success rate of axillary brachial plexus block. Canadian Journal of Anaesthesia-Journal Canadien D Anesthesie, 2007. 54(3): p. 176-82.

[30] Sites, B.D., et al., Ultrasound guidance improves the success rate of a perivascular axillary plexus block. Acta Anaesthesiol Scand, 2006. 50(6): p. 678-84.

[31] Kapral, S., et al., Ultrasonographic guidance improves the success rate of interscalene brachial plexus blockade. Reg Anesth Pain Med, 2008. 33(3): p. 253-8.

[32] Liu, F.C., et al., Efficacy of ultrasound-guided axillary brachial plexus block: a comparative study with nerve stimulator-guided method. Chang Gung Med J, 2005. 28(6): p. 396-402.

[33] Williams, S.R., et al., Ultrasound guidance speeds execution and improves the quality of supraclavicular block. Anesthesia and Analgesia, 2003. 97(5): p. 1518-23.

[34] Gurkan, Y., et al., Comparison of nerve stimulation vs. ultrasound-guided lateral sagittal infraclavicular block. Acta Anaesthesiol Scand, 2008. 52(6): p. 851-5.

[35] Taboada, M., et al., Is Ultrasound Guidance Superior to Conventional Nerve Stimulation for Coracoid Infraclavicular Brachial Plexus Block? Regional Anesthesia and Pain Medicine, 2009. 34(4): p. 357-360

[36] Sia, S. and M. Bartoli, Selective Ulnar Nerve Localization Is Not Essential for Axillary Brachial Plexus Block Using a Multiple Nerve Stimulation Technique. Regional Anesthesia and Pain Medicine, 2001. 26(1): p. 12-16.

[37] Warman, P. and B. Nicholls, Ultrasound-guided nerve blocks: efficacy and safety. Best Pract Res Clin Anaesthesiol, 2009. 23(3): p. 313-26.

[38] Hadzic, A., X. Sala-Blanch, and D. Xu, Ultrasound guidance may reduce but not eliminate complications of peripheral nerve blocks. Anesthesiology, 2008. 108(4): p. 557-8.

[39] Fredrickson, M.J. and T.K. Danesh-Clough, Ambulatory continuous femoral analgesia for major knee surgery: a randomised study of ultrasound-guided femoral catheter placement. Anaesth Intensive Care, 2009. 37(5): p. 758-66.

[40] Abrahams, M.S., et al., Ultrasound guidance compared with electrical neurostimulation for peripheral nerve block: a systematic review and meta-analysis of randomized controlled trials. Br J Anaesth, 2009. 102(3): p. 408-17.

[41] Fredrickson, M.J. and D.H. Kilfoyle, Neurological complication analysis of 1000 ultrasound guided peripheral nerve blocks for elective orthopaedic surgery: a prospective study. Anaesthesia, 2009. 64(8): p. 836-44.

[42] Borgeat, A., et al., Evaluation of the lateral modified approach for continuous interscalene block after shoulder surgery. Anesthesiology, 2003. 99(2): p. 436-442.

[43] Loubert, C., et al., Complication during ultrasound-guided regional block: accidental intravascular injection of local anesthetic. Anesthesiology, 2008. 108(4): p. 759-60.

[44] Zetlaoui, P.J., J.P. Labbe, and D. Benhamou, Ultrasound guidance for axillary plexus block does not prevent intravascular injection. Anesthesiology, 2008. 108(4): p. 761.

[45] Russon, K. and R. Blanco, Accidental Intraneural Injection into the Musculocutaneous Nerve Visualized with Ultrasound. Anesthesia & Analgesia, 2007. 105(5): p. 1504-1505.

[46] Schafhalter-Zoppoth, I., I.D. Zeitz, and A.T. Gray, Inadvertent Femoral Nerve Impalement and Intraneural Injection Visualized by Ultrasound. Anesthesia & Analgesia, 2004. 99(2): p. 627-628.

[47] Koff, M.D., et al., Severe Brachial Plexopathy after an Ultrasound-guided Single-injection Nerve Block for Total Shoulder Arthroplasty in a Patient with Multiple Sclerosis. Anesthesiology, 2008. 108(2): p. 325-328

[48] Bhatia, A., et al., Pneumothorax as a Complication of the Ultrasound-Guided Supraclavicular Approach for Brachial Plexus Block. Anesthesia & Analgesia, 2010. 111(3): p. 817-819.

[49] Neal, J.M., et al., ASRA Practice Advisory on Neurologic Complications in Regional Anesthesia and Pain Medicine. Regional Anesthesia and Pain Medicine, 2008. 33(5): p. 404-415.

[50] Carty, S. and B. Nicholls, Ultrasound-guided regional anaesthesia. Continuing Education in Anaesthesia, Critical Care & Pain, 2007. 7(1): p. 20-24.

[51] Hebl, J.R., Ultrasound-guided Regional Anesthesia and the Prevention of Neurologic Injury: Fact or Fiction? Anesthesiology, 2008. 108(2): p. 186-188

[52] Hopkins, P.M., Ultrasound guidance as a gold standard in regional anaesthesia. Br J Anaesth, 2007. 98(3): p. 299-301.

[53] Peterson, M.K., F.A. Millar, and D.G. Sheppard, Editorial I. British Journal of Anaesthesia, 2002. 88(5): p. 621-624.

[54] Denny, N.M. and W. Harrop-Griffiths, Editorial I: Location, location, location! Ultrasound imaging in regional anaesthesia. British Journal of Anaesthesia, 2005. 94(1): p. 1-3.

[55] McCartney, C.J.L., Ultrasound guidance for regional anaesthesia. British Journal of Anaesthesia, 2007. 99(1): p. 139-142.

[56] Koscielniak-Nielsen, Z.J., Ultrasound-guided peripheral nerve blocks: What are the benefits? Acta Anaesthesiologica Scandinavica, 2008. 52(6): p. 727-737.

[57] Horlocker, T.T. and D.J. Wedel, Ultrasound-guided regional anesthesia: in search of the holy grail. Anesthesia and Analgesia, 2007. 104(5): p. 1009-11.

[58] Tsui, B., Ultrasound-guidance and nerve stimulation: implications for the future practice of regional anesthesia. Canadian Journal of Anesthesia / Journal canadien d'anesthésie, 2007. 54(3): p. 165-170.

[59] Marhofer, P., H. Willschke, and S. Kettner, Current concepts and future trends in ultrasound-guided regional anesthesia. Current Opinion in Anesthesiology, 2010. 23(5): p. 632-636.

[60] Steinfeldt T, Poeschl S, Nimphius W, et al. Forced needle advancement during needle nerve contact in a porcine model: histological outcome. Anesth Analg 2011; 113: 417-20

[61] Hadzic A, Dilberovic F, Shah S, et al. combination of intraneural injection and high injection pressure leads to fascicular injury and neurologic deficits in dogs. Reg Anesth Pain Med 2004; 29: 417-23.

[62] Sala-Blanch X, Ribalata T, Rivas E et al. Structural injury to the human sciatic nerve after intraneural needle insertion. Reg Anesth Pain Med 2009; 34: 201-5.

[63] Shah S, Hadzic A, Vloka JD et al. Neurologic complication after anterior sciatic nerve block. Anesth Analg 2005; 100: 1515-7.

[64] Reiss W, Kurapati S, Shariat A, Hadzic A. Nerve injury complicating ultrasound / electrostimulation-guided supraclavicular brachial plexus block. Reg Anesth, Pain Med 2010; 35: 400-1.

[65] Cohen J.M., Gray A.T., Functional deficits after intraneural injection during interscaleneblock.RegAnesthPainMed2010;35:397-99.

[66] Kalvøy H, Frich L, Grimnes S, Martinsen ØG, Hol PK, Stubhaug A. Impedance-based tissue discrimination for needle guidance. Physiological measurement. 2009;30(2):129.

[67] Kinouchi Y, Iritani T, Morimoto T, Ohyama S., Fast in vivo measurements of local tissue impedances using needle electrodes. Med Biol Eng Comput. 1997;35(5):486-92.

[68] Slaughter G. E., Hobson R., An impedimetric biosensor based on PC 12 cells for the monitoring of exogenous agents, Biosensors and Bioelectronics 24 (2009) 1153–1158

[69] Kalvoy, H., et al., Electrical Impedance of Stainless Steel Needle Electrodes. Annals of Biomedical Engineering, 2010. 38(7): p. 2371-2382.

[70] Kalvoy, H., et al., Determination of tissue type surrounding a needle tip by electrical bioimpedance, 30th Annual International IEEE EMBS Conference Vancouver, British Columbia, Canada, August 20-24, 2008

[71] Lisa Helen, Walter Messina, Brian O'Donnell and Eric Moore, Investigation of tissue bioimpedance using a macro-needle with a potential application in determination of needle-to-nerve proximity, Proceedings of the 8th International Conference on Sensing Technology, Sep. 2-4, 2014, Liverpool, UK

Chapter 6

6 CONCLUSIONS AND FUTURE WORK

6.1 CONCLUSIONS AND FUTURE WORK

Impedance spectroscopy (IS) and impedance based sensors are commonly used to characterise systems and to extract valuable information about them. A system is broadly defined as an element or material in electrical contact with electrodes which can be a solid-solid (in the case of many chemical sensors) or solid-liquid (when examining concentration of a species in a liquid) interface. IS can be used to obtain information about the element itself and the interface between the element and electrode.

IS takes advantage of the fact that a small voltage potential applied to the interface will polarize the interface. The manner in which the interface polarizes, combined with the rate at which it changes when the applied potential is reversed, it characterises the interface. This allows the user to extract information about the system interface, such as adsorption/reaction rate constants, diffusion coefficients, and capacitance. It is also possible to estimate information on the dielectric constant, conductivity, mobility of charge equilibrium, constituent concentrations, and bulk generation/recombination rates of the element (i.e. the sensor or substance under investigation).

For these reasons impedance based sensors have been used in this thesis to study the behaviour of cell cultures exposed to toxic compounds and to analyse the bioimpedance of animal tissues to create an efficient tool in peripheral nerve block procedures.

Nanopillars have been successfully fabricated on the interdigitated impedance electrodes using the e-beam lithography technique combined with evaporation and photolithography methods in order to investigate the possibility of increasing the sensitivity of techniques for studying the cytotoxicity.

The fabrication procedure created a lot of problems at the start of the project and lot of work and time was dedicated to the troubleshooting. However, once all the parameters and procedure were defined and finalised, the fabrication proved to be a relatively easy and fast process but still quite expensive. It has been estimated that the total cost would be ~20-22 € per device including the labour and all the consumables used. Hopefully in future the costs might decrease making this technique more economically appealing for the fabrication of nanopillars.

More fabrication attempts will be done in the future using materials different from gold, like platinum or again ITO which would also allow a certain electrode transparency very useful for imaging the cells growing on the devices. Other layouts and pillar height will be also examined.

Three cell lines have been imaged using both an optical microscope and a scanning electron microscope. On the two different kinds of electrodes the cells appeared quite healthy and reached confluence; however, it seemed that the cells growing on the standard electrode had a larger surface area compared to those growing on the nanostructured device. The nanostructures did not prevent the cells from growing on the culturing surface but it was necessary a further analysis of the cells with the aid of a scanning electron microscope.

Expected results were observed through the images obtained with the aid of a scanning electron microscope. The A549 and HeLa cells appeared round and less spread growing on the nanopillars than those observed on the flat surface electrodes, achieving a confluent layer of cells comparable to that formed on the standard electrode. The BALB c3T3 cells, however, did not show any differences between those grown on the flat and nanostructured electrode. Larger gaps between the basal membrane of the cell and the impedance electrode surface where easily noticed on the first two types of cells growing

on the nanostructured electrodes which in theory, during the ECIS measurement, should have showed some differences in the impedance figures collected during the analysis.

Little or no differences were noticed in the impedance analysis carried out over time with a fixed frequency of 10 kHz on A549 cells. The main reason for this negative result resided in the fact that the cells were placed manually on the electrodes and the attachment to the substrate happened always in a different way and did not follow a precise and repeatable process. There could not be an absolute certainty that the same amount of cells would attach on the electrode in the same way and at the same time. Only in a couple of experiments carried out on A549 cells growing on the nanostructured electrodes exposed to Nicotine was noticed an increase of sensitivity, but a larger amount of data will be needed to achieve a higher level of statistical significance to prove this with absolute confidence.

Future work on this kind of assay will be carried out in order to get more statistical data with the impedance analysis confirm these findings. Other cell lines will be also used to have a broader view about this kind of assay.

The performances of the devices comprising the nanopillars on the interdigitated impedance electrodes were compared with their flat counterpart toward the simultaneous detection of dopamine and uric acid; the nanostructured electrodes showed better sensitivity and the peaks in the voltammograms reported in this thesis were higher and better defined compared to the smaller and broader ones of the flat electrodes. This was due to the fact that the nanostructures increased the surface area of the electrode; for this reason the nanopillars fabricated on the interdigitated electrode enhanced the electron transfer property of the flat version of this electrode.

Experiments are currently being carried out to investigate the effects of different nanopillar configurations, especially in terms of pillar height, diameter and spacing to optimize the detection of DA and UA. More tests will be performed including the detection of Ascorbic acid which is often reported in many papers as an element that could mask the peaks of the other two elements in the voltammogram as they often overlap.

The tests carried out with the macro needle showed that it is feasible to use an impedance electrode fabricated on the needle tip to differentiate several tissues from the nerve tissue. In these preliminary studies bioimpedance measurement was applied in the field of anaesthesia and more specifically to ultrasound guided peripheral nerve block. It was possible to distinguish, between muscle, fat, bone, connective tissues and eventually nerve tissue using meat samples.

Several techniques for the fabrication of the impedance electrode have been explored and the fabrication is still on going, although the shadow masking technique looked the most promising for this type of fabrication.

More tests are being carried out using a thin polyamide sheet with gold tracks and pads fabricated on it. This thin membrane-like electrode is wrapped around the needle, packaged and connected to the impedance analyser, giving very good results in term of tissue differentiation.

Chapter 7

7 APPENDIX

7.1 LIST OF PAPERS, ORAL PRESENTATIONS AND POSTER PRESENTATIONS

7.1.1 List of papers

Walter Messina, Michelle Fitzgerald, Una Crowley, Eric Moore

Fabrication of gold nanopillars on gold interdigitated impedance electrodes for biological applications

Proceedings of the 8th International Conference on Sensing Technology, Sep. 2-4, 2014, Liverpool, UK

Lisa Helen, Walter Messina, Brian O'Donnell and Eric Moore

Investigation of tissue bioimpedance using a macro-needle with a potential application in determination of needle-to-nerve proximity

Proceedings of the 8th International Conference on Sensing Technology, Sep. 2-4, 2014, Liverpool, UK

Walter Messina and Eric Moore

Nanopillars: a review on applications, fabrication methods and materials

Submitted to the Analyst Journal

Walter Messina, Lisa Helen, Brian O'Donnell, Eric Moore and George Shorten
Bioelectrical impedance as a tool for safer peripheral nerve block procedures.
Submitted to the British Journal of Anaesthesia

Una B. Crowley, Walter Messina, Miloslav Pravda, Jeremy D. Glennon, Eric Moore.
Electrochemical property of screen printed electrode modified with gold nanoparticles for the simultaneous determination of Dopamine and Uric acid
Accepted and in press, Journal of Electroanalytical Chemistry.

Una B. Crowley, Siriboon Mukdasai, Walter Messina, Xiaoyun He, Supalax Sriharanai, Ekaterina P. Nesterenko, Pavel N. Nesterenko , Brett Paull, Miloslav Pravda, Jeremy D. Glennon, Eric Moore
Electrochemical properties of carbon monolith with gold nanoparticles modified screen printed electrode for the simultaneous determination of Dopamine and Uric acid
Submitted to Electroanalysis Journal.

7.1.2 List of oral presentations

Walter Messina, Una Crowley, Michelle Fitzgerald, Eric Moore
Fabrication of gold nanopillars on gold interdigitated impedance electrodes for biological and electrochemical applications
8th International Conference on Sensing Technology (ICST 2014) Liverpool 2-4 September 2014

Walter Messina, Una Crowley, Michelle Fitzgerald, Eric Moore
Fabrication of gold nanopillars on gold interdigitated impedance electrodes for biological and electrochemical applications
International Conference and Exhibition Nanotech MEET Tunisia 2014, April 24-26, 2014, Hammamet, Tunisia

Walter Messina, Eric Moore

Fabrication of gold nanopillars on gold interdigitated impedance electrodes for biological applications

Conference of Analytical Science in Ireland, CASi 2013 July 1st 2013 Cork

Walter Messina, Brian O'Donnell, George Shorten, Eric Moore

Development of a needle integrated with an impedance sensor to determine nerve proximity

NanoBio Europe Conference July 18-20 Varese, Italy

7.1.3 List of poster presentations

Walter Messina, Lisa Helen, Niall Savage, Brian O'Donnell, Martin O'Sullivan and Eric Moore

Impedance sensors for biomedical and bioassay applications

Irish Universities Chemistry Research Colloquium June 19-20th 2014

Walter Messina, Eric Moore

Fabrication of gold nanopillars on gold interdigitated impedance electrodes for biomedical applications

SSI Smart System Integration, International Conference and Exhibition on Integration Issues of Miniaturized Systems, Vienna 26-27 March 2014

Walter Messina, Eric Moore

Fabrication of gold nanopillars on gold interdigitated electrodes for impedance and electrochemical measurements on biological samples

MNBS 2013 and EPoSS General Assembly & Annual Forum 2013, Cork 24-26th September 2013

Walter Messina, Eric Moore

Nano-structured sensor arrays for toxicity monitoring of cells relevant to human health.

Tyndall Industrial Days, September 17th 2013

Walter Messina, Eric Moore

Development of miniaturized biomedical sensor devices

Royal Academy of Medicine in Ireland Annual Meeting 2013, 20th june 2013

Walter Messina, Eric Moore

Nano-structured sensor arrays for toxicity monitoring of cells relevant to human health

NanoWeek 2012 Conference, 17th – 18th September 2012, Trinity College Dublin.